DEVELOPMENT AND CHARACTERISATION OF A NON-THERMAL PLASMA SOURCE SUITABLE FOR BIOLOGICAL APPLICATION, AND ITS EFFECTS ON MAMMALIAN CELLS, WITH A PARTICULAR FOCUS ON FIBROBLASTS AND MACROPHAGE-LIKE CELLS

A thesis presented in fulfilment of the requirement for the degree of

Doctor of Philosophy

Rachael B. Pirie

2023

Electronic and Electrical Engineering

University of Strathclyde

Glasgow, UK

Declaration of Authenticity and Author's Rights

'This thesis is the result of the author's original research. It has been composed by the author and has not been previously submitted for examination which has led to the award of a degree.'

'The copyright of this thesis belongs to the author under the terms of the United Kingdom Copyright Acts as qualified by University of Strathclyde Regulation 3.50. Due acknowledgement must always be made of the use of any material contained in, or derived from, this thesis.'

Signed: Rachael B. Pirie

Date: 28 August 2023

Acknowledgements

Firstly, I would like to thank my Supervisors Dr Tao Wang (Electronic and Electrical Engineering (EEE)) and Professor Mary Grant (Biomedical Engineering (BME)) for their support, assistance and expertise throughout my study. Without them, I could not have completed this work. I would also like to thank my secondary supervisor, Professor Scott Macgregor.

Several members of the University's technical staff have also provided assistance to me over the course of my study, for which I am very grateful. Mrs Catherine Henderson, chief technician in BME, has provided consistent assistance and support throughout the project, and I have benefited greatly from her extensive technical knowledge. Dr Rothwelle Tate from the Strathclyde Institute of Pharmacy and Biomedical Science (SIPBS) and Dr Peter Childs (BME) both helped me to understand and carry out RT-qPCR. Mr Graeme Mackenzie (SIPBS) provided technical assistance for the more advanced imaging techniques used during the project. Mr Sean Doak and Mr Andy Carlin (EEE) manufactured my reactor designs.

I have also enjoyed the support of several fellow PhD students. From EEE, I would particularly like to thank Yiyi Zhao for her early encouragement in the field of plasma research, as well as Yingjia Zhou, Zhongshu Zhang, and Biye Cao. From BME, Sara Gomez Arnaiz, Laura Beattie and Jamie Dow.

Lastly, I could of course not have completed this work without the endless support of my family and friends. In particular, I would like to thank my mother, Elaine Pirie, brother, Chris Pirie, and friend Alan Robertson.

Abstract

Plasma medicine is the research field investigating the use of non-thermal plasmas (NTP) for medical treatment. NTP is already used clinically in areas such as the enhancement of wound healing. The motivation behind this work performed on this project was to further develop understanding of the biomedical effects of NTP, particularly those relating cells of the immune system.

In this project, a dielectric barrier discharge (DBD) NTP source, with a pin-plate style electrode arrangement, was designed to apply NTP to aqueous liquid which either contained *in vitro* mammalian cell samples (direct treatment), or which was later added to such samples (plasma-activated medium (PAM) treatment). During liquid exposure to NTP for 30 minutes in the designed device, concentrations of hydrogen peroxide (H_2O_2) and nitrite (NO_2^-), two key substances in plasma medicine, rose linearly to 5.2 mM and 13.0 mM respectively. These are within the range used for similar work in the literature. Testing on cells also showed that the designed device was capable of reducing viability with both directly and via PAM. Together, this chemical and biological data showed the suitability of the designed NTP source for use in plasma medicine research. The precision of the pin-plate DBD design style was also demonstrated.

A range of dilutions of PAM from the device were applied to a pro-inflammatory macrophage-like cell line, differentiated U937, and resulting in several novel findings. Sublethal PAM treatments did not influence phagocytic ability, nor the expression of two genes related to antioxidants superoxide dismutase 1 and 2 (SOD1 and SOD2). The release of pro-inflammatory chemokines and other cytokines was altered however, and notably the

overall cytokine profile was dependent upon the PAM dilution used. This raises the possibility of fine-tuning the inflammatory environment through NTP.

Table of Contents

List of tables

List of figures

Abbreviations

ACBC	AC barrier corona
Akt	Protein kinase B
ANOVA	Analysis of variance
APC	Antigen-presenting cell
BCDF	B cell differential factor
BCGF-1	B cell growth factor 1
BME	β-mercaptoethanol
BSA	Bovine serum albumin
BSF-1	B cell stimulatory factor 1
BSF-2	B cell stimulatory factor 2
CAM	Cell adhesion molecules
CCL	Chemokine (C-C motif ligand),
cDNA	Complementary DNA
$C_{19}H_{14}O_5S$	Phenol red
C_q	Quantification cycle
CXCL	Chemokine (C-X-C motif) ligand
DAMP	Damage-associated molecular pattern
DAPI	4',6-diamidino-2-phenylindole, dihydrochloride
DBD	Dielectric barrier discharge
DEPC	Diethylpryrocarbonate
DMEM	Dulbecco's modified Eagle's medium
DMEM-PAM	PAM made from FBS-free DMEM
DMSO	Dimethylsulfoxide

DNA	Deoxyribonucleic acid
DPBS	Dulbecco's phosphate buffered saline
DPBS-PAM	PAM made from DPBS
DTT	DL-dithiothreitol
EDTA	Ethylenediaminetetraacetic acid
ELISA	Enzyme-linked immunosorbent assay
FACS	Fluorescence-activated cell sorting
FBS	Foetal bovine serum
FE	Floating electrode
FINCA	Fibrosis, neurodegeneration, and cerebral angiomatosis
FITC	Fluorescein isothiocyanate
FOXO	Forkhead box O
GAPDH	Glyceraldehyde 3-phosphate dehydrogenase (also known as G3PDH)
Gluc	Glucocorticoid
GM-CSF	Granulocyte macrophage colony-stimulating factor
gDNA	Genomic DNA
HNO_2	Nitrous acid
HNO_3	Nitric acid
HO-1	Haem oxygenase 1
HO_2	Hydroperoxyl radical
H_2O_2	Hydrogen peroxide
H_3PO_4	Phosphoric acid
HRP	Horseradish peroxidase

H_2SO_4	Sulphuric acid
IC	Immune complex
ICCD	Intensified charge-coupled device
ICD	Immunogenic cell death
IFN-γ	Interferon γ
IGIF	IFN-γ inducing factor
IL	Interleukin
iNOS	Inducible nitric oxide synthase
LPS	Lipopolysaccharide
MEM	Minimum essential medium
MHC	major histocompatibility complex
mRNA	Messenger RNA
MTT	3-[4,5-dimethylthiazole-2-yl]-2,5-diphenyltetrazolium bromide
$NaHCO_3$	Sodium bicarbonate
$NaNO_2$	Sodium nitrite
NEAA	Non-essential amino acids
NHLRC2	NHL-repeat-containing protein 2
NK cell	Natural killer cell
NKSF	Natural killer cell stimulatory factor
NKT cell	Natural killer T cell
NMR	Nuclear magnetic resonance
NO	Nitric oxide
NO_2	Nitrogen dioxide

NO_2^-	Nitrite ion
NO_3^-	Nitrate ion
nrf2	Nuclear factor erythroid 2-related factor 2
NTP	Non-thermal plasma
$^1O_2$	Singlet oxygen
O_2^-	Superoxide
O_3	Ozone
OES	Optical emission spectra
OH·	Hydroxyl radical
$ONOO^-$/ONOOH	Peroxynitrite
O_2NOO^-	Peroxynitrate
PAM	Plasma-activated medium
PAMP	Pathogen-associated molecular pattern
PBS	Phosphate buffered saline
PCR	Polymerase chain reaction
PDGF	Platelet-derived growth factor
PES	Polyethersulfone
PI	Propidium iodide
PMA	Phorbol 12-myristate 13-acetate
ppm	Parts per million
PRR	Pattern recognition receptors
PTFE	Polytetrafluoroethylene
PVC	Polyvinyl chloride
qPCR	Quantitative PCR

RANTES	Regulated upon activation, normal T cell expressed and excreted
RNA	Ribonucleic acid
RNS	Reactive nitrogen species
RONS	Reactive oxygen and nitrogen species
ROS	Reactive oxygen species
rpm	Revolutions per minute
RPMI 1640	Roswell Park Memorial Institute 1640 medium
RPMI-PAM	PAM made from FBS-free RPMI 1640
RT-PCR	Reverse transcription PCR
RT-qPCR	Quantitative reverse transcription PCR
SD	Standard deviation
SE	Standard error
SIPBS	Strathclyde Institute of Pharmacy and Biological Sciences
SOD	Superoxide dismutase
SOD1	Superoxide dismutase 1
SOD2	Superoxide dismutase 2
SSIV	SuperScript IV Reverse Transcriptase
TAM	Tumour-associated macrophage
TGF-β	Transforming growth factor β
Th1	T helper 1 cell
Th2	T helper 2 cell
T_m	Melting temperature
TM2D1	TM2 containing domain 1

TMB	3,3’,5,5’-tetramethylbenzidine
TNF	Tumour necrosis factor
TNF-α	Tumour necrosis factor α
TUNEL	Terminal deoxynucleotidyl transferase dUTP nick end labelling
UV	Ultraviolet
VEGFA	Vascular endothelial growth factor A
V_m	Peak voltage

Chapter 1 Introduction

1.1 Summary of project

This project involved the development of a non-thermal plasma (NTP) source capable of applying NTP to *in vitro* eukaryotic cells, and the subsequent investigation of its electrical properties and ability to chemically modify aqueous liquids, as well as its effects on murine fibroblasts, used for basic biological testing of the NTP source, and a human macrophage-like cell line.

The initial stage of the project involved the development and characterisation of a dielectric barrier discharge (DBD) style NTP source which was suitable for application to cells held within cell culture vessels (Chapter 3). This was then followed by the assessment of the designed reactor's ability to chemically modify liquid, via the assessment of two biologically-relevant indicator species, hydrogen peroxide (H_2O_2) and the nitrite ion (NO_2^-). Alongside this work, levels of liquid evaporation, changes in temperature and changes in pH in the treated liquid were also considered (Chapter 4). Chapters 5 and 6 considered basic biological testing of the effects of the generated NTP, using both the direct and plasma activated medium (PAM) methods of treatment, terms which are explained below in 1.2.3.4. This work used the NIH3t3 murine fibroblast cell line. Finally, Chapter 7 considered some of the effects of the PAM treatment produced by the designed reactor on the U937 human monocytic cell line, differentiated to a macrophage-like cell, specifically with regards to inflammatory profile, phagocytic ability, and the expression of antioxidant enzyme genes.

The purpose of this project was to further develop understanding of the potential of NTP for future medical treatments. There were several novel findings within the work, particularly with regards to understanding the effects of PAM treatment on the inflammatory profile of macrophage-like cells, and how this could be varied by the use of the different PAM dilutions, as well as the lack of impact of sublethal strengths of PAM on phagocytosis and the expression two antioxidant enzyme genes.

1.2 Background

1.2.1 Eukaryotic cells and the mammalian immune system

1.2.1.1 Eukaryotic cells

Eukaryotic cells are those which have a clearly-defined nucleus holding the genetic material of the cell, in comparison to prokaryotic cells which do not [1][2]. As well as this, eukaryotic cells are larger and more complex than prokaryotic cells [2], contain intracellular compartments, and have a larger genome [2]. While the prokaryotic organism group consists entirely of bacteria (eubacteria) and archaea (archaebacteria), all other organisms, including multicellular ones such as animals and therefore humans, are eukaryotic [1][2]. A typical example of a eukaryotic cell is shown in Figure 1.1.

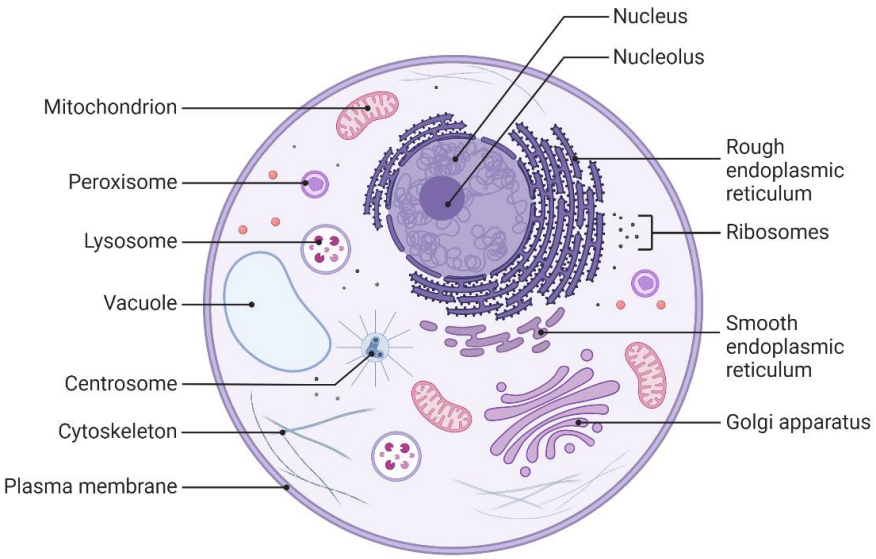

Figure 1.1. Typical eukaryotic cell, in this case from an animal. Adapted from "Structural Overview of an Animal Cell" by BioRender.com (2022). Retrieved from [3].

1.2.1.2 The mammalian immune system

Much of the latter work of this project involved the application of NTP to human immune cells, specifically macrophage-like cells. The mammalian immune system is vital to the survival of the animal, protecting it from external threats of many types, such as viruses, bacteria, protozoa, fungi and parasites [4]. The system is made up of a mixture of cellular components, derived from haematopoietic stem cells (Figure 1.2, Table 1.1) and humoral, or non-cellular components, which include substances such as cytokines and antibodies.

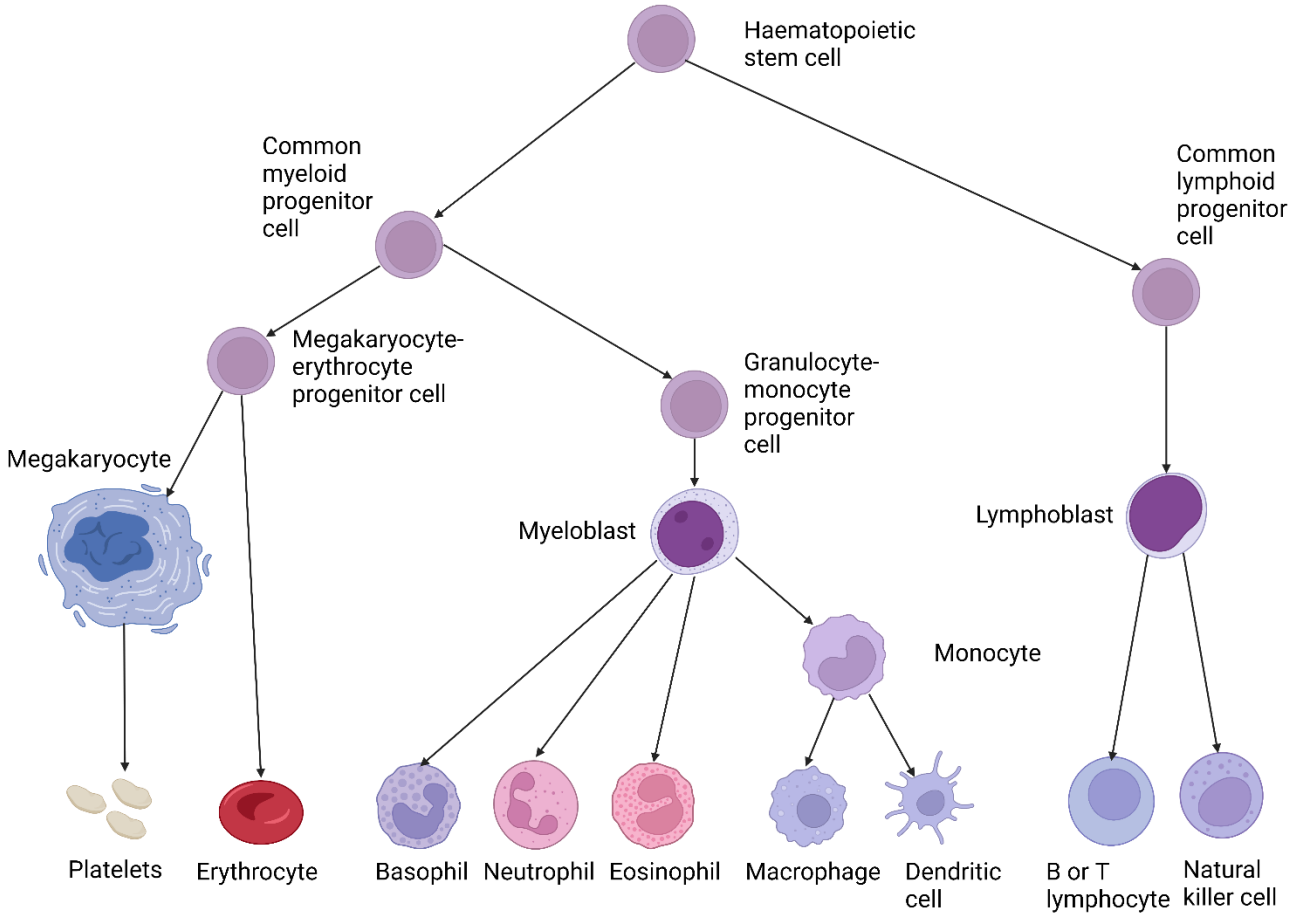

Figure 1.2. Origin of haematopoietic cells from progenitor cells. Based on diagram from [5]. Some intermediate stages have been omitted for clarity. Created with BioRender.com [6].

Table 1.1. Haematopoietic cells with immune functions [4].

Cell type	**Main location found**	**Main actions**
Monocytes	Blood	Differentiation into macrophages when required
Macrophage	Tissue	Phagocytosis, defence against bacteria, antigen presentation
Neutrophil	Blood	Phagocytosis and defence against bacteria
Basophil	Blood	Defence against parasites, involvement in allergic reactions
Eosinophil	Blood	Defence against parasites, involvement in allergic reactions
Dendritic cell	Tissue	Antigen uptake and presentation
B-lymphocyte	Blood and lymph tissue	Differentiate into plasma cells which secrete antibodies
T-lymphocyte	Blood and lymph tissue	Depending on T-cell type may act against intracellular pathogens, or regulate the behaviour of other cells
Natural killer cell	Blood and lymph tissue	Defence against viruses

The immune system consists of two parts: the innate immune system and the acquired immune system. A high-level comparison of these is given in Table 1.2. The innate and acquired immune systems do not operate completely separately, with acquired immunity also being reliant on the work of the innate system to operate [4].

Table 1.2. Comparison between the features of the innate and acquired immune systems. Based on information within [7].

	Innate	**Acquired**
Key components involved	Phagocytes, such as macrophages, barriers such as skin, plasma proteins of the complement system	B- and T-lymphocytes, antibodies
Specificity	Not specific to pathogen, recognises common pathogen sequences instead	Highly specific to pathogen
Response time	Minutes and hours	Days
Reaction to repeat exposure to antigen	Does not change from initial exposure	Becomes more effective with repeated exposures

1.2.1.2.1 Macrophages

The human immune cells used during this project were of the U937 monocyte cell line, differentiated to be macrophage-like. Macrophages are, along with neutrophils, the main phagocytes of the immune system. Phagocytes are cells which are capable of carrying out phagocytosis, which is where the cell ingests particles from its surroundings by engulfing

them with its plasma membrane, and thereby capturing them in an intracellular vesicle known as a phagosome (Figure 1.3) [8]. The most common phagocytic target of the macrophage is bacteria [9], which are destroyed by the cell once ingested [8].

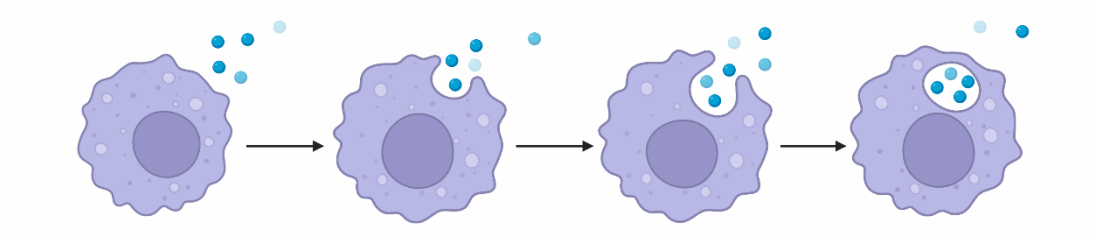

Figure 1.3. Phagocytosis of particles by cell. Adapted from "Phagocytosis 2", by BioRender.com (2022). Retrieved from [3].

As well as providing such direct defence against pathogens, however, macrophages have other roles as well. They are, alongside monocytes and dendritic cells, an antigen-presenting cell (APC), capable of displaying peptides from the pathogens they have ingested to T-lymphocytes via their major histocompatibility complex (MHC) class II receptors on the outside of the cell [10][11]. They are also capable of influencing the behaviour of other cells via secretions [11][12], playing important roles in inflammation [13] and having involvement in tissue remodelling and wound healing [9].

The exact range of functions that a specific macrophage is able to carry out is dependent upon its polarisation. Traditionally, it has been considered that macrophages can be differentiated from a monocyte, and polarised to either a "classically activated" or M1, phenotype, or an anti-inflammatory, "alternatively activated" M2 phenotype (with M2a, M2b, and M2c subtypes), depending upon the mix of stimulants present within its environment (Figure 1.4). However, research in recent years has suggested that the

situation is more complex than this, with a range of likely macrophage phenotypes between the two extremes of M1 and M2 *[14]*, and appreciation of the variances within macrophage phenotypes is only beginning to be appreciated. Regarding their role in inflammation, M1 macrophages encourage inflammation, and their role is discussed more fully in 1.2.1.2.1.1. M2 macrophages are those which are involved in resolution of inflammation (Figure 1.5). Macrophages also have plasticity, meaning that their phenotype is not fixed and can change with further stimulus *[15]*. Furthermore, it is possible that monocytes can be differentiated to a macrophage which is unpolarised, known as an M0 macrophage, which may then, subject to further stimulus from the environment, polarise to a pro- or anti-inflammatory phenotype *[16]*. It should also be noted that monocytes themselves are phagocytic, but that this ability is enhanced when the cell differentiates to become a macrophage *[11]*.

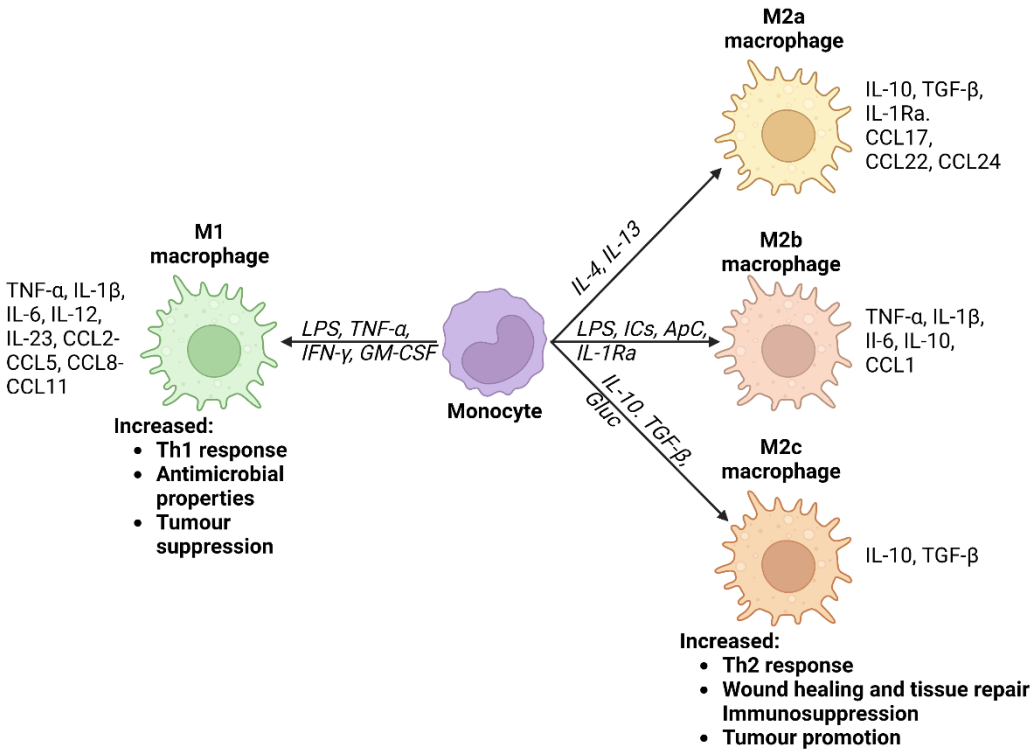

Figure 1.4. Differentiation of monocyte to M1 (pro-inflammatory) and M2 (anti-inflammatory) macrophages, including M2 subtypes. LPS = lipopolysaccharide, TNF-α = tumour necrosis factor α, IFN-γ = interferon γ, GM-CSF = Granulocyte macrophage colony-stimulating factor, ICs = immune complexes, ApC = apoptotic cells, IL= interleukin, Gluc = glucocorticoids, TGF-β = transforming growth factor β, CCL = chemokine (C-C motif ligand), CXCL = chemokine (C-X-C motif) ligand, Th1 = T helper 1 cells, Th2 = T helper 2 cells. Based on diagram within [11]. Created with BioRender.com [6].

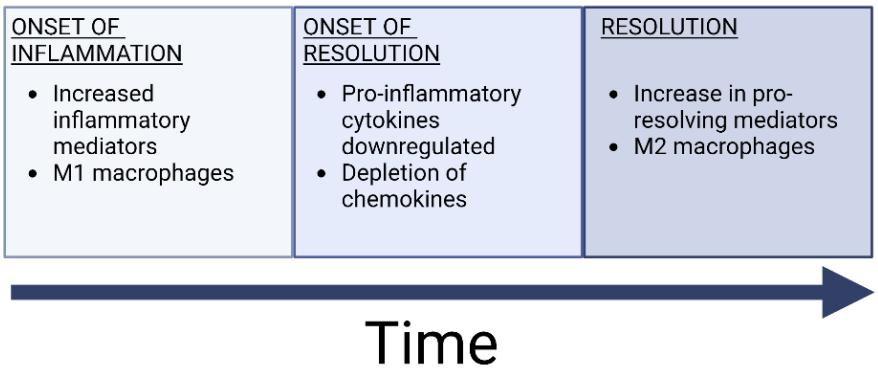

Figure 1.5. Macrophages in acute inflammation. Modified from diagram within [13]. Created with BioRender.com [6].

It has been observed that the differentiation of U937 monocytes by phorbol 12-myristate 13-acetate (PMA), the substance used to trigger differentiation in this project, results in cells which lean towards pro-inflammatory M1 phenotype as opposed to M2 *[17][18]*.

1.2.1.2.1.1 Pro-inflammatory macrophages

In nature, a number of substances may act as a trigger for a monocyte to transform to a pro-inflammatory M1-phenotype macrophage (Figure 1.4), and these substances can be divided into two groups. Firstly, they may be an undesirable item, usually a pathogen-associated molecular pattern (PAMP), such as LPS [19][20][4]. The plasma proteins of the complement system may also bind to these proteins, something which enhances their identification by phagocytes [21]. Macrophage pattern recognition receptors (PRRs) identify PAMPs [22] or complement proteins [23], and binding to these receptors results in both the phagocytosis of the pathogen, and also polarisation of the macrophage to a pro-inflammatory phenotype, which triggers the macrophage to release certain cytokines such as TNF-α. It is some of these cytokines which form the second group of substances capable

of causing polarisation to an M1 phenotype, thus one macrophage is able to polarise others. Activation of a macrophage to an M1 phenotype also causes changes to the cell, including increased MHC II expression [24], which assists the cell in its role as an APC.

Cytokines are low molecular weight proteins that function as signalling molecules [11] and several pro-inflammatory cytokines are released by M1 macrophages (Table 1.3). These have a variety of effects, depending on the specific cytokine, including attracting and activating other cells, increasing the permeability of local blood vessel walls, and inducing fever [11].

*Table 1.3. Key pro- and anti-inflammatory cytokines, excluding chemokines, produced by macrophages. Based on information in [11][25][26] and [9]. * = known to have both pro- and anti-inflammatory functions.*

CYTOKINE	ALTERNATIVE NAME
Pro-inflammatory	
Tumour necrosis factor α (TNF-α)	Tumour necrosis factor (TNF)
Interleukin 1α (IL-1α)	-
IL-6	B cell stimulatory factor 2 (BSF-2) B cell differential factor (BCDF)
IL-1β	-
IL-12	Natural killer cell stimulatory factor (NKSF)
IL-18	Interferon γ (IFNγ) inducing factor (IGIF) Interferon-α inducing factor
IL-23	-
IL-27	-
Interferon γ (IFN-γ)*	-
Anti-inflammatory	
IL-1Ra	-
IL-4	B cell growth factor 1 (BCGF-1) B cell stimulatory factor 1 (BSF-1)
IL-10	Cytokine synthesis inhibitory factor
IL-13	p600
Transforming growth factor β (TGF-β)	-
Vascular endothelial growth factor A (VEGFA)	-

A subset of the cytokines, the chemokines, have the main function of attracting other cells to the area, a process known as chemotaxis [11][12]. Several of these are also released by pro-inflammatory macrophages (Table 1.4).

*Table 1.4. List of key chemokines in M1 macrophages and their functions. Based on information in [27][27], [28][29][8] and [11]. * = known to have both pro- and anti-inflammatory functions.*

Chemokine	**Alternative name**	**Cell type attracted**
CCL2	Monocyte chemoattractant protein 1 (MCP-1)	Monocytes, CD4 and CD8+ T cells, NK cells, dendritic cells.
CCL3	MIP-1 alpha	Monocytes, macrophages, Th1 lymphocytes, NK cells
CCL4	MIP-1 beta	Monocytes, macrophages, Th1 lymphocytes, NK cells
CCL5	Regulated upon activation, normal T cell expressed and excreted (also known as RANTES)	Monocytes, macrophages, Th1 lymphocytes, NK cells, basophils, eosinophils, dendritic cells
CXCL5	ENA-78	Neutrophils, endothelial cells
CXCL8*	IL-8	Neutrophils, basophils, eosinophils, CD8 cells, keratinocytes, endothelial cells
CXCL9	Monokine induced by gamma interferon (MIG)	Monocytes, macrophages, Th1 lymphocytes, NK cells
CXCL10	IP-10	Monocytes, macrophages, Th1 lymphocytes, NK cells
CXCL11	I-TAC	Monocytes, macrophages, Th1 lymphocytes, NK cells
CXCL16	Sexckine	Activated T cells, NKT (natural killer T) cells, endothelial cells

Once phagocytosis by a macrophage has taken place, a pathogens is killed by a range of toxic substances available within the cell. Some of these contact the pathogen when the phagosome merges with a lysosome [30], another vesicle type already present within the

cell which contains a range of digestive enzymes called hydrolases [31]. However, the production of some of the other toxic substances involved, specifically those which are reactive oxygen species (ROS) and reactive nitrogen species (RNS), occurs within the phagosome itself, triggered by the binding of the pathogen to the cell. This process is known as "oxidative burst" or "respiratory burst" and it commences with the conversion of molecular oxygen (O_2) to superoxide (O_2^-) within the phagosome itself, with NADPH oxidase acting as a catalyst, along with the conversion of L-arginine to NO with inducible nitric oxide synthase (iNOS) as catalyst. A number of further ROS and RNS, collectively known as reactive oxygen and nitrogen species (RONS), are then produced following these initial reactions (Figure 1.6). Many of these have the potential to contribute to the destruction of the pathogen, although there is some uncertainty around the relative importance of each of these in the process [32].

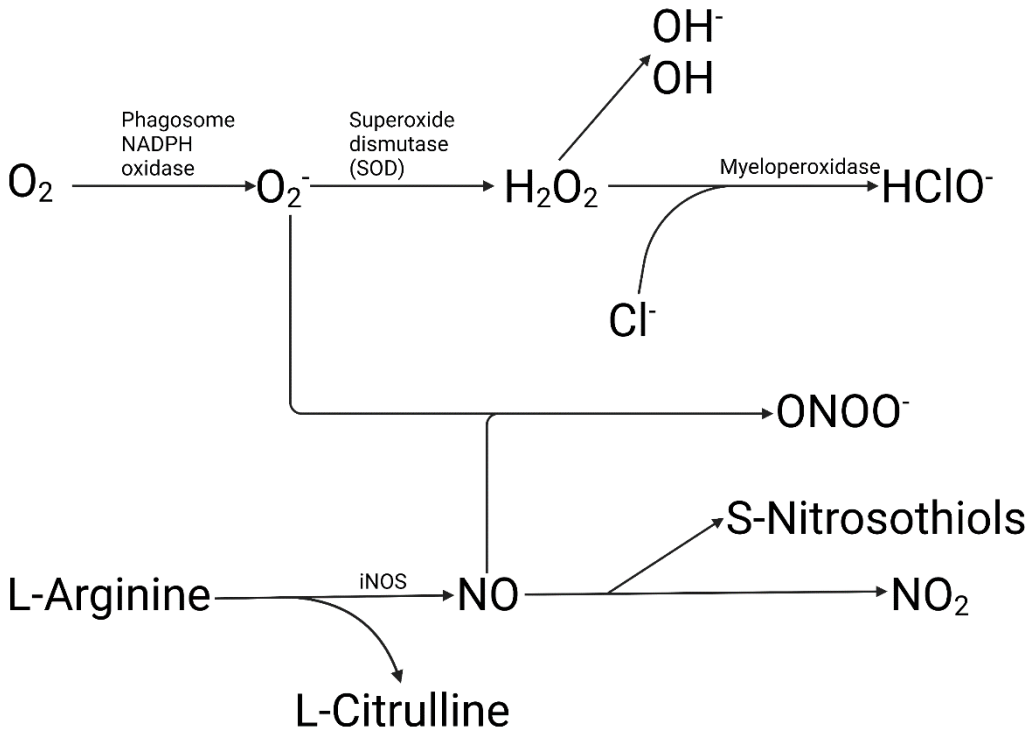

Figure 1.6. Respiratory burst in phagocytes. Based on diagram within [33]. Created with BioRender.com [6].

1.2.1.3 Antioxidants

In nature cells have constant contact with RONS (Table 1.5). In some situations these species can be beneficial, for example when acting as signalling molecules [34], or being part of the respiratory burst to kill pathogens, as discussed in 1.2.1.2.1.1 above. However, given their reactive nature, RONS can be highly dangerous to the cells themselves [35]. It is therefore important that a balance is maintained between these and antioxidant substances which can counteract them to ensure that oxidative stress, defined as an imbalance in favour of the oxidants, does not occur, as this may affect cell signalling and also cause molecular damage [36]. Antioxidants can be either enzymatic or non-enzymatic (Figure 1.7).

Table 1.5. Selected ROS common in biology [37].

Reactive oxygen species (ROS)	**Reactive nitrogen species (RNS)**
H_2O_2	Nitric oxide (NO)
Superoxide (O_2^-)	Nitrogen dioxide (NO_2)
Hydroxyl (OH)	Nitrous acid (HNO_2)
Singlet oxygen ($^1O_2$)	Nitrosyl cation (NO^+)
Hydroperoxyl (HO_2)	Nitroxyl anion (NO^-)
Peroxynitrate (O_2NOO)	
Peroxynitrous acid, (ONOOH)	
Peroxynitric acid, (O_2NOOH)	
Peroxynitrite, ($ONOO^-$)	

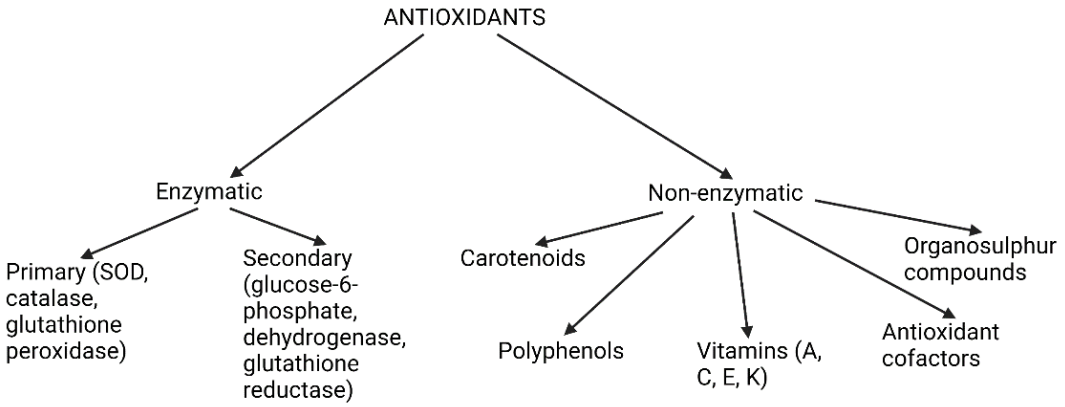

Figure 1.7. Antioxidants. Summarised version based on diagram within [38]. Created with BioRender.com [6].

There are several known antioxidant enzymes, such as catalase and glutathione peroxidase, both of which act on H_2O_2 [39], but that which has been examined as part of the work presented in the later parts of this project (7.4.6) is superoxide dismutase (SOD), an enzyme which dismutates O_2^- to H_2O_2 [40]. There are three different forms of the SOD enzymes present in humans (Table 1.6).

Table 1.6. Members of SOD enzyme family which occur in humans. Based on information within [40] and [41].

Enzyme name (alternative name)	**Metal cofactor**	**Location**
SOD1 (CuZn-SOD)	Copper, zinc	Cytoplasmic, nucleus, mitochondrial intermembrane space
SOD2 (Mn-SOD)	Manganese	Mitochondrial matrix
SOD3 (extracellular-SOD)	Copper, zinc	Extracellular matrix, endothelium surface

O_2^- can be involved in signalling within cells [41], but there are also a number of ways by which it can be damaging to the cell, hence the need for SOD. Some of mechanisms of damage are direct, such as inactivation of Fe-S enzymes and impairment of metabolic processes. However, with others it is the product of reactions involving O_2^- that cause the damage, given that O_2^- is involved in the production of $ONOO^-$, and furthermore the highly reactive OH radical (Figure 1.6). This latter substance is produced via the Haber-Weiss reaction if O_2^- is in the presence of H_2O_2, and transition metal ions such as iron or copper function as catalysts (Equations 1.1 to 1.3 show examples with the iron ion as catalyst) [39].

$$Fe(III) + O_2^{\cdot -} \rightarrow Fe^{2+} + O_2 \quad (1.1)$$

$$\underline{Fe^{2+} + H_2O_2 \rightarrow OH^{\cdot} + OH^- + Fe(III)} \quad (1.2)$$

$$\boldsymbol{H_2O_2 + O_2^{\cdot -} \rightarrow O_2 + OH^{\cdot} + OH^-} \quad (1.3)[39]$$

OH and $ONOO^-$ are involved in such damaging processes as enzyme inactivation, lipid peroxidation and DNA damage [39]. It is also known that a portion of the O_2^- will

protonate, resulting in the hydroperoxyl radical (HO_2), also known as hydrogen superoxide – the protonated form of superoxide. This fraction is likely to be small unless at low pH values, such as those that can be found near membranes, and there is some speculation that HO_2 may cause membrane damage [39].

1.2.2 Basics of non-thermal plasma

Plasmas are defined as a subdivision of the ionised gases, specifically ones which are quasi-neutral [42], by which it is meant that they contain equal numbers of positively and negatively charged particles. A plasma may be either a thermal plasma or an NTP, with NTPs, also known as cold or non-equilibrium plasmas, being ones in which the ion temperature is considerably lower than the electron temperature [43]. In the case of this project, the NTP used to apply to cell samples has been formed from ambient, atmospheric pressure air.

NTPs can be produced by placing a voltage across a gas in a process known as gas discharge [43]. At a certain voltage, the gas becomes able to conduct a current and thus completes the circuit, causing an increase in current, a point that is known as breakdown [44]. There are known to be two different forms of breakdown, Townsend and streamer [45][46], but in the initial stages both follow the same path [42], known as an electron avalanche. With this, the applied electric field causes any free electrons within the gas to begin to move towards the anode. In doing so, these then collide with molecules within the gas, causing ionisation and the production of other free electrons. These steps then repeat, giving increasing numbers of ions and free electrons (Figure 1.8).

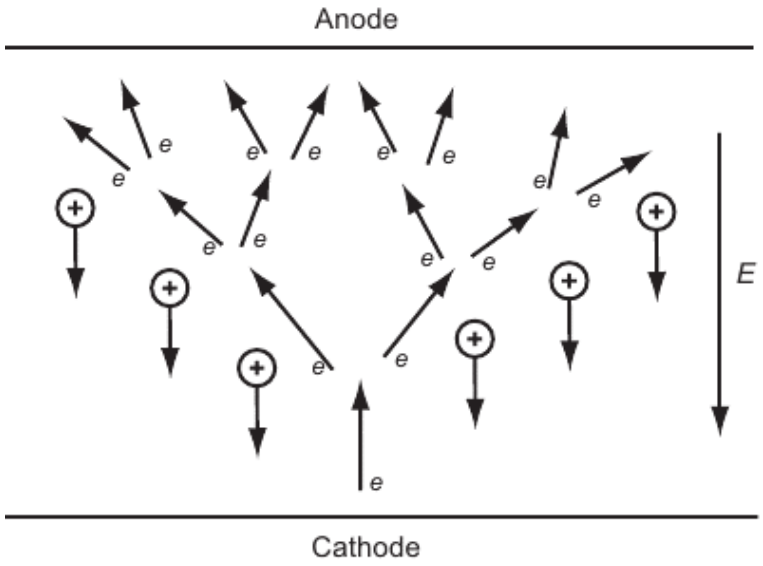

Figure 1.8. Electron avalanche. E represents an electric field, e represents an electron. Reproduced from [46] with modification.

The progression of breakdown beyond this point, to Townsend or streamer form, depends on pressure and the distance between the two electrodes, with Townsend occurring at low pressure and with small electrode separations. The streamer form, on the other hand, occurs at higher pressures and larger gap sizes, under conditions which allow the Meek criterion, where the electric field resulting from the space charge within the avalanche becomes equal to that of external field, to be met [46].

1.2.2.1. Reactive species in NTP

As seen in the simple model presented within Figure 1.8, the application of the electric field results in electron collisions producing ions. In reality, however, the situation is much more complex than this. Electrons may be involved in collisions which do not produce ions, but instead result in radicals or excited state molecules. As well as this, newly formed ions themselves may also undergo further reactions, whether with electrons, other ions, or

uncharged species. This means that a large range of substances, many of which are highly reactive, will be produced within a gas discharge [47]. The presence of these reactive species is what makes plasma useful in for practical application, as they have the ability to cause chemical changes to a target substance.

A summary of some of the reactions which would be expected in atmospheric pressure air containing a small percentage of water, such as was used throughout this project, is shown in Equations 1.4 to 1.27 [47]. It should be noted that some of these substances, although formed in the gas phase, can then dissolve into a bulk liquid if that is in proximity to the gas.

- Electron collision resulting in ionisation, for example:

$$e + N_2 \rightarrow N_2^+ + 2e \quad (1.4)$$

$$e + O_2 \rightarrow O_2^+ + 2e \quad (1.5)$$

$$e + H_2O \rightarrow H_2O^+ + 2e \quad (1.6)$$

$$e + O_2 \rightarrow O_2^- \quad (1.7)$$

$$e + O_2 \rightarrow O^- + O \quad (1.8)$$

$$e + H_2O \rightarrow OH^- + H \quad (1.9)$$

- Electron-ion collisions, for example:

$$\mathrm{e} + \mathrm{N}_2^+ \rightarrow N^* + N \quad (1.10)$$

$$e + H_2O^+ \rightarrow OH + H \quad (1.11)$$

- Collisions between ions, for example:

$$\mathrm{N}_2^+ + \mathrm{O}_2^- \rightarrow \mathrm{N}_2 + \mathrm{O}_2 \quad (1.12)$$

- Reactions producing radical and excited state substances, for example:

$$e + N_2 \rightarrow N_2(v) + e \quad (1.13)$$

$$e + N_2 \rightarrow N_2^* + e \quad (1.14)$$

$$e + N_2 \rightarrow 2N + e \quad (1.15)$$

$$e + O_2 \rightarrow 2O + e \quad (1.16)$$

$$e + O_2 \rightarrow O_2^* + e \quad (1.17)$$

$$e + H_2O \rightarrow OH + H + e \quad (1.18)$$

- Charge exchange reactions, for example:

$$N_2^+ + N_2 \rightarrow N_4^+ \quad (1.19)$$

$$N_2^+ + H_2O \rightarrow H_2O^+ + N_2 \quad (1.20)$$

$$H_2O^+ + H_2O \rightarrow H_3O^+ + OH \quad (1.21)$$

- Other reactions, for example:

$$O + O_2 \rightarrow O_3 \quad (1.22)$$

$$O^* + H_2O \rightarrow 2OH \quad (1.23)$$

$$OH + O_3 \rightarrow HO_2 + O_2 \quad (1.24)$$

$$H + O_2 \rightarrow HO_2 \quad (1.25)$$

$$N^* + O_2 \rightarrow NO + O \quad (1.26)$$

$$N + OH \rightarrow NO + H \quad (1.27)[47]$$

Throughout these equations, an asterisk represents electronic excitation, while *v* represents vibrational excitation.

1.2.3 Plasma medicine

Due to their highly reactive nature, as well as the fact that they can be targeted with precision [48], NTPs have already proved useful across a range of industries including electronics, materials science and agriculture [49]. The possibility of expanding this usefulness into the medical field was initially considered with regard to the sterilisation and decontamination abilities of NTP [50]. However, the application of such treatments to mammalian biology started to gain increasing interest in the early 2000s, notably in the work of Stoffels and colleagues who showed the ability of NTP to cause non-lethal cell detachment [51][52][53][54][55], and since then this has developed into a significant area of research, known as plasma medicine.

1.2.3.1 NTP source types in plasma medicine

There is no standardised device used to supply NTP within the field of plasma medicine, with most groups of researchers developing their own. However, those that exist can be divided into two main types: dielectric barrier discharge (DBD) sources (Figure 1.9) and plasma jets (Figure 1.10) [56]. With a DBD-style reactor, the NTP is produced from a gas, usually air, between two electrodes, which are separated by one or more dielectric layers. The produced NTP is either then in direct contact with the sample to be treated (Figure 1.9(a) and (b)), or is able to defuse towards due to the use of mesh as one of the electrodes (Figure 1.9(c)). Further detail of physics of DBD is given in 1.2.3.2 below. With a plasma jet, the NTP is produced distant from the sample, in a gas flow that is then directed towards the sample to be treated (Figure 1.10(a) and (b)). This project has used a DBD design throughout all work performed however, as of 2017, it has been estimated that around 70 % of papers published on the topic of plasma medicine have instead used plasma jets [57].

There are several important differences between the plasma jets and DBD-style NTP sources. Firstly, most, but not all, DBD devices are designed in a way that results in the biological sample being within the circuit producing the NTP, something which is not the case with plasma jets. This therefore means that target samples treated in such a DBD-style device would be subjected to electric field effects and charged particles, unlike samples treated with a plasma jet. Secondly, DBD devices usually, but not always, use atmospheric pressure air as the basis for the NTP, thus forming air NTPs [58][59], although there have been examples of their use with N_2 [60] and He [51]. On the other hand, plasma jets can use a range of gases, but usually use one of the noble gases such as Ar or He, often with the addition of a percentage of air or O_2 [61], with the NTP formed then mixing with ambient air as the jet heads towards the sample. This therefore means that there may differences in the reactive species supplied to the target sample by the two device types. Thirdly, some DBD-style devices also use flat plate electrodes, and thus create a much larger interface area between the plasma and treatment liquid than the narrow plasma jet.

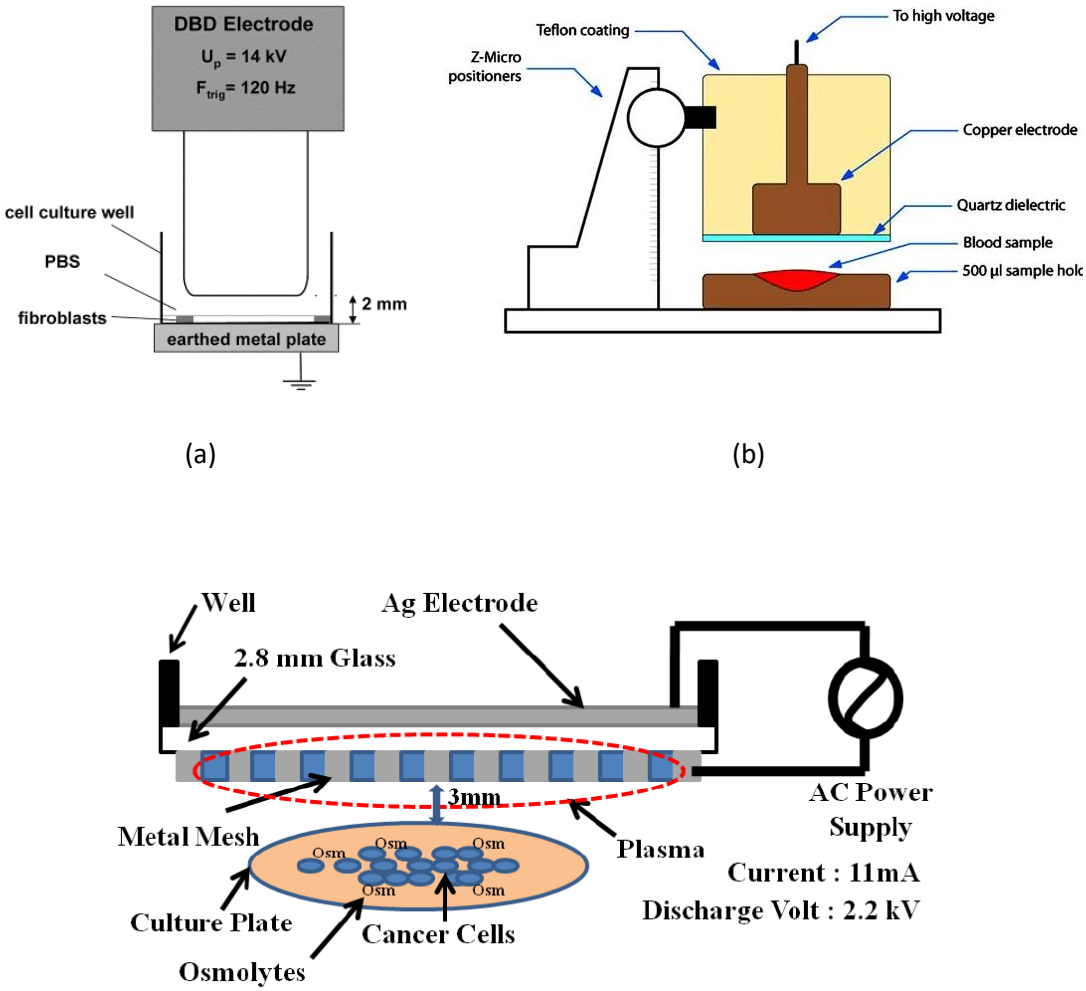

Figure 1.9. Schematics of three example DBD devices used within plasma medicine research (a) DBD device with metal grounding plate, used for work on fibroblasts by Balzer et al. (2015). Diagram taken from [62] (b) floating-electrode DBD device, used for work on blood by Fridman et al. (2006). Diagram taken from [63] (c) DBD device with grounded mesh above samples, with diffusion of NTP to sample. Diagram taken from Kaushik et al. (2013) [59].

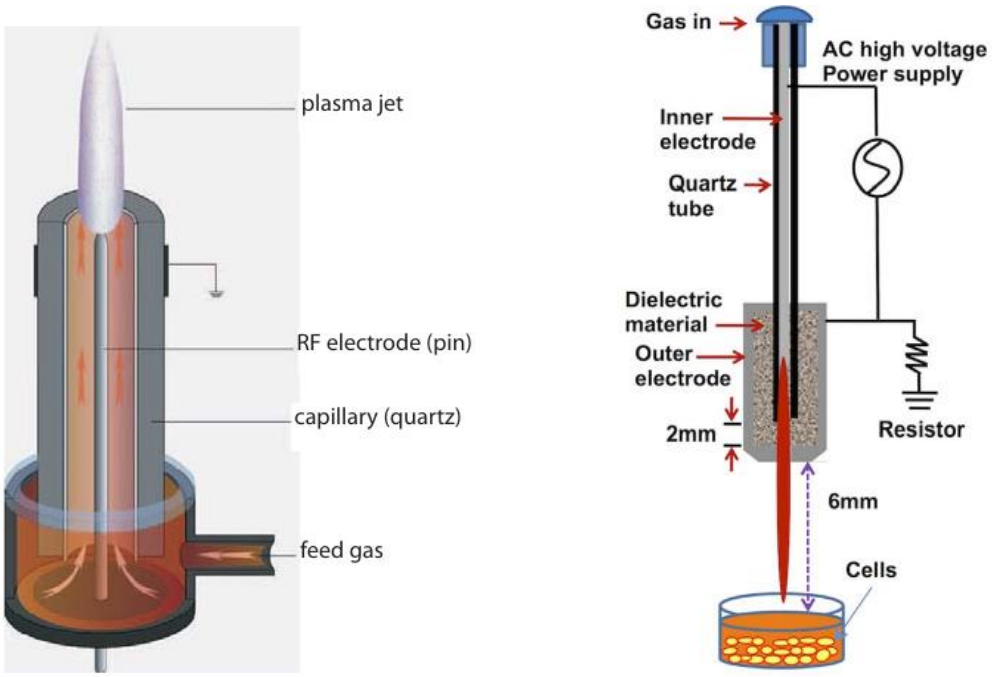

(a) (b)

Figure 1.10. Schematics of two example plasma jet devices used within plasma medicine research (a) plasma jet design which formed the basis of the kINPen series of devices. Diagram taken from Weltmann et al. (2009) [64] (b) plasma jet design used by Kaushik et al. (2015), diagram taken from [65].

It should also be noted that plasma jets themselves usually produce the NTP using a DBD arrangement internal to the housing prior to the plasma being ejected from the device towards the sample.

1.2.3.2 Dielectric barrier discharge

1.2.3.2.1 Dielectric barrier discharge in plasma medicine

This project used DBD-style devices to produce NTP. The earliest example identified of the use of DBD to carry out work on eukaryotes related to work on blood coagulation carried

out in 2006 [63]. Since then, a number of other groups have considered the use of DBD systems applied to mammalian biology, mainly in the field of cancer research (Table 1.7).

Table 1.7. Selected plasma medicine papers in which a DBD-style NTP source was used.

	Author	Description of DBD source used	Application
1	Conway *et al.* [66]	DBD with sample held between two layers of dielectric. Supply 120 kV AC, 50 Hz	Cancer cell research. Application times of up to three minutes.
2	Gerber *et al*. [67]	Cylindrical electrodes suspended above wells of 96-well plate. Supply 15 kV AC, 50 Hz.	Prototype for application to cancerous cells.
3	Kalghatgi *et al.* [68]	DBD with quartz covered powered electrode and grounded dish. 10 kV pulsed supply, 0.5 – 1.5 kHz, 1.65 µS pulse width with 5 V/ns rise time.	Cancer cell research. NTP application times of up to 50 s.
4	Karki *et al.* [69]	Needle-style electrode with dielectric layer, suspended above grounded petri dish. 12 kV pulsed supply, 1 kHz, 10 µS pulse width.	Cancer cell research. NTP application times of up to two minutes.
5	Kim *et al.* [70]	DBD operated in air, without sample being part of circuit (diffusion down to sample dish). Supply 6 kV AC, 22 kHz.	Cancer cell research. NTP application times of up to 30 s.
6	Panngom *et al.* [71]	DBD with mesh ground electrode, allowing diffusion of RONS to sample. Supply 600 V AC, 60 Hz.	Cancer cell research. NTP application times of up to 5 minutes.
7	Song *et al.* [72]	DBD in flowing He atmosphere. Supply 15 kV AC, 43 kHz	Cancer cell research. NTP application times of up to 4 minutes.

	Author	Description of DBD source used	Application
8	Vandamme *et al.* [73]	Floating electrode DBD (FE-DBD). 23 kV µs-pulsed, 2 kHz	Cancer cell research. NTP application times of up to 30 s.

1.2.3.2.2 Theory of dielectric barrier discharge

A schematic of the main reactor used for this project, Reactor 1, will be given in the following chapter (2.1.1.1). The design of this reactor, with a dielectric, or insulating, layer situated between the two electrodes, would be expected to produce the DBD form of discharge, which is also occasionally referred to as silent discharge. This form of discharge has already proved to have a number of uses including in other areas such as in plasma screens, ozone production, and excimer lamps [74].

The presence of a dielectric barrier in such a reactor limits current during discharge [75], making it highly suitable for biological use. Dielectric substances do not allow the passage of direct current, and thus DBD needs to have an applied voltage which changes with time to operate [76]. Assuming this applied voltage is AC, the current in the circuit producing the DBD would be expected to have a similar form to that shown in Figure 1.11.

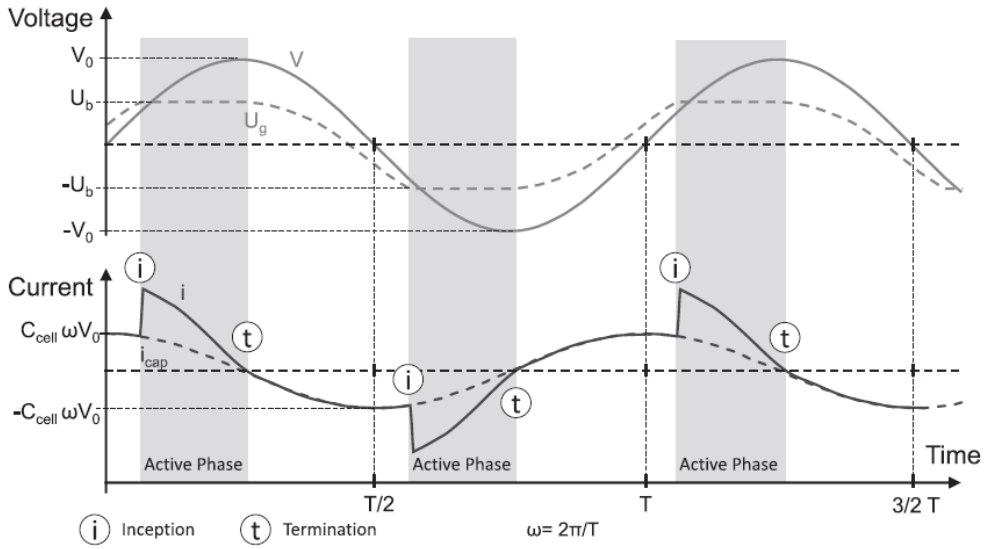

Figure 1.11. Relationship between applied sine wave voltage and current in DBD circuit. Diagram reproduced from [77]. V_0 = applied voltage magnitude, U_g = voltage across gas, C_{cell} = total capacitance of the reactor, U_b = breakdown voltage, ω = angular velocity, i_{cap} =capacitive component of current, T = period of wave.

There are several things to note from Figure 1.11:

- The points at which the discharge is seen in the current wave occurs when the breakdown voltage, U_b, is reached across the gas [77]. However, once the rate of change of the voltage becomes zero the discharge is terminated as, as has already been stated, DBD requires an applied voltage which changes with time. There is then no discharge until the breakdown voltage is again reached on the next half-period of the applied voltage wave. This therefore means that discharge is only present in two quarters of the wave period.
- As well as the discharging current, there is also an underlying capacitive component to the current present even in the absence of discharge and which relates to

polarising of the dielectric. In Figure 1.11 this is labelled as i_{cap} and is a sine wave [77].

- The discharge in Figure 1.11 is shown as having a diffuse nature throughout the discharging time but it is often of a more filamentary nature, with current spikes visible in the current trace [77].

Devices generating DBD can have a range of different structures, with differing electrode arrangements, and variations in the number and location of dielectric layers (Figure 1.12).

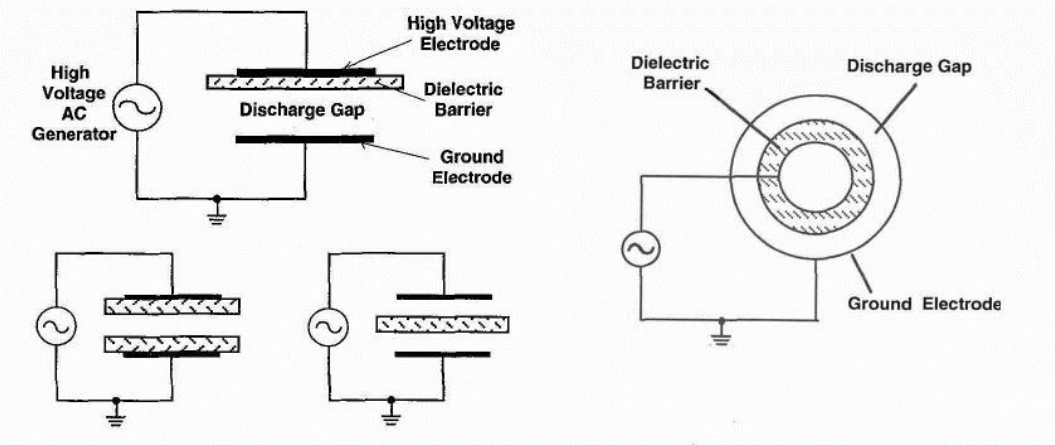

Figure 1.12. Examples of common dielectric placements in DBD. Reproduced from [74].

1.2.3.3 Key findings in plasma medicine

It should be noted that the key findings in plasma medicine that are presented here are given at a very high level, and therefore the discussion is not a comprehensive representation of research within field. In particular, many of the detailed biochemical effects, such as effects on specific signalling pathways [78][79][80][78], and changes in intracellular RONs [60][48][81][82][83][84][85] have not been included for brevity.

1.2.3.3.1 Inhibition of cell function

It has been noted that both necrosis (uncontrolled cell death) and apoptosis (controlled cell death) may be caused by NTP treatment, depending on circumstances [86]. Apoptotic cells die by a controlled process which follows specific established pathways, and which avoids an inflammatory response and the associated damage. Under normal circumstances, with the cells within an organism rather than *in vitro*, they would then be phagocytosed by macrophages or other cells to dispose of them fully [87][88]. This method of cell death contrasts with that of necrosis, which is uncontrolled and in which the cells, instead of being neatly packaged up then engulfed by phagocytes, instead burst open, with their contents spilling out and triggering inflammation (Figure 1.13(b)) [87].

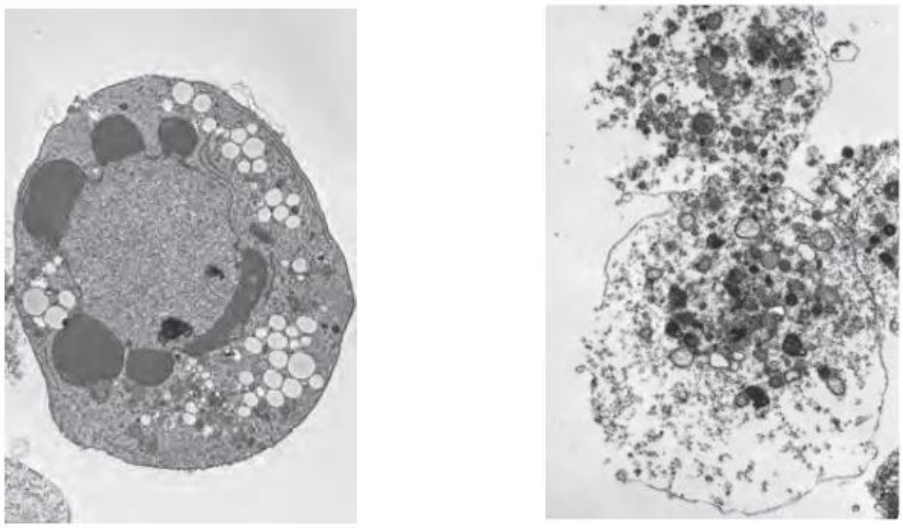

(a) (b)

Figure 1.13 (a) Apoptotic cell, maintaining membrane integrity and (b) necrotic cell, with contents spilling out due to loss of membrane integrity. Photographs reproduced from [87].

One possible contributory factor to cell death occurring with NTP treatment is that it is known that NTP can cause damage to the deoxyribonucleic acid (DNA) within cells [89][73][90][91][92][68], an effect which appears to be dose dependent [82]. DNA is a

double-stranded molecule which contains the genetic information of the cell, represented by a code produced by four different nucleobases, adenine (A), cytosine (C), guanine (G) and thymine (T) (Figure 1.14) [93]. One of the two strands of DNA acts as the coding strand, which can undergo transcription and ultimately be translated into proteins, with the other being a complementary strand to the coding strand, pairing adenine to cytosine and guanine to thymine [93][94]. A number of papers [89][73][92][68] have shown that NTP treatment resulted in increases in γ-H2AX, which is an indicator of double-stranded DNA breaks [92][89]. This type of damage, which is often seen with exposure to ionising radiation such as x-rays and radon emissions [95], is known to generate RONS itself within cells [96]. It may be possible for the cell to repair DNA damage in some cases, but in other cases it results in the death of the cell, by either apoptosis or necrosis, usually depending upon the severity of damage [97].

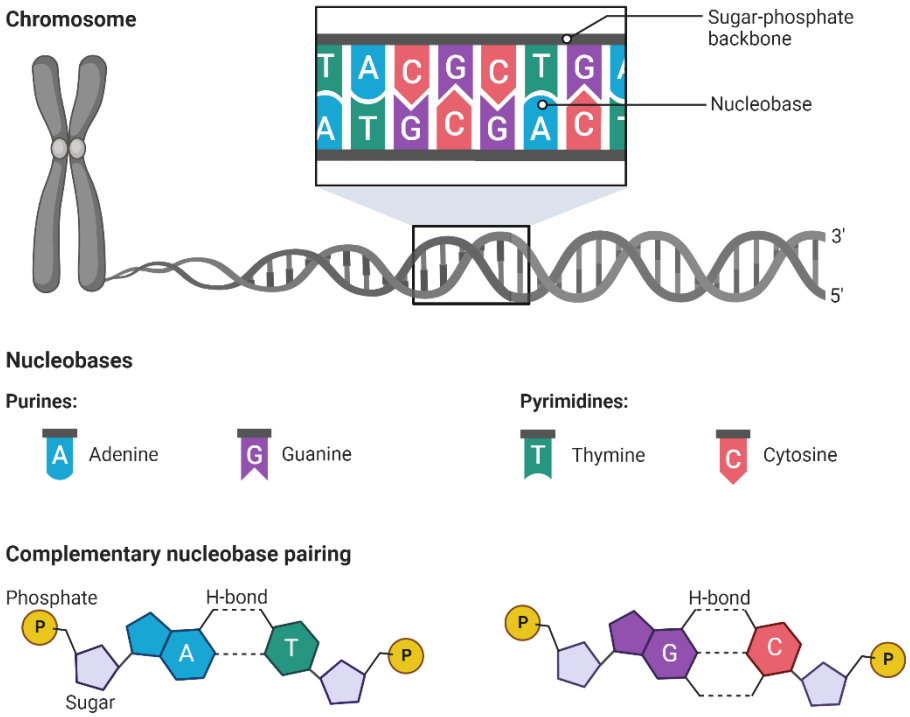

Figure 1.14. Double helix structure of DNA. Reprinted from "DNA structure", by BioRender.com (2022). Retrieved from [3].

It has also been shown that exposure to NTP can interfere with the progress of a cell through the cell cycle, the series of steps which cells go through in order to replicate (Figure 1.15). A number of studies have found that NTP treatment causes cells to stall during this cycle, with the most common observation being that this occurs at the G2/M checkpoint [89][98][91], a point at which both the health of the cell and suitability of its surroundings would be assessed to ensure the cell does not divide in unfavourable conditions.

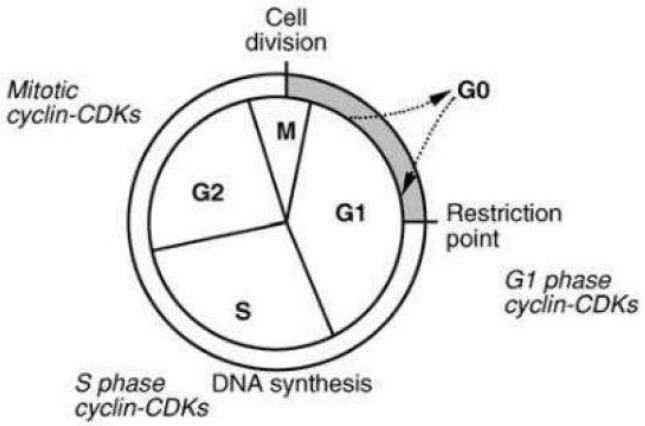

Figure 1.15. Cell cycle stages. Taken from [99]. S phase: synthesis stage in which cells duplicate their chromosomes. M phase: mitosis stage, where the chromosomes are split into two identical sets. G0: gap 0 stage. G1: gap 1 phase. G2: gap 2 stage. During the gap stages, cells grow and the cell and surroundings are monitored to ensure the cycle does not progress unless conditions are favourable [31].

Cell adherence, important for the correct functioning of many cell types, have also been shown to be reduced by NTP [51][86], even in situations where the applied treatment is not fatal to the cells [51][100]. This effect has been attributed to the treatment affecting the cell adhesion molecules (CAMs) (integrins and cadherins) on the surface of the cell [51].

1.2.3.3.2 NTP treatment of immune cells

In recent years research has begun to consider whether the human immune system can be modulated by the use of NTP treatment, and this area has been furthered explored in this project during the work of Chapter 7. Work seen in the literature has considered such areas as the effect of such a treatment on the viability of immune cells and on the release of inflammatory mediators [101][102][103][104], and it has also been established that sublethal NTP doses can increase proliferation in immune cells [101][60][78]. As well as

this, some research has also found that non-immune cells treated with NTP are considered differently by the cells of the immune system, an area of research titled immunogenic cell death (ICD). This is where damage-associated molecular patterns (DAMPs), in this case created on the surface of cells by NTP treatment, make it clearer to the cells of the immune system that the cell is abnormal and should be destroyed. ICD has been explored in papers such as [105][106] and [107] with, for example, Lin *et al.* showing that NTP pre-treatment of the CNE-1 nasopharyngeal carcinoma cell line resulted apparent stimulation of THP-1 macrophages when the two cell types were mixed, resulting in a higher death rate of CNE-1 than if that cell line had not been exposed to NTP [105]. A small amount of *in vivo* work has also been performed in this area [108].

1.2.3.3.2.1 Macrophages

NTP treatment applied specifically to macrophages, of particular relevance to this project, is a niche area of research. Many of the papers which have been published on this topic have considered the effects of NTP treatment on macrophage viability [109][110][101][90][60] rather than examining the effects on its immune-related functions. It has also been established that sub-lethal NTP doses can increase macrophage proliferation [101][60][78].

Some researchers, however, have also considered whether NTP treatment can enhance some of the specific features and abilities of macrophages. It has been demonstrated that the migratory ability of macrophages may be enhanced by NTP exposure [101][60], and other work has established that NTP-treated macrophages may be more effective at killing or inhibiting the invasive abilities of cancer cells [105][111][18]. Morphological changes to macrophages, with cells appearing more like dendritic cells, have also been noted following NTP treatment, with the cells also developing increased migratory ability [60]. Some

research has also observed that differentiation of monocytes to macrophages can be enhanced by NTP treatment [18], or possibly even triggered by it in the absence of other differentiation stimuli [109]. A number of researchers have also found that NTP can modify the chemokine and cytokine secretion profiles of macrophages [18][110][60][112][109][113], as well as their polarisation [18][109][114][112].

1.2.3.3.2.2 Other immune cell types

Other immune cells have also been subject to NTP treatment, either directly or using PAM, in the literature (Table 1.8).

Table 1.8. Key papers covering the NTP treatment of other immune cell types.

Immune cell type	**Relevant papers**
Monocyte	[102][115][116][117][118][119][120][121]
Neutrophils	[48][122][123][124]
Lymphocytes	[103][125][118][126][120][121][127]
PMBC generally	[104][128][118][123][122][129][130]
Dendritic cells	[131]

There is evidence that immune cells are, like other cell types, vulnerable to plasma treatment to the extent that it can cause their death. However, there is some difference in the response of different types of immune cells, with monocytes and macrophages appearing to be more robust in terms of cell viability than lymphocytes [132][118].

Although many of the papers in Table 1.8 had the inhibiting effects of NTP treatment as a focus, such as a reduction of viability, a small number of papers have considered NTP-induced enhancement of cell functions in the listed immune cell types, such as increases in metabolism [102], changes to the inflammatory profile [102][131], and the enhanced release of neutrophil extracellular traps, thought to assist in disabling bacteria [124].

1.2.3.3.3 Other significant areas of research in plasma medicine

1.2.3.3.3.1 Cancer cells

It has become apparent that there is differential effect of NTP treatment on cancerous and non-cancerous cells, with the cancerous cells being more vulnerable to NTP [68][84][133][80]. These effects have been attributed to endogenous ROS being higher within the cancerous cells in comparison to those which are not cancerous, and thus cells are more vulnerable when exposed to further ROS from NTP [133]. The increased ROS in endogenous ROS in cancer cells in comparison to non-cancerous cells has been attributed to a variety of processes, notably mitochondrial malfunction, increased metabolic rate and oncogene signalling [134]. It has been observed that p-53 deficient cancer cells are particularly vulnerable to NTP treatments, likely due to their particularly high endogenous ROS levels [133]. A reducing effect on the migration and invasive abilities of cancer cells has also been noted in response to NTP exposure [135][69].

A number of studies have considered *in vivo* use of NTP against cancers and confirmed the inhibitory effects of NTP [136][137][138]. However, to date, a very limited amount of clinical trial work has been performed to determine the suitability of NTP as an addition to established cancer treatments in humans. One study of note considered the effect of

multiple applications NTP to patients with inoperable locally advanced oropharyngeal cancer, however the results of this were mixed [139].

1.2.3.3.3.2 Wound healing

The possibility of using NTP to assist in wound healing has been extensively investigated in the literature. There are two ways in which NTP is able to do this. Firstly, NTP has a well-documented antimicrobial effect. Although its effects against fungi are disputed [140], it is firmly established of having the effect of killing a range of bacteria, including *Eschericia coli (E. coli)*, *Bacillus subtilis (B. subtilis)* [141], *Staphylococcus aureus (S. aureus)* and *Enterococcus faecalis (E. faecalis)* [142], as well as perhaps enhancing vulnerability of bacteria to antibiotics [143]. Secondly, NTP is known to have a range of effects on cells which can enhance their ability to resolve the wound, for example by increasing vascularisation and modifying inflammation (Figure 1.16) [144].

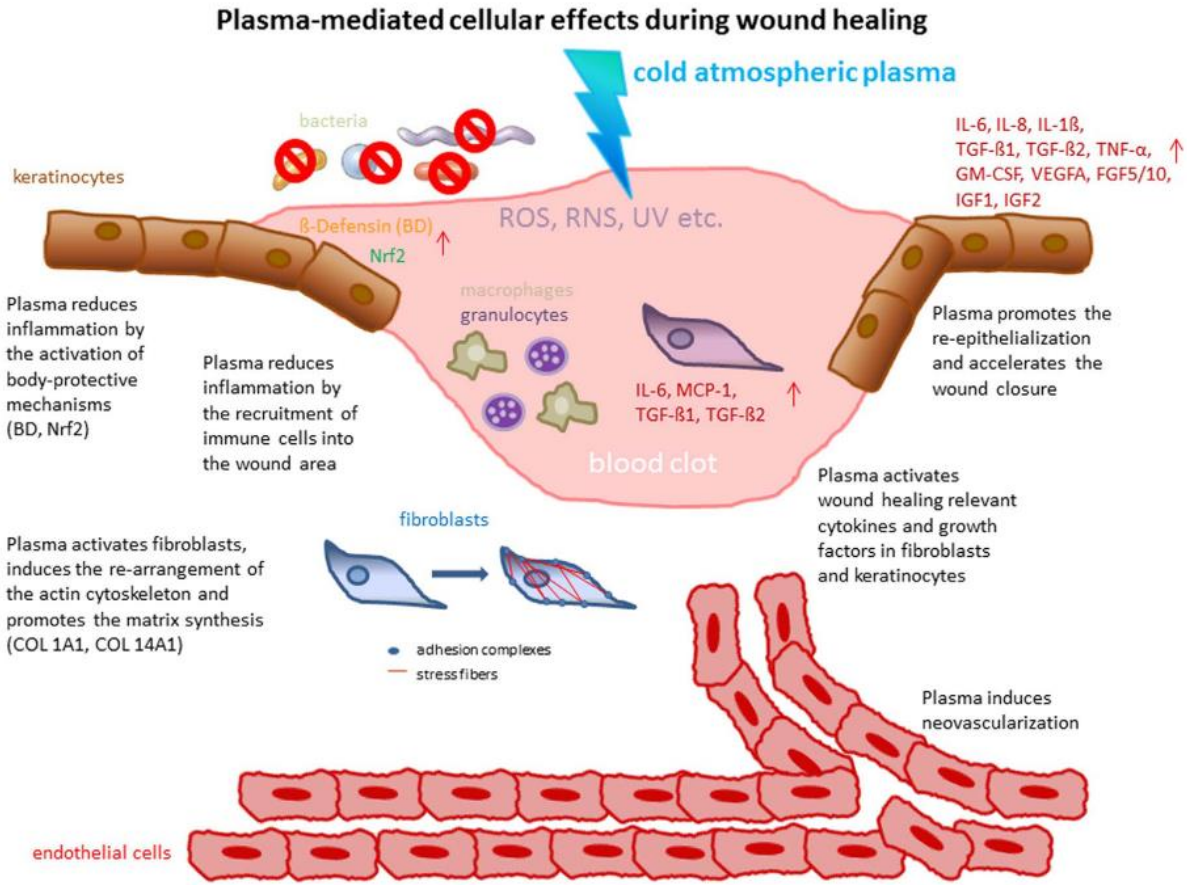

Figure 1.16. Effects of plasma treatment on wound healing. Reproduced from [144].

The use of NTP in wound healing is an area of research in which work has progressed far enough for commercial devices to be available. These include the PlasmaDerm, a DBD-style device made by CINOGY System GmbH, which claims to be able to improve healing of both acute and chronic wounds by both its antimicrobial actions and its effects on human tissue (Figure 1.17(a)) [145]. The kINPenVET, a plasma jet produced by neoplas GmbH, is also available to assist wound healing in veterinary care(Figure 1.17(b)) [146].

(a)

(b)

Figure 1.17. Promotional photographs of (a) the PlasmDerm, photograph reproduced from [147] (b) the kINPenVET, photograph reproduced from [146].

1.2.3.3.3.3 Stem cells

Stem cells are undifferentiated cells which are capable of continuously dividing to act as a source for differentiated cells [148]. In recent years there has been much interest in them in medical science as a whole, due to the potential of using them to regenerate tissues in the body [149]. A number of studies have determined that plasma treatment has the ability to enhance cell differentiation, notably of muscle stem cells [150] and bone stem cells [151]. This has been attributed to the ROS resulting from NTP treatment enhancing signalling processes related to differentiation, however the exact details of this appear to remain unclear [151][150]. Other work has also found that it may be possible to improve the viability of stem cells by repetitive NTP treatments [133].

1.2.3.4 Interactions between NTP and biological targets

There are two main methods of creating and applying an NTP treatment: directly or via PAM. Direct treatment is used to describe a situation where the sample is in contact with the NTP as it is being produced (Figure 1.18(a)), meaning that there is exposure to not only the long-lived chemical species within the NTP, but also short-lived species, as well as visible light, ultraviolet (UV) light and any heating effects. PAM treatment, on the other hand, involves liquid being subjected to NTP prior to it being transferred to the biological sample being treated (Figure 1.18(b)). In this situation, the biological sample only encounters the long-lived chemical substances produced in the liquid by the NTP. PAM treatment is sometimes referred to as indirect treatment, or occasionally with other terminology such as liquid NTP [152].

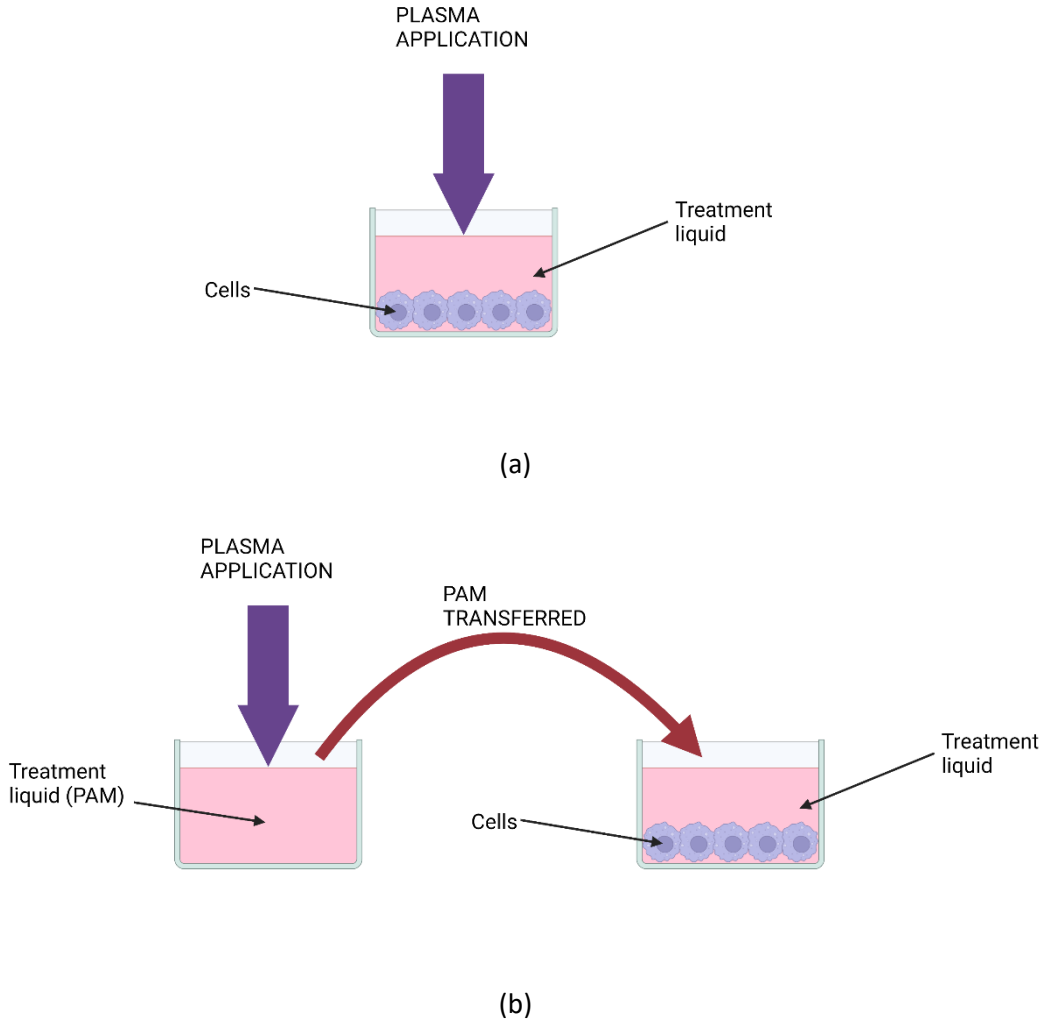

Figure 1.18. Schematics of the application of a) direct treatment and b) PAM, or indirect, treatment to in vitro *samples. This terminology also applies to NTP treatments* in vivo *experiments or in clinical trials. Created with Biorender.com [6].*

Much of the early work in plasma medicine considered direct treatment only, and it became well established cell viability can be reduced by direct NTP treatment, for example through the work of Vandamme *et al.* [73] using an FE-DBD device to reduce viability in the U87MG glioma cell line (2012), Hoentsch *et al.* [153] using an Ar plasma jet to do the same with the mHepR1 murine hepatocyte cell line (2011), and Yan *et al.* [154] the same with the

HepG2 human hepatocellular carcinoma cell line (2012). As the 2010s progressed, the use of PAM began to appear in the literature, firstly with the work of Tanaka *et al.* [80], who looked at the ability of PAM to kill glioblastoma cells, as well as its effect of downregulating the AKT signalling pathway.

Unlike with direct treatment, cells subject to PAM would not encounter the effects of the any short-lived chemical species produced by the treatment, as the cells are not present at the time that the PAM is created. As well as this, depending on the design of the NTP source, directly treated samples may also be sitting within an electric field, which would not be the case with PAM treatments. It may be thought that these factors could lead to a difference in effect between the two treatment types. For the most part, however, investigations have shown little difference in the extent of viability reduction between the two treatments. This has been confirmed for a range of cell types, for example dermal fibroblasts [62], and epithelial cells [73][155][155][156][157], and therefore suggests that the short-lived species, visible and (UV) light, and heating effects present in direct treatment have little contribution to the cell death seen with NTP treatment. Notably, however, Saadati *et al.* found that direct treatment was significantly more effective at reducing cell viability than PAM in the B16F10 murine melanoma cell line [158], although the reasons for this unusual finding were not clear [159].

1.2.3.5 H_2O_2 and NO_2^-, two key RONS in plasma medicine

Since work began on plasma medicine in the mid-2000s, a significant amount of effort has been expended towards understanding the chemical or electrical factors responsible for the biological effects observed. However, at this time, these remain incompletely understood. An observation has been made by a number of researchers that the effects of direct NTP

treatment and those of PAM on cell viability are usually similar, suggestive of the involvement of long-lived chemical species rather than either short-lived species or electric field effects [155][157][73][104][156][62]. There are a number of these long-lived species which may form during the interaction between NTP and aqueous liquids, such as the nitrate ion (NO_3^-) [72][160][161][162][163], ozone (O_3) [164], [165] and $ONOO^-$ (peroxynitrite) [156], but the two which have been most strongly implicated in the biological effects of NTP are H_2O_2 and NO_2^- (Table 1.9).

Table 1.9. Key papers showing importance of H_2O_2 and NO_2^- in plasma medicine.

	Authors	Cell type	Relevant findings
1	Balzer *et al.* [62]	Normal primary human fibroblasts	H_2O_2 inhibited proliferation to a similar degree as PAM.
2	Bekeschus *et al.* [129]	Primary human T helper cells	Addition of catalase, which converts H_2O_2 to water and O_2, resulted in a smaller cell viability reduction in both NTP-treated and H_2O_2-treated cells. The effect was approximately equal for the two groups of cells.
3	Bekeschus *et al*. [128]	Primary peripheral blood mononuclear cells (PBMC)	Catalase addition eliminated the cell viability reduction caused by direct NTP treatment.
4	Bundscherer *et al.* [78]	1. Jurkat ($CD4^+$ helper cells) cell line 2. THP-1 (monocytes) cell line	p38 MAPK and JNK1/2 pathways, which relate to apoptosis, were found to be similarly activated by H_2O_2 and PAM.
6	Girard *et al*. [161]	1. Normal primary human skin fibroblasts 2. MRC5Vi (normal human lung fibroblast) cell line 3. Lu1205 (human melanoma) cell line	No significant difference between viability of cells treated with PAM made from PBS, and those treated a combination of H_2O_2 and NO_2^-. NO_2^- alone had no effect on viability.

	Authors	Cell type	Relevant findings
		4. HCT116 (human colorectal carcinoma) cell line	
7	Kurake *et al.* [166]	U251SP (human glioma) cell line	Concluded that H_2O_2 was responsible for the bulk of the cell viability reduction seen with PAM treatment, but that there was also a synergistic effect with NO_2^-. Addition of NO_2^- alone had no effect on cell viability.
8	Winter *et al.* [167]	HaCaT (human keratinocyte) cell line	Cell viability reduction with PAM treatment was similar to that of H_2O_2 alone.

Although H_2O_2 and NO_2^- have been strongly implicated in the biological effects of NTP treatment, there is also evidence that some of the other substances formed may also contribute, with several of the papers from Table 1.9 finding that H_2O_2 and NO_2^- could not completely explain their own observed findings [62][129][166]. At this stage is not clear what other substances would bridge this gap. It is also apparent from the literature that work towards understanding the chemical species responsible for the biological effects of NTP has largely focused on the inhibiting effects observed in plasma medicine, such as reduction in cell proliferation or viability, rather than considering the substances responsible for the stimulating effects which have been observed, such as enhancement of immune cell activity [60][101][105][112][122][113][116], stem cell differentiation and improvement in viability [133][151][168], and encouragement of wound healing [144][75][169][170][171]. It is therefore not determined at this time whether these effects are also reliant on H_2O_2 and NO_2^- from the NTP, however, some evidence has shown that they may not be, at least in some stem cells [172]. Despite this, it is clear that H_2O_2 and NO_2^- remain among the most important substances in plasma medicine.

H_2O_2 is a non-radical with known biological effects, and it is able to move easily into cells both by diffusion and through aquaporin channels in the cell membrane (Figure 1.19) [173] [157]. It is involved in cell signalling processes within the cell [174], such as acting as a second messenger in the stimulation of smooth muscle cells by platelet-derived growth factor (PGDF) [175] and the modulation of transcription factors [176]. H_2O_2 also has roles in processes such as proliferation and migration [177] and inflammation [177], as well as being linked to improved angiogenesis and wound healing [178][179]. However, above certain levels it is also damaging to the cell, and indeed is eventually fatal [180][181]. Some of this damage is caused by H_2O_2 directly, due to such actions such as its interference

with glyceraldehyde 3-phosphate dehydrogenase (GAPDH or G3PDH) and peroxiredoxin, but other damage, such as degradation of DNA, RNA and lipids is more likely to be caused by OH, produced when H_2O_2 reacts with either copper or iron ions also within the cell [180]. Intracellular H_2O_2 levels are thought to normally be in the range of picomolar to nanomolar (Figure 1.20) [176][182].

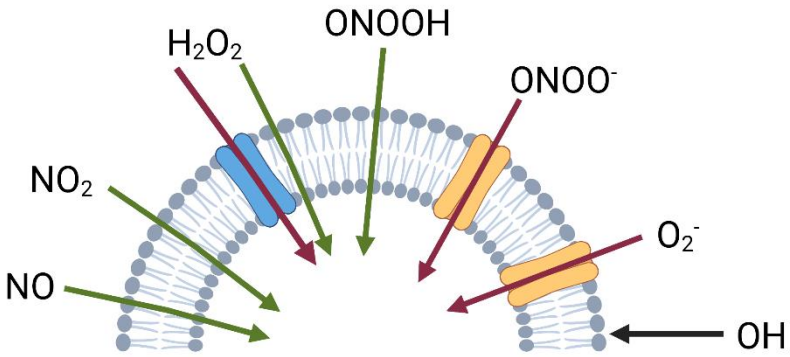

Figure 1.19. Behaviour of RONS at cell membrane. Green arrow = diffusion, red arrow = passage through channel, black arrow = acts on outside of membrane. Blue channel = aquaporin, yellow channel = anion exchange protein channel. Based on diagram within [173]. Created with Biorender.com [6] .

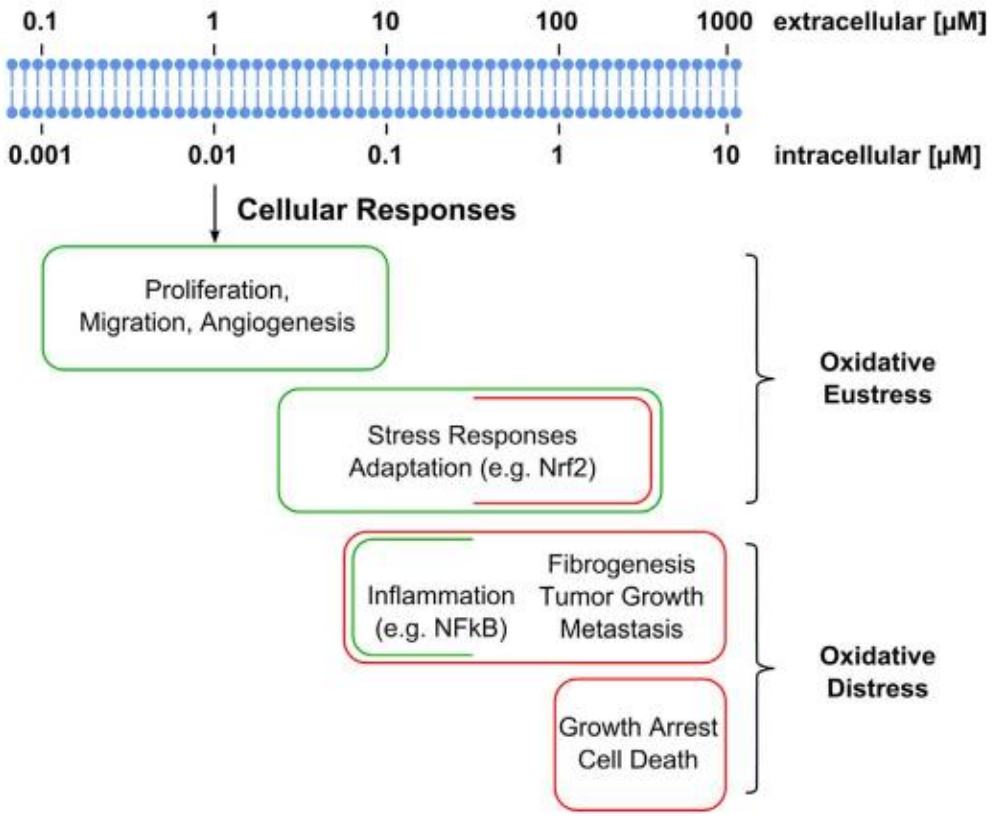

Figure 1.20. Effects of increasing intracellular H_2O_2 concentrations. Diagram reproduced from [177]. Note that, as stated in the paper, the concentration gradient values are given for illustration only, and will vary depending on circumstances. The green box outline represents effects which are beneficial to the cell, whereas the red outline represents detrimental effects.

NO_2^- has often been considered biologically inactive, and only important as a reservoir of NO (Figure 1.21), which is a free radical with an important role in a number of areas of human biology, such as vasodilation, neurotransmission and immunity, and which has also been implicated in medical conditions such as septic shock, strokes and chronic inflammation [180]. However, in recent years, it has been established that NO_2^- does have its own direct effects in the cell without conversion to NO, such as involvement in

signalling, post-translational modifications of proteins [183], and the modification of sites within mitochondria which are related to mitochondrial regulation [184].

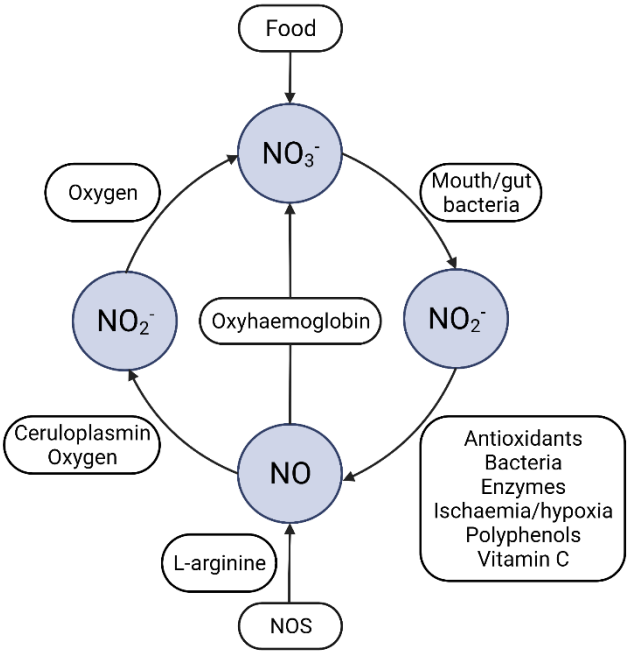

Figure 1.21. The NO_3^--NO_2^--NO· pathway in mammals. Based on diagram from [185]. Created with Biorender.com [6].

The mechanisms by which NTP-produced NO_2^- affects cells are not clear. The NO_2^- cannot cross the cell membrane from the NTP-treated liquid by diffusion due to its charge [186], nor does it appear that any ion channels or transporters have been identified in mammals which would allow it to do so by other means. Reduction of NO_2^- to NO which, unlike NO_2^-, can easily cross the cell membrane (Figure 1.19), may seem like a possible area to explore, and there are a range of reactions by which NO can be formed from NO_2^- [187][188], but there is no evidence that these are occurring with NTP treatment, and it is not certain whether the correct conditions for these reactions are present. An increase in NO levels in NTP-treated cells has been observed [79], although it has not been determined whether the

original source of this is the NO_2 being produced in the surroundings of the cell by NTP, or if another NO-producing pathway is being triggered by other substances formed during the treatment.

A possible explanation for the cell viability effects of NO_2^- produced by NTP treatment on cancerous cells specifically, and its identified synergy with H_2O_2, has been proposed by Bauer and colleagues [189][190][191][192]. This relies upon the finding that, unlike non-cancerous cells, tumour cells can have membrane-bound catalase [189][190]. The process relies on the formation of singlet oxygen ($^1O_2$) via Equations 1.28 to 1.37, with the reactants of the initial reaction being H_2O_2 and NO_2^-. The protons (H^+) necessary for the reactions are thought to be provided by membrane-bound proton pumps, moving the ion out of the cell.

$$NO_2^- + H_2O_2 \rightarrow ONOO^- + H_2O \quad (1.28)$$

$$ONOO^- + H^+ \rightarrow ONOOH \quad (1.29)$$

$$ONOOH \rightarrow NO_2 + OH \quad (1.30)$$

$$OH + H_2O_2 \rightarrow H_2O + HO_2 \quad (1.31)$$

$$NO_2 + HO_2 \rightarrow O_2NOOH \quad (1.32)$$

$$O_2NOOH \rightarrow O_2NOO^- + H^+ \quad (1.33)$$

$$O_2NOO^- \rightarrow {}^1O_2 + NO_2^- \quad (1.34)\ [191]$$

$$ONOO^- + H^+ \rightarrow ONOOH \quad (1.35)$$

$$HO_2 + O_2^- + H^+ \rightarrow H_2O_2 + {}^1O_2 \quad (1.36)[192]$$

$$O_2NOO^- \rightarrow O_2^- + NO_2 \quad (1.37)[191]$$

The $^1O_2$ produced in Equations 1.34 and 1.36 would then act upon the membrane-bound catalase, causing its inactivation, and therefore preventing the breakdown of H_2O_2 and $ONOO^-$, allowing greater amounts of these to enter the cell via diffusion or ion channels

(Figure 1.19). The effects of high levels of intracellular H_2O_2 have already been discussed above, while high levels of $ONOO^-$ are known to lead to oxidation and nitration of lipids, DNA strand breaks, and modification of both DNA bases and amino acids [180]. As well as the inactivation of the membrane-bound catalase via $^1O_2$ production, the series of reactions from Equations 1.28 to 1.30 also produces OH, which can itself damage the cell membrane (Figure 1.19). Nitrogen dioxide (NO_2) is formed in Equation 1.30, and the breakdown of the peroxynitrate (O_2NOO^-) formed in Equation 1.33 can also result in the formation of more NO_2 via Equations 1.34 and 1.28 to 1.30 as well as via Equation 1.37, with this latter equation also yielding superoxide (O_2^-). Both of these substances can cross the cell membrane (Figure 1.19), with NO_2 having a variety of effects including lipid peroxidation and the oxidation of amino acids [193], while O_2^- can cause the oxidation and peroxidation of lipids as well as single strand DNA damage.

The hypothesis based on Equations 1.28 to 1.37 would explain the observations of [166] in Table 1.9, and also some of those in [161], specifically that NO_2^- alone does not appear to have a toxic effect on cancerous cells in its own right, but that it heightens the toxicity of H_2O_2 when that is also added. However, [161] also found that the same effect from NO_2^- addition was found in normal primary fibroblasts, which would not be expected to have membrane-bound catalase. Therefore, it does not appear that the role of NO_2^- in NTP treatment is fully understood at present.

1.2.3.5.1 Origins of H_2O_2 and NO_2^- in NTP treatment

As is notable from Figure 1.18(a), even when direct treatment is used the NTP does not in fact contact the cells directly, but rather the liquid in which the cells are sitting. Thus, in both direct and PAM treatment, the chemical modifications made by NTP are to liquid

which either is, or will be, in contact with the cells, rather than directly to the cells themselves. It is therefore from this liquid that the cells will encounter the H_2O_2, NO_2^- and other RONS which occur as a result of NTP treatment. The liquids which are used for *in vitro* plasma medicine research are usually those which are in common *in vitro* use generally, such as a range of cell media, phosphate-buffered saline (PBS) or Dulbecco's phosphate-buffered saline (DPBS). A common feature of all these liquids is that they are aqueous and, fortunately, there is a large body of work considering the chemical effects of NTP interactions with water from the water treatment literature which gives an indication of the types of chemical species that would be expected to occur in the interaction between NTP and these *in vitro* liquids (Figure 1.22). The substances produced are a mix of short- and long-lived species (Table 1.10).

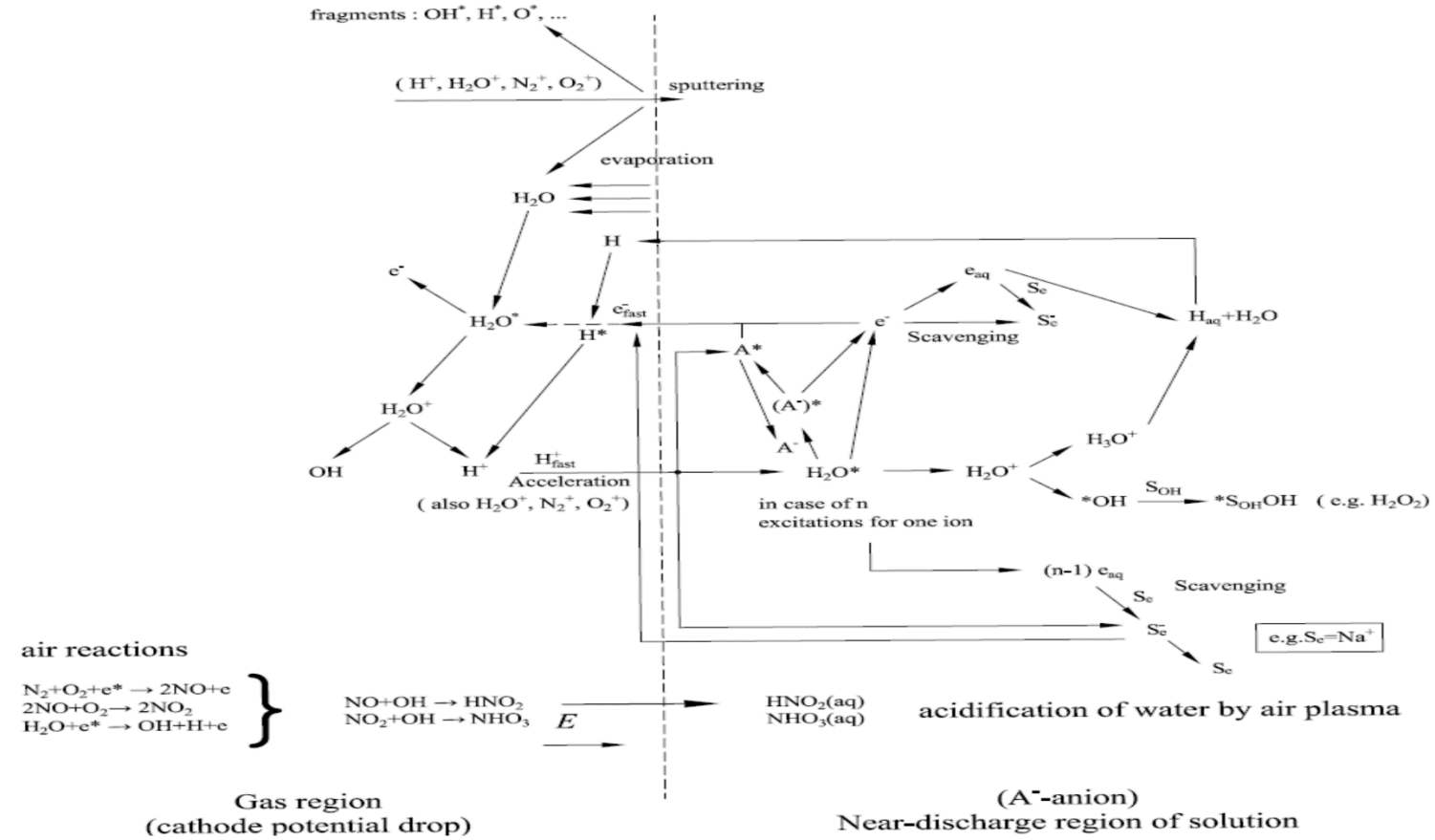

Figure 1.22. Key reactions in the interaction between air NTP and liquid. The dotted line representing the interface between the gas and liquid. Diagram reproduced from [194].

Table 1.10. Half-lives for selected substances produced in interactions shown in Figure 1.22.

Substance	**Half-life**
H_2O_2	Not applicable, considered [195]
OH	10^{-10} s s[195]
NO	0.05-1 s [196]
NO_2	Approximately 1 s [195]
NO_2^-	Varies with environment, but stable in water [197]
NO_3^-	5-8 hours [196]

As discussed above, two of the most important substances in plasma medicine are thought to be H_2O_2 and NO_2^-. Several pathways have been identified by which NTP can form H_2O_2 in water, with it being thought that much of the H_2O_2 produced comes from the dimerization of OH (Equation 1.38), but some may also be formed via Equations 1.39 and 1.40. In Equations 1.39 and 1.40, H_2O^* signifies a water molecule which has a higher level of excitation due to collision with an electron.

$$OH + OH \rightarrow H_2O_2 \quad (1.38)[198][199]$$

$$2H_2O^* \rightarrow H_2O_2 + H_2 \quad (1.39)$$

$$OH + H_2O^* \rightarrow H_2O_2 + H \quad (1.40)[200]$$

Two of the above reactions forming H_2O_2 rely on the presence of OH, and there are several identified pathways by which OH can be produced by the interaction between NTP and water (Equations 1.41 to 1.44).

$$e^- + H_2O \rightarrow H + OH + e^- \quad (1.41)$$

$$e^- + H_2O \rightarrow H^- + OH \quad (1.42)[199][198]$$

$$H_2O^* + H_2O \rightarrow H + OH + H_2O \quad (1.43)[201][200]$$

$$H + H_2O^* \rightarrow OH + H_2 \quad (1.44)[201]$$

As with H_2O_2, there are several routes by which NO_2^- can be formed. The first pathway for NO_2^- production involves the production of NO, followed by nitrous acid (HNO_2), which then, being a weak acid, partially dissociates in the water giving H^+ and NO_2^- (Equations 1.45 to 1.47). The NO produced in Equation 1.42 can also react to give NO_2^- via an alternative pathway (Equation 1.48).

$$N_2 + O_2 + e^{-*} \rightarrow 2NO + e^- \quad (1.45)$$

$$NO + OH \rightarrow HNO_2 \quad (1.46)[194]$$

$$HNO_2 \rightarrow H^+ + NO_2^- \quad (1.47)[202]$$

$$4NO + O_2 + 2H_2O \rightarrow 4NO_2^- + 4H^+ \quad (1.48)[203]$$

Caution must be applied when considering how these reactions forming H_2O_2 and NO_2^- apply to the aqueous liquids used in plasma medicine research, as there are two important differences between these and water alone. Firstly, most liquids used for *in vitro* work, and therefore, for plasma medicine research, are buffered. pH may affect the speed of a reaction, and indeed whether it occurs at all, and little work has been identified where the prominence of the different pathways above has been considered in these buffered liquids. As well as this, liquids used for *in vitro* work, particularly cell medium, are much more chemically complex than water (Appendix A), and therefore it might be expected that other, as-yet unidentified reactions take place when it is treated with NTP. However, given the aqueous nature of *in vitro* liquids, it is likely that many of the above reactions are indeed taking place, and are responsible for at least some of the H_2O_2 and NO_2^- formation observed.

1.3 Aims of this project

The aims of the present study were:

1. To develop a simple DBD-type NTP source suitable for application to *in vitro* cell samples, and carry out appropriate electrical, chemical, and biological testing to develop an understanding of its operation and confirm its suitability for use in plasma medicine research. This style of device was selected for ease of construction, but is also novel.
2. To investigate the effect of NTP treatment generated by this reactor on the cells of the human immune system. Specifically, this would consider the U937 monocyte cell line, differentiated to be macrophage-like.
    (a) For this work, there would be a particular focus on the use of PAM of different dilutions.
    (b) Measures would include those relating to viability, phagocytic ability, antioxidants, chemokines and other cytokines.

Much of this work is novel. The differentiated U937 cell line, and indeed macrophage-like cells generally, have rarely been used in plasma medicine studies. No other work has been identified in which the effects of NTP treatments on the phagocytic abilities, or the expression of phagocytosis-related genes, in macrophage-like cells has been considered. Similarly, no work to consider the effects of NTP treatment on cytokine secretion by U937 has been considered, nor has any other work been identified in which the effects of different strengths of PAM on cytokine secretion has been considered in any cell type. The effects of PAM treatment on the expression of antioxidant genes has been considered

elsewhere, but not in the differentiated U937 cell line, nor using PAM created with the novel device developed for project.

Chapter 2 Methodology

2.1 Electrical design and measurement

2.1.1 Plasma reactor designs

2.1.1.1 Main reactor (Reactor 1)

Most plasma treatment within this project was performed with a DBD pin-plate style reactor (Reactor 1), which was built to treat liquid samples of 325 µL within a 96-well plate well, and which was designed as part of this project (Figure 2.1). The tip of the needle was kept at a fixed position above the plate for all experiments. This position was set as 0.1 mm above the top of the well, determined using a 0.1 mm glass spacer. The needle itself had a 0.5 mm diameter tip. All plates used within the reactor were Nunc microwell 96-Well Nunclon delta-treated, flat-bottom microplates (Thermo Scientific; Waltham, Massachusetts, USA).

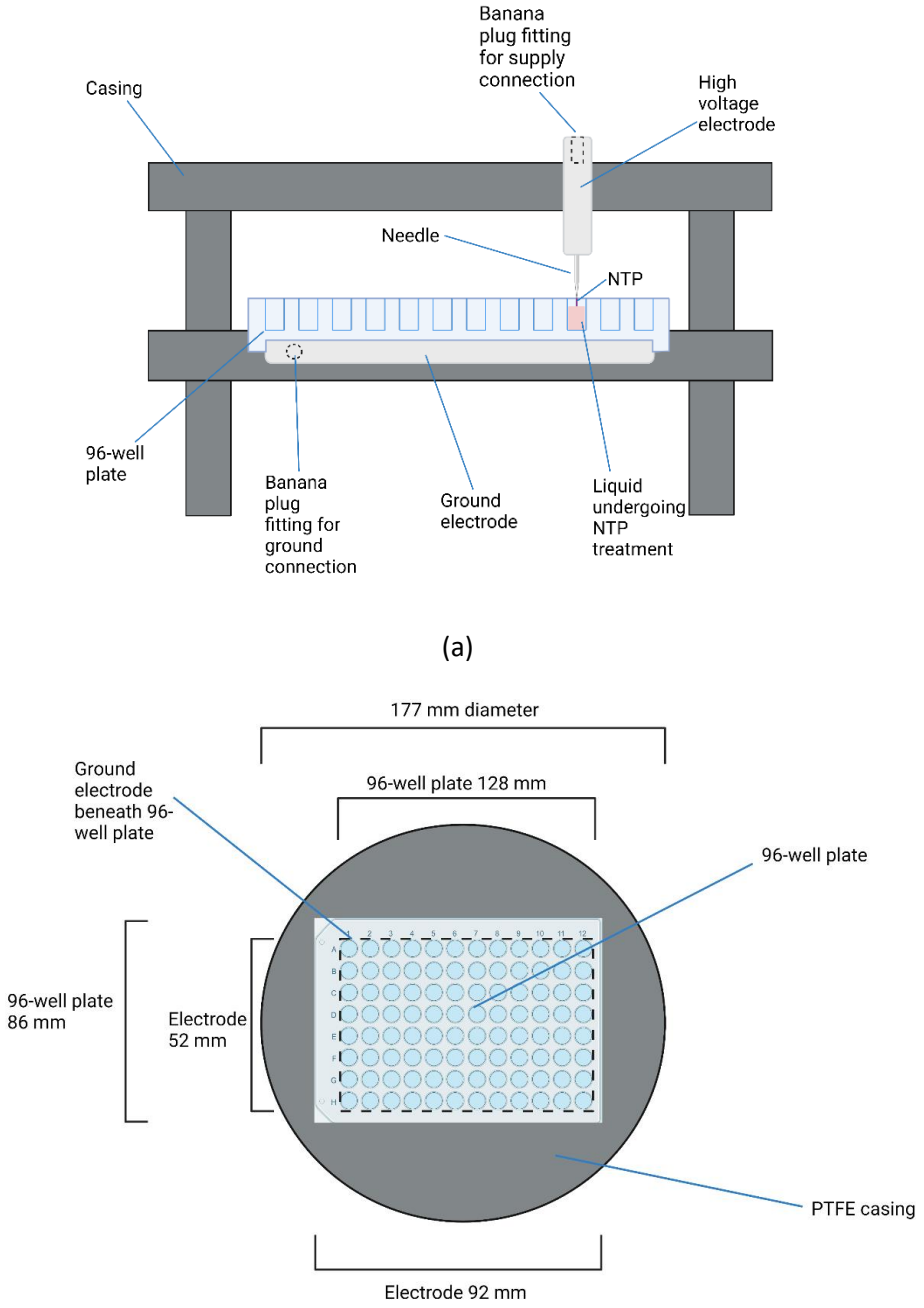

Figure 2.1. Reactor 1 (a) detailed diagram and (b) view from above showing location of ground electrode below 96-well plate. Note that the electrode dimensions given are those which are in contact with the bottom of the 96-well plate. The base of the electrode, as fitted in to the casing, was slightly larger, at 100 mm by 60 mm, with a curved transition between the two sets of dimensions. Both diagrams created with Biorender.com [6].

The reactor can be represented by the equivalent circuits in Figure 2.2.

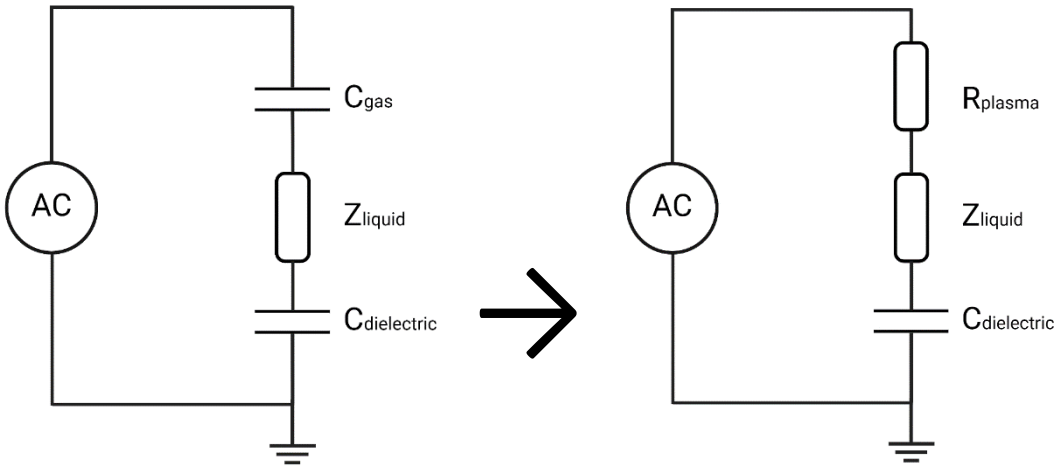

(a) (b)

Figure 2.2. Equivalent circuits for Reactor 1 (a) no discharge (b) discharge. C_{gas} = capacitance of gas, $C_{dielectic}$ = capacitance of dielectric, Z_{liquid} = impedance of liquid, R_{plasma}= resistance of plasma. Created with Biorender.com [6]. The black arrow between the two circuits indicates breakdown.

Although a more unusual arrangement for DBD than many of those shown in Figure 1.12, similar devices have been used elsewhere in non-plasma medicine NTP research, for example by Tian *et al.* [204]. The most similar reactor design identified in the plasma medicine literature specifically was that of Sato *et al*. [205], which also used a needle-style electrode, and which also had the plastic container holding the treatment liquid functioning as the dielectric layer (Figure 2.3(a)). However, a microtube was used rather than a 96-well plate, and the pulsed power supply was also different from the AC supply used with Reactor 1

(Figure 2.3(b)), meaning that the operating characteristics of the Sato *et al.* reactor are unlikely to be directly comparable to Reactor 1.

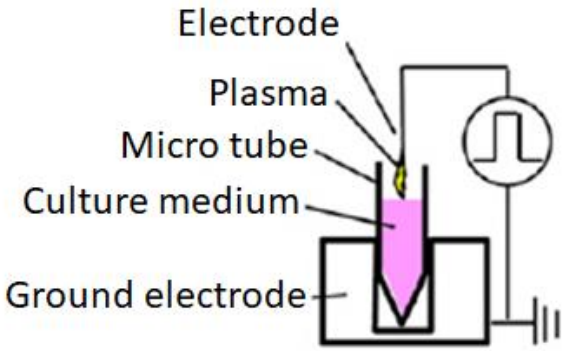

(a)

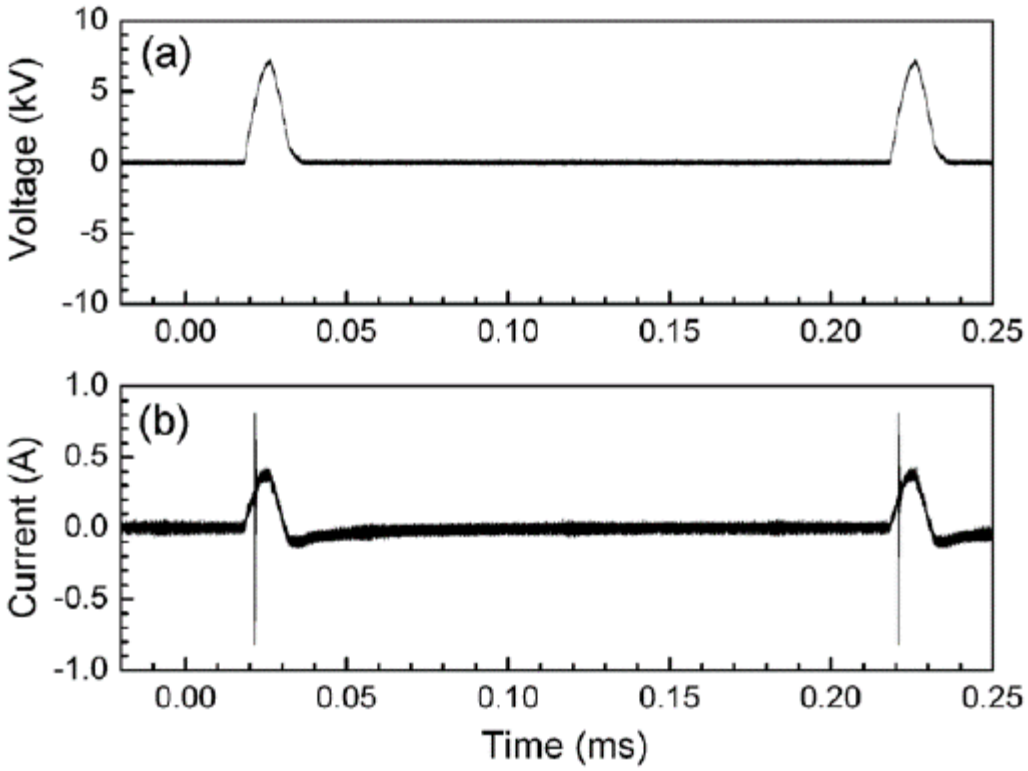

(b)

Figure 2.3. The reactor of Sato et al. (a) reactor diagram (b) electrical supply and resultant current. Reproduced from [205].

2.1.1.2 Petri dish reactor (Reactor 2)

A small amount of work within the project (section 4.4.5) was carried out with a modified reactor of similar design to the main reactor described above, but which used 9.6 cm^2 Petri dishes rather than a 96-well plate (Reactor 2, Figure 2.4). All Petri dishes used with this were Falcon 35 mm diameter easy-grip tissue culture dishes (Corning; Corning, New York, USA), and the starting liquid volume at the beginning of plasma treatment was always 2 ml. The needle point was fixed during all experiments, approximately 0.5 mm above the liquid surface. The needle tip diameter was 0.5 mm.

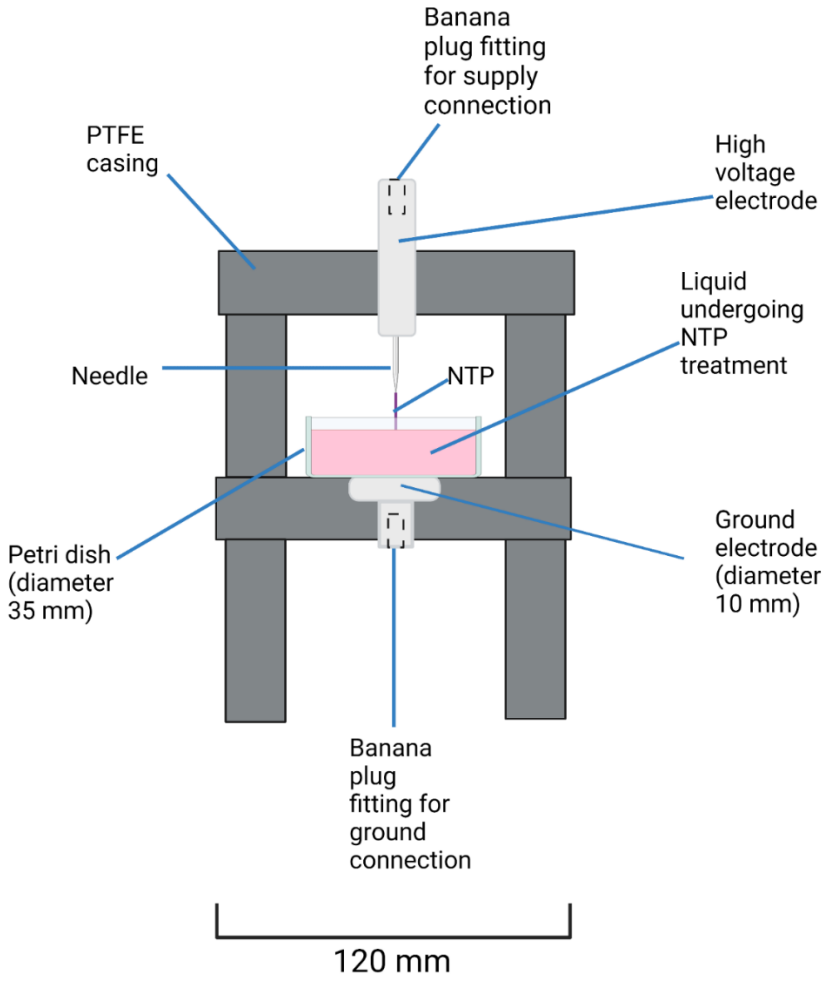

Figure 2.4. Reactor 2. Created with Biorender.com [6].

2.1.1.3 Manufacturing and other reactor designs

All manufacturing of reactors was carried out by the in-house workshop within the High Voltage Technologies research group within the Department of Electronic and Electrical Engineering, University of Strathclyde. All electrodes were made from stainless steel, with the casings of the reactors being made from polytetrafluoroethylene (PTFE) and polyvinyl chloride (PVC).

Other reactors designed for use on this project, but which proved unsuitable for biological work, are shown in Appendix B.

2.1.2 Electrical supply

The electrical supply for all NTP experiments was provided by an AMX-112 AC power source with UPC-12 controller (Pacific Power Source Inc.; Invine, California, USA) operating at a frequency of 4 kHz. For the main reactor used, Reactor 1, the peak output voltage of the was 180 V_m, which was then connected to a commercially-purchased step-up 220:10000 transformer, resulting in a secondary voltage of approximately 8 kV_m, which was applied across the reactor. A diagram showing the circuit used to operate Reactor 1 is given in Figure 2.5.

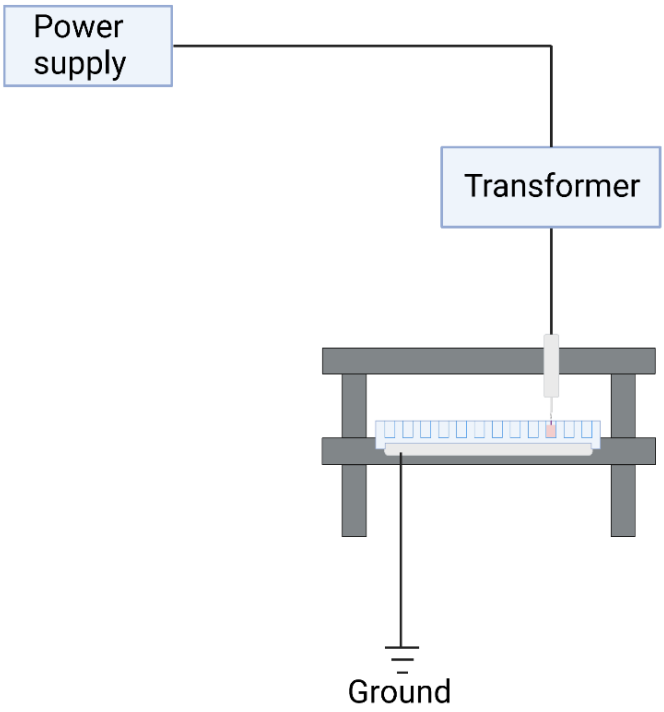

Figure 2.5. Circuit used to operate Reactor 1. Created with Biorender.com [6].

The same arrangement of connections was used for Reactor 2, and thus this has not been separately illustrated here. The selection of the voltage used with Reactor 2 is covered within section 4.3.

2.1.3 Electrical measurements

2.1.3.1 Oscilloscope

The oscilloscope used for all electrical measurements was a DPO3034 digital oscilloscope (Tektronix; Beaverton, Oregon, USA).

2.1.3.2 Applied voltage measurement

Applied voltage across the reactors was measured with a P6015A high voltage oscilloscope probe (Tektronix; Beaverton, Oregon, USA) placed across the reactor, and an oscilloscope.

2.1.3.3 Current measurement

Measurement of the external current in the circuit containing Reactor 1 was made using a 50 Ω coaxial cable with 50 Ω resistance stub (Figure 2.6). The oscilloscope (50 Ω internal impedance) was used with an attenuation setting of 0.02 to convert the voltage across the resistance stub to the equivalent current. The voltage applied to the reactor was also measured at the same time as the current.

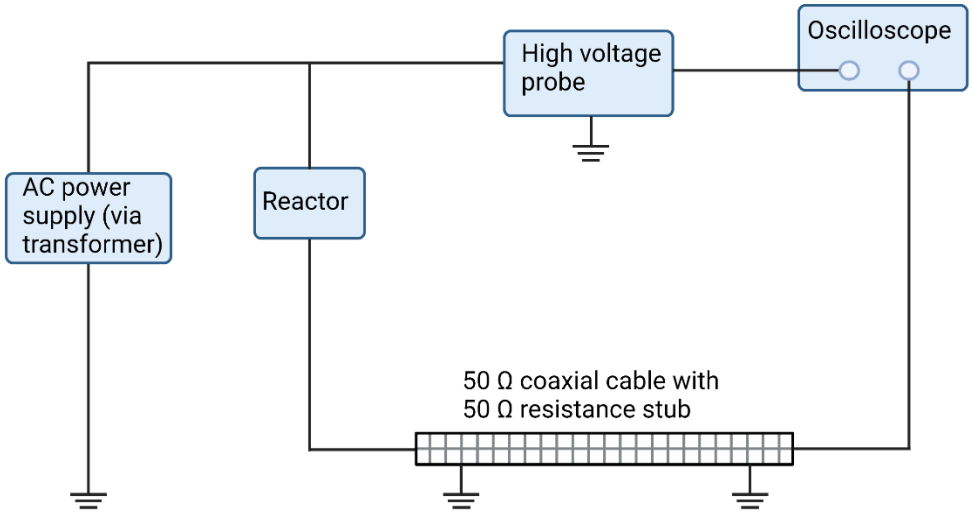

Figure 2.6. Measurement of current using a 50 Ω coaxial cable. Also shown is the measurement of the voltage across the reactor, measured by high voltage probe alongside the current. Created with Biorender.com [6].

Measurement of Reactor 2 current was not within the scope of the project.

2.1.3.4 Discharge power measurement

Measurement of the discharge power of Reactor 1 was made using the Lissajous method, frequently used with DBD devices, and as described in [206]. This involves creating a

Lissajous diagram, sometimes also called a Q-V diagram (Figure 2.7), in which applied voltage and charge transfer for the reactor are plotted against each other at a large number of timepoints throughout an applied voltage wave period.

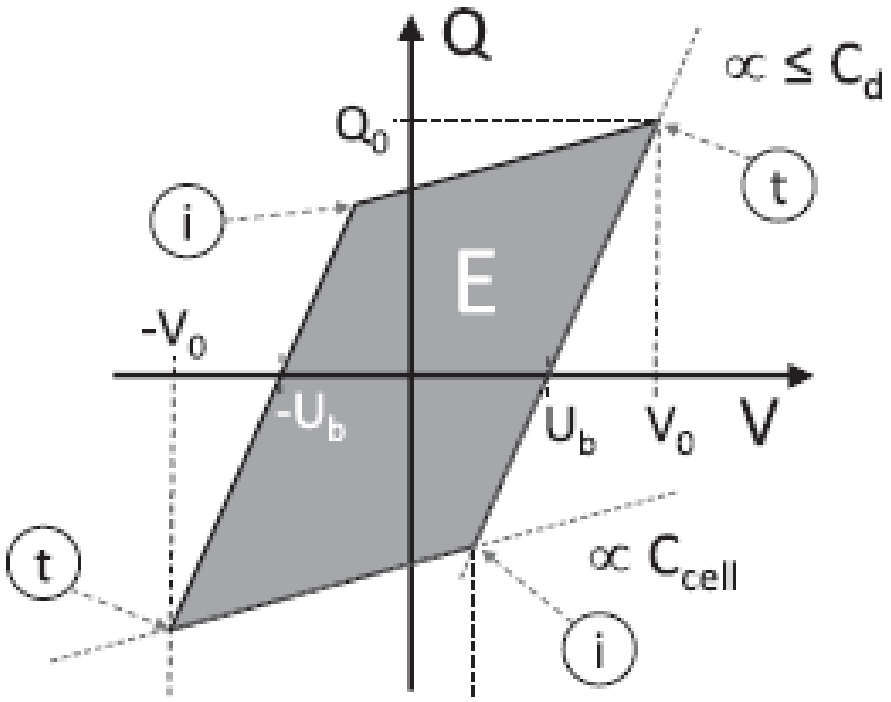

Figure 2.7. Example Lissajous diagram. The inception (i) and termination (t) points correspond to those shown in in the current in Figure 3.1. C_d = dielectric capacitance, V_0 = voltage magnitude, C_{cell} = total capacitance of the reactor, U_b = breakdown voltage. Reproduced with modification from [77].

To create the Lissajous, both the voltage applied to the reactor and the voltage across a 10 nF capacitor in series with the reactor were measured simultaneously, with a sampling interval of 40 ns (Figure 2.8).

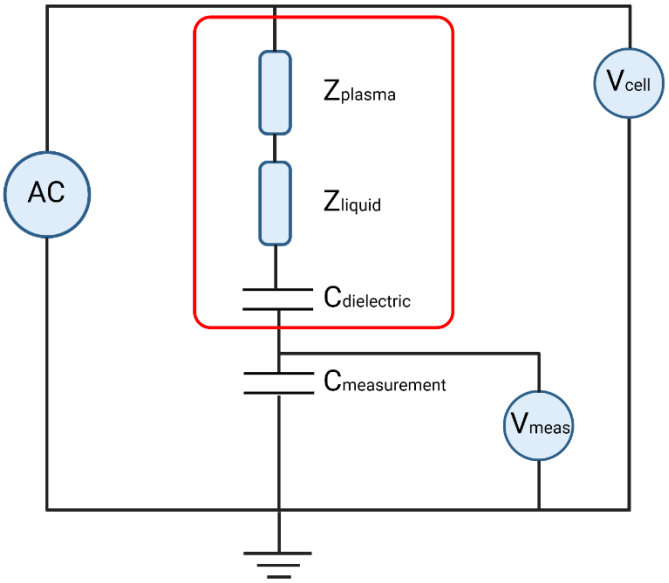

Figure 2.8. Discharge power measurement circuit for Reactor 1, shown as equivalent circuit. Area circled in red represents the reactor cell. V_{cell} = high voltage probe across entire reactor cell, V_{meas} = low voltage probe across measurement capacitor, $C_{measurement}$ = measurement capacitor. Created with Biorender.com [6].

The applied voltage was measured using the technique described in 2.1.3.2, while the capacitor voltage was measured using a TPP0101 passive voltage probe (Tektronix; Beaverton, Oregon, USA). From this latter measurement, the charge transfer could be calculated (Equation 2.1) and thus allowing the creation of the Lissajous figure over one AC cycle.

$$Q = CV \tag{2.1}$$

where Q is charge in Coulombs (C), C is capacitance in Farads (F) and V is voltage in Volts (V).

It is established that the area enclosed by the voltage-charge plot must always represent the energy of one cycle [76][207]. From this area the discharge power can then be determined (Equation 2.2).

$$P = \frac{E}{t} \tag{2.2}$$

Where P is power in Watts, E is energy in Joules and t is time in seconds.

A MATLAB script was written to convert the raw data of the two measured voltages measured by the oscilloscope, the applied voltage and the voltage across the measurement capacitor, into a value for discharge power via a calculation of the area of the Lissajous diagram (Appendix C).

Figure 2.7 above shows the Lissajous plot as a perfect parallelogram. However, in reality, this is often not the case and it may, for example, have rounded corners [77], or even be oval-shaped [76], depending on the nature of the discharge. Such variance away from the parallelogram may mean that the interpretation of the figure is not straightforward [77].

2.2 Physical and chemical measurements

2.2.1 Temperature measurement

Temperature measurement of treated liquid was carried out using a thermocouple.

2.2.2 Evaporation measurement

Liquid volumes were measured to the nearest 10 µL by removing liquid within the well 5 µL at a time using a micropipette. This allowed rounding to the nearest 10 µL.

2.2.3 pH measurement

Due to the small liquid volumes being tested, pH test strips were used (Sigma; Darmstadt, Germany and Precision Laboratories; Cottonwood, Arizona, USA).

2.2.4 H_2O_2 measurement

An Amplex Red Hydrogen Peroxide/Peroxidase Assay Kit (Invitrogen; Waltham, Massachusetts, USA) was used to measure H_2O_2 in NTP-treated liquid. The process was carried out following the instructions supplied by the kit manufacturer, which are briefly described below.

Firstly, the required stock solutions were prepared. To create a 10 mM Amplex Red reagent stock solution, a vial of Amplex Red was warmed to room temperature from the kit storage temperature of -20 °C. Dimethylsulfoxide (DMSO, Sigma-Aldrich; Darmstadt, Germany) was also warmed to room temperature. 60 µL of this was then added to the Amplex Red vial and pipetted gently up and down to ensure full dissolving of the Amplex Red. A 1X reaction buffer was also made up using 4 ml of the 5X reaction buffer supplied with the kit, and 16 ml of deionised water. A 10 U/ml horseradish peroxidase (HRP) solution was then prepared by adding 1 ml of the 1X reaction buffer to the supplied vial of HRP. This was aliquoted and that not required immediately was frozen at -20 °C for storage.

To carry out the assay, 50 µL of the sample liquid was added to a well, if necessary being pre-diluted using 1X reaction buffer beforehand to ensure it was in the range of H_2O_2 detectable by the kit. An Amplex Red/HRP solution was made from 50 µL of the Amplex Red solution above, 100 µL of the 10 U/ml HRP stock solution above, and 4.85 ml of the 1X reaction buffer. 50 µL of this Amplex Red/HRP solution was then added to each of the wells

containing a sample. The plate was then incubated at room temperature for 30 minutes, wrapped in foil to protect the reaction from light. Absorbance was then measured at 560 nm using a Multiscan GO plate reader (Thermo Scientific; Waltham, Massachusetts, USA).

So that the absorbance readings could be converted into a concentration of H_2O_2, a standard curve was created at the same time as the samples were assayed. To do this, a 20 mM H_2O_2 working solution was also prepared by diluting 22.7 µL of the 3.0 % H_2O_2 supplied with the kit with 977 µL of the 1X reaction buffer previously prepared. This was then diluted to a series of concentrations of a range of 0 – 10 µM H_2O_2, and 50 µL of each of these was subjected to the assay as described above. The H_2O_2 concentrations of experimental samples were then established by comparison against the absorbance values of the known concentrations of H_2O_2.

2.2.5 NO_2^- measurement

The method used to measure the nitrite ion (NO_2^-) in NTP-treated liquid was based on that proposed in [208], known as the Greiss reaction. The two required reagents were prepared. For Reagent A, 2% (w/v) sulphanilamide was dissolved in 4% (v/v) H_3PO_4 (lab stock; source unknown). For Reagent B, 0.2% (-w/v) naphtylethylenediamine di-HCl (lab stock; source unknown) was dissolved in deionised water. Both reagents were stored refrigerated and protected from light until use.

To measure NO_2^- in a sample, Reagents A and B were mixed in equal volumes immediately prior to use. 100 µL of this combined liquid was then added to 100 µL of sample liquid in a 96-well plate well. If necessary, to ensure the samples were within the range of concentrations which could be measured by the Greiss technique, they were pre-diluted

with deionised water prior to addition to the plate. Once the samples and reagents had been combined, the plate was then gently agitated on an orbital shaker for 10 minutes, before the absorbance was measured at 540 nm using a Multiscan GO plate reader (Thermo Scientific; Waltham, Massachusetts, USA).

To derive NO_2^- levels from these absorbance values, a standard curve was created using $NaNO_2$ (Sigma-Aldrich; Darmstadt, Germany). A 200 µM solution of this was made up in deionised water. Following this, a series of dilutions was made with deionised water to give 100 µM, 50 µM, 20 µM, 10 µM and 5 µM solutions. 100 µL of each of these was then subjected to the Greiss process as outlined above, allowing a standard curve to be created.

2.3 Biological methods

2.3.1 Cell culturing and sample creation

All biological experiments were carried out using either the NIH 3t3 (ECACC 93061524) [209] cell line, or the U937 (ECACC 85011440) [210] cell line. Both of these were already held in stock within the University.

Where incubation was carried out, this was done at standard conditions, specifically at 37 °C with 5 % CO_2.

2.3.1.1 NIH 3t3

NIH 3t3 ('3t3') are fibroblasts derived from Swiss albino mouse embryonic tissue [209], and were cultured in complete Dulbecco's modified Eagle's medium (DMEM). This was created by adding 5 ml of antibiotics (5000 units/ml penicillin and 5 mg/ml streptomycin) (Sigma-Aldrich; Darmstadt, Germany), 5 ml of non-essential amino acids (NEAA) (Lonza; Basel,

Switzerland), and 50 ml of foetal bovine serum (FBS) (Biosera; Nuaillé, France) to each 500 ml bottle of DMEM (Lonza; Basel, Switzerland, or Gibco; Waltham, Massachusetts, USA).

For the 3t3 cell line, all experiments were performed with cells seeded at a 1 x 10^5 cells/cm^2 density two days prior to plasma treatment. The reason for the selection of this seeding density was due to its success with the neutral red assay, as discussed in 2.3.4.1, and it was retained throughout all further 3t3 experiments to ensure comparable conditions. At the 24-hour point following cell seeding, serum starvation was carried out, as detailed below.

2.3.1.1.1 Serum starvation process

Initial biological experiments with 3t3 yielded inconsistent results between different biological replicates. In order to reduce this effect, a serum starvation process was used, which is known to align mammalian fibroblasts into the G_0 stage of the cell cycle [211] (Figure 1.15).

Low serum medium was made up using a 500 ml bottle of DMEM, 5 ml of both penicillin/streptomycin and NEAA, but with only 0.5 ml of FBS added instead of 50 ml. To carry out the serum starvation process on the 3t3 cells, the complete DMEM was removed from the cells 24 hours after cell seeding. The wells were then washed twice with 400 µL of sterile PBS, prepared as described in 2.3.3, for each wash. Following removal of the PBS, 200 µL of low serum medium was then added to each well, and the plates were returned to the incubator for 24 hours prior to experimentation, allowing time for the cells to align in the G_0 stage.

2.3.1.2 U937

U937 is a monocyte cell line, derived from a histiocytic lymphoma [210], but which can be stimulated to differentiate into a cell with macrophage-like characteristics by use of a number of substances, including PMA [212][213][17]. The cells were used in this differentiated form for most experiments during this project. U937 was cultured in complete Roswell Park Memorial Institute 1640 (RPMI 1640, 'RPMI') medium. This was created by adding 5 ml of antibiotics (5000 units/ml penicillin and 5 mg/ml streptomycin) (Sigma-Aldrich; Darmstadt, Germany), 5 ml of 200 mM glutamine (Gibco; Waltham, Massachusetts, USA), and 50 ml of FBS (Biosera; manufacturer number FB-1090/500) to each 500 ml bottle of RPMI 1640 (Lonza; Basel, Switzerland).

To create cell samples for NTP treatment, the cells were first pelleted by centrifuging at 800 rpm for 5 minutes, before being resuspended in fresh complete RPMI 1640 with 16.2 nM PMA and seeded in a 96-well plate at 2 x 10^5 cells/cm^2. The reason for the selection of this specific seeding density was, as with 3t3, due to its success with the neutral red assay (2.3.4.1), and the seeding density was the same throughout all further U937 experiments to ensure comparable conditions. Experiments were carried out on the sample at 24 hours following the addition of PMA. The serum starvation technique used with 3t3 was not used for U937 as it proved unnecessary to achieve consistent results, and it was also not clear whether reducing the serum level could interfere with the PMA activation of the cells.

2.3.1.2.1 PMA

PMA powder (Sigma-Aldrich; Darmstadt, Germany), used to differentiate U937 to a macrophage-like cell, was dissolved in DMSO (Sigma-Aldrich; Darmstadt, Germany) to give stock solutions of 5 µM or 10 µM. This was stored at -20 °C until time of use. 16.2 nM PMA

was used for all plasma experiments using, and this was created from the 5 µM or 10 µM stock solutions by the addition of complete RPMI. The reason for the selection of this specific concentration for experimentation are discussed in Appendix D.

2.3.2 NTP treatments

Specific details around methods, timings and liquids used in each experiment performed in this project are stated alongside the results.

2.3.2.1 Direct and indirect treatment

For the purposes of this project, direct plasma treatment is defined as the cells being within the treatment liquid as it is being treated in the reactor. PAM treatment is defined as the liquid being treated in the reactor in the absence of cells, before then being added to cell samples. The difference between these two types of treatment is illustrated in Figure 1.18.

2.3.2.2 NTP treatment liquid

For most experiments, whether direct treatment or PAM, the NTP treatment was applied to room-temperature cell medium. The medium used (DMEM for experiments involving 3t3 and RPMI for those using U937) was taken straight from the bottle, without the addition of FBS, antibiotics, NEAA or l-glutamine. In a small number of experiments, Dulbecco's phosphate buffered saline (DPBS) with calcium and magnesium (Lonza; Basel, Switzerland) was used as the NTP-treated liquid rather than medium. In the experiments where this was the case, it is clearly stated.

In all experiments the complete or low-serum medium that the cells were sitting in prior to the experiment was removed before the application of the treatment liquid. Following the

completion of the treatment, cells were then either immediately subjected to further experiment such as assay, or, where this was to be carried out the following day, complete medium (DMEM for 3t3, and RPMI for U937) was added at a volume of 200 µL for a 96-well plate well or 2 ml for a Petri dish, and the cells were returned to the incubator for 24 hours. In this context, complete medium is that which used for cell culture as described in 2.3.1.1 and 2.3.1.2, specifically:

- For 3t3, per 500 ml bottle of DMEM, 50 ml of FBS, 5 ml of antibiotics (5000 units/ml penicillin and 5 mg/ml streptomycin) and 5 ml of NEAA were added.
- For U37, per 500 ml of RPMI 1640, 50 ml of FBS, 5 ml of antibiotics (5000 units/ml penicillin and 5 mg/ml streptomycin) and 5 ml of 200 mM glutamine were added.

2.3.2.3 PAM dilution treatments

In some experiments, the treatment liquid consisted of PAM created using a standardised time of 15 minutes with identical electrical conditions each time, then diluted down to lower concentrations. Where this was the case, the PAM was created in Reactor 1 using RPMI directly from the bottle, with no additives, for 15 minutes. Immediately upon completion, the liquid was then diluted by fresh RPMI, again with no additives. The dilutions used are shown in Table 2.1.

The NTP exposure time of 15 minutes was obtained after studying the data for previous experiments which showed that PAM created with such a treatment time was sufficient to cause a significant reduction in cell viability for the U937 cell line.

Table 2.1. PAM dilutions.

Dilution	Treated liquid volume (µL)	Untreated liquid volume (µL)
1	50	0
1/2	25	25
1/4	12.5	37.5
1/10	5	45

When these PAM dilutions were used, which was always in 96-well plates, the treatment liquid volume added to each well was 40 µL.

2.3.3 Preparation of PBS

PBS was made using PBS tablets (Sigma-Aldrich; Darmstadt, Germany), following the instructions of the manufacturer: 1 tablet fully dissolved in 200 ml of deionised water. If sterility was required, this liquid was then passed through a 0.22 µm sterile syringe filter unit with polyethersulfone (PES) membrane (Millex-GP; Darmstadt, Germany).

2.3.4 Neutral red assay

The neutral red assay was used to determine the level of cell viability in cells subjected to NTP treatment. This assay works by the dye diffusing passively into the cell, before it then moves into the lysosomes, organelles containing digestive enzymes, and then binds to the anionic and phosphate groups of the lysosomal matrix within. When lysosomes are damaged or destroyed, such as by the application of an NTP treatment, less neutral red is bound in this way [214][215], and thus the level of neutral red measured during the subsequent assay process is reduced, giving an indication of reduced viability in the sample.

The assay was carried out by following the protocol described by Repetto *et al.* [214]. 40 mg of neutral red powder (Sigma-Aldrich; Darmstadt, Germany) was dissolved in 10 ml PBS, giving a concentration of 4 g/l. This stock solution could be stored in the dark for several weeks. To use for the assay, the stock solution was then diluted 1:100 with complete cell medium containing FBS (DMEM for 3t3 use, RPMI 1640 for U937 use), giving a concentration of 40 µg/ml. This was then placed in a 37 °C oven for 24 hours, before being filtered through a 0.22 µm Millex-GP sterile syringe filter unit with PES membrane (Merck; Darmstadt, Germany) to remove crystals. To carry out the neutral red assay in a 96-well plate, any liquid already present in the well was removed and discarded. 100 µL of the 40 µg/ml neutral red solution was then added to the well, and the plate was placed in an incubator at 37 °C with 5 % CO_2 for 3 hours. The neutral red solution was then removed. The well was washed with 200 µL of PBS, which was then removed. 100 µL of de-staining liquid, made up as described below, was then added to the well, and the plate was gently agitated for 30 minutes using an orbital shaker. The absorbance was then measured at 540 nm in a Multiscan GO plate reader (Thermo Scientific; Waltham, Massachusetts, USA).

The required de-staining liquid was obtained by combining 49 ml of deionised water, 1 ml of glacial acetic acid (BDH; Darmstadt, Germany) and 50 ml of ethanol (Fisher Scientific; Waltham, Massachusetts, USA).

2.3.4.1 Determination of suitable seeding density

The seeding densities for both cell lines used consistently throughout the project were determined during work using the neutral red assay. For the 3t3 cells, a larger number of cells was used than that recommended by the Repetto *et al.* protocol (recommended number of 5,000 versus number used of 32,000). Smaller numbers of cells were attempted, up to

and including 16,000 cells, however, this meant that all samples, including controls, gave low absorbance readings when assayed. The advice given in the Repetto *et al.* protocol for this situation, increasing the cell numbers, was therefore followed.

According to Repetto *et al.*, the recommended quantity of macrophages per 96-well plate well for the neutral red assay is 100,000, seeded 48 hours prior to assay. During the work of this project, the number of U937 cells used, based on the seeding density of 1 x 10^5 cell/cm^2, was lower at 64,000 per well. However, the absorbance values obtained when this seeding density were large enough to suggest that this number of cells was sufficient.

2.3.5 MTT assay

3-[4,5-dimethylthiazole-2-yl]-2,5-diphenyltetrazolium bromide (MTT) was also used to determine the viability of cells subjected to NTP. This assay measures metabolic activity, specifically the production of nicotinamide adenine dinucleotide (NADH). NADH is a substance which is produced during cellular respiration [216], and which is necessary for the conversion of MTT into the formazan detectable during the assay process (Figure 2.9). Thus, lower levels of formazan production are indicative of reduced metabolism, and thus reduced cell viability.

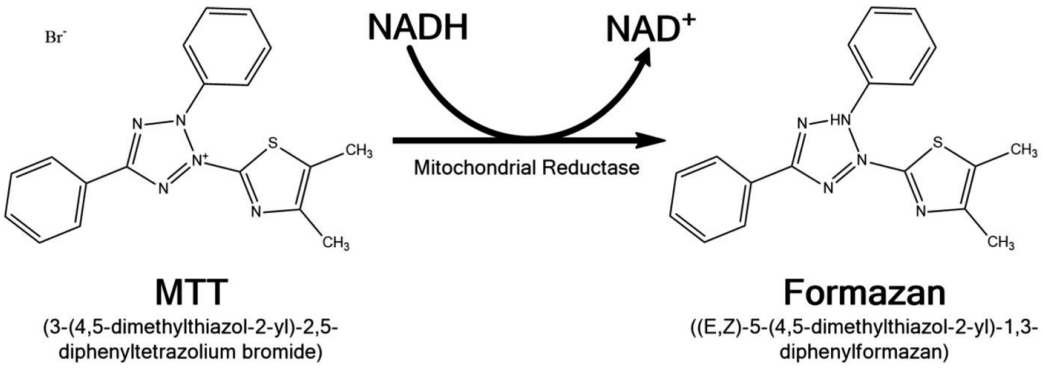

Figure 2.9. Reduction of MTT to formazan requiring NADH. Reproduced from [217].

For the MTT assay, an MTT solution was made up with 0.4142 g of MTT powder (Sigma-Aldrich; Darmstadt, Germany) and 100 ml of pH 6.75 PBS. This was then stirred to ensure that the powder had fully dissolved, before being filtered through a 0.22 µm sterile syringe filter unit with a PES Membrane (Millex-GP; Darmstadt, Germany) to ensure no clumps of powder remained. This solution could then be stored in the fridge for up to two weeks prior to use. To carry out the assay, 50 µL of the MTT solution was placed with 200 µL of medium already present within the well of the 96-well plate. This was then placed in the incubator at 37 °C with 5 % CO_2 for four hours. After this time, the MTT-medium mix in the well was fully removed by pipette, and 200 µL of DMSO was added to the well. The plate was then mixed on an orbital shaker for approximately 30 minutes, and the absorbance then measured in a Multiscan GO plate reader (Thermo Scientific; Waltham, Massachusetts, USA) at 540 nm.

2.3.6 Phalloidin-FITC and DAPI staining and imaging

The phalloidin-fluorescein isothiocyanate (FITC) and 4',6-diamidino-2-phenylindole, dihydrochloride (DAPI) stains were used in a combined method. DAPI is a nuclear stain,

while phalloidin binds to actin, which forms part of the cell cytoskeleton. Thus use of this combined staining process allowed damage caused by NTP application to be visualised. All cells to be stained were cultured on 96-well plate wells. At the time of staining, they were washed with 200 µL of 37 °C PBS and, once this PBS was removed, 100 µL of 4 % (w/v) formalin in PBS (Sigma-Aldrich; Darmstadt, Germany) was added to each well and left in place for 20 minutes to fix the cells. The formalin was then removed, and the well washed three times with 200 µL PBS for each wash. Following removal of the PBS, 100 µL of 0.1 mg phalloidin-FITC (Sigma-Aldrich; Darmstadt, Germany) dissolved in 1 ml methanol was added to each well, and the plate was then left for one hour in a 37 °C incubator with 5 % CO_2 in a moist chamber. The samples then underwent a further three washes with PBS, with the PBS being left on the cells for five minutes during each wash. After the final wash, the PBS was removed and discarded.

A stock solution of DAPI (Invitrogen; Waltham, Massachusetts, USA) of 5 mg/ml in deionised water was made up and stored at -20 °C in the dark. At time of use, the stock solution was then diluted to 286 nM using PBS. Following completion of the phalloidin-FITC staining process above, 100 µL of this DAPI solution was added per well, and the plate was then left at room temperature in the dark for two minutes. The DAPI was then removed, and three 200 µL PBS washes were then carried out. The plate was wrapped in foil to protect the stains from light until imaging took place, which was as soon as possible after the completion of the staining process.

Imaging was carried out with an Eclipse TE300 inverted epifluorescent microscope (Nikon; Amsterdam, Netherlands). The focus of this imaging was to observe the actin, stained by the phalloidin-FITC, to observe whether it remained web-like, or if it had collapsed.

2.3.7 Diffusion area measurements

For measurements of the area of reduction of cell viability 4.4.5, which was carried out in Petri dishes, 2 ml of fresh complete DMEM was added to the dish after the plasma treatment liquid was removed. The dish was then placed into an incubator at 37 °C for 24 hours. 0.5 ml of MTT, made up as described in 2.3.5, was then added, and the dish returned to the incubator for a further 4 hours before the liquid was completely removed. The dishes were then placed on top of graph paper with 1 cm squares visible and photographed from above. ImageJ opensource software was then used to determine the unstained area, indicative of little or no cell viability, by manually highlighting this area, determining the pixel number of this area, then comparing it to the pixel number of a grid square.

2.3.8 Latex bead preparation and use

FITC-labelled latex beads were used for the assessment of phagocytosis in the U937 cell line, as the cells are capable of phagocytosing these beads, and this can be seen by microscopy.

2.3.8.1 Latex bead preparation

Carboxylate-modified polystyrene latex beads, fluorescent green 1.0 µm diameter, 2.5 % in aqueous solution (Sigma-Aldrich; Darmstadt, Germany) were used to consider the phagocytic activity of U937 in response to plasma treatment. To prepare the beads for use, 200 µL of the bead mixture was added to 20 ml of sterile-filtered PBS, then shaken. 1 ml of this was added to each of 20 centrifuge microtubes, before they were centrifuged at 13,000 rpm for 10 minutes. Following this, all but around 50 µL of the PBS was removed from each microtube. The remaining pellet of beads was then resuspended in the remaining PBS

using a pipette. The resuspended bead liquid from all 20 tubes was then combined in a single sterile container.

2.3.8.2 Use of latex beads to assess phagocytosis

For assessment of phagocytosis, 10 µL of the bead mixture prepared as described in 2.3.8.1 was added per 200 µL of liquid within a 96-well plate well, already containing the differentiated and NTP-treated U937 cells to be analysed, and left for 24 hours. All the liquid was then removed, and the well washed twice with 300 µL of DPBS with calcium and magnesium (Lonza, Basel, Switzerland) to remove non-phagocytosed beads prior to examination by microscopy. This microscopy was carried out with inverted microscopes (Carl Zeiss; Cambridge, UK or Motic; Barcelona, Spain), a SP8 inverted confocal microscope (Leica; Wetzlar, Germany) and a ZOE fluorescent imager (Bio-Rad; Hercules, California, USA).

2.3.9 PI staining and imaging

For staining with propidium iodide (PI), a nuclear stain, cells were first fixed in a 96-well plate with 100 µL of 4 % (v/v) formalin in PBS (Sigma-Aldrich; Darmstadt, Germany) per well. The formalin was left for 20 minutes before being removed, and the wells were then each washed three times with 200 µL of PBS. Following the removal of the PBS, 100 µL of PI (20 µg/ml, diluted with pH 7.4 PBS) was added to each of the wells. The plate was then stored in the dark for two minutes by wrapping in metal foil. The PI was then removed, and the wells each received a further three 200 µL PBS washes. Finally, 200 µL of PBS was added to each well and left there until imaging was completed to prevent desiccation of the samples.

Imaging was carried out with an SP8 inverted confocal microscope (Leica; Wetzlar, Germany).

2.3.10 ELISA

The enzyme-linked immunosorbent assay (ELISA) technique was used to measure the concentration of chemokines and other ctyokines. There are several different ELISA types, however, the one used for all experiments in this project is the sandwich form (Figure 2.10). In summary, two antibodies specific for the target substance are used: a capture antibody, coated onto the plate to capture the target molecule within the sample, and a labelled detection antibody which then also binds to the target molecule, allowing its detection.

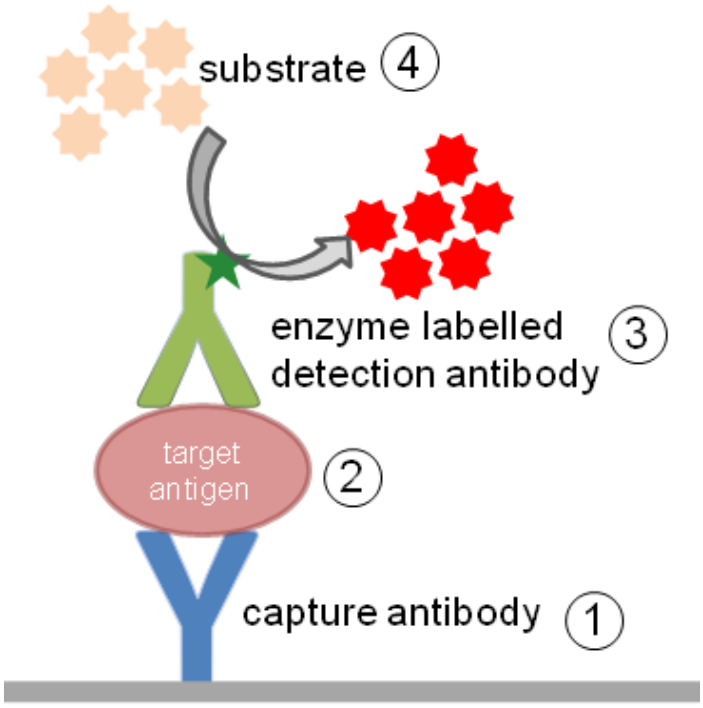

Figure 2.10. Schematic of sandwich ELISA. Reproduced from [218].

During this project, sandwich ELISAs were used to measure a total of 8 chemokines and cytokines. The following ELISA kits were used: IL-8 human uncoated ELISA kit with plates (product number 88-8086-22), MCP-1/CCL2 human uncoated ELISA kit with plates (88-7399-22), human RANTES uncoated ELISA kit (88-50287-88), MIG/CXCL9 human ELISA kit (EHCXCL9), TNF-α Human uncoated ELISA kit with plates (88-7346-22), IFN-γ human uncoated ELISA kit with plates (88-7316-22), IL-6 human uncoated ELISA kit with plates (88-7066-22), and IL-1β human uncoated ELISA kit with plates (88-7261-22) (Invitrogen; Waltham, Massachusetts, USA).

The cell supernatant subject to ELISA was harvested into 2 ml microcentrifuge tubes, which were then centrifuged at 1600 rpm for 10 minutes in a microcentrifuge to separate out any cell debris. The supernatant from these tubes was then removed and placed in fresh tubes, then frozen at -80 °C until use. When the samples were required for the ELISA, they were defrosted at 37 °C and assayed immediately. The ELISA kits were then used in accordance with the instructions. For most kits, the instructions were similar to those of the TNF-α kit.

For the TNF-α kit, a coating buffer was first made up by diluting the 10X PBS supplied with the kit to 1X using deionised water. The supplied 250X capture antibody was then diluted to 1X with this coating buffer before 100 µL of this capture antibody solution was added to each of the wells of the supplied 96-well plate. The plate was sealed with an adhesive plate sealer and placed in the fridge at 4 °C overnight. The following day, the liquid was removed from the wells, and the wells were washed three times with 250 µL of 0.05 % (v/v) Tween 20 (Sigma-Aldrich; Darmstadt, Germany) in PBS, with one minute of soaking time per wash, followed by vigorous blotting to remove all liquid. The supplied 5X ELISA/ELISPOT diluent was diluted to 1X with deionised water, and 200 µL of this 1X ELISA/ELISPOT was added to

each of the wells to block, with the plate then being resealed and incubated at room temperature for one hour. The liquid was then removed from the wells once again, and the wells were washed once with 250 µL 0.05 % Tween, with vigorous blotting afterwards to remove all liquid.

To create a standard curve, the TNF-α standard supplied with the kit was diluted to 500 pg/ml with deionised water. 100 µl of this was added to each of two wells. 100 µl of 250 pg/ml, 125 pg/ml, 62.50 pg/ml, 31.25 pg/ml, 15.63 pg/ml, 7.81 pg/ml, and 3.91 pg/ml TNF-α, all diluted down from the 500 pg/ml sample using 1X ELISA/ELISPOT diluent, were then also added to two wells each. 100 µL of each of the experimental samples was then also added to a well, as was 100 µL of 1X ELISA/ELISPOT diluent to act as a blank. The plate was then sealed and kept overnight in the fridge. Following this, the wells were again aspirated, washed five times with 0.05 % Tween, with one minute of soaking time per wash, and then vigorously blotted after the final wash to remove all liquid.

The supplied 250X detection antibody was then diluted with 1X ELISA/ELISPOT diluent, and 100 µL of this diluted detection antibody solution was added to each well, both those of containing the samples and those containing the standards. The plate was sealed and left for one hour at room temperature. Following this, the liquid was removed and the wells washed five times with 250 µL of 0.05 % Tween per wash, with one minute of soaking time per wash, and vigorously blotted after the final wash to remove all liquid. The supplied 100X streptavidin-HRP was diluted to 1X with 1X ELISA/ELISPOT diluent, and 100 µL of this 1X streptavidin-HRP was then added to each well. The plate was then sealed and incubated for 30 minutes at room temperature. The wells were then aspirated and washed seven

times with 250 µL 0.05 % Tween for each wash and blotted vigorously after the final wash to remove all liquid.

100 µL of the supplied 3,3',5,5'-tetramethylbenzidine (TMB) solution was added to each well, and the plate resealed and incubated at room temperature for 15 minutes. Following this, 2N sulphuric acid (H_2SO_4) (Fisher Scientific; Waltham, Massachusetts, USA) was added to the wells to stop the reaction. The plate was read at 450 nm and 570 nm in the plate reader, and the absorbance calculated as the 450 nm reading minus the 570 nm reading. Of the two sets of standard curve data generated, the one selected for use was the one that aligned most closely with the exemplar supplied with the kit.

This process outlines the method specific to the TNF-α kit. Most of the kits used a very similar series of steps, however, in some cases there were some slight variations. Specifically, some kits did not include the coating step as they were purchased pre-coated. Others used proprietary washes and stop solutions supplied as part of the kit rather than 0.05% Tween 20 and 2N H_2SO_4. Specified timings could also vary. In all cases, the instructions provided for the specific kit being used were followed.

2.3.11 RT-qPCR

The RT-qPCR technique was employed measure the effect of PAM treatment on the expression of several specific genes in differentiated U937 which relate to phagocytosis and antioxidant enzymes.

2.3.11.1 Background

As has been explained in 1.2.3.3.1, DNA molecules contain the genetic information of the cell, and the information within this is used to create specific functional substances, namely

proteins, as required by the cell (Figure 2.11). This process is known as genetic expression [219]. The intermediate step in the process is transcription of messenger ribonucleic acid (mRNA) from the gene within the DNA.

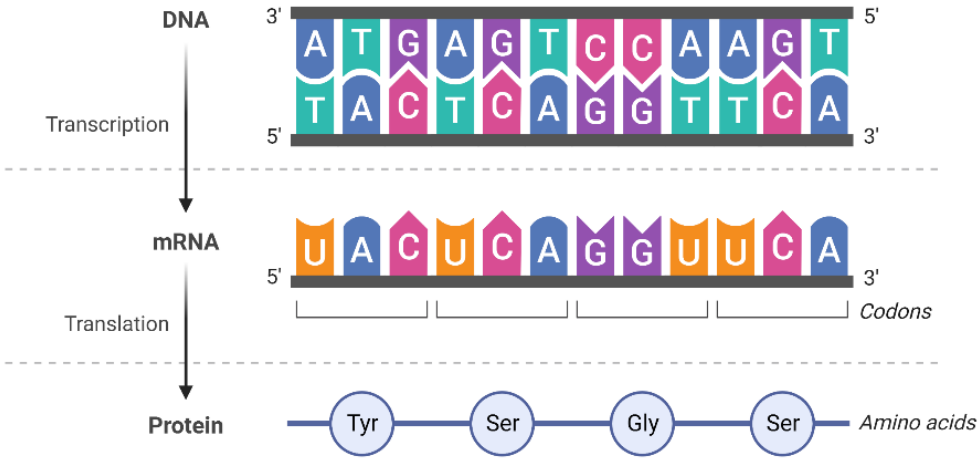

Figure 2.11. Genetic expression via transcription of DNA to mRNA, and subsequent translation of mRNA to protein. Reprinted from "Central Dogma", by BioRender.com (2023). Retrieved from [3].

Polymerase chain reaction (PCR) is a well-established technique amplifying specific sections of nucleotides [220]. A modification of this, known as RT-qPCR (quantitative reverse transcription polymerase chain reaction), or sometimes reverse transcription PCR (RT-PCR) or quantitative PCR (qPCR), is capable of quantifying the level of expression of a gene [220]. In order to do this, the mRNA from the cell which, as shown in Figure 2.11, will give an indication of the expression of a gene, is first isolated. Following on from this, a reverse transcription process is carried out to create DNA complementary to this, the amount of which will reflect the amount of the complementary mRNA present. This DNA is then subjected to the amplification process of PCR.

2.3.11.2 RT-qPRC methods

There were several stages to the preparation of RT-qPCR samples, and the RT-qPCR process itself used during this project (Figure 2.12). Each of these processes is covered sequentially in the following sections.

Diluted PAM treatment of U937 cell samples

↓

Lysis of treated cells

↓

Total RNA isolation and assessment of RNA concentration

↓

Production of cDNA

↓

RT-qPCR cycles

↓

Interpretation of results

Figure 2.12. RT-qPCR process from PAM treatment of samples through to interpretation of results.

2.3.11.2.1 Plasma treatment of U937 cell samples and lysis of these cells

All RT-qPCR experiments were carried out using diluted PAM applied to differentiated U937. To ensure that there would be sufficient RNA to carry out the RT-qPCR, two samples of PAM were combined for each replication of the experiment, allowing sufficient PAM to apply to four wells of cells to create each RNA sample. 40 µL of PAM was added to each well for one hour.

Upon removal of the PAM, the cells were washed with 200 µL of PBS. When this was also fully removed, each set of 4 wells was then lysed in a total volume of 250 µL of lysis solution. This lysis solution was made up of 10 µL of 2-mercaptoethanol to 1 ml of proprietary lysis buffer, both supplied as part of a GenElute Mammalian Total RNA Miniprep Kit (RTN70) RNA isolation kit (Sigma-Aldrich; Darmstadt, Germany). This lysis solution was left within the sample wells for two minutes, with rocking and tapping of the plate, before being harvested and the liquid from the four wells combined, and then frozen at -80 °C in microcentrifuge tubes until the RNA isolation stage.

A range of timings between treatment applications and cell lysis for mRNA isolation appear in the plasma medicine literature, with Shi *et al.* adding PAM for one hour only prior to immediate isolation [221], as opposed to Adachi *et al.* who applied PAM for three [222] or six hours prior to mRNA harvesting [223][224]. Considering work performed outside of plasma medicine, Archer *et al.* [225] found that mRNA in murine cells reached peak transcription rate at 30 minutes to one hour following dexamethasone exposure, and peak absolute mRNA was between six and eight hours after exposure. Taking all this information into account, it was decided that the treatment and lysing protocol used on this project would involve the cells being subjected to one hour of PAM exposure followed by immediate lysing. This decision was made as these timings should be sufficient to detect any change in mRNA production triggered by the PAM application, but at the same time would keep the applied treatment in line with those carried out during other experiments throughout the project. It is acknowledged, however, that any change in mRNA levels triggered by PAM application might be more pronounced if cell lysis was carried out at a later timepoint, and with a longer exposure to PAM.

2.3.11.2.2 Total RNA isolation and assessment of RNA sample purity

The cell lysate samples were defrosted at room temperature for a few minutes prior to the commencement of RNA isolation. The isolation process was performed using the GenElute Mammalian Total RNA Miniprep Kit mentioned above.

Samples were first filtered using the filtration columns supplied by the kit. This involved the filtration column being placed in a 2 ml microcentrifuge tube, and the cell lysate sample being pipetted into the column. The microcentrifuge tube containing the column was then centrifuged at 16,000 g for two minutes. The column was then discarded.

250 µL of 70 % ethanol solution (Honeywell Riedel-de Haën; Seelze, Germany) was then added to the lysate. A binding column was set up in a new microcentrifuge tube, and this mixture of lysate and ethanol was then pipetted into the column. The tube containing the column was then centrifuged at 16,000 g for 15 seconds. The liquid in the tube was discarded, then the binding column was returned to the tube. 500 µL of the supplied Wash Solution 1 was added to the binding column, and the tube and column were again centrifuged at 16,000 g for 15 seconds. The tube and liquid were then discarded, and the binding column was placed in a new microcentrifuge tube.

60 ml of 100 % ethanol (Honeywell Riedel-de Haën; Seelze, Germany) was then added to the supplied bottle of Wash Solution 2. 500 µL of this was then added to the binding column, and the binding column and tube were then centrifuged at 16,000 g for 15 seconds. The liquid was then discarded. A second wash with the mix of ethanol and Wash Solution 2 was then carried out, using the same volume, but with a longer centrifuging time of two minutes, extended to three minutes if the binding column still appeared wet. The binding column was then placed in a new microcentrifuge tube. 50 µL of the supplied

Elution Solution was then added to the column, and the tube and column were centrifuged for one minute. The binding column was subsequently discarded.

Following this, the sample was subjected to DNase to remove any DNA present within it. Amplification Grade DNase (Sigma-Aldrich; Darmstadt, Germany) was used, following the instructions supplied by the manufacturer. 5 µL of the supplied 10X reaction buffer was added to the eluted RNA sample, alongside 5 µL of Amplification Grade DNase I. This was then incubated at room temperature for 15 minutes. 5 µL of the supplied Stop Solution was then added to the sample, and the sample was heated at 70 °C in a water bath for 10 minutes. The extracted RNA was then frozen at -80 °C until reverse transcription was carried out.

2.3.11.2.3 Production of cDNA

Prior to carrying out reverse transcription on the RNA samples, the samples were defrosted at room temperature and the concentration of the RNA was measured using a NP80 nanophotometer (Implen; Westlake Village, California, USA).

SuperScript IV Reverse Transcriptase (200 U/µL) (SSIV) (Invitrogen, Waltham, Massachusetts, USA) was used as the reverse transcriptase for the creation of complementary DNA (cDNA). 700 ng of RNA, calculated from the measured concentration and which, assuming a 1:1 conversion from RNA to cDNA, would result in 700 ng of cDNA, was added to a 0.1 ml PCR tube. The volume was then made up to 11 µL with diethylpryrocarbonate (DEPC)-treated water (Invitrogen; Waltham, Massachusetts, USA). 1 µL of 50 µM Oligo d(T)20 primer (Invitrogen; Waltham, Massachusetts, USA) and 1µL of 10 mM dNTP mix (10 mM each) (Invitrogen; Waltham,

Massachusetts, USA) were added, giving a total volume of 13 µL in the tube. This was gently mixed by pipette, and the tube centrifuged at 0.2 g for one minute. The tube was then heated in a SimpliAmp thermal cycler (Applied Biosystems; Waltham, Massachusetts, USA) at 65 °C to anneal the primer to the RNA, following which the sample was placed on ice for one minute.

A reverse transcription reaction master mix was then prepared in a sufficient quantity for all samples. The volumes per sample were 1 µL of SSIV, 4 µL of 5x SSIV buffer (supplied with the SSIV pack), 1 µL of 100 mM DL-dithiothreitol (DTT) (supplied with the SSIV pack), and 1 µL of RNaseOUT Recombinant RNase Inhibitor (Invitrogen; Waltham, Massachusetts, USA). This was gently mixed by pipette and centrifuged at 0.2 g for one minute. An amount of 7 µL of this master mix was then added to each 700 ng RNA sample, bringing the total volume to 20 µL. The tubes were heated in the thermocycler set to a programme of 50 °C for 10 minutes, then 80 °C for a further 10 minutes. 1 µL *E.coli* RNase H (Invitrogen; Waltham, Massachusetts, USA) was then added to each sample before the sample was returned to the thermocycler at 37°C for 20 minutes to remove any remaining RNA. The cDNA was then diluted to a concentration of 2 ng/µL with DEPC water and the samples were stored at -20 °C until use in the RT-qPCR process.

Alongside the production of the cDNA samples, a parallel set of samples was produced for all RNA samples, exactly following the same process, but using 1µL of DEPC-treated water in the master mix instead of 1 µL SSIV. These samples were used a control during the RT-qPCR process to confirm the elimination of genomic DNA (gDNA).

2.3.11.2.4 RT-qPCR process

For each biological replicate, RT-qPCR was carried out on three technical replicates, with the resultant quantification cycle (C_q) values then averaged for use in the analysis of the results.

2.3.11.2.4.1 Primers and probes

Probe-based chemistry was used for all PCR experiments. All primers and probes were from the PrimeTime standard qPCR assay range (Integrated DNA Technologies; Coralville, Iowa, USA), which gives a combined mix of primers and probes. Both forward and reverse primers were supplied in amounts of 5 nmol, and all probes were supplied in amounts of 2.5 nmol and labelled with 5' 6-FAM/ZEN/3' IB FQ. The primers and probes came in powdered form and were diluted with 500 µL of proprietary "IDTE" (10 mM Tris and 0.1 mM Ethylenediaminetetraacetic acid (EDTA)) pH 8.0 buffer (Integrated DNA Technologies; Coralville, Iowa, USA), before being frozen at -20 °C until use, as specified in the manufacturer instructions. Further details of the individual primers and probes used for each gene are shown as part of the experimental work in 7.4.4.2 and 7.4.6, with those used for reference genes given in 2.3.11.2.4.4 below.

2.3.11.2.4.2 PCR master mix

The master mix used for all RT-qPCR experiments was Primetime Gene Expression Master Mix (Integrated DNA Technologies; Coralville, Iowa, USA), which was the recommended master mix for the probes and primers used. This was stored at -20 °C until use, at which point it was defrosted at room temperature and vortexed.

This master mix required the use of an added reference dye (carboxyrhodamine or ROX) for use with the RT-qPCR machine model available, and this dye was supplied with the master mix. In line with the manufacturer's instructions, 4 µL of this reference dye was added to 1 ml vials of the master mix, and 20 µL added to the 5 ml vials. This mixture was thoroughly vortexed prior to use to ensure even distribution of the dye throughout the liquid.

2.3.11.2.4.3 RT-qPCR cycles

All RT-qPCR experiments were carried out using a QuantStudio 5 Real-Time PCR System (Figure 2.13) and associated software (Applied Biosystems; Waltham, Massachusetts, USA) and MicroAmp Optical 96-Well Reaction Plate with Barcode (Applied Biosystems; Waltham, Massachusetts, USA).

Figure 2.13. QuantStudio 5 Real-Time PCR System. Photograph reproduced from [226].

For each cDNA sample, the volumes shown in Table 2.2 were used per well, with three technical replicates being run per sample. As well as the samples being tested, a control was run alongside for each gene on the plate, made up as in Table 2.2 but replacing the 2 µL of sample with 2 µL of DEPC water. Following addition of the liquid to the plate, the plate was sealed with an adhesive PCR plate seal (Thermo Scientific; Waltham, Massachusetts, USA), and was then centrifuged in a mini plate centrifuge for 20 seconds, before being placed in the RT-qPCR machine, and the thermocycling process being run.

Table 2.2. Liquid volumes used per well for RT-qPCR process. Liquids used as described above.

Substance	**Volume (µL)**
Sample (2 ng/µL cDNA)	2 µL
Master mix	10 µL
Primer/probe (20 X)	1 µL
Water	7 µL

The thermocycling process carried out by the RT-qPCR machine consisted of an initial stage of 95 °C for three minutes for polymerase activation, followed by an activation stage of 40 cycles of denaturisation at 95 °C for 15 seconds and an annealing/extension phase of 60 °C for one minute. C_q data was saved at the end of each 60 °C section.

2.3.11.2.4.4 Reference genes

Four potential reference genes were identified from literature related to plasma-cell interactions and work relating to U937: HRPT1, B2M, GAPDH and β-actin. Further details of the papers which were consulted to reach this conclusion are shown in Appendix E. Details

of the primers and probes used (Integrated DNA Technologies; Coralville, Iowa, USA) for each of these reference genes are given in Table 2.3.

Table 2.3. Reference gene primers and probes. Shown are the nucleobase sequences for the two primers, forward and reverse, which were supplied, as well as the sequence of the probe. Also shown for the probe are the fluorophore (56-FAM) and quencher (3IABkFQ). Also shown in the GC content, which is optimally between 40 % and 60 % of the bases in the primer [227], and the melting temperature (T_m) which is ideally between 55 °C and 70 °C, and within 5 °C for the primer pair [228].

Gene and manufacturer sequence name	**Primer/probe**	**Number of bases**	**Sequence**	**GC content (%)**	**T_m (50 mM NaCl (°C))**
GAPDH (human) Hs.PT.39a.22214836	Primer 1 (forward)	22	TGT AGT TGA GGT CAA TGA AGG G	45.5	54.39479321
	Primer 2 (reverse)	19	ACA TCG CTC AGA CAC CAT G	52.6	54.93481027
	Probe	25	/56-FAM/AAG GTC GGA /ZEN/GTC AAC GGA TTT GGT C/3IABkFQ/	52.0	60.84055582
HPRT1 (human) Hs.PT.58v.45621572	Primer 1 (forward)	21	GCG ATG TCA ATA GGA CTC CAG	52.4	55.10686976
	Primer 2 (reverse)	22	TTG TTG TAG GAT ATG CCC TTG A	40.9	53.79487134
	Probe	31	/56-FAM/AGC CTA AGA /ZEN/TGA GAG TTC AAG TTG AGT TTG G/3IABkFQ/	41.9	59.8228233
B2M (human) Hs.PT.58v.18759587	Primer 1 (forward)	20	ACC TCC ATG ATG CTG CTT AC	50.0	54.87680537
	Primer 2 (reverse)	23	GGA CTG GTC TTT CTA TCT CTT GT	43.5	53.78807331
	Probe	23	/56-FAM/CCT GCC GTG /ZEN/TGA ACC ATG TGA CT/3IABkFQ/	56.5	61.72417168
ACTB (human) Hs.PT.39a.22214847	Primer 1 (forward)	17	CCT TGC ACA TGC CGG AG	64.7	56.89996923
	Primer 2 (reverse)	17	ACA GAG CCT CGC CTT TG	58.8	55.16512452
	Probe	21	/56-FAM/TCA TCC ATG /ZEN/GTG AGC TGG CGG /3IABkFQ/	61.9	62.09733267

To determine which of the reference genes were the most suitable for use with the treated samples being examined, RT-qPCR was run on three biological replicates of cDNA samples, and on three technical replicates of each biological replicate, for each of the four possible reference genes. This was achieved using the volumes stated in Table 2.2 and using the thermocycling programme detailed above. Once the data had been obtained, the C_q data generated for each of the technical replicates for each gene were entered into the RefFinder website [229][230], which ranked the genes for suitability as shown in Table 2.4. From this, it could be concluded that B2M was the most appropriate housekeeping gene, and it was therefore this that was used as the reference gene for all following work.

Table 2.4. Reference gene recommendations from RefFinder, which uses C_q data to determine suitability of a gene relative to others based on its stability with treatment. To do this, it analyses the results from four different methods of assessment (Delta C_t, Bestkeeper, Normfinder and Genorm) before determining an overall recommendation.

Method	**Ranking**			
	1	2	**3**	**4**
Delta C_t	B2M	GAPDH	HRPT1	ACTB
Bestkeeper	B2M	ACTB	HRPT1	GAPDH
Normfinder	B2M	GAPDH	HRPT1	ACTB
Genorm	HRPT/B2M	-	GAPDH	ACTB
Recommended comprehensive ranking	**B2M**	**HRPT1**	**GAPDH**	**ACTB**

The absence of contamination of gDNA in all samples was also confirmed at this stage by performing RT-qPCR portions of these samples which had not undergone reverse transcription to create cDNA. The absence of detection of a commonly expressed gene, specifically the β-actin gene, provided confirmation that there was no gDNA contamination.

2.3.11.2.4.5 Selection of genes of interest

Potential genes of interest were confirmed as being expressed in white blood cells using the "Illumina bodyMap2 transcriptome" gene expression data for each individual gene, accessed via the gene's page on the National Center for Biotechnology Information's website [231].

2.3.11.2.4.6 Analysis of PCR results

In order to determine gene expression fold changes, the $\Delta\Delta C_T$ method of calculation, as described at [232], was used.

When analysed for gene expression, water-only samples should ideally give a C_q value which is undetermined, indicating that the qPCR machine has not been able to identify the presence of cDNA after the full programme of cycles. However, in some situations a C_q value may be obtained in a water-only sample, indicative of contamination of one or more of the reagents in the well from sources such as from handling of pipettes, or contamination of, for example, the water being used. The presence of a value for C_q for water-only samples may not be a problem as long as the C_q value is much higher than that of the test samples, due to the exponential nature of the $\Delta\Delta C_T$ method. Therefore, for the qPCR work undertaken on this project, replicates were discounted only if there was a

difference of less than 10 in the C_q values for any of the treated samples versus that of a water-only sample tested for the same gene.

2.3.12 Image processing, data processing, statistical analysis and figure creation

Image processing was carried out on some microscopy photographs, specifically adjustment of brightness of images, addition of scale bars, colouration of fluorescent images, and the addition of arrows. This was mostly carried out using ImageJ opensource software, with some work being performed using Zen Blue software (Zeiss; Oberkochen, Germany).

Numerical data from biological experiments was entered into Excel (Microsoft; Redmond, Washington, USA), and this software was used for calculations using these data. Assessment of statistical significance was performed using SPSS version 27 and earlier versions (IBM; Armonk, New York, USA). Graphs were created using Origin 2018 and its predecessors (OriginLab, Northampton, Massachusetts, USA) or, for straightforward graphs, using Excel.

Chapter 3 Electrical characterisation of reactor

3.1 Aims

The aim of this chapter was to develop a basic understanding of the electrical characteristics of Reactor 1, the reactor used throughout this project, as well as how these characteristics changed over a treatment time of 30 minutes.

3.2 Introduction

Reactor 1 (shown in 2.1.1.1, with electrical parameters given in 2.1.2) produces DBD. An explanation of this discharge type was given in 1.2.3.2.

3.3 Methods

3.3.1 Treatment liquid

For all experiments within this chapter, Reactor 1 was operated with a starting volume per 96-well plate well of 325 µL of room temperature, FBS-free DMEM without added antibiotics or NEAA.

3.3.2 Measurement of discharge power

Measurement of the discharge power of Reactor 1 was made using the Lissajous method, as described in 2.1.3.4. Measurements of the discharge power were taken immediately following switching the power on (3.4.1) and at intervals up to 30 minutes of run time (3.4.2).

3.3.3 Current measurement

Current was measured as described in 2.1.3.3.

3.4 Results

3.4.1 Initial discharge power and external current

Lissajous diagrams, as described in 2.1.3.4, were produced from measurements taken at the beginning of a treatment in Reactor 1, as soon as possible after the power was switched on (Figure 3.1). It was possible to identify two discharging and two non-discharging sections, as would be expected, with the transitions between the non-discharging and discharging sections well defined. It was found that the discharge power was an average of 438.5 mW (SE = 23.7 mW, n= 5), using the MATLAB code of Appendix C. The breakdown voltage, which is taken as the crossing point of the Lissajous figure with the x-axis, was found to average -1439 V (SE = 258 V, n=5). This figure was based on the discharging section between C and D, as this is approximately linear on the Lissajous diagram, rather than on the section other discharging section from A to B, which has a stepped appearance and therefore may be less accurate to use as a basis for the assessment of the breakdown voltage (Figure 3.1).

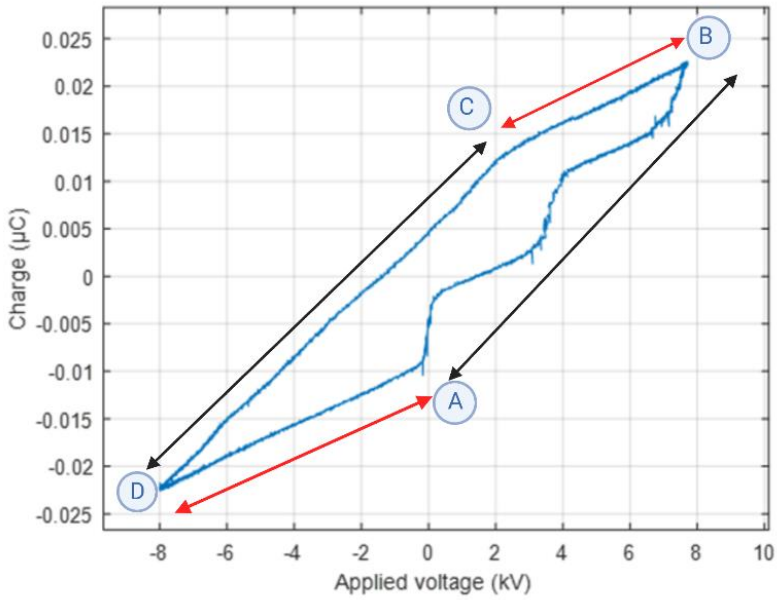

Figure 3.1. Reactor 1 Lissajous figure immediately following commencement of discharge. Lissajous figure plotted from oscilloscope data in blue, non-discharging regions identified with red arrows, discharging regions identified with black arrows. Created with Biorender.com [6] using data gathered from experimentation.

From the Lissajous diagram, it can be observed that the charge transfer across the discharging sections is in the region of 30 nC. As has already been noted, there is a clear difference in character between the discharging regions in the positive and negative parts of the cycle, with the negative half of the applied voltage wave (CD) giving discharge which appears as a straight line, suggestive of a discharge which occurs steadily throughout the discharging period, whereas the form of the discharging region in the positive part (AB) is likely to be indicative of the discharge consisting of groupings of pulses [77]. It would be expected that, in the sections of AB which are parallel with the non-discharging sections (BC and DA), no discharge would be occurring, with the discharge instead only occurring in the

parts of AB which have a steep gradient. From Figure 3.1, this would suggest that there are three pulses of discharge within AB.

This difference in discharge character between the positive and negative part of the cycle is not unexpected as such an effect has been observed elsewhere in similar reactor designs, notably with the similarly designed reactor of Tian *et al.* In their work, they found that the positive part of the cycle had streamer-type discharge emanating from the needle with some of these reaching the liquid beneath, while with the negative part of the cycle, the discharge had a diffuse, glow-like form (Figure 3.2).

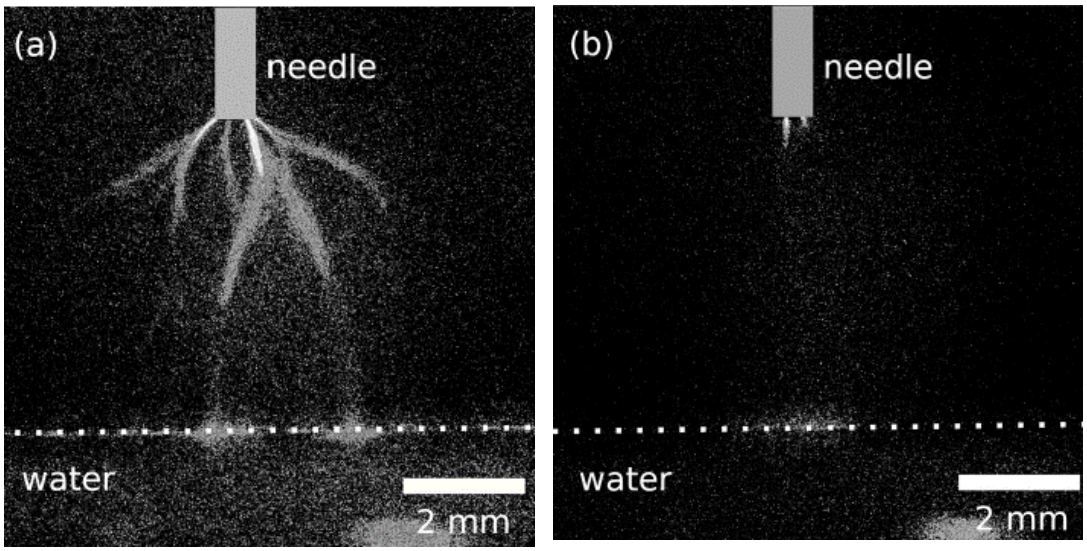

(a) (b)

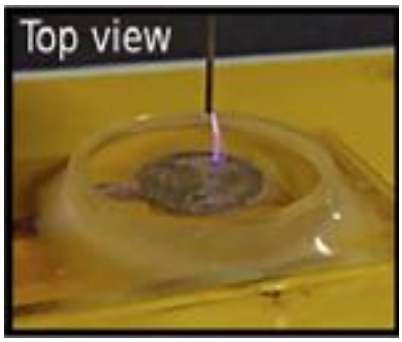

(c)

Figure 3.2. Discharge of Tian et al. reactor with 12 kV AC supply (a) in positive half-period (b) in negative half-period (c) photograph of reactor showing needle electrode suspended above grounded Petri dish containing water. All photographs reproduced from [204].

As well as considering the Lissajous diagram, the size and form of the current of the circuit was also assessed at the commencement of treatment (Figure 3.3). Here it was again apparent that the discharge in the positive and negative parts of the cycle were not of the same character, with the current trace demonstrating the pulsed nature of the positive half-period discharge and the more continuous, diffuse nature of the negative half-period.

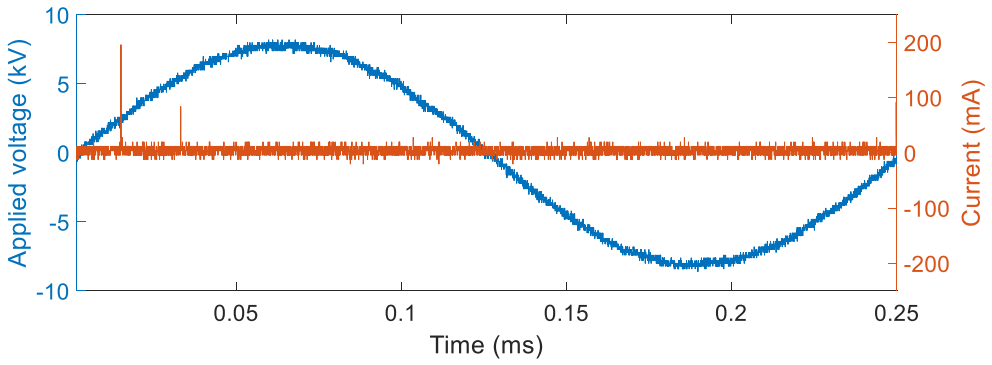

Figure 3.3. Reactor 1 current trace immediately following commencement of NTP treatment, alongside applied voltage wave.

The individual pulses in the positive part of the wave were also assessed. They were found to have a duration of around 0.1 µs and a magnitude in the region of 100-200 mA (Figure 3.4).

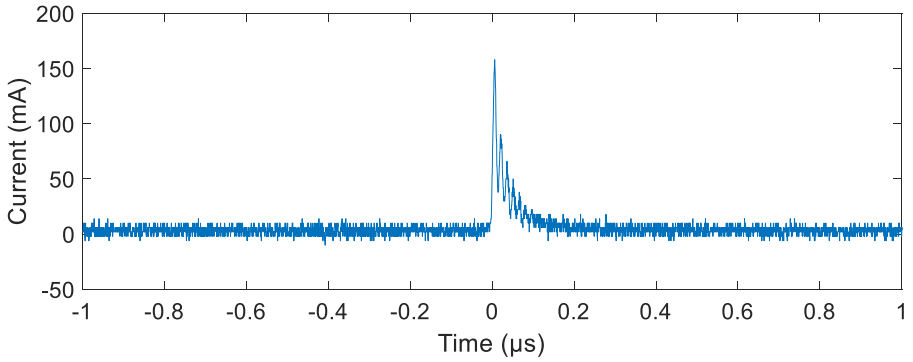

Figure 3.4. Individual discharge current pulses in increasing section of positive half-period of applied voltage wave, immediately following commencement of Reactor 1 treatment.

Assuming a magnitude of 200 mA, a duration of 0.1 µs, and a pulse which is perfectly triangular, this would suggest the charge per pulse is around 10 nC. Given that the charge transfer in Figure 3.1 is around 30 nC across the positive discharge part of the cycle, this would suggest that there should be around 3 of these pulses per across this discharge

section, something which agrees with the appearance of 3 bursts of discharge within Figure 3.1.

3.4.2 Evolution of discharge type over time

Following on from the measurements taken at the commencement of NTP treatment with Reactor 1, as discussed in 3.4.1, further Lissajous figures were produced following 15 and 30 minutes of continuous treatment (Figure 3.5). The Lissajous diagram from Figure 3.1 has also been reproduced as Figure 3.5(a) for ease of comparison against those from the later timepoints of 15 and 30 minutes.

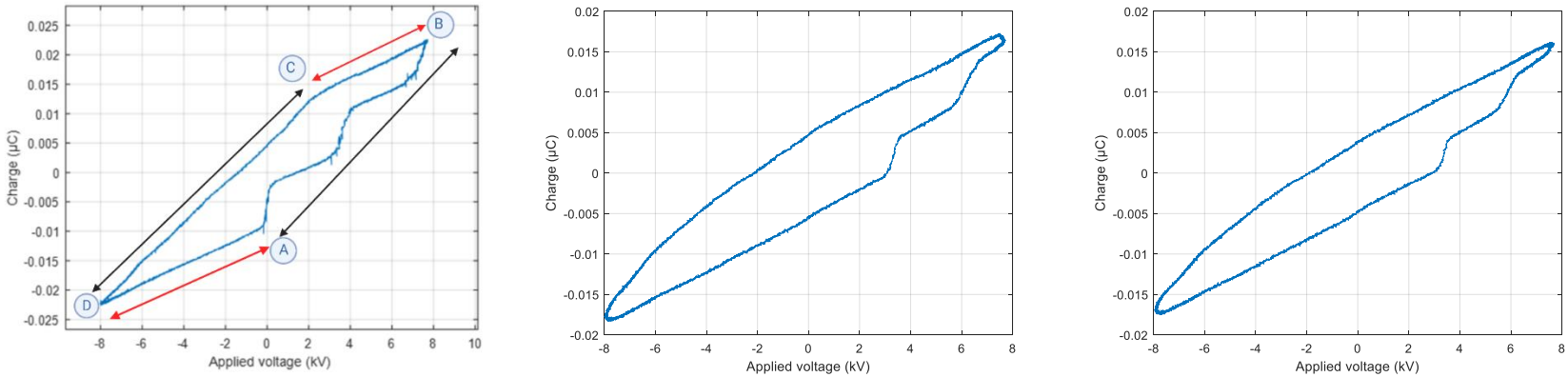

(a) (b) (c)

Figure 3.5. Lissajous diagrams of Reactor 1 discharge (a) at the beginning of treatment (b) following 15 minutes of continuous treatment and (b) following 30 minutes of continuous treatment. Figure 3.5(a) is reproduced from Figure 3.1, created with Biorender.com [6].

The discharge power after 30 minutes of continuous treatment was found to be an average of 468.6 mW (SE = 26.3 mW, n=5). The difference between this and the values for the discharge power immediately following the commencement of treatment were not found to be statistically significant (p = 0.420, independent t-test (two-tailed significance)) (Figure 3.6).

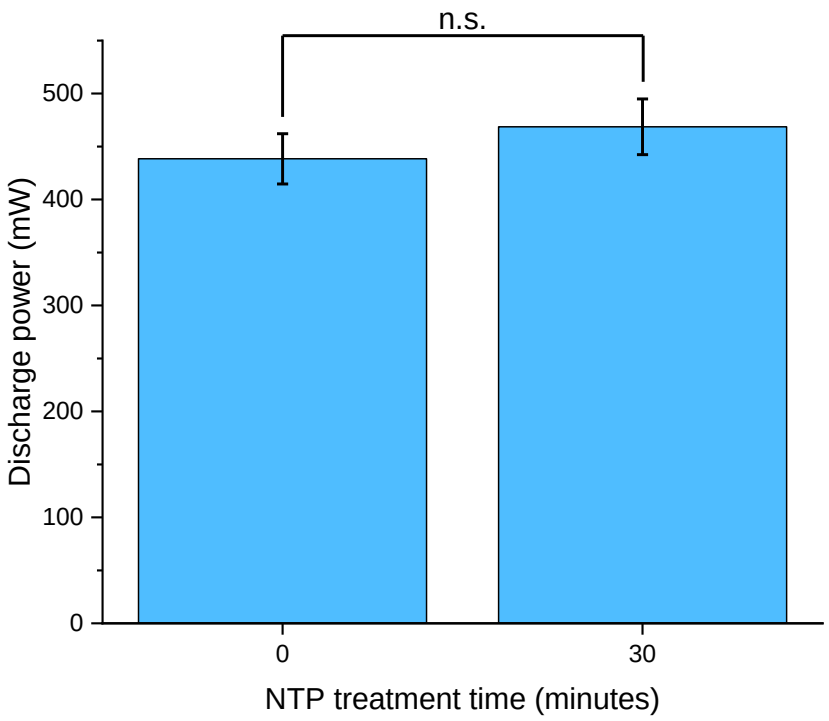

Figure 3.6. Discharge power of Reactor 1 calculated by Lissajous method immediately following the commencement of treatment and following 30 minutes of continuous treatment. n=5, SE shown, n.s. = not statistically significant, independent t-test.

It was noted that the breakdown voltage was an average of -2353 V (SE = 146 V, n = 5) following 30 minutes of continuous treatment. This had increased from the -1439 V average of the 0-minute Lissajous figures. In a homogenous field, the expected breakdown voltage can be calculated using Equation 3.1, where *p* represents pressure in Torr

(atmospheric pressure = 760 Torr), *d* represents the gap size in cm and V_b is the breakdown voltage in kV.

$$V_b = 6.72\sqrt{pd} + 24.36(pd) \quad (3.1)[233]$$

Using Equation 3.1, it was possible to calculate, with MATLAB, the equivalent gap size for the determined breakdown voltages at atmospheric pressure, assuming that they had occurred within a homogenous field. These were found to be 0.0750 cm or 0.75 mm for the 0-minutes breakdown voltage of -1439 V and 0.1236 cm or 1.24 mm for the 30-minutes breakdown voltage of -2353 V. It would be expected that in a non-homogenous field such as that created by a needle electrode [234], the gap sizes would be smaller for the same breakdown voltage than that calculated for a homogenous field, and thus it can be assumed that the gap size at the beginning of a Reactor 1 treatment is less than the 0.75 mm calculated above.

The situation beyond this timepoint is more complicated than it may at first appear. Certainly, the breakdown voltage after 30 minutes of treatment exceeds that at 0 minutes, which would be expected given that the liquid level would be reducing due to evaporation (4.4.3). However, although it is not possible to accurately measure the distance between the needle tip and the liquid surface due to the narrow confines of the well combined with the surface tension of the liquid, it is apparent that the gap size increases by several millimetres over a 30-minute treatment, with it being visibly clear that the distance between the needle tip and water surface far exceeds 1.24 mm as calculated above. Thus, it can be said that the breakdown voltage at this time is unexpectedly low. It was also notable from Figure 3.5(b) and Figure 3.5(c) that there is, in comparison to Figure 3.5(a), a loss of clarity between the non-discharging section B to C with the discharging section C to

D, with the whole section from B to D instead forming a smooth curve. This, coupled with the observations about the breakdown voltage raises questions as to whether there is a change in the mode of discharge somewhere between the beginning of the NTP treatment and the 15-minute timepoint.

To further investigate this, a series of Lissajous were taken at shorter time intervals in the period between the beginning of a treatment and the 5-minute timepoint (Appendix F). From a review of this series of diagrams, the change in discharge type was not gradual over the first 15 minutes of treatment, but rather occurred somewhere in the region of 1 minute 45 seconds to 2 minutes (Figure F.1(h) and (i)). The breakdown voltage was also determined for the same timepoints (Figure 3.7). This was found to have increased gradually over the 5 minutes of treatment before reaching approximately that of the 30-minute treatment by 5 minutes (average of -2353 V, SE of 147 V for a 30-minute treatment versus average of -2355 V, SE of 113 V for 5-minute treatment). Further investigation found that, between the 5-minute and 30-minute timepoints of treatment, the breakdown voltage remained stable (Figure 3.8). There is therefore significant evidence that there is a change in the discharge mode occurring somewhere in the first 5 minutes of a treatment, and this new mode continues throughout the remainder of a full 30-minute treatment.

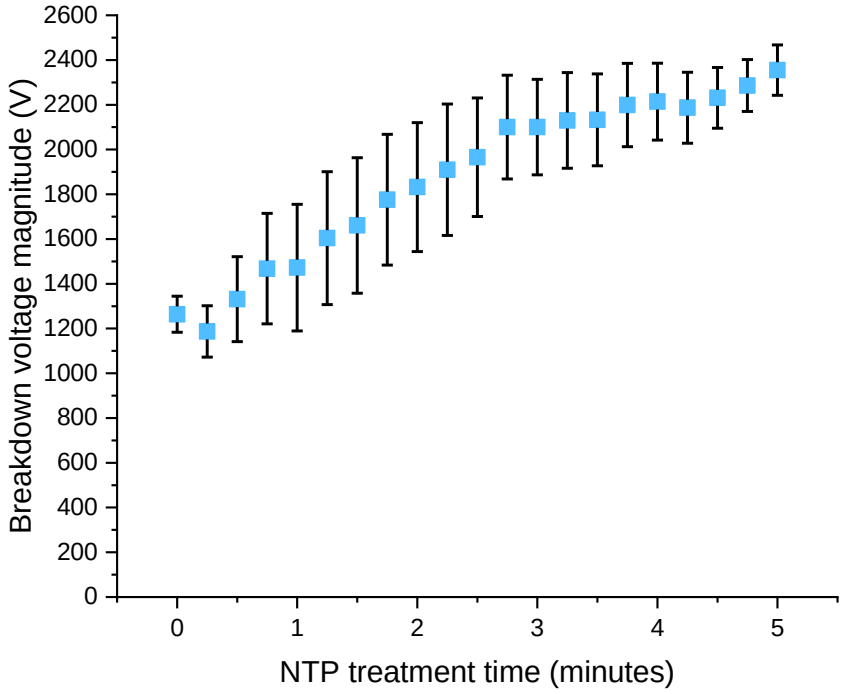

Figure 3.7. Breakdown voltage derived from Lissajous figures at 15 second intervals for 5 minutes. n=6, SE shown.

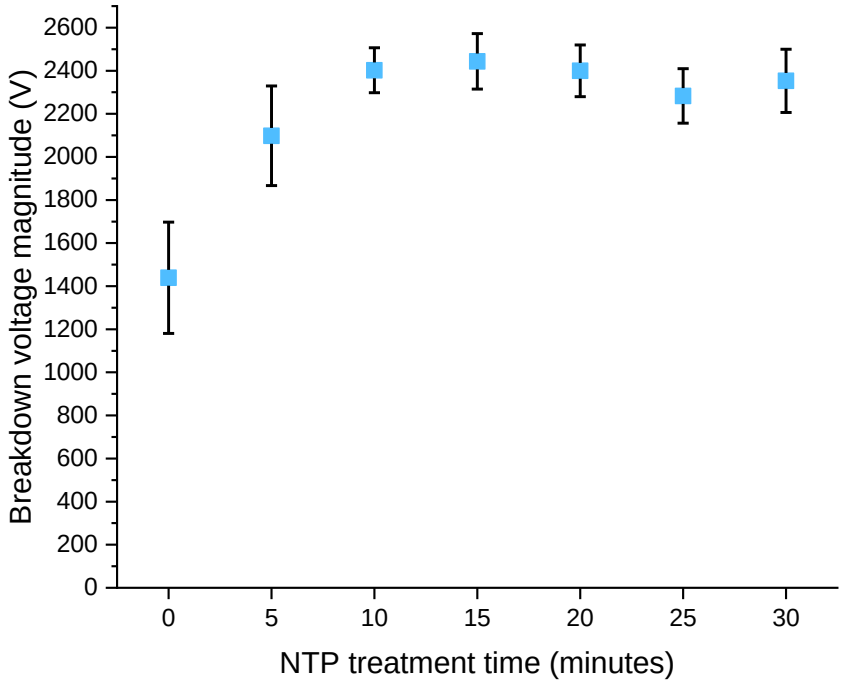

Figure 3.8. Breakdown voltage derived from Lissajous figures at 5-minute intervals for 30 minutes. n=5, SE shown.

This is supported by considering the current traces at the 15- and 30-minute timepoints (Figure 3.9). It was noted that the maximum discharging current peak appears to be lower after 15 and 30 minutes than at the beginning of the treatment, in the region of 40 to 60 mA (Figure 3.10), which would not be expected if the discharge mode remained the same as it has been observed that increasing a DBD gap size should increase the current in the circuit [235]. There is also apparent lengthening of individual pulses by 30 minutes (Figure 3.11) in comparison with those at the beginning of treatment (Figure 3.4).

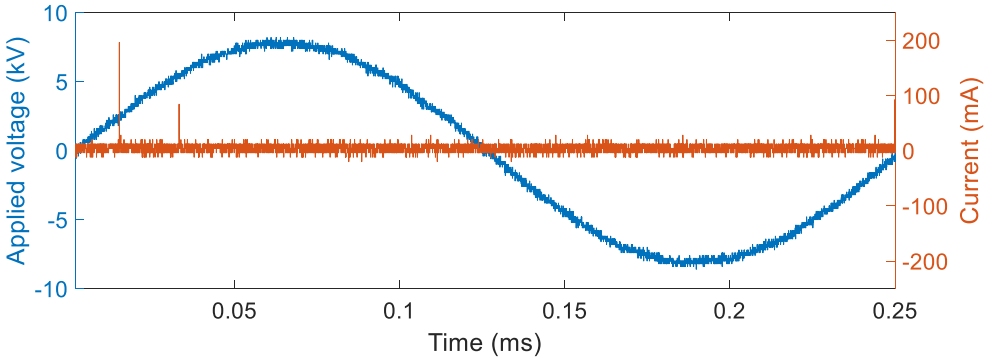

(a)

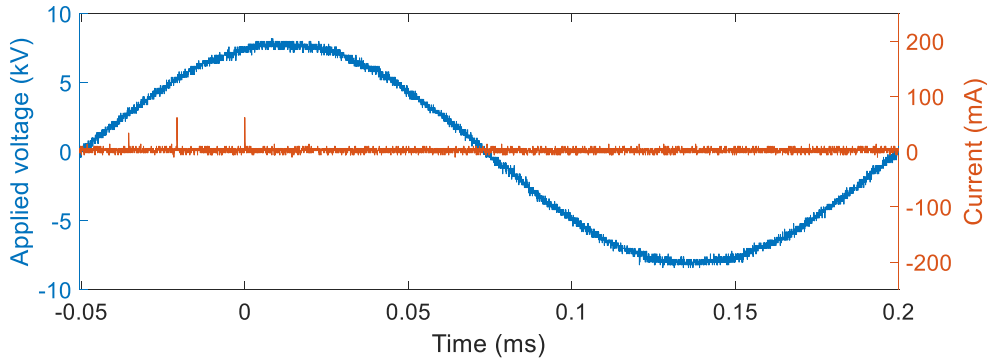

(b)

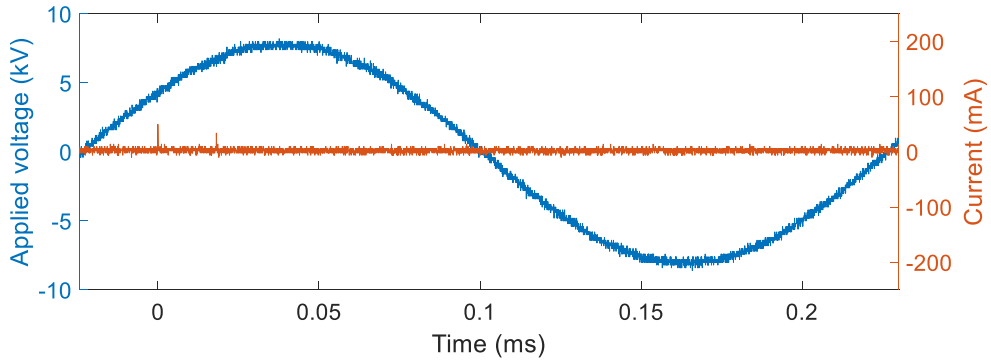

(c)

Figure 3.9. Current traces of Reactor 1 (a) immediately after commencement of treatment (b) after 15 minutes (c) after 30 minutes.

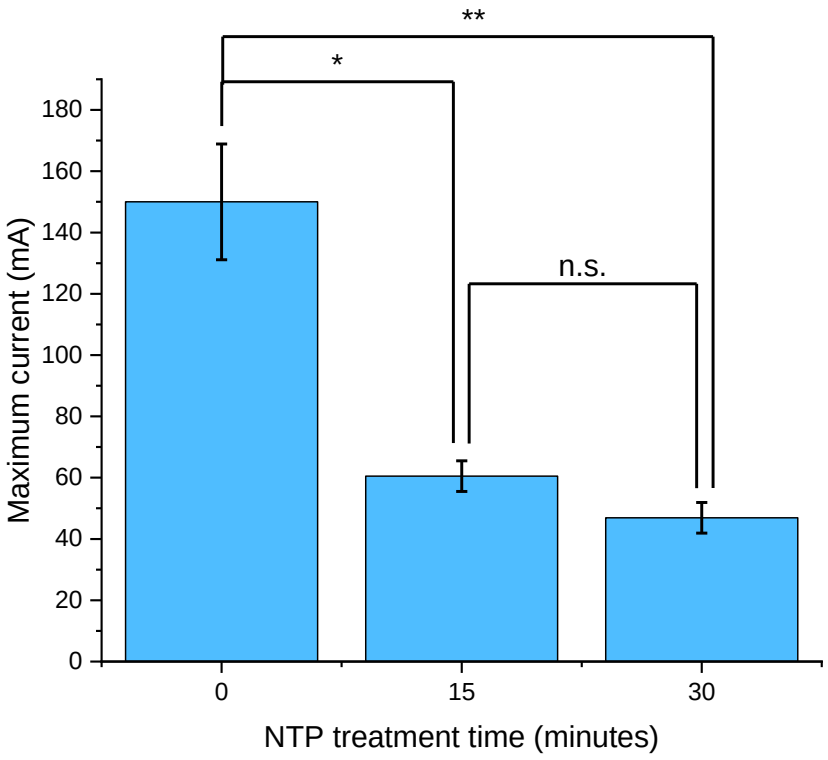

*Figure 3.10. Average peak current of Reactor 1. n=4, SE shown, *: p<0.05, **: p< 0.001, n.s: not statistically significant, ANOVA with Tukey HSD post-hoc. Difference between 0 and 15 minutes, and between 0 and 30 minutes statistically significant (p = 0.001 and p < 0.001 respectively). Difference between 15 and 30 minutes not statistically significant (p = 0.697).*

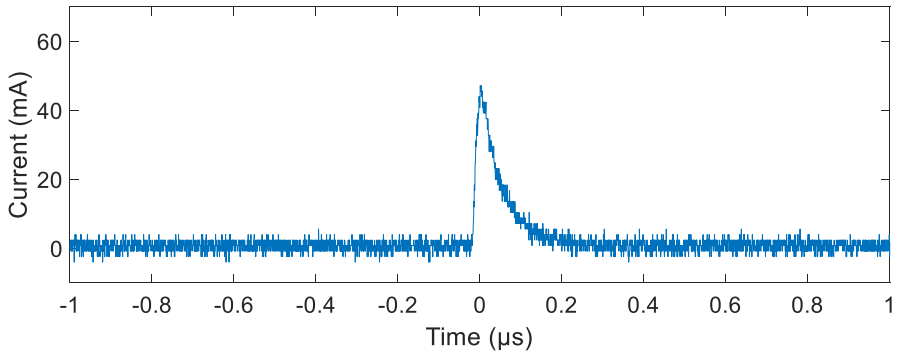

Figure 3.11. Individual discharge current pulse of Reactor 1 at 30 minutes.

3.5 Discussion

It was notable from the analysis of the discharge performed in 3.4.1 and 3.4.2 that there was a probable change in the form of the discharge between the commencement of an NTP treatment in Reactor 1 and the 15-minute timepoint. Further analysis revealed this change occurred early on in the treatment period, possibly as early as one to two minutes from commencement, but certainly by the 5-minute timepoint. Beyond this, the discharge appeared to stabilise in its new form.

It is thought that the most likely cause for the change in form is that, as the liquid level drops with increasing treatment time, the discharge switches from being between the needle and the surface of the liquid, with the base of the plate acting as the dielectric, to instead occurring between the needle tip and the side of the well as this becomes nearer the needle than the liquid surface (Figure 3.12). Due to the ground electrode being situated below the base of the wall, it is assumed that the discharge involving the wall results in a surface discharge down the side of the wall, especially given the walls will be wet, which is able to interact with the remaining liquid at the bottom, thus continuing to modify it chemically.

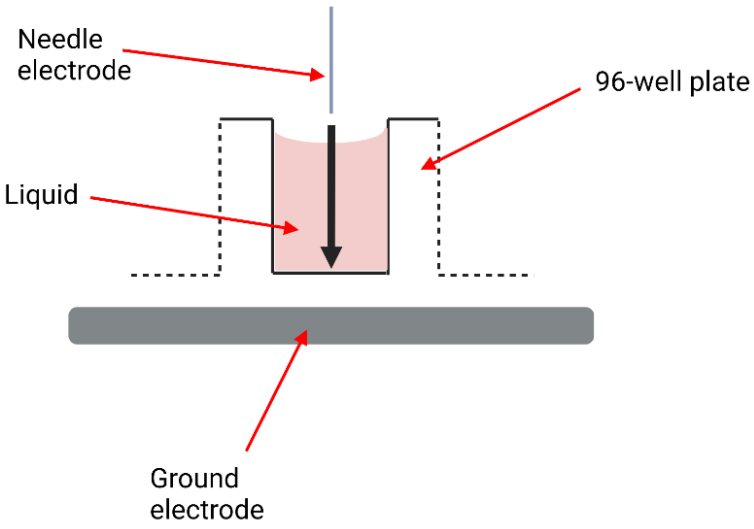

(a)

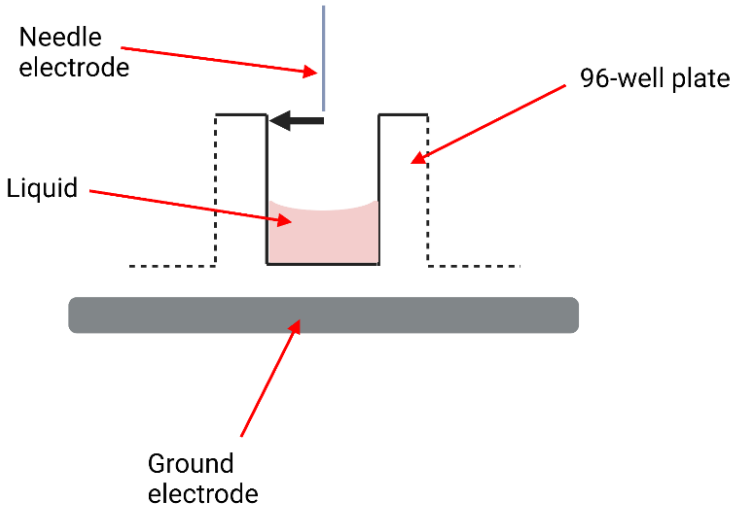

(b)

Figure 3.12. Schematic of assumed interaction between plate and discharge (a) form of initial discharge (b) discharge against wall after 30 minutes of treatment. Black arrows show direction of interaction between powered electrode and dielectric. Created with Biorender.com [6].

It was also considered whether the change in discharge mode discharge could be due to it transitioning to a form of corona discharge known as AC barrier corona (ACBC). One of the requirements for a corona discharge is a field enhancement in an area, something which occurs with needle-type electrodes [236], such as those which are present in Reactor 1. Lissajous figures for ACBC are known to show a similar loss of the sharp transition between non-discharging and discharging sections seen in Figure 3.5(b) and (c) (Figure 3.13). However, it is felt that the interaction with the side wall of the well is the more likely explanation given the stability of the discharge beyond the 5-minute timepoint despite the continually falling liquid level, with ACBC being less likely, given that the side wall of the well is in close proximity to the needle (given an area of the bottom of the well of 0.32 cm^2, the radius, and also approximately the distance between the needle tip and the side wall, would be around 3 mm).

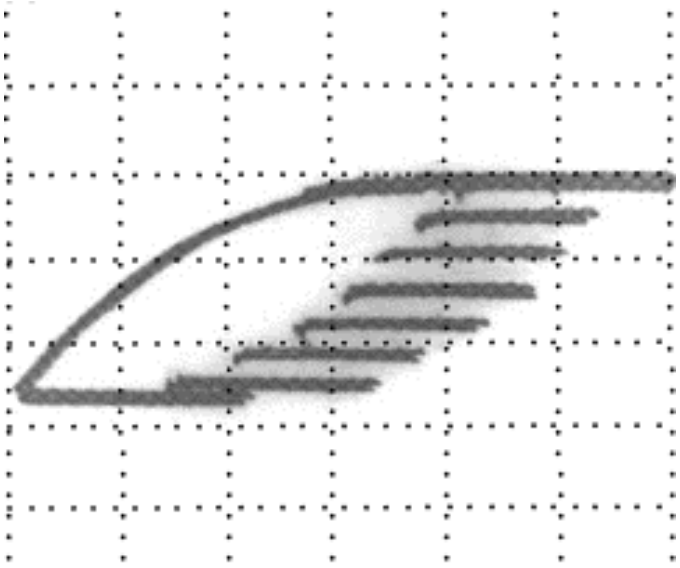

Figure 3.13. Lissajous figures for ACBC of Akishev et al. Reproduced from [237]. Note absence of sharp transition between non-discharging and discharging sections of the negative half period of the applied voltage wave.

The discharge mode was not analysed in detail until late on in the project, by which time a large portion of the work performed in Chapters 4 to 7 had already been performed. Although some biological work remained to be completed beyond this time, it was thought most appropriate to continue using Reactor 1 in the same manner as it had been used to that point in order to ensure comparability with earlier results. However, for future experiments, it would be proposed that the operating conditions of Reactor 1 are modified to remove the change in discharge mode so that the mode is consistent throughout an entire 30-minute treatment. If the speculation about the discharge in the latter part of a treatment occurring between the needle and side wall of the well is correct, then the modification may be as simple as slightly reducing the starting liquid level.

3.6 Conclusion

This chapter has detailed the investigation of the electrical characteristics of Reactor 1, designed to be used for the NTP treatment of *in vitro* cell samples. There were a number of key findings:

1. The initial discharge power was found to be an average of 439 mW. This remained stable over a 30-minute treatment time.
2. The discharge in the positive and negative half-periods of the applied voltage was found to differ in character. This is in line with the findings of other researchers using similar reactors.
3. The character of the discharge was found to change across a 30-minute treatment time. It is thought that the change occurred within the first five minutes of the treatment, and it is likely due to the reducing liquid level causing the discharge to be formed between the needle and side wall of the well.

Chapter 4 Chemical profile of reactor and illustration of diffusion effects in pin-plate DBD reactors

4.1 Aims

This chapter focuses on developing an understanding of the interactions between the NTP formed by Reactor 1 and liquid contained within the reactor at treatment times of up to 30 minutes, in order to gain an understanding of the environment that cells treated with the reactor would be subjected to. Specifically, the aims of the work discussed in this chapter were:

1. To measure concentrations of H_2O_2 and NO_2^- within the treated liquid and use these values for comparison against other NTP sources used for similar work in the field of plasma medicine. These two substances are not the only ones which it would be expected would arise, however they were used as indicator species due to their recognised biological prominence in NTP treatments, as well as their relative ease of measurement.
2. To measure temperature change, pH change and level of evaporation in the liquid treated in the reactor for up to 30 minutes in order to confirm that these would not have negative effects on biological samples in their own right.
3. To demonstrate the precision of NTP treatment with a pin-plate style of DBD reactor, using a modified version of Reactor 1 (Reactor 2) in terms of the affected cell layer area and show how this area varies both with treatment time, and also with time following the end of treatment.

4.2 Introduction

As Reactor 1 is a novel design for plasma medicine use, it was important to understand its production of H_2O_2 and NO_2^-, given their clear role in producing the effects of NTP treatment on cells (1.2.3.5). It was determined from the work performed within this chapter that the concentrations of both of these substances produced in liquid treated in Reactor 1 were of a suitable level for use in plasma medicine research, in comparison to those levels see in related literature.

It is also important to consider temperature and pH changes in liquid treated in Reactor 1 so that it can be confirmed that any biological effects of the treatment are due to factors specifically related to the NTP, rather than simply excessive heat or extremes of pH. Evaporation over the NTP treatment time has also been assessed below for Reactor 1 as this allows an assessment both of maximum running time of the reactor, as well as a better understanding of the formation of H_2O_2 and NO_2^-.

Alongside these measurements, work has been performed to understand the size of the area of the cell layer affected by a pin-plate DBD arrangement such as Reactor 1, using Reactor 2, and how this varies both with treatment time and diffusion beyond the end of the NTP exposure. This work is important because it shows the level of precision of the design when used for direct treatment, and also shows how this precision will reduce under certain circumstances. Understanding of this is critical for the development of such designs for *in vivo* or clinical work in the future. The issue of the effects of post-treatment diffusion do not appear to have been considered elsewhere.

4.3 Methods

All experiments in this chapter, except for those in 4.4.5, were carried out using Reactor 1 (2.1.1.1) using its standard electrical parameters (2.1.2). The diffusion experiments in 4.4.5 used direct plasma treatment provided by Reactor 2 (2.1.1.2), with the voltage applied to the reactor, determined as described as within Appendix G, being around 4.5 kV_m. H_2O_2 and NO_2^- measurement experiments used phenol red-free, FBS-free DMEM as the liquid subject to plasma treatment, whereas the pH measurement experiments used both this, and DPBS. For all other experiments, the treated liquid was FBS-free DMEM with phenol red. All liquid volumes at the beginning of the treatment were 325 µL where Reactor 1 was used and 2 ml where Reactor 2 was used, regardless of liquid type. H_2O_2 was measured using Amplex Red (2.2.4), and NO_2^- was measured using the Greiss method (2.2.5).

Temperature and evaporation were measured using the techniques described in 2.2.1 and 2.2.2, and pH was measured using pH sticks (2.2.3). All chemical analysis of the liquid was carried out as soon as practicable following the end of the treatment, and the treated liquids were thoroughly mixed by pipette prior to testing to ensure even distribution of any substances to be measured. NIH 3t3 cell samples were set up following the process in 2.3.1.1 and the area measurements carried out in 4.4.5 used MTT (2.3.5, 2.3.7).

Treatment times of up to 30 minutes of liquid exposure to NTP were considered throughout these experiments. This time was chosen as scoping experiments showed that this length of treatment gave a clear reduction in cell viability with 3t3.

4.4 Results and discussion

4.4.1 H_2O_2 and NO_2^-

4.4.1.1 H_2O_2 concentration

H_2O_2 concentration in treated liquid, created in Reactor 1 with standard electrical parameters (2.1.2), with treatment times of up to 30 minutes, was measured (Figure 4.1). In untreated liquid, an average concentration of 0 mM H_2O_2 (SE = 0 mM, n=5) was detected, rising to 0.8 mM (SE = 0.1 mM, n=5) with 5 minutes of NTP treatment, 1.1 mM (SE = 0.3 mM, n=5) with 10 minutes, 2.5 mM (SE = 0.3 mM, n=5) with 15 minutes and 5.2 mM (SE = 0.6 mM, n=5) with 30 minutes. It was found that the increase in concentration was approximately linear (r^2=0.85851), and occurred at a rate of ~175 µM/min.

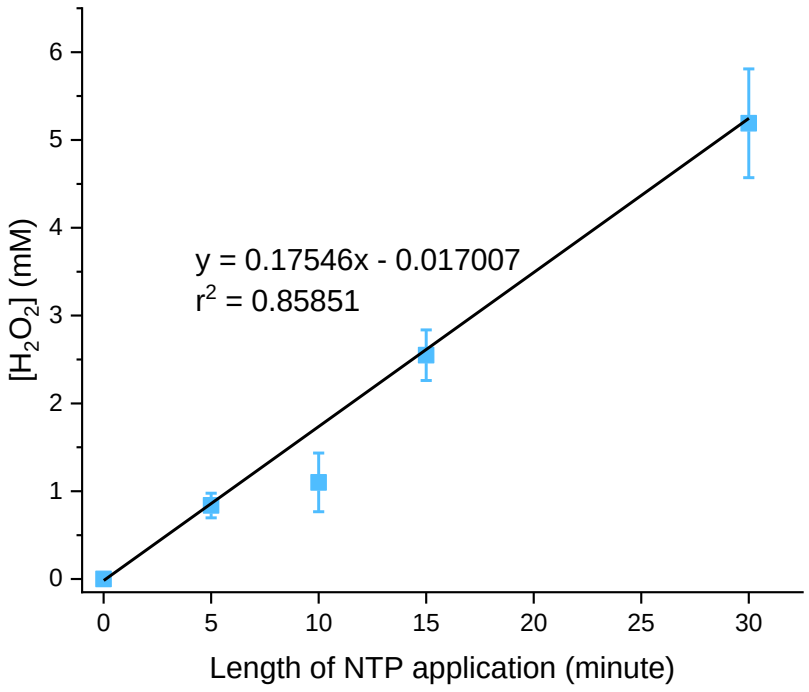

Figure 4.1. H_2O_2 concentration in serum-free, phenol red-free DMEM treated in Reactor 1, operated with standard electrical parameters. n=5, SE shown.

To summarise the results from Figure 4.1, concentrations of up to 5.2 mM of H_2O_2 were achieved in liquid treated in Reactor 1, and this concentration was reached in a manner that was approximately linear with time. Unexpectedly, the observed change in discharge mode around 1 minute 45 seconds to two minutes into treatment, as discussed in sections 3.4.2 and 3.5, and the apparent reduction in charge transfer in the discharging sections with longer treatments (Figure 3.5), did not appear to affect this linearity.

Elsewhere, it has been observed that, at least with fibroblasts, applied H_2O_2 concentrations of <0.1 mM have no toxic effect, with values of between 0.1 mM and 10 mM having a slow-acting toxic effect and >10 mM having a rapid toxic effect [181]. Assuming the treated liquid was applied to cells as a well-mixed PAM, this would therefore suggest that with fibroblasts, such as the NIH 3t3 cell line, Reactor 1 treatment times of below 40 s would not give a cytotoxic effect, and treatment times of between 40 s and 57 minutes would give a slow cytotoxic effect, based on regression analysis and the data in Figure 4.1, and assuming that the increase in concentration remains linear indefinitely beyond 30 minutes. This latter point is unlikely in reality given the rate of evaporation measured below (4.4.3).

Comparative H_2O_2 values for other NTP devices used in similar research operated are shown in Table 4.1, with final concentrations being as low as around 20-30 µM and as high as 1300 µM. Reactor 1 can give H_2O_2 concentrations at the top of this range within a reasonable timescale, approximately 7.5 minutes. Comparing Reactor 1 to the NTP sources within Table 4.2, the rate of increase in H_2O_2 concentration which could be described as moderate.

Table 4.1. H_2O_2 concentrations produced in selected biomedical NTP devices. The inclusion or omission of FBS is stated as it is known that this substance may reduce the concentration of H_2O_2 in NTP treatments, possibly due to the iron in the FBS initiating a Fenton reaction with the H_2O_2 [177][166]. Only papers in which the device is operated in its usual conditions have been considered, and thus papers such as [238] and [167], in which the surroundings were modified from the usual environment of air, have been omitted.

	Author	**NTP source**	**Treated liquid volume (µL)**	**Liquid type**	**Linear concentration increase?**	**Maximum H_2O_2 concentration measured (µL) with associated treatment time (s) in brackets**	**Rate of H_2O_2 concentration increase (µM/min)**
1	Balzer *et al.* [62]	DBD with flat electrodes	250	PBS	Yes	440 (450)	59
2	Bekeschus *et al.* [129]	kINPen argon (Ar) plasma jet	1000	RPMI 1640 with FBS	Yes	60 (60)	60
3	Chauvin *et al.* [163]	Helium (He) plasma jet	100	DMEM with and without FBS	Yes	600 with FBS (150) 600 without FBS (150)	640
4	Kurake *et al.* [166]	Ar plasma jet	3000	DMEM with FBS and without FBS	Yes	110 without FBS (300) 90 with FBS (300)	22 without FBS 18 with FBS

	Author	NTP source	Treated liquid volume (µL)	Liquid type	Linear concentration increase?	Maximum H_2O_2 concentration measured (µL) with associated treatment time (s) in brackets	Rate of H_2O_2 concentration increase (µM/min)
5	Girard *et al.* [161]	He plasma jet	500	PBS	Yes	1300 (240)	325
6	Horiba *et al.* [239]	Ar plasma jet, with wide plasma source.	4000	DMEM without FBS	No	90 µM (180)	Linear beyond 1 minute of treatment at rate of 40
7	Liu *et al.* [240][241]	He plasma jet	1000	RPMI 1640 with FBS	Yes	33 (75)	26
8	Mohades *et al.* [242]	"Plasma pencil" He jet	500	Minimum Essential Medium (MEM), assumed no FBS.	Linear for lowest voltage (5 kV) up to 1 minute, then at higher voltages saturated more quickly.	20-30 dependent on applied voltage (240)	n/a

	Author	NTP source	Treated liquid volume (µL)	Liquid type	Linear concentration increase?	Maximum H_2O_2 concentration measured (µL) with associated treatment time (s) in brackets	Rate of H_2O_2 concentration increase (µM/min)
9	Nguyen *et al*. [155]	Air plasma jet	Not stated	DMEM with FBS	Not known	40-45 (300)	n/a
10	Sato *et al.* [205]	DBD using pin anode and microtube	1000	MEM with FBS.	Yes	304 (210)	87
11	Wende *et al.* [243]	kINPen Ar plasma jet, moved over liquid surface	5000	RPMI 1640 with FBS	Yes	50 (180)	17
12	Wende *et al.* [156]	Radio frequency (RF) Ar plasma jet	100	PBS with 1g/l glucose.	Unknown	200 (60)	n/a

4.4.1.2 NO_2^- concentration

NO_2^- concentration in treated liquid, created in Reactor 1 with treatment times of up to 30 minutes under standard electrical operating parameters, was measured (Figure 4.2). In untreated medium, the concentration was found to be 0 (SE = 0), and it rose to 2.1 mM (SE = 0.1 mM) after 5 minutes of NTP treatment, 3.7 mM (SE = 0.4 mM) after 10 minutes, and 5.8 mM (SE = 0.1 mM) after 15 minutes, and 13.0 mM (SE = 0.3 mM) after 30 minutes. The increase in NO_2^- concentration was found to be approximately linear (r^2= 0.98988), with a rate of increase of ~424 µM/min.

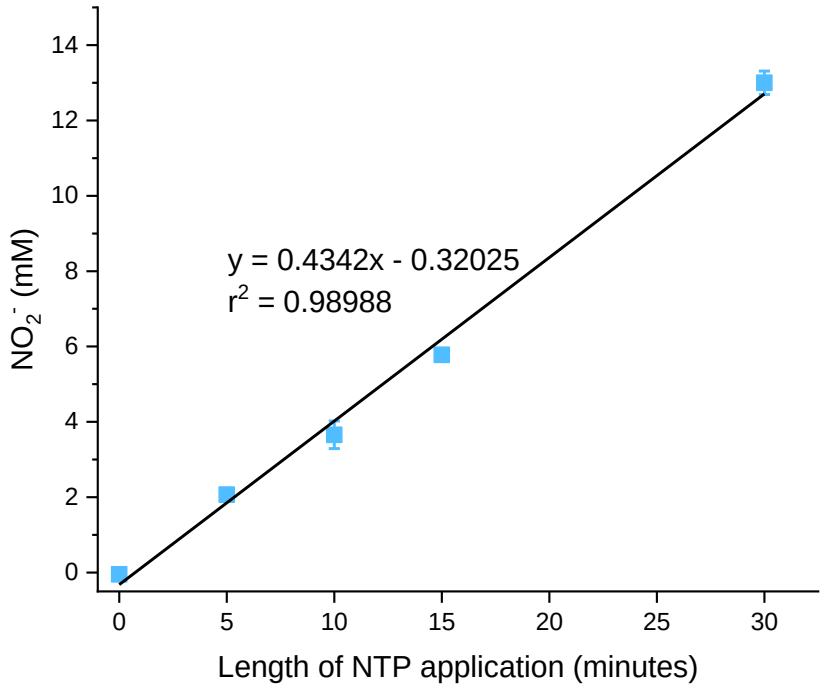

Figure 4.2. NO_2^- concentration in serum-free, phenol red-free DMEM treated in Reactor 1 operated using standard electrical parameters, against NTP treatment time. n=3, SE shown.

As with H_2O_2, NO_2^- also appears to have importance in the effects of NTP treatment on cells (1.2.3.5) although its role is less well understood. From Figure 4.2, NO_2^- concentrations of

up to an average of 13.0 mM were obtained in liquid treated in Reactor 1 for periods of up to 30 minutes, again with a linear increase. As with H_2O_2, the change in discharge mode early on in a treatment with Reactor 1 appeared to have little effect on this linearity. NO_2^- concentrations measured for a variety of NTP sources used for similar work are given for comparison (Table 4.2). From this, it can be seen that the range of maximum concentrations used in the research was from 10 µM to 3250 µM. Reactor 1 can obtain the highest of these concentrations within around 8.2 minutes of treatment, based on regression analysis (Figure 4.2).

Table 4.2. NO_2^- concentrations produced in selected biomedical NTP devices. Whether or not FBS is included within the treatment liquid is shown in the table as it is known that this substance may increase the amount of NO_2^- produced in NTP treatment [166].

	Author	**Device**	**Treated liquid volume (µL)**	**Liquid type**	**Linear concentration increase?**	**Maximum NO_2^- concentration measured (µM) with associated treatment time in brackets (s)**	**Rate of NO_2^- concentration increase (µM/min)**
1	Balzer *et al.* [62]	DBD with flat electrodes	250	PBS	Yes	400 (450)	53
2	Rödder *et al*. [244]	kINPen Ar plasma jet	1000	RPMI with FBS, or PBS	No	50 (20 s) for RPMI 60 (20) for PBS	n/a
3	Bekeschus *et al.* [129]	kINPen Ar plasma jet	1000	RPMI 1640 with FBS	Yes	32 (60)	32
4	Chauvin *et al*. [163]	He plasma jet	100	DMEM with and without FBS	Yes	540 (150) with FBS 210 (150) without FBS	84 without FBS 216 with FBS
5	Girard *et al.* [162]	He/N_2 plasma jet	2000	PBS	Yes	590 (600)	59
6	Girard *et al.* [161]	He plasma jet	500	PBS	Yes	1600 (240)	400

	Author	Device	Treated liquid volume (µL)	Liquid type	Linear concentration increase?	Maximum NO_2^- concentration measured (µM) with associated treatment time in brackets (s)	Rate of NO_2^- concentration increase (µM/min)
7	Horiba *et al.* [239]	Ar plasma jet device, with wide plasma source.	4000	DMEM without FBS	Yes	1450 (180)	483
8	Kurake *et al*. [166]	Ar plasma jet	3000	DMEM with and without FBS	Yes	2750 (300) without FBS 3250 (300) with FBS	550 without FBS 650 with FBS
9	Nguyen *et al*. [155]	Air plasma jet	Volume treated is not stated.	DMEM with FBS.	Not known	10-15 (300)	n/a
10	Wende *et al*. [243]	kINPen Ar plasma jet	5000	RPMI 1640 with FBS	Yes	13 (180)	4.2
11	Wende *et al.* [156]	Radio frequency Ar jet	100	"Phosphate buffer", thought to be PBS with glucose but not clear.	Not known	200 (360)	n/a

4.4.2 Temperature change

Temperature change in the bulk medium treated within Reactor 1 was measured for an NTP treatment time of 30 minutes only, with the medium allowed to acclimatise to room temperature prior to treatment. The treated liquid was mixed prior to measurement. On average, temperature changed from a starting temperature of 20.7 °C (SE = 0.3 °C) prior to the commencement of treatment, to a temperature of 21.9 °C (SE = 0.5 °C) following the 30-minute treatment, therefore giving a temperature rise of 1.2 °C (SE = 0.2 °C) (n=3). The maximum temperature increase observed was 1.5 °C, from 21.0 to 22.5 °C. Given the low starting temperature and the small increase observed with a 30-minute application of NTP, treatment in Reactor 1 for this time period would not result in thermal damage to biological samples.

It should be noted that these temperature changes are within the bulk medium, mixed, rather than directly underneath the needle electrode, where it would be predicted that there could be localised heating.

4.4.3 Evaporation

The volume of liquid remaining following treatment in Reactor 1 was measured (Figure 4.3). The average volume fell from 325 µL at the beginning of treatment (SE = 0 µL), to 217 µL (SE = 3 µL) after 5 minutes of treatment, 187 µL (SE = 3 µL) after 10 minutes, 180 µL (SE = 0 µL) after 15 minutes and 80 µL (SE = 6 µL) after 30 minutes. This represented a reduction in volume of 75 % between the beginning and end of a 30-minute treatment. It was found to be a non-linear relationship with reduction from 0 min to 5 min of 108 µL, giving an average evaporation rate of 22 µL/min, but a reduction from 0 minutes to 30 minutes of 245 µL, an

average evaporation rate of 8µL/min. The data more closely approximated a 2nd order polynomial fit than linear.

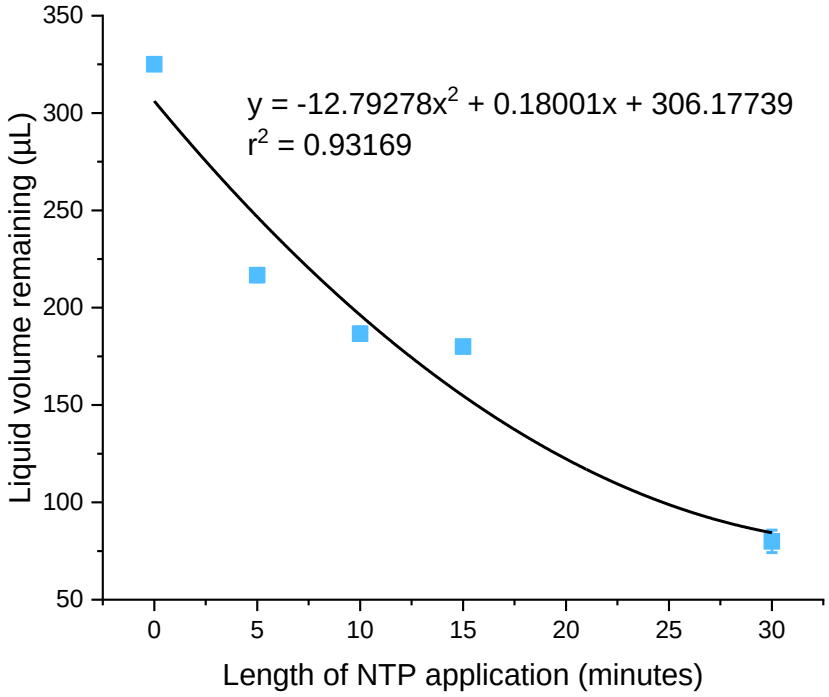

Figure 4.3. Remaining volume of serum-free, phenol red-free DMEM against treatment time in Reactor 1. n= 3, SE shown.

Although little temperature change was observed in the bulk liquid (4.4.2), a significant amount of evaporation took place, presumably due to localised heating, with around 75 % of the liquid having evaporated with a 30-minute treatment. This evaporation rate does limit the length of time that the reactor can be operated for, as it cannot be used for treatments much in excess of 30 minutes without running dry. This therefore suggests that Reactor 1 is not capable of producing the levels of H_2O_2 necessary for a rapid cytotoxic effect, as discussed in 4.4.1.1, but rather only for a slow effect.

Evaporation was also not found to proceed at a constant rate, but instead the rate appeared to reduce as treatment progressed. Two possible reasons for this observation have been identified. Firstly, it could be that there was a genuine reduction in evaporation rate, likely due to the effects of the falling liquid level and consequent increased gap size. This could be related to the change in discharge mode partway through the 30-minute treatment as has been discussed in sections 3.4.2 and 3.5. Alternatively, it could be that the evaporation rate is, in reality, linear, but that there are instead inaccuracies in the 5- and 10-minute liquid volume measurements. The measurement method used, which involved using a pipette in increments of 5 µL, is not likely to be highly accurate, and, if these two data points are omitted, the relationship between the remaining points, 0, 15 and 30 minutes, is linear ($r^2 = 0.98671$). Further replication of this experiment may give clarity around which of these two possible explanations is correct.

While the liquid level remaining in the well continues to fall throughout the 30-minute treatment time, the concentration of H_2O_2 and NO_2^- increases approximately linearly (Figure 4.1 and Figure 4.2). This, therefore, must mean that the rate of increase in molar mass of H_2O_2 and NO_2^- slows down over the course of the treatment time. An approximate calculation of the average molar mass within the treated liquid has therefore been carried out, based on the average concentration of H_2O_2 and NO_2^-after different treatment times shown in Figure 4.1 and Figure 4.2, and the evaporation data given in Figure 4.3 (Table 4.3). It should be noted that the evaporation and the H_2O_2 and NO_{2-} measurements were not carried out on the same set of samples, and, as well as this, there were of course errors within all three sets of data, which will compound when considered together. This means that the values in the table are unlikely to be highly accurate.

From the values in Table 4.3, the data does not rule out the possibility that, towards the later stages of a 30-minute NTP treatment with Reactor 1, the molar mass of H_2O_2 and NO_2^- is not increasing at all. If this is correct, this would mean that the increase in NO_2^- concentration in the latter stages of treatment is solely due to evaporation of the liquid, rather than to the formation of new NO_2^-, presumably an effect of the increasing gap size. The available data do not rule out this effect also happening with H_2O_2, however the situation with this substance is further complicated as, unlike NO_2^-, it is also liable to evaporation. In order to determine whether the suspicion of failure of NO_2^- and H_2O_2 production towards the end of 30 minutes of NTP treatment is in fact correct, further data would need to be gathered, with optimised experimentation to reduce variances.

Table 4.3. Approximate number of moles of H_2O_2 and NO_2^- within wells treated by Reactor 1 operating under standard electrical settings at various time points up to 30 minutes of NTP exposure. Calculation of number of moles based on liquid volume remaining following treatment (Figure 4.3) and the concentration of H_2O_2 or NO_2^- (Figure 4.1 and Figure 4.2) detected.

Treatment time (min)	**Average volume of liquid remaining (µL)**	**Average [H_2O_2] (mM)**	**Calculated number of moles of H_2O_2 in (nmol)**	**Average [NO_{2-}] (mM)**	**Calculated number of moles of NO_2^- (nmol)**
5	217	0.8	174	2.1	456
10	187	1.1	206	3.7	692
15	180	2.6	468	5.8	1044
30	80	5.2	416	13.0	1040

4.4.4 pH

The available pH meter could not be used as the liquid volume remaining in a well following 30 minutes of treatment was insufficient, and therefore the measurement could only be taken using pH strips. Given the very small changes in pH, and the inaccuracy inherent in interpreting these strips, it proved impossible to take measurements that were sufficiently precise, and the only conclusion that could be drawn was that any change in pH was minimal, staying close to the value of around pH 7.7 for the untreated liquid (DMEM and DPBS).

As well as extremes of temperature, extremes of pH can be fatal to cells, and it is known that pH reduction occurs in water treated with NTP, due to the accumulation of H^+ ions produced by reactions such as Equations 1.47 and 1.48. This effect is evidenced in works such as [245], which showed that this was particularly the case when air was used. However, many liquids used in *in vitro* work, such as DMEM and DPBS, contain buffers, and so it may be expected any change in pH with NTP exposure would be small. There are a number of papers in which pH change in NTP-treated buffered liquids has been considered. In PBS and DPBS, it has mostly been observed that there is either no change in pH [238], [246][247] or a slight tendency to acidity [62][162][248], and the results here for DPBS do not contradict this. With cell medium, some have found a slight increase in pH with NTP treatment with, for example, one paper giving a change from 7.8 to 8.3 over the course of the treatment time [238][246][247][132]. All of the papers identified in which this effect had occurred used plasma jets as the NTP source, and therefore the tendency to alkalinity observed has been largely attributed to "degassing" of carbon dioxide (CO_2) present within the liquid due to gas flow [238][247][132], something which would not be expected with a design such as Reactor 1. It has also been suggested that reactive species in the NTP itself

may contribute to the effect, either by acting on the sodium bicarbonate ($NaHCO_3$) buffer [247] or on some of the organic substances present within the medium [246]. Both of these are present within DMEM (Appendix A) and therefore, although not detected with the pH measurement tools available, it may be that there is a slight shift to alkalinity when this is treated in Reactor 1.

4.4.5 Diffusion effects

The small cell layer area when a 96-well plate was used made it difficult to carry out any experimentation to determine the spread of the effect of the NTP treatment with Reactor 1. Therefore, a similar reactor, Reactor 2 (Figure 2.4), was designed, but which instead used a Petri dish to house the cells and treatment liquid to allow for a larger cell layer area. With this, it was possible to give an illustration of the change in the affected area of cells with treatment time with a DBD reactor with needle electrode, as well as allowing the effect of post-treatment diffusion to be observed.

4.4.5.1 Diffusion effects during treatment

15- and 30-minute direct NTP treatments, as well as a short treatment of 30 s, were applied to adherent 3t3 cells within a Petri dish using Reactor 2, with the treatment liquid being removed immediately following cessation of the NTP application. It was then replaced with untreated medium, before the MTT-based measurement technique described in 2.3.7 was carried out the following day.

Example images of control samples, and samples which received the 15- and 30-minute NTP treatments in Reactor 2 are shown in Figure 4.4. From an area of reduced viability of 0 with the control samples (SE = 0), the average area rose to 0.174 cm^2 (SE = 0.009 cm^2) with

a 15-minute plasma treatment, and then 1.338 cm^2 (SE = 0.267 cm^2) with a 30-minute plasma treatment (Figure 4.5, areas indicated by blue arrows). The increase in area was not linear with increasing treatment time, with a greater increase between 15- and 30- minute treatments than between control and 15-minute treatments. It was also noted that there was no area of reduced viability with very short treatment times (30 s), with no visible reduction in MTT colour intensity (Figure 4.4(d)). It is acknowledged that there is an element of subjectivity to the measurement, however, an area was assumed to be of reduced viability if there was an evident reduction in the strength of the MTT colouration in that area, even if some cells in the area were apparently still viable.

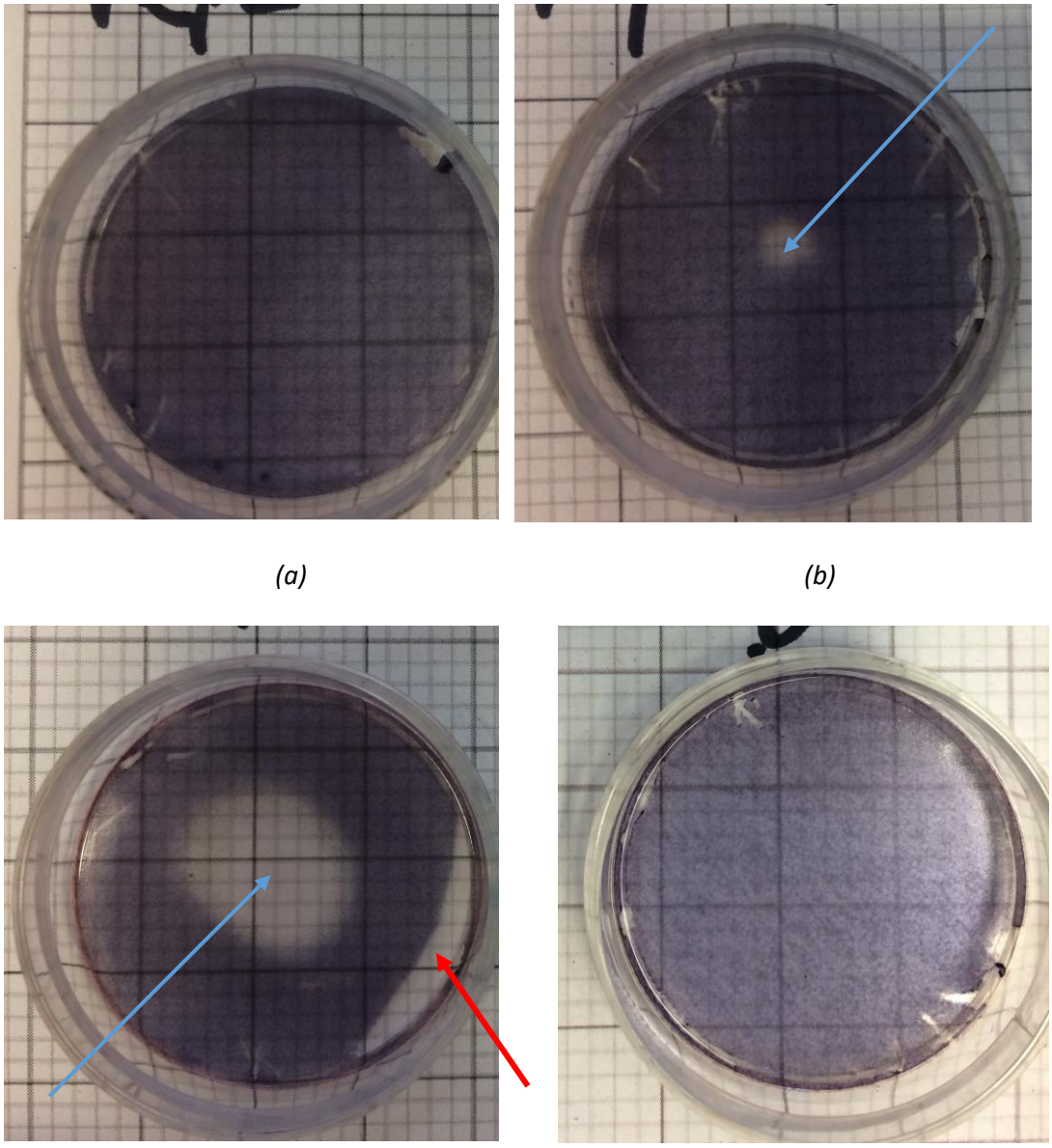

(a) *(b)*

(c) *(d)*

Figure 4.4. MTT-stained Petri dishes 24 hours following (a) no NTP treatment (b) 15-minute treatment in Reactor 2 (c) 30-minute treatment in Reactor 2 (d) MTT-stained Petri dish 24 hours following 30-second treatment in Reactor 2. Area of damage due to direct NTP treatment indicated by blue arrow. Damage to the cell layer at the right-hand side of the Petri dish shown in c) (red arrow) is thought to be due to the need to tip the dish to one side

to remove the treated liquid with a pipette tip after completion of the NTP treatment, and therefore this has not been included in the measurement of the area of reduced viability.

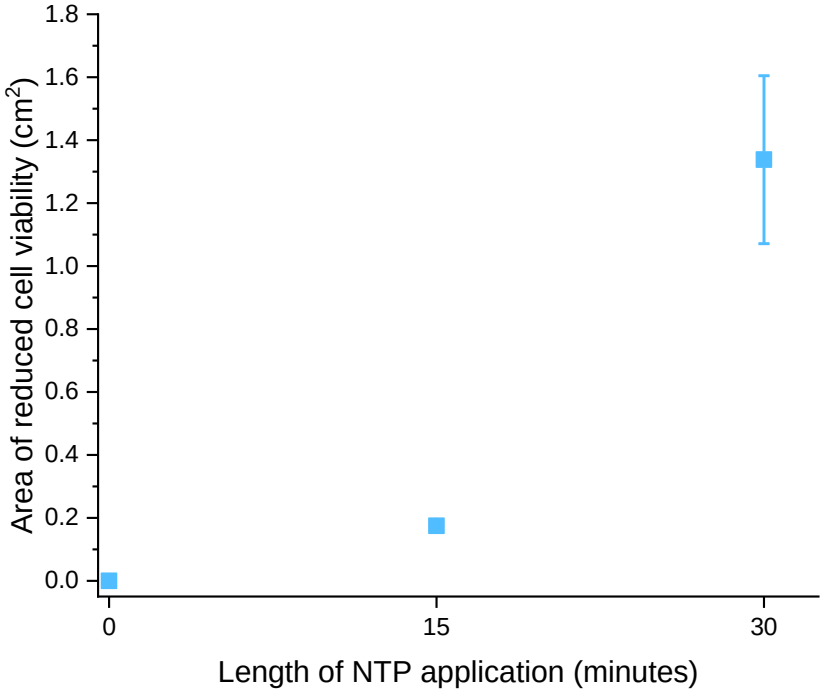

Figure 4.5. Area of reduced cell viability, considered 24 hours after plasma treatment, against NTP treatment time. n=5, SE shown.

It is possible to draw several conclusions from these findings. The absence of an area of non-viable cells after short treatments (Figure 4.4(d)) shows that the effect of NTP on the cells was not instantaneous, adding further evidence to support the involvement of high concentrations of long-lived RONS in the cell viability effects of NTP, with insufficient concentrations being reached in any area of the dish with these shorter treatment times. This would also account for the highly focused area of non-viable cells directly below the needle electrode tip with a 15-minute treatment (Figure 4.4(b)): this is the area above which the NTP is contacting the liquid surface, and, therefore, where the chemical reactions

resulting in long-lived RONS, such as H_2O_2 and NO_2^-, are occurring. The 15-minute treatment, having an evident reduction of cell viability, but in a very small area directly underneath the needle, shows the potential for precision application of NTP with this style of device.

Increasing the treatment time from 15 to 30 minutes would result in more of the long-lived RONS being produced by NTP-liquid interaction, thus increasing the concentration gradient of these between the liquid in the area immediately below the needle, and areas further towards the edges of the dish. This therefore results in increasing diffusion of these substances, enhanced by the longer time period while this extended treatment continues, resulting in a larger, but still approximately circular, area of the dish having concentrations of RONS sufficient to be toxic to cells (Figure 4.4(c)). The non-viable area achieved with a 30-minute treatment was, on average, 769 % of the size of that of the 15-minute treatment. Assuming the affected area was a perfect circle then, based on the area measurements, the radius of the affected area for the 15-minute treatments would be on average 0.24 cm, whereas for the 30-minute treatment, it would be 0.65 cm, approximately 2.7 times greater. This means that neither the increase in area, nor the radius of the area, were linear with treatment time.

4.4.5.2 Diffusion effects following treatment

A 30-minute NTP treatment was applied to 3t3 cells with Reactor 2, with the treatment liquid either being removed immediately or left undisturbed in the Petri dish for a further 30 minutes before removal. Once removed, the liquid was replaced with untreated medium, before the previously described MTT area measurement technique was applied the following day. Example photographs showing a Petri dish which had the treated liquid

immediately removed, and one which had it removed 30 minutes later, are shown in Figure 4.6. The average area of reduced viability was 1.456 cm^2 (SE = 0.181 cm^2) when the treatment liquid was removed immediately following the completion of the NTP treatment, and 2.123 cm^2 (SE = 0.110 cm^2) when there was a 30-minute delay (Figure 4.7). This therefore meant leaving the dish undisturbed for 30 minutes following the end of the NTP treatment increased the area of reduced cell viability by an average of 45.8 %. This increase was statistically significant ($p = 0.034$).

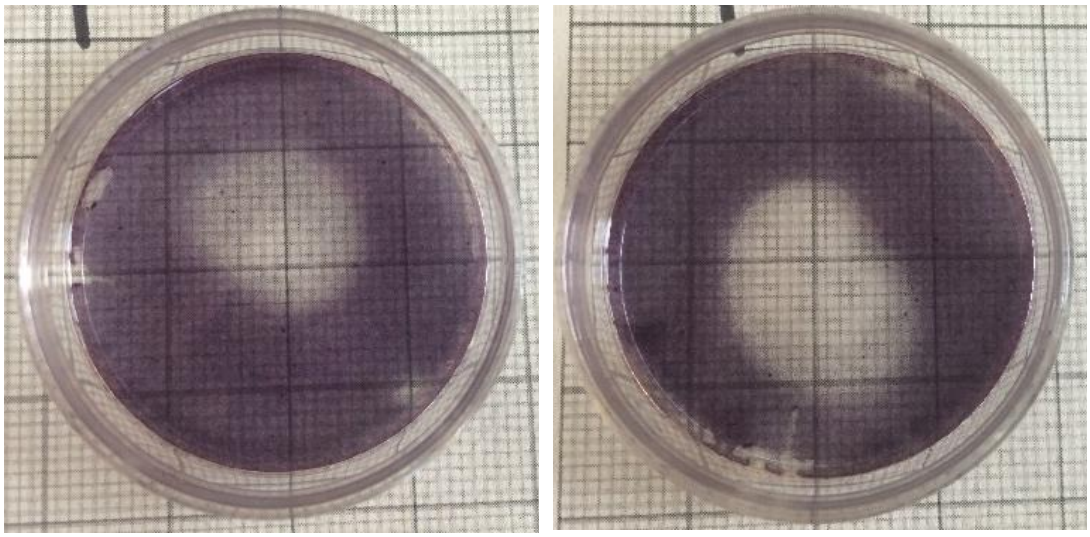

a) b)

Figure 4.6. Example of area of reduced cell viability with a) no diffusion time following 30 minutes of NTP treatment in Reactor 2 b) 30 minutes of diffusion time following 30 minutes of NTP treatment in Reactor 2.

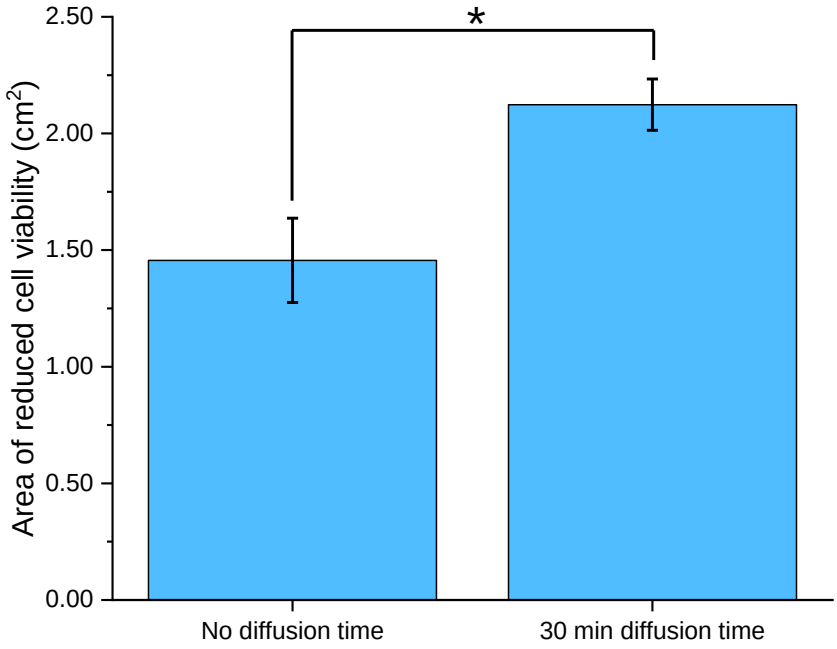

*Figure 4.7. Area of reduced 3t3 cell viability for samples with no diffusion time, and with 30 minutes of diffusion time, following 30 minutes of direct treatment in Reactor 2. n=3, SE shown, *: p< 0.05, independent samples t-test (two-tailed significance).*

From Figure 4.7, it is evident that, if the liquid remains undisturbed, diffusion continues along the concentration gradient beyond the end of the NTP-treatment, with the area of fatal concentrations of NTP-generated RONS increasing from an average of 1.46 cm^2 immediately following the cessation of treatment, to 2.12 cm^2 30 minutes later. This difference in the area immediately affected by the NTP treatment, versus that following post-treatment diffusion does not seem to have been considered elsewhere in the literature as far as has been determined, however, it is an important consideration if such treatments are applied to *in vivo* or clinical work, as the affected area may be significantly larger than the area targeted, possibly resulting in the application of the treatment to unwanted areas.

4.4.5.3 Overall discussion of diffusion effects

The only work similar to the area measurement work that has been carried out here which has been identified is that of Karki *et al*. [69], which used the reactor design shown in Figure 4.8. Although of differing design to Reactor 1, with an added dielectric layer, it also gives a plasma which is highly focused on a central area of the well. Treating A549 lung adenocarcinoma cells, they also found that the central area beneath the needle electrode was the focus of the treatment, with dead cells in the centre of this area, surrounded by an area of absent cells. The combined area of dead and absent cells would be equivalent to the non-viable area measured with the MTT technique, which is not able to make this distinction. Unlike the work performed here, however, Karki *et al.* found that the increase in area was linear with treatment time. There was also some evidence that a small proportion of cells beyond the main area of dead and absent cells was apoptotic, suggesting that, although there was a highly targeted effect at the centre of the well, there were some effects at the periphery as well, but perhaps just for the more vulnerable cells. A further point of note is that they left the NTP-treated on the cells for 1 hour following treatment, rather than removing it immediately, thus the cleared area that they observed is also inclusive of any post-treatment diffusion effects. The treatment is therefore more alike that of (b) in Figure 4.6, rather than (a).

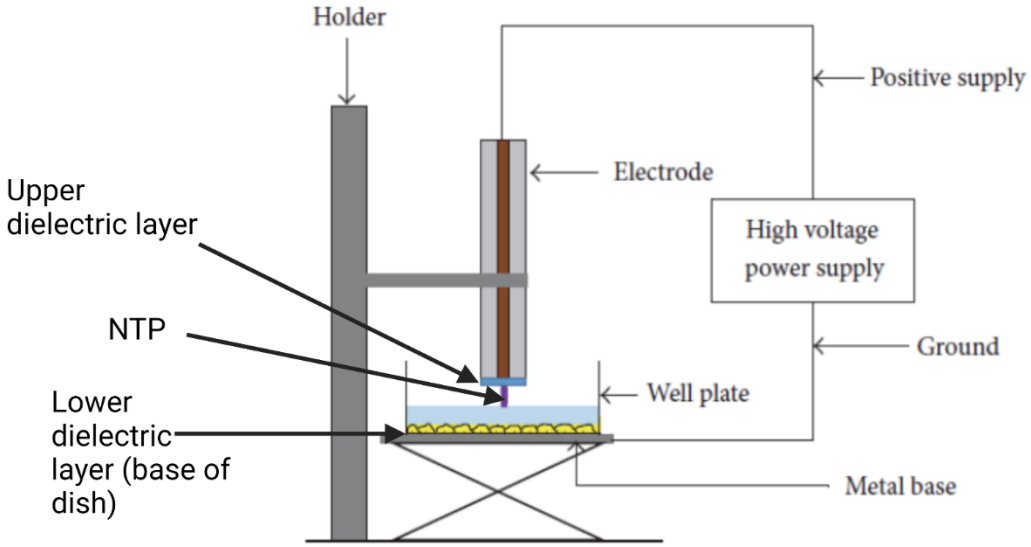

Figure 4.8. Reactor used by Karki et al. (2017). Like Reactor 1, it uses a DBD design with the treatment liquid and cells within the electrical circuit, but unlike Reactor 1, it has two separate dielectric layers: one covering the needle, and one being the base of the tissue culture container. A pulsed 12 kV power supply was used, set at 1000 Hz and a 10 μs pulse width. Diagram taken from [69], modified to add additional labelling. Modifications created with Biorender.com [6].

4.5 Conclusions

H_2O_2 and NO_2^- have been identified throughout the plasma medicine literature as key substances involved in observed biological effects, as well as being useful indicator species for RONS production generally in the NTP treatment. Reactor 1 was found to produce both of these RONS in suitable concentrations for plasma medicine experimentation, in line with the levels seen with other NTP sources used for similar work. It also did this within a reasonable timeframe. As well as this, the increase in concentration of both substances was approximately linear with treatment time, allowing predictable application of treatment.

Temperature and pH change with treatment of buffered liquid in Reactor 1 was minimal, meaning biological effects observed within this project are not due to extremes of either of these. Evaporation was, however, quite high, with around 75 % of the liquid being evaporated by 30 minutes of NTP exposure. This therefore limits the length of treatment time that can be achieved with Reactor 1 to a little more than 30 minutes, although given the concentrations of H_2O_2 and NO_2^- that are achievable with a 30-minute treatment, and the cytotoxicity of these, this is likely to be sufficient for most experimental purposes. It is also possible that there is minimal production of H_2O_2 and NO_2^- with longer treatment times with Reactor 1, and that the increase in concentration of these two substances at these time points is largely due to the continuing evaporation of the treatment liquid, but there is at this stage insufficient evidence to fully conclude this, and further work would need to be carried out to determine whether this is indeed true.

Several conclusions could be drawn about the style of design of Reactor 1 from the work performed with Reactor 2. It was found that, at moderate treatment times (15 minutes), the cell viability reduction was highly targeted to a specific area. However, it is also shown that this is lost with longer treatments, and also with by post-treatment diffusion. This possibility of this post-treatment diffusion following NTP treatments does not seem to have been considered elsewhere, despite its importance.

Overall, this chapter showed the acceptability of the design of Reactor 1 (2.1.1.1), as well as the electrical parameters selected for its operation (2.1.2), as it produced levels of the indicator species H_2O_2 and NO_2^- which were comparable with those measured for other NTP sources seen in plasma medicine work in the literature, with minimal temperature or pH change seen in the treated medium. As well as this, the work performed in the chapter also

demonstrated a benefit of such a pin-plate design of reactor via Reactor 2, specifically that it can be very precisely targeted to a small area. This work also demonstrated the biological effect of post-treatment diffusion of RONS, something that does not appear to have been considered elsewhere.

Chapter 5 Direct NTP treatment of NIH 3t3 with reactor

5.1 Aims

Following on from the electrical characterisation of Reactor 1 (Chapter 3), and investigation of the chemical effects on liquid treated within it (Chapter 4), it was important to confirm that Reactor 1 as designed was also capable of causing biological effects using both the direct and PAM treatment methods, thus confirming its suitability for employment in further biomedical research. Initially, in the work presented in this chapter, the effect of direct NTP treatment with Reactor 1 was investigated, with the effect of PAM treatment being considered in the following chapter.

For Chapter 5, the aims of the work performed were:

1) To confirm the ability of direct NTP treatment in Reactor 1 to cause biological effects by measuring its impact on the viability of the 3t3 cell line, and on also on its morphology.
2) To understand whether the observed effect on viability was immediate.
3) To investigate whether the NTP-related degradation of phenol red, observed in liquid treated by Reactor 1, was involved in the reduction in viability of 3t3.
4) To understand whether the use of DPBS versus DMEM as the treatment liquid in Reactor 1 affected the level of viability reduction in 3t3.

5.2 Introduction

All experiments in this chapter have used direct NTP application as the treatment applied to the cell samples. The meaning of the term "direct treatment" has already been explained in 1.2.3.4, and is illustrated in Figure 1.18.

All of the NTP treatments carried out within the chapter were of 15 or 30 minutes. As has been discussed in 1.2.3.5, two of the most important substances produced in NTP treatment for biological effects are H_2O_2 and NO_2^-. From the work performed in sections 4.4.1, it has been established that the 15-minute treatments would result in an H_2O_2 concentration of 2.5 mM and a NO_2^- concentration of 5.8 mM on average whereas the 30-minute treatments would give an average concentration of 5.2 mM of H_2O_2 and 13.0 mM of NO_2^-. These concentrations were determined from work performed with FBS-free DMEM, but it is assumed that the concentrations produced in the other liquid used in this chapter, DBPS, would be similar given that much of the H_2O_2 and NO_2^- is likely to be produced by the aqueous reactions listed in 1.2.3.5.1. It should also be noted that the H_2O_2 and NO_2^- measurements in 4.4.1 were taken using NTP-treated liquid which had been thoroughly mixed prior to assay. With direct treatment in Reactor 1, it may well be that the concentrations of these two substances, plus any others produced, are not homogenous throughout the treated liquid, particularly considering the Reactor 2 results given in 4.4.5.

H_2O_2 concentrations over 10-100 µM are thought to induce cell toxicity [180] and it has been established that the human L939 cell line, also a fibroblast cell line like the 3t3 line used during this project, is at the higher end of this scale, with concentrations of 0.1 mM required to give any observable cytotoxic effect, concentrations between this and 10 mM giving a slow-acting cytotoxic effect, and levels above this giving a more rapid effect [181].

From this, it might therefore be expected that the 15- and 30-minute treatments used here would give H_2O_2 concentrations within the range which would produce such a slow cytotoxic effect (4.4.4.1), assuming a fairly even distribution of the substance throughout the liquid.

5.3 Methods

5.3.1 Direct NTP treatment

All direct treatment within this chapter was carried out using Reactor 1, as described in 2.1.1.1 and with the electrical parameters of 2.1.2, with cells already present in the well to be treated at the time of NTP application. Following the completion of the NTP application, the treated liquid was removed immediately from the cells and, if assay or staining were not to take place immediately, it was then replaced with complete DMEM until the time of analysis.

For most experiments, DMEM with phenol red and without the addition of FBS, NEAA or antibiotics was used as the liquid exposed to NTP. The exception to this was the work performed in 5.4.3 in which DPBS, with and without phenol red, was used. Where the phenol red was added to the DPBS, 45 µL of 0.5% phenol red solution was added to 15 ml of DPBS. As with the previous chapters, the starting volume of liquid in a well treated in Reactor 1 was always 325 µL.

5.3.2 NIH 3t3

The cell line used for all of the experiments in this chapter was 3t3, with the samples being set up in accordance with the process described in 2.3.1.1, including the serum starvation process described in 2.3.1.1.1.

5.3.3 Cell viability and morphology assessments

Cell viability was measured using either a neutral red or MTT assay, following the procedures described in sections 2.3.4. and 2.3.5. Where combined DAPI and phalloidin-FITC staining was used for microscopy, this was carried out using the procedure described in 2.3.6.

5.4 Results and discussion

5.4.1 Cell viability of 3t3 24 hours following direct NTP treatment in DMEM

An assessment of 3t3 cell viability at 24 hours following direct plasma treatment was performed by neutral red assay (Figure 5.1). The viability was standardised against the control values (length of NTP application of 0 minutes, instead allowing the cells to sit in serum-free DMEM for the same length of time as the treated samples were exposed to NTP), which were taken as having an average of 100 % (SE = 3.90 % of this value). For a 15-minute treatment, the cell viability was 76.24 % compared with control (SE = 2.52 % of the average control value), whereas for the 30-minute treatment cell viability was 37.13 % of the control value (SE = 9.29 % of the control value). 15 and 30 minutes were chosen as treatment times, as scoping experiments showed that times of these magnitudes were giving a measurable reduction in viability.

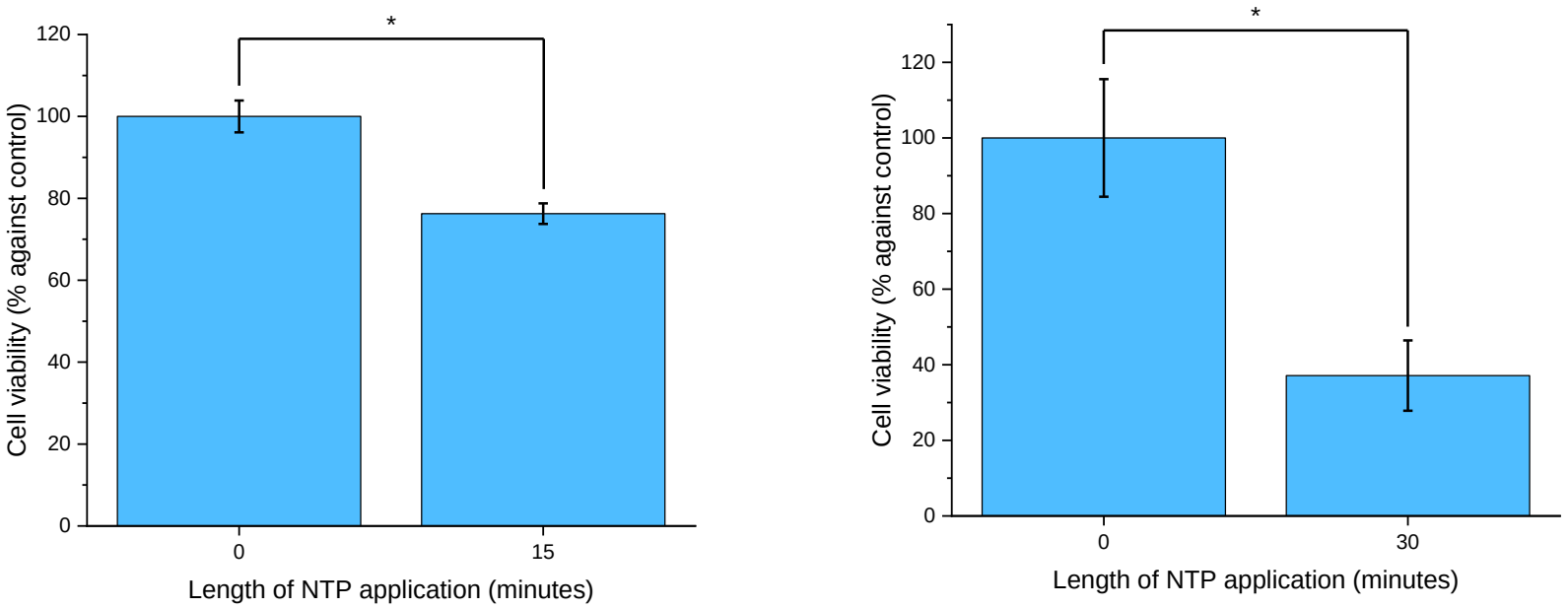

*Figure 5.1. Comparison of viability of directly Reactor 1-treated 3t3 samples against control, measured by neutral red assay, at 24 hours post-treatment (a) 15-minute NTP treatment, n=4, SE shown, *: $p < 0.05$, independent t-test with two-tailed significance and (b) 30-minute NTP treatment, n=4, SE shown, *: $p < 0.05$, independent t-test with two-tailed significance.*

Both the 15- and 30- minute direct treatments resulted in a statistically significant reduction in cell viability ($p = 0.002$ and $p = 0.006$ respectively), a result which is not surprising given the large number of papers demonstrating cell viability reduction when measured at least 24 hours following application of NTP treatments (Table H.1). As well as this, the H_2O_2 concentrations present in the 15- and 30-minute treatments are of the level which were predicted to be cytotoxic to 3t3, and so the results of Figure 5.1 are as expected.

The average cell viability of the 30-minute treatment in Figure 5.1 was approximately 48 % of that of the 15-minute treatments. These results could suggest that the change in viability was linear with treatment time, however, it was clear from informal work carried out prior to this experiment that there was a minimum treatment time of the order of several minutes for any reduction in cell viability to be seen, an observation which concurs with the work using the similar Reactor 2 in 4.4.5.1.

Due to the geometry of the 96-well plate, it was not possible to get any meaningful information from an assessment of the affected area of the cell layer such as was carried out with Reactor 2 in 4.4.5. However, it cannot be ruled out that the area is also increasing with treatment time with Reactor 1 which would mean that this effect could be at least partially responsible for the larger viability reduction in 30-minute treatments versus the 15-minute ones.

5.4.1.1 Comparison between different viability assay methods

There are a number of different ways of assessing cell viability, such as assessing whether there is physical damage to specific parts the cells, or investigating whether the metabolic

processes of the cells are failing. One of each of these two types of methods was used during this project, the neutral red assay for the former and the MTT assay for the latter, to detect if there was a difference in the viability levels measured by each, as this could provide some indication of the effects of NTP on the cells.

As discussed in 2.3.4, the neutral red assay, used in Figure 5.1, assesses lysosomal damage to determine cell viability. The MTT assay, on the other hand, measures metabolic activity (2.3.5).

For MTT, against the average control viability value set as 100 % (SE = 4.82 % of this value), it was found that a 15-minute direct NTP treatment in Reactor 1 gave an average viability of 87.79 % (SE = 3.75 % of the average control value), measured at 24 hours following the NTP application, and the viability with a 30-minute treatment was 22.21 % (SE = 7.07 % of the average control value). Only the 30-minute treatment resulted in a statistically significant reduction in cell viability from the control ($p < 0.001$ versus $p = 0.142$ for 15 minute treatment). There was also a statistically significant reduction in viability between the 15 and 30 minute treatments ($p < 0.001$) (Figure 5.2).

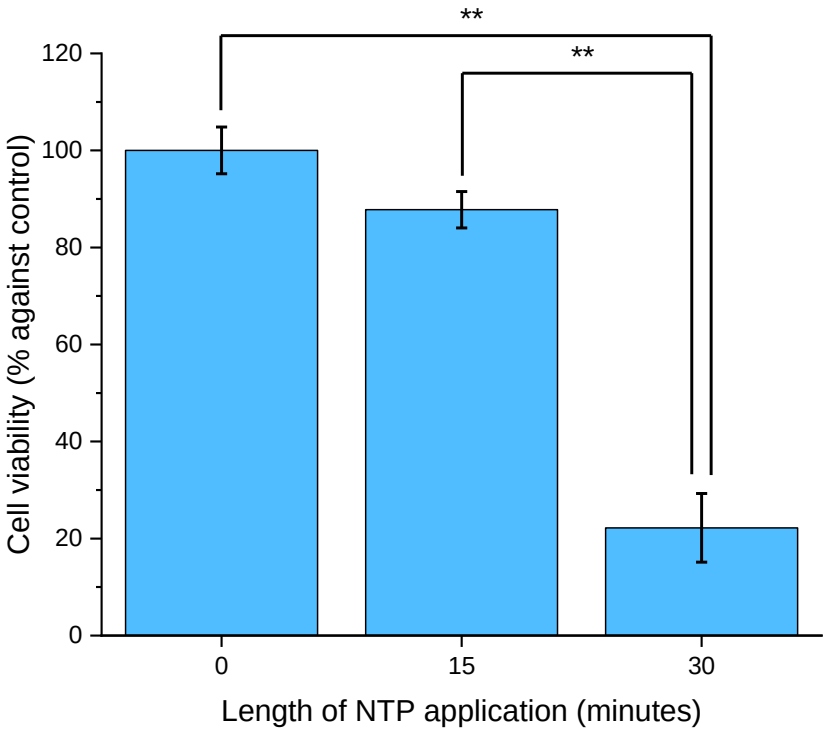

*Figure 5.2. Cell viability 24 hours following direct NTP treatment, measured using MTT cell viability assay. n=3, SE shown, **: p < 0.001, ANOVA with Tukey HSD post-hoc.*

Comparing the results from the two assay techniques, it was found that the results were broadly similar, but that the viability of the 15-minute treatment appeared smaller when measured by MTT rather than neutral red, whereas the reduction for the 30-minute treatment appeared larger (Table 5.1). Unlike the neutral red assay, where the 30-minute treatment gave a viability equivalent to 48 % of that of the 15-minute treatment, with the MTT method it was 25 %. However, the variances in some of the results are quite large, and it therefore cannot be definitively stated that the differences obtained between the two methods are truly indicative of a difference in the viabilities of the cell populations. Further work would need to be performed to obtain a clearer set of results before this can be concluded. It has been established from papers such as [161][249] and [250], via the use of MTT, that direct NTP treatment impacts NADH production, and thus cell metabolism.

However, few papers have been identified where neutral red has been used with NTP treatment, and none where the two methods have been compared.

Table 5.1. Comparative average cell viability values as percentage of control from the data in Figure 5.1. and 5.2, both showing a measurement of cell viability following 15 and 30 minutes of direct NTP treatment of 3t3 in Reactor 1.

Assay	**15-minute treatment**	**30-minute treatment**
Neutral red (n=4)	76.24 % (SE = 2.52 %)	37.13 % (SE = 9.29 %)
MTT (n=3)	87.79 % (SE = 3.75 %)	22.21 % (SE = 7.07 %)

5.4.1.2 Comparison of viability results with the findings of other researchers

Ideally, the results presented above could be compared to the work of other researchers to understand the relative effects of Reactor 1 versus other NTP source designs. However, this is, in reality, problematic. It is known that different cell types have different vulnerabilities to NTP treatments [90][157][71][161], with possible explanations for this including the level of aquaporin expression [157] or relative growth rates [71], thus comparisons between works where different cell types have been used is not meaningful. A of number of papers have investigated the direct NTP treatment of fibroblasts specifically (Table 5.2), and all of these showed a reduction in viability resulting from the treatment. It was also apparent that different fibroblast types, had a different level of response to the treatment, with Girard *et al.* showing that MRC5Vi (human lung fibroblast) cell line was less vulnerable than the primary fibroblasts used. All treatments were also shorter than the

shortest applied here (15 minutes), with the maximum being 10 minutes. This latter work, by Iseki *et al.* [251], resulted in viability levels of around 80 % of control for two different fibroblast cell lines, which is higher than that found here. The reasons for this difference are difficult to determine due to the lack of information available about the NTP source used by Iseki *et al.*, and the chemical species it produces, but it may be that an increase in treatment time would have resulted in them achieving a greater viability reduction. It was also noted that one paper, that of Girard *et al.* [161], achieved a much larger viability reductions than those of this project, even with a shorter treatment time. The reasons for this were not clear, but could be due to the effects of using a different NTP source than that used here, the relative vulnerability of their cells compared to 3t3, or the fact that they left their cells in the NTP-treated liquid for 24 hours, whereas here it was removed immediately following the end of the NTP application.

None of the papers in Table 5.2 were truly comparable with the results of Figure 5.1 or Figure 5.2 for several reasons. For example, some papers measured the viability at a 48-hour time point rather than 24-hour [251][252], while others left the cells sitting in the treated liquid well beyond the end of the NTP exposure rather than immediately changing to untreated medium [84][62][161]. As well as this, the work with 3t3 on this project employed a serum starvation process to align the 3t3 cells in the samples into the G_0 phase, where cells are removed from the cell cycle (Figure 1.15), and are non-dividing [253]. The reason for the use of this process was that large variances were being encountered during preparatory experiments, something which was eliminated when serum starvation was employed. However, such standardising techniques have not been identified within any of the papers in Table 5.2, and therefore it is assumed that the cells within their samples would be distributed throughout the cell cycle. Although it has not proved possible to find

anything within the plasma medicine literature which compares the vulnerability of cells in different stages of the cell cycle to NTP treatment, it is still thought likely that cells in some parts of the cycle may be more vulnerable than those in other parts when considering other fields of research involving the application of RONS to eukaryotic cells [254][255].

Table 5.2. Delayed cell viability reaction (fibroblasts) after direct NTP treatment.

	Author	**Summary of results**
1	Ahn *et al.* [84]	Direct NTP treatment was applied to MRC5 (human foetal lung fibroblast-like) for 300 s prior to cells being left in the treated liquid for a further 24 hours. At this point, viability was found to be approximately 80 % of control value.
2	Balzer *et al.* [62]	Direct treatment was applied to primary human foreskin fibroblasts for periods of up to 300 s prior to cells being left in the treated liquid for a further 24 hours. At this point, the samples which had been subjected to a 300 s treatment was found to be 66 % of control.
3	Girard *et al.* [161]	NTP treatment was applied to primary human skin fibroblasts for a range of different times. Cells were then left in the treated liquid for one hour, prior to assay then being performed 24 hours later. 120s of NTP treatment was found to give a cell viability of 3-4 % of control, with a 240 s or 480 s treatment instead giving a result in the range of 1-2 %.

	Author	Summary of results
		NTP treatment was applied to MRC5Vi (human lung fibroblast) cell line following the same protocol. A 120 s NTP treatment gave a viability against control of 10-20 %, a 240 s treatment gave approximately 5 %, and a 480 s treatment gave a viability somewhere in the range of 1-2 %.
5	Iseki *et al.* [251]	The WI-38 (human foetal lung fibroblast-like) cell line was subjected to 600 s of direct NTP treatment, before then being left in the treated liquid for 72 hours. At this point, viability was found to be approximately 80 % of control. The MRC5 cell line was also subjected to the same treatment protocol, with viability also being found to be approximately 80 % of control.
6	Tiede *et al.* [252]	The GM00637 (human skin fibroblast) cell line was subjected to 270 s of direct treatment followed by 48 hours within the same treatment liquid and was then found to have a viability of 54 % of control. Primary fibroblasts which were subjected to 360 s of direct treatment followed by 48 hours within the same treatment liquid were found to have a viability of 52 % of control.

5.4.2.3 Morphological effects

DAPI and FITC-phalloidin staining was carried out on cells 24 hours following direct NTP treatments of 15 and 30 minutes with Reactor 1 (Figure 5.3).

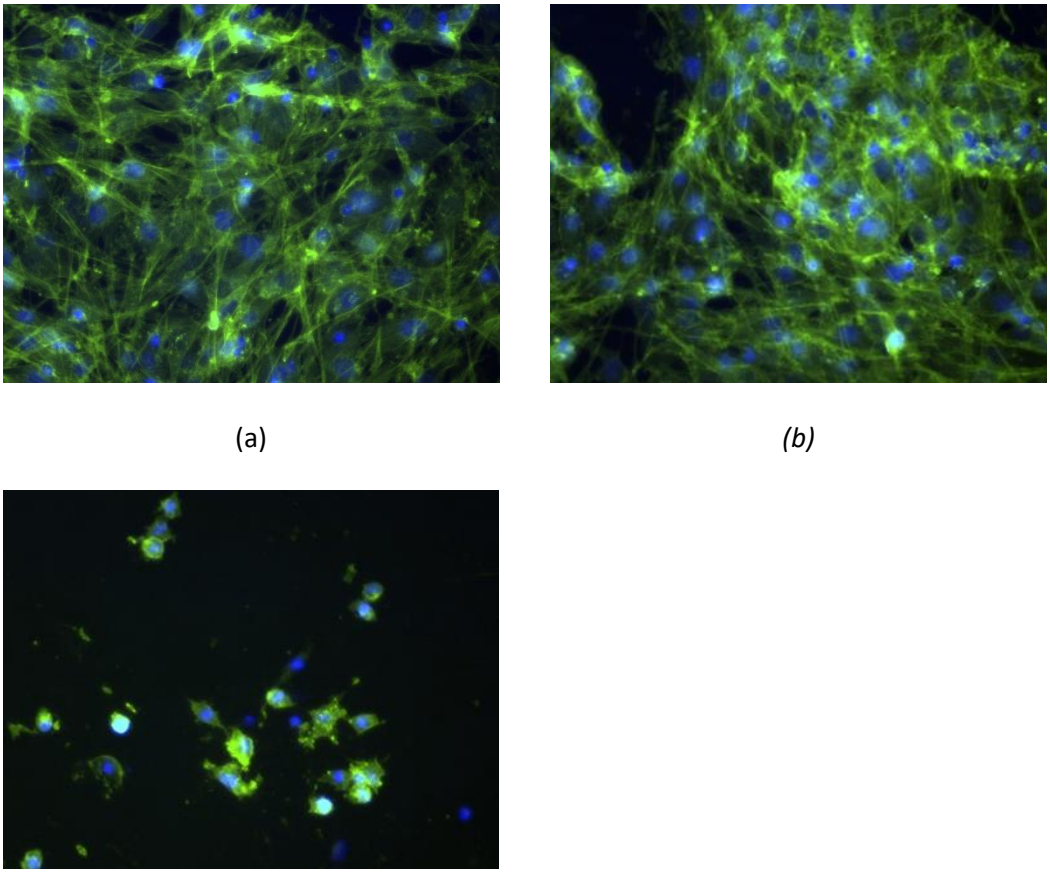

(a) *(b)*

(c)

Figure 5.3. DAPI and phalloidin-FITC staining of 3t3, 24 hours following direct NTP treatment in Reactor 1. Phalloidin-FITC, which stains actin filaments, is green, and DAPI, a nuclear stain, is blue (a) control (no NTP treatment) (b) 15-minute treatment and (c) 30-minute plasma treatment.

With the cells subject to 30-minutes of direct NTP treatment, (Figure 5.3(c)), the morphology was clearly different to that of the control samples (Figure 5.3(a)). It was observed that there

was a reduced number of cells adhering to the plate surface, suggesting detachment, and, of those cells which were still present, there was a collapsing of the cytoskeleton, demonstrated by the phalloidin-FITC staining of the actin being less clear and filamentary, and with the cells becoming smaller and more dense. Actin is one of the three components within the cytoskeleton which contribute to the cell's ability to maintain its shape and strength, and this observation of cell shrinkage with an increase in density and cytoskeleton collapse is indicative of controlled apoptotic cell death (Figure 1.13(a)) [256]. This observation of apoptosis from Reactor 1 treatment would concur with the expectation of a slow cytotoxic effect, as discussed in 5.2. A number of other researchers, for example [100][257][80][68][258] and [238], have also found that NTP treatment can induce apoptosis, using a range of techniques such as simple visual confirmation, Annexin V staining, caspase 3/7 detection or the terminal deoxynucleotidyl transferase dUTP nick end labelling (TUNEL) method.

However, unlike the cells subjected to 30 minutes of treatment, the morphology of those given 15 minutes of treatment (Figure 5.3(b)) still appeared similar to that of the control cells (Figure 5.3(a)). This may be surprising given both the results of Figure 5.1 and the H_2O_2 concentrations present. A possible explanation for this apparent contradiction could be that there is indeed an increasingly large affected area of the cell layer with increasing treatment time, and that the photographs taken for the 15-minute samples, which were taken at random points in the well, did not happen to coincide with the relatively small areas of apoptosis.

5.4.2 Cell viability of 3t3 immediately following direct NTP treatment in DMEM

Cell viability was also measured by neutral red assay immediately following the completion of a 30-minute direct plasma treatment (Figure 5.4), rather than 24 hours later, as was carried out in the experiments shown in Figure 5.1 and Figure 5.2. With the control average taken to be 100 % (SE = 22.58 % of this value) the comparative cell viability after a 30-minute treatment was 20.38 % (SE = 13.52 % of control average). This difference was statistically significant ($p = 0.037$).

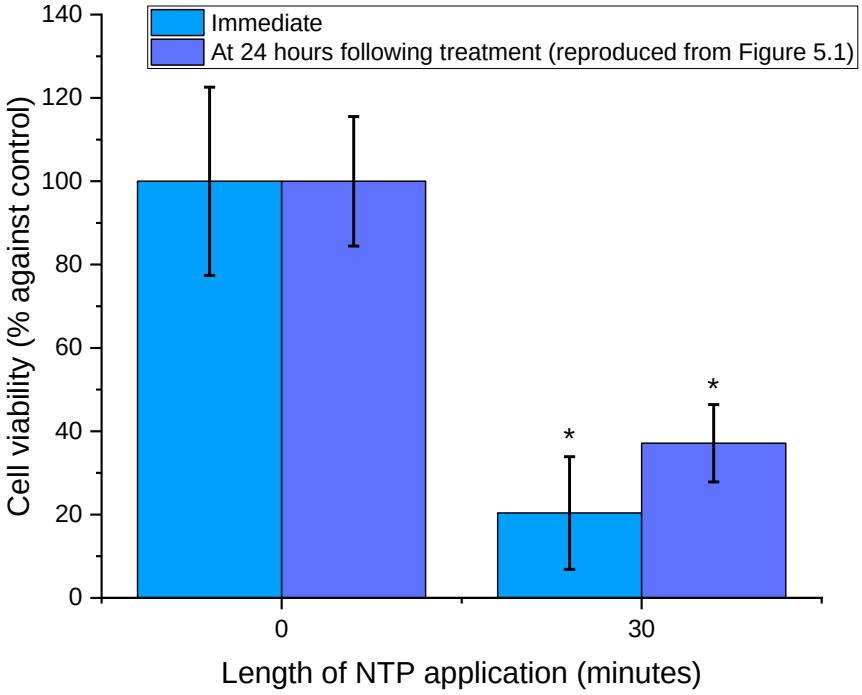

*Figure 5.4. 3t3 viability, measured with neutral red assay, immediately following direct NTP treatment of 30 minutes, against control (0 minutes of NTP treatment). Equivalent data for measurement at 24 hours is also reproduced from Figure 5.1. SE shown, n = 3, *: $p < 0.05$, independent t-test. Significance measured against relevant control bar (0 minute bars, for either immediate measurement or measurement at 24 hours, as appropriate).*

It is therefore apparent that NTP-induced reduction in 3t3 cell viability is an immediate effect. A surprising finding was that the viability measured in Figure 5.4 was lower than that of Figure 5.1 (20.38 % against control, versus 37.13 % against control), suggesting that the cell samples may recover from the treatment to some extent in the hours following the treatment. A possible explanation for the difference in results between Figure 5.4 and Figure 5.1 could be that, if a cell is vulnerable to the NTP dose supplied, then they immediately become non-viable, but that cells which survive the NTP exposure are still able to divide, thus meaning there are new, healthy cells 24 hours later. Alternatively, it could be that a proportion of the "non-viable" cells are in fact temporarily impaired but then recover, although a literature search has produced no evidence of this possibility.

Few researchers have considered the immediate effect of NTP treatment on viability. The closest comparison with the work performed here appears to be that of Balzer *et al*. [62] who found that a 5-minute direct treatment of primary human fibroblasts with their DBD-style NTP source gave an immediate reduction of viability to 66 % of the control value. However, the H_2O_2 and NO_2^- levels in their treatments were only 200 µM and 300 µM respectively, not unexpected given the far shorter treatment time, and therefore it is difficult to draw any conclusions between the relative effectiveness of treatment with their device and that of Reactor 1.

5.4.2.1 Morphological effects

DAPI and FITC-phalloidin staining was performed to show the morphological difference between 3t3 cells immediately following a 30-minute direct NTP treatment, and control cells (Figure 5.5).

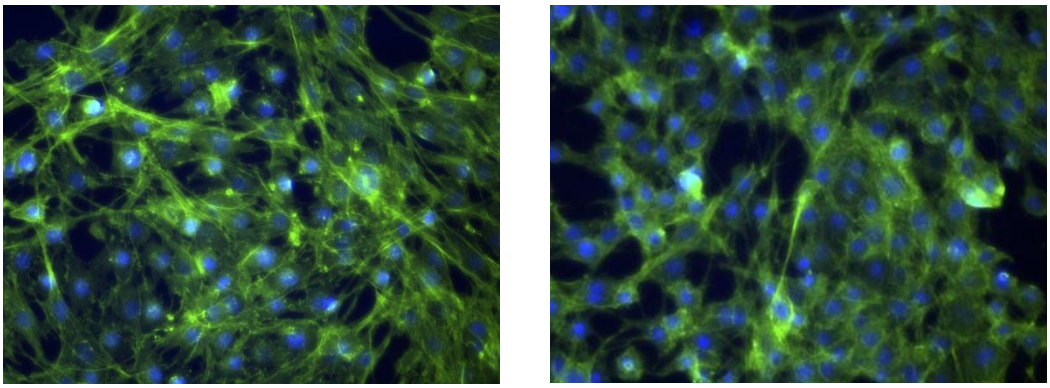

(a) (b)

Figure 5.5. DAPI and phalloidin-FITC staining of 3t3 immediately following direct treatment (a) control and (b) 30-minute direct NTP treatment. n=3.

There was little difference apparent between the morphology of the treated and untreated samples. It was notable, however, that the treated samples looked clearly different from those which had been subjected to the exactly the same NTP treatment but were instead viewed 24 hours later (Figure 5.3(c)). Specifically, unlike the photographs above where the treated samples appeared much like the control, treated samples considered at the later time point showed very small numbers of adherent cells remaining, with those cells still present appearing smaller and with increased density. It can therefore be determined that cytoskeletal collapse and cell detachment are not immediate effects from direct NTP treatment in Reactor 1, but that lysosomal damage is (Figure 5.4). The difference between the appearance at the two time points is likely to the progression of apoptosis, with the cells in the immediately-viewed photographs, although damaged, not having advanced far into this process and thus still appearing physically normal.

5.4.3 Effect of NTP-induced phenol red degradation on cell viability

Phenol red is present in many cell media, including specific formulae of DMEM, as it is a pH indicator. It was observed that the colouration of DMEM with phenol red ($C_{19}H_{14}O_5S$), which was used as the treatment liquid for the experiments in sections 5.4.1 and 5.4.2, was degraded when the liquid was exposed to NTP in Reactor 1 (Figure 5.6).

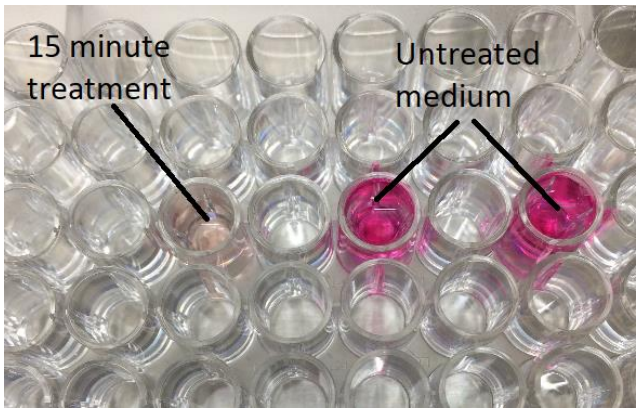

Figure 5.6. Phenol red degradation following 15 minutes of NTP treatment in Reactor 1. By 30 minutes of treatment, the liquid was colourless (not shown).

To understand whether the toxic effect of direct NTP treatment observed in Figure 5.1, Figure 5.2 and Figure 5.4 related in any way to the breakdown products of the phenol red, a comparison was made between the effect of direct NTP treatment on 3t3 when DPBS with added phenol red was used as the treatment liquid versus when DPBS without phenol red addition was used (Figure 5.7). Against a control (untreated 3t3 left in phenol red-containing DPBS for 30 minutes) taken as 100 % (SE = 20.42 % of this value), untreated samples in DPBS without phenol red had a viability of 79.85 % (SE = 14.56 % of phenol red-containing control average), samples treated with NTP in DPBS plus phenol red had a viability of 12.93 % (SE =3.31 % of control average), and samples treated in DPBS in the absence of phenol red had a viability of average 5.70 % of the viability of the control (SE =

2.37 % of control average). There were no statistically significant differences between the two treated samples. There were, however, significant differences between the untreated samples and their treated counterparts, which would not be unexpected (p = 0.006 for samples with phenol red and p = 0.014 for samples without).

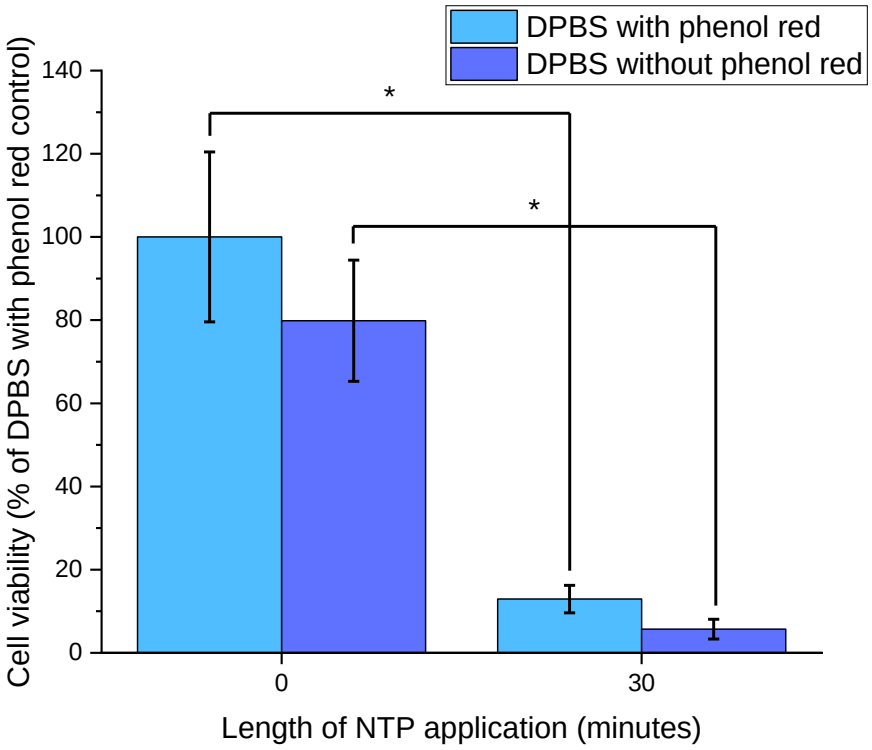

*Figure 5.7. Cell viability of 3t3 , measured by neutral red assay, following 30 minutes of NTP exposure using DPBS with or without phenol red. Viability was measured 24 hours following treatment using the neutral red assay. n=3, SE shown, *: p < 0.05 ANOVA with Tukey HSD post-hoc. Standardised to DPBS with phenol red control.*

It was not possible to determine the likely breakdown products of NTP-treated phenol red from the literature as this is not an area that appears to have been explored, however, there was a suspicion that, given its chemical formula, its breakdown could result in an

increase in ROS, which could in turn be partially responsible for the reduction in cell viability seen with NTP treatment. Alternatively, it is possible that the phenol red acts to quench the NTP-produced ROS, thus reducing the effect of the NTP treatment. However, Figure 5.7 shows that, although there was clear degradation of the phenol red caused by NTP treatment, this did not contribute to the reduction in cell viability that was caused by the same treatment. Given this conclusion no further work was attempted in this area.

A comparison between the viability values obtained from Figure 5.7, where DPBS with phenol red was used as the treatment liquid for 3t3 for a direct NTP treatment, and Figure 5.1(b), where FBS-free DMEM (also containing phenol red) was used, is given in Table 5.3. Although this comparison has been made with the phenol-red containing DPBS, the values for DPBS without phenol red would also be similar (Figure 5.7).

Table 5.3. Comparison between cell viability of 3t3, determined by neutral red assay, for cells subject to direct treatment in Reactor 1 in DMEM (Figure 5.1) and DPBS (Figure 5.7). Viability measured at 24 hours following treatment in both cases.

Treatment liquid	**Standardised control average (%)**	**SE of control (% of control average)**	**Average viability against control average following 30-minute NTP exposure (%)**	**SE of treated samples (% of control average)**
DMEM (n=4)	100	15.54	37.13	9.29
DPBS (n=3)	100	20.42	12.93	3.31

Interestingly, it does appear that direct treatment carried out with the cells in DPBS may be more effective than that carried out in DMEM. This is unexpected as it would be assumed that most of the RONS causing the reduction in viability would be due to aqueous NTP interactions, such as those described in 1.2.3.5.1, and thus it would be expected that the quantities of these in the two treated liquids would be similar. The reasons for this apparent difference in viability levels between the two liquid types are therefore not clear, and it is particularly confusing given that, as will be described in 6.4.6, this result was not repeated with PAM treatment, where both liquids gave similar viability results. Further experimentation is necessary to clarify the results in this area, and it would also be beneficial to carry out H_2O_2 and NO_2^- measurements in the DPBS treated in Reactor 1, as to date these measurements have only been carried out in DMEM.

5.5 Conclusions

An important conclusion from the work performed in this chapter was that the designed reactor, Reactor 1, was capable of giving reproducible, consistent and measurable biological effects on eukaryotic cells, and it could thus be concluded that it was suitable for further biomedical research work.

A number of specific conclusions could also be drawn from the work on Reactor 1 direct treatment presented within this chapter. 15- and 30-minute exposures caused significant reductions in cell viability when considered 24 hours following the completion of treatment, with apparent apoptosis also being observed microscopically in the samples subjected to a 30-minute treatment. The 15-minute treatment, however, did not show any morphological evidence of apoptosis, despite the fact that such a treatment did give a significant reduction in viability with one of the assays used to measure this. The reasons

for this are not known, but it is possible that it is due to the non-viable cells being concentrated in a specific area of the well, but that the microscopy photographs, taken at random positions in the sample, did not identify this.

It was also found that there was a bigger cell viability reduction against control in cells immediately following NTP treatment than in those considered 24 hours following the completion of the treatment. The reasons behind this finding have not been determined at this stage, and further work is necessary in this area. However, it is possible that this is due to cells which survived the NTP treatment then dividing in the following 24 hours. Morphological assessment at this time point showed little difference from control, despite the viability assay results, and this is likely to be due to the cells still being in an early stage of apoptosis.

There were two findings around the effects of using different treatment liquid the effectiveness of Reactor 1 treatment. Firstly, it was confirmed that the degradation of phenol red by the NTP did not in itself result in toxic by-products. Secondly, it was also found that DBPS as a treatment liquid during direct NTP application was more effective at reducing viability than DMEM. This is counterintuitive and appears to contradict the results obtained with PAM during similar experiments in the following chapter.

Chapter 6 PAM treatment with reactor

6.1 Aims

The aims of the work performed in this chapter were:

1. To confirm that PAM created in Reactor 1 is capable of causing biological effects, using cell viability as a measure.
2. To investigate the viability effects on 3t3 of one hour of exposure to PAM created with treatment times of up to 30 minutes in Reactor 1. This work would examine the cells both at 24-hours following the removal of PAM, and also immediately after the removal of PAM.
3. To observe the morphological changes in 3t3 following the treatments in Point 2.
4. To compare the effects of PAM and direct NTP treatments with Reactor 1 on 3t3 and investigate the effects of combined treatment.
5. To investigate whether Reactor 1 PAM loses its ability to affect 3t3 when kept in refrigerated storage.
6. To compare shorter and longer exposures to PAM with respect to their impact on cell viability.
7. To determine whether the use of DPBS to create PAM rather than cell medium changes its effect on 3t3.

6.2 Introduction

This chapter considers the application of PAM treatment to cells using Reactor 1. An explanation of PAM treatment, and how it varies from direct treatment, has been given in 1.2.3.4 and Figure 1.18.

6.3 Methods

6.3.1 Creation and use of PAM

The PAM used for all experiments within this chapter was created using Reactor 1. Unless stated otherwise, the PAM (40 µL) was used immediately after creation using the electrical parameters and treatment volumes stated in 2.1.1.1 and 2.1.2, and was then left in the well of cell samples for one hour following the removal of the cell medium, before then being removed itself. Where the subsequent analysis work was not carried out immediately following the treatment, complete medium was added following PAM removal, and the samples were then placed in the incubator (37 °C, 5 % CO_2) until the time of evaluation. The length of NTP exposure to create the PAM for each experiment is included alongside the results, as this varies.

Experiments using (i) DMEM without FBS and (ii) DPBS to form the PAM were carried out within this chapter. This was in line with the recommended media for the cell line. PAM created from these liquids will be referred to as DMEM-PAM, and DPBS-PAM as appropriate throughout this chapter. As with all previous Reactor 1 work, the starting volume in the 96-well plate well prior to the commencement of treatment was 325 µL.

Cells were seeded in a separate 96-well plate from that placed in Reactor 1 to hold the treatment liquid. In order to treat the cells with PAM, the PAM was mixed by pipette while still in its treatment well, to ensure even distribution of the products of the NTP exposure, before then being pipetted into the 96-well plate containing the cell samples. A volume of 40 µL of PAM was added per well of cells once the existing medium had been removed.

6.3.2 NIH 3t3

The setting up of cell samples for the 3t3 experiments described below was carried out in accordance with the description in 2.3.1.1, inclusive of the serum starvation process in 2.3.1.1.1. Cell viability was measured using the neutral red assay following the process described in 2.3.4. Where combined DAPI and phalloidin-FITC staining was used for microscopy, this was carried out using the processes described in 2.3.6.

6.3.3 Concentrations of H_2O_2 and NO_2^- in PAM

As the PAM was mixed prior to addition to cell samples, it can be assumed that all cells within a sample were subject to exactly the same concentrations of H_2O_2, NO_2^- and other RONS when this PAM was added, regardless of their position within the monolayer of cells in the well of the 96-well plate. The approximate concentrations of H_2O_2 and NO_2^- that would be encountered by these cells for the PAM treatments used in this chapter can be deduced from the work performed in 4.4.1 (Table 6.1).

Table 6.1. Concentrations of H_2O_2 and NO_2^- achieved by Reactor 1 in DMEM-PAM for the treatments used in this chapter. All concentration values are the result of the experiments carried out in 4.4.1, aside from that for a one-minute treatment, where the H_2O_2 and NO_2^- concentrations have been estimated using the line-of-best-fit equations determined in those sections.

NTP treatment time (minutes)	**H_2O_2 (mM)**	**NO_2^- (mM)**
0	0	0
1	0.2	0.1
5	0.8	2.1
15	2.5	5.8
30	5.2	13.0

6.4 Results and discussion

6.4.1 Viability at 24 hours following DMEM-PAM exposure

A large body of research has shown the ability of PAM to affect cell viability, across a range of different cell types (Table H.2), however, it was still important to confirm that the PAM produced by Reactor 1 was capable of doing so as well. Therefore, the viability of 3t3 at 24 hours following a one-hour application of DMEM-PAM made using 5 or 15 minutes of NTP treatment, was measured (Figure 6.1(a)). It was found that the DMEM-PAM created using 5 minutes of NTP gave a cell viability that was 43.27 % of that of the control (SE = 7.64 % of control average) whereas for the 15-minute treatment this value was 14.14 % (SE = 2.64 % of control average). Both results were found to be statistically different from control ($p = 0.044$ and $p = 0.008$ respectively). Separately to this experiment, a longer NTP treatment

time of 30 minutes to create DMEM-PAM was also considered (Figure 6.1(b)). This was found to give a cell viability of 7.92 % of control (SE = 1.12 % of control average), again a statistically significant change ($p = 0.015$).

DMEM-PAM created using a 15-minute NTP treatment gave a viability that was around one third of that created with a 5-minute treatment, and the 30-minute treatment gave a viability of around half of the 15-minute treatment. However, the reduction between 0 and 5 minutes did not fit in with this pattern.

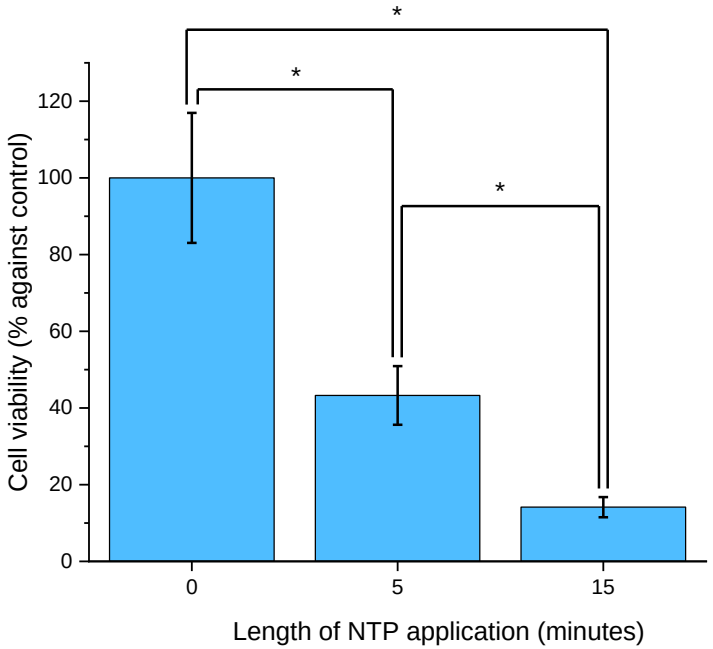

(a)

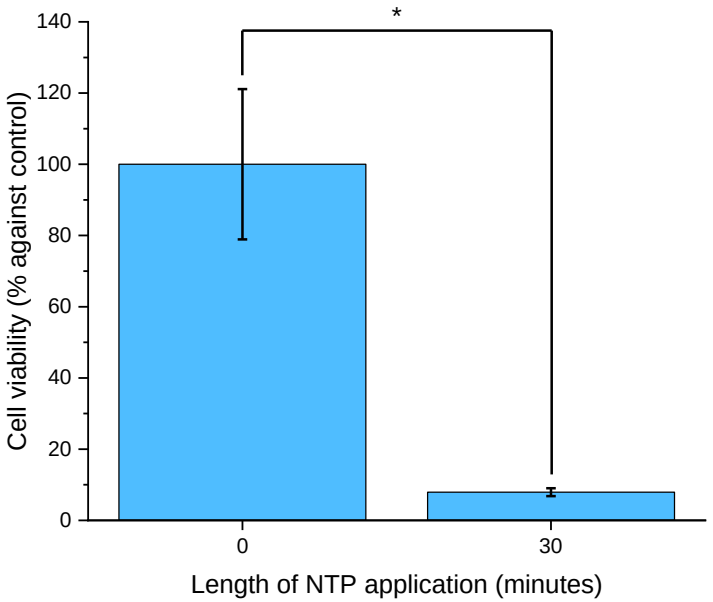

(b)

*Figure 6.1. Cell viability measured at 24 hours following one hour of DMEM-PAM application (a) PAM created by NTP treatment of 5 or 15 minutes in Reactor 1. n=6, SE shown, *: $p < 0.05$, Welch test with Games-Howell post-hoc (b) PAM created by 30 minutes of NTP treatment in Reactor 1, n=3, SE shown, *: $p < 0.05$, independent t-test.*

A small number of papers have been identified which considered viability following the application of PAM to fibroblasts (Table 6.2), and these were of particular interest for comparison against Reactor 1. All of these papers demonstrated a reduction in cell viability from the treatment. However, as was found in the previous chapter with direct treatment, most were, in reality, not truly comparable with the work performed here due to major differences in the time of exposure of the cells to PAM. Nguyen *et al.* [81], Tiede *et al.* [252] and Torii *et al.* [259] used cell exposure times which greatly exceeded that used in the work of this project, with each of them leaving the cells in the PAM for at least a day. Balzer *et al.* [62], on the other hand, added PAM to their cells for a very short period of only 5 minutes. As will be shown, and discussed, in 6.4.5, the length of time the cells are exposed to PAM greatly affects its impact. Two of the papers in Table 6.2 did, however, apply their PAM treatments in a similar manner to the work performed here, with the treatment liquid being applied for one hour only prior to its replacement with fresh, untreated medium until assay 24 hours later, specifically the work of Hara *et al*. [260] and of Girard *et al.* [161].

Hara *et al.* [260] showed that an application of their PAM, created by 2 minutes of NTP treatment, for one hour reduced viability by 20 % of the control value. Although not measured, this may be of a similar scale of effect that would be obtained by PAM created by a similar length of treatment in Reactor 1, as a 5-minute treatment gave a reduction that was 57 % of the control value (Figure 6.1(a)).

Girard *et al.* [161] found that, with PAM created using 2 minutes of NTP treatment, one hour of exposure resulted in primary human skin fibroblasts having a viability of 2-3 % of control, and the MRC5Vi fibroblast cell line having a viability of 10-20 % of control. With a

4-minute treatment, viability was in the region of 2-3 % for the primary fibroblasts and around 5 % for MRC5Vi. The H_2O_2 and NO_2^- concentrations with these treatments were approximately 700 µM H_2O_2 and 750 NO_2^- µM for 2-minute PAM and 1300 µM and 1600 µM for 4-minute PAM. Comparing with the results from 4.4.1, the H_2O_2 concentration of the liquid subjected to 2 minutes of NTP by Girard *et al*. is very close to that of the 5-minute treatment with Reactor 1, but the viability results of their work were much lower than that seen for such a treatment (Figure 6.1(a)). The reason for the apparently stronger biological effect is not clear. Possibilities could include higher concentrations of substances other than H_2O_2 present in the PAM, or perhaps differing qualities of the fibroblasts used. It would be interesting to try PAM produced by both the Girard *et al.* NTP source and Reactor 1 on the same cell line to clarify this.

It is also worthwhile to consider the application of H_2O_2 alone, rather than PAM, to 3t3 in the literature. Laurent *et al*. [261] found that exposure to 2 µM of H_2O_2 was enough to reduce cell viability in 3t3 to around 20-25 % of control. 2 µM is around $1/400$ of the final concentration of H_2O_2 for a 5-minute NTP treatment with Reactor 1, yet treatment with this 5-minute PAM gave less of a reduction in viability than was found by Laurent *et al.* A possible explanation for this difference is that they left the H_2O_2-containing liquid on their cells for 48 hours, which far exceeds the exposure time used on this project. This therefore suggests the possibility of the effect of H_2O_2 application, and therefore of H_2O_2 within an PAM treatment, being a function of both concentration and time, rather than simply of concentration itself.

Table 6.2. Papers which have considered the effect of application of PAM on the viability of fibroblasts, 24 hours or longer after application of PAM. Nakamura et al. [262] investigated WI-38 fibroblasts and PAM, however, there was some difficulty in understanding exactly what the applied treatment actually was, as dilutions were used and it was not clear when these were being used, therefore this has been omitted from the table.

	Author	**NTP source**	**Treatment liquid**	**Cell type**	**Measurement point (hours)**	**NTP treatment time to create PAM (s)**	**Cell viability (% of control)**	**Length of cell exposure to PAM (mins)**
1	Balzer *et al.* [62]	DBD with flat electrodes	PBS	Human foreskin fibroblasts	24	300	55 %	5
2	Girard *et al.* [161]	He plasma jet	PBS	Primary normal human skin fibroblasts	24	120, 240, 480	120 s PAM: 2-3 % 240 s PAM: 2-3 % 480 s PAM: 1-2 %	60
3	Girard *et al.* [161]	He plasma jet	PBS	MRC5Vi (normal human lung fibroblast cell line)	24	120, 240, 480	120 s PAM: 10-20 % 240 s PAM: ~5 % 480 s PAM: ~2 %	60
4	Hara *et al.* [260]	Ar plasma jet	DMEM without FBS	Normal human fibroblasts (not otherwise specified)	20	180, then diluted with 20 µL PAM per 100 µL	80 %	60

	Author	NTP source	Treatment liquid	Cell type	Measurement point (hours)	NTP treatment time to create PAM (s)	Cell viability (% of control)	Length of cell exposure to PAM (mins)
5	Nguyen *et al.* [81]	Air plasma jet	DMEM with FBS	WI38 fibroblasts	24	300	70 %	1440 (24 hours)
6	Tiede *et al.* [252]	DBD with flat electrodes	PBS	GM00637 fibroblasts	48	360	91 %	5 in full strength PAM, then another 2875 (48 hours minus 5 minutes) in diluted PAM
7	Tiede *et al.* [252]	DBD with flat electrodes	PBS	Primary human skin fibroblasts	48	600	83 %	5 in full strength PAM, then another 2875 (48 hours minus 5 minutes) in diluted PAM

	Author	NTP source	Treatment liquid	Cell type	Measurement point (hours)	NTP treatment time to create PAM (s)	Cell viability (% of control)	Length of cell exposure to PAM (mins)
8	Torii *et al.* [259]	Ar jet	RPMI, not clear whether FBS was present	WI-38 fibroblasts	24	300	25 - 30 %	1440 (24 hours)

6.4.1.1 Morphological effects

DAPI and phalloidin-FITC staining of 3t3 treated with DMEM-PAM created with 30 minutes of NTP treatment was also carried out at 24 hours following the completion of the PAM treatment (Figure 6.2).

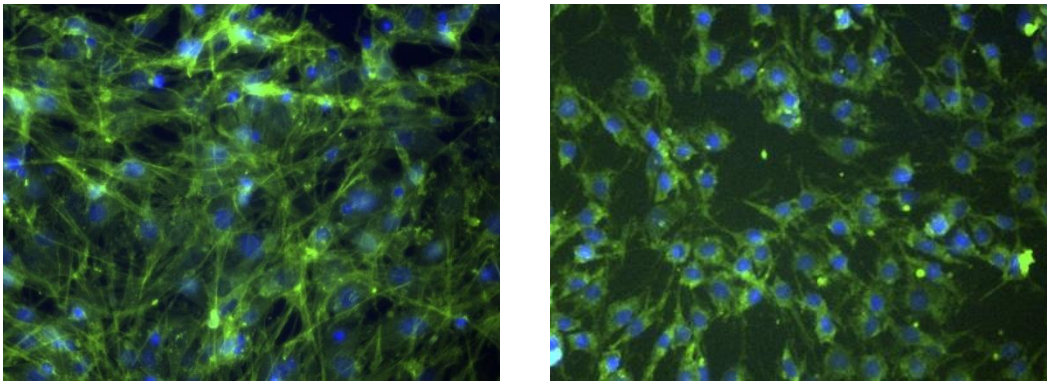

(a) *(b)*

Figure 6.2. Phalloidin-FITC and DAPI staining of 3t3 (a) control (b) 24 hours following one hour exposure to DMEM-PAM created with 30-minute NTP treatment.

It is evident that, although the treated cells (Figure 6.2(b)) do appear to have some collapse of the cytoskeleton in comparison to the control samples (Figure 6.2(a)), this is not to the same extent as was observed in the equivalent direct sample (Figure 5.3(c)), even though the viability assay showed a lower viability with the PAM treatment than the direct sample (Figure 6.1(b), Figure 5.1(b)). The reason behind this difference in the cell appearance is not clear, but it is suggestive that the cells subjected to PAM, although no longer viable, are not as far advanced through the apoptosis pathway as the direct cells were at this timepoint. Why this would be the case is, however, not known.

6.4.2 Cell viability and morphology immediately following DMEM-PAM exposure

The cell viability of 3t3 immediately following a one-hour application of DMEM-PAM created with 30 minutes of NTP treatment, rather than 24 hours later, is shown in Figure 6.3. Compared with the control value set at 100 % (SE = 29.81 % against control average), a viability of 86.23 % was measured (SE = 26.04 % of control average). This difference from control was not statistically significant (p = 0.746). Comparative microscope photographs are shown in Figure 6.4.

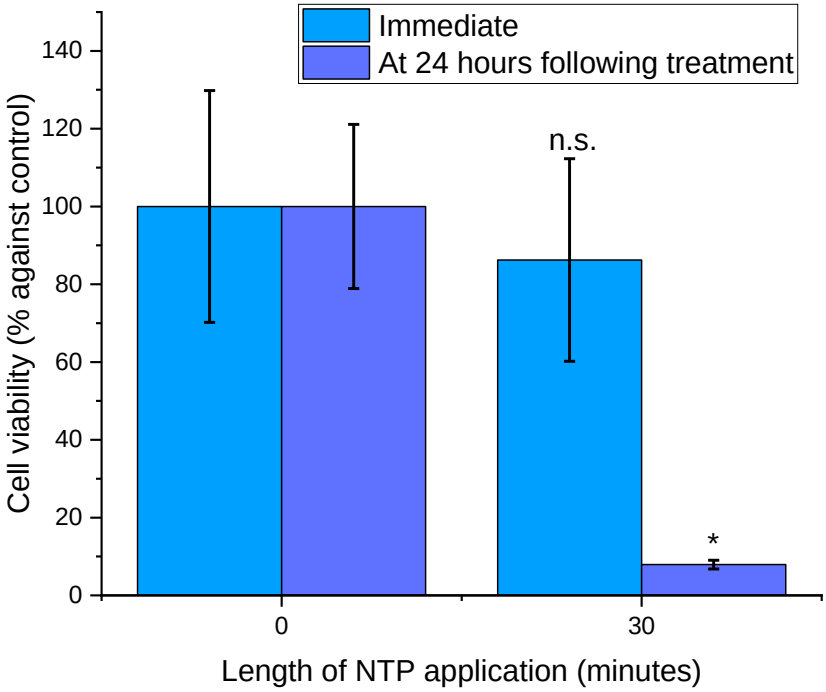

Figure 6.3. Cell viability of 3t3 measured immediately following one hour of exposure to DMEM-PAM, created with a 30-minute NTP treatment, shown against control (0 minutes of NTP application). Equivalent data for measurement at 24 hours is also reproduced from Figure 6.1 for comparison. n=3, SE shown, n.s.=difference not statistically significant, independent t-test. Significance measured against relevant control bar (0 minute bars, for either immediate measurement or measurement at 24 hours, as appropriate).

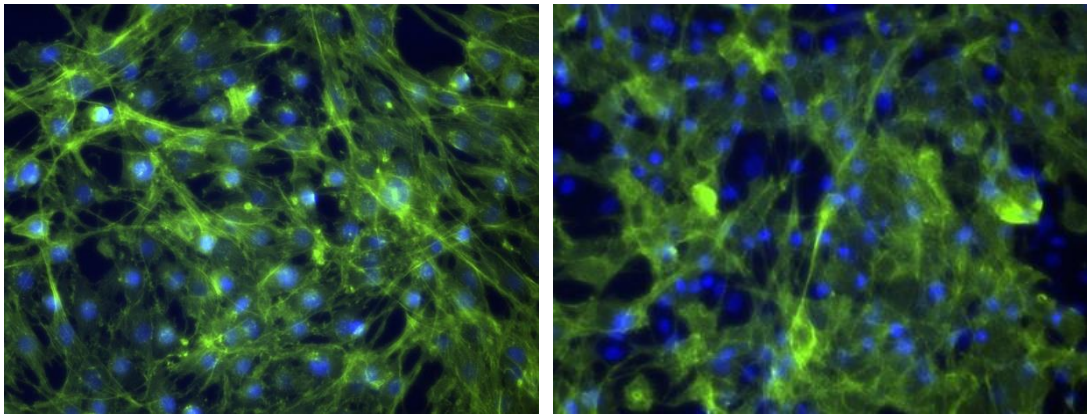

(a) (b)

Figure 6.4. Phalloidin-FITC and DAPI staining of 3t3 (a) control (b) immediately after one hour exposure to PAM created by 30-minute NTP treatment.

The results from Figure 6.3 contrasts to 7.92 % of the average control value for the viability measurement taken 24 hours following DMEM-PAM exposure (Figure 6.1(b)), indicating that there is a period of time required post-treatment for the negative effects to be realised by the cell.

The previous chapter considered the immediate effect of direct treatment on 3t3 viability (5.4.2), finding that a 30-minute application of NTP gave an average of 20.38 % of control, compared with the equivalent value for DMEM-PAM of 86.23 % given above. It would therefore appear that direct treatment was able to immediately reduce viability of 3t3, whereas the equivalent PAM treatment could not. The reasons for this difference in results for the two treatment types is not presently clear, but may be due to factors such as short-lived RONS and electrical effects being present in direct treatment but not in PAM. Both direct and PAM samples did, however, maintain apparently normal morphology in the

period immediately following the removal of the treatment liquid (Figure 5.5(b) and Figure 6.4(b)).

A small number of papers have been identified where viability has been measured immediately following a short PAM treatment, some of which were on fibroblasts [62][263]. The experiments of Balzer *et al.* [62] were the most comparable to those performed here. They obtained an immediate 55 % reduction in the viability of human primary fibroblasts with PAM which contained 200 µM H_2O_2 and 300 µM NO_2^-, and which was created using 300 s of treatment in a DBD-style device. Their result is different from that of Figure 6.3 where an immediate effect was absent, somewhat surprising given the longer contact time used in the Figure 6.3 work, and the much higher concentrations of H_2O_2 and NO_2^- produced by Reactor 1, which, it might be thought, would result in a faster cell response. The results of Balzer *et al.* also appear unusual as, reading outside of the fibroblast literature, others have found that, much like the results in Figure 6.3, the measured reduction in viability with PAM treatment was not immediate [264][242].

6.4.3 Combined direct and PAM treatment

At 24 hours following treatment, direct treatment applied to 3t3 in Reactor 1 for 30 minutes resulted in a viability of 37 % of control (Figure 5.1(b)), whereas DMEM-PAM created using the same 30-minute treatment gave a viability of 8 % (Figure 6.1(b)). This therefore suggests that the PAM treatment was more effective than the direct treatment at reducing viability, something which is at odds with the findings of most other researchers who have found that there was no significant difference between the two treatments [155][157][73][104][155][156][62].

A possible reason behind the difference in the findings of these papers, and those in this project, is that with this work the treatment liquid in a direct application was immediately removed at the end of the NTP exposure, meaning a maximum exposure time for the cells of 30 minutes, with the liquid also having low levels of NTP-produced RONS for the earlier part of the treatment. This contrasts to the approach that is usually used by researchers carrying out a direct application, where the cells would be left in the directly treated liquid until the point of assay, which is likely to be at least 24 hours later, resulting in something which could be described as a combined direct-PAM treatment.

An experiment was carried out with Reactor 1 to compare a PAM treatment with such a combined direct-PAM treatment. To carry out this work, 3t3 cell samples were either subjected to 10 minutes of direct treatment, followed by 50 minutes remaining in the treatment liquid, or alternatively one hour of exposure to DMEM-PAM created by 10 minutes of NTP treatment (Figure 6.5). In both cases, the liquid was removed at the end of these times and replaced with untreated medium until assay 24 hours later. Compared with control (SE = 4.87 % of control average), the DMEM-PAM treatment had an average cell viability of 63.57 % (SE = 2.78 % of average control value), whereas the combined treatment had an average of 50.69 % (SE = 4.83 % of average control value). While both the PAM and combined treatments were statistically significantly different from the control ($p < 0.001$ for both), as would be expected, they were not from each other ($p = 0.138$). It was therefore possible to conclude that the results from Reactor 1 agree with the accepted findings in the literature in terms of the similarity of effect between PAM and direct treatments.

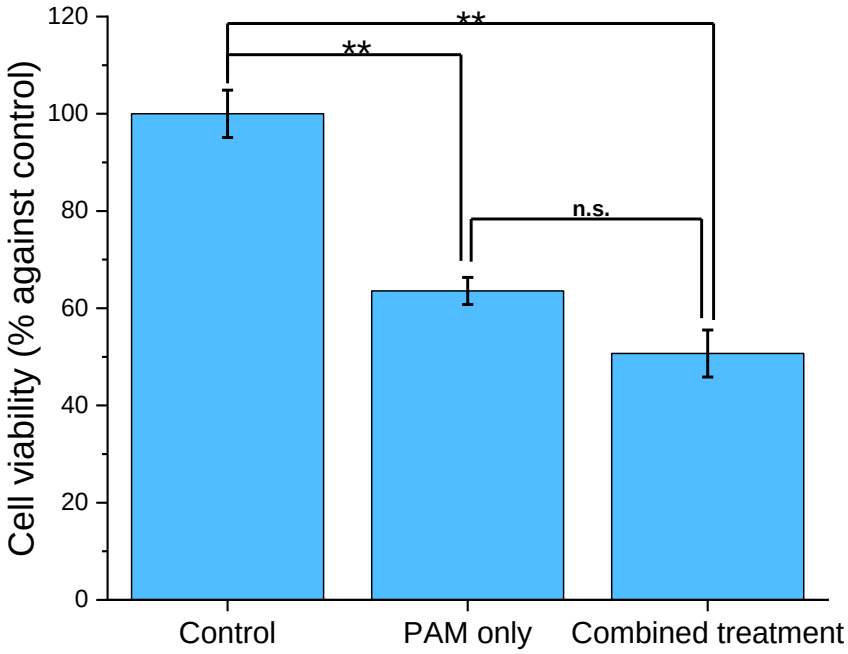

*Figure 6.5. Comparison between combined treatment and PAM only treatment. n=4, SE shown, **: p < 0.05, *: p < 0.001, n.s. = difference not statistically significant, ANOVA with Tukey HSD post-hoc.*

6.4.4 Effect of cold storage on DMEM-PAM efficiency

If the use of PAM progresses to clinical use, it is unlikely to be produced immediately before application to a patient. Consequently, it is necessary to develop a complete understanding of the extent to which PAM maintains its biological efficacy when stored for prolonged periods, and what its optimum conditions of storage are. A comparison was therefore carried out on the viability of 3t3 treated with DMEM-PAM used immediately after its production with a 30-minute treatment in Reactor 1 versus DMEM-PAM used after 48 hours of 4 °C refrigerated storage post-production (Figure 6.6). Against a control value set to 100 % (SE = 21.11 % of control average), DMEM-PAM used immediately gave a viability

of 7.92 % (SE = 1.12 % of the average control value) whereas the DMEM-PAM stored for 48 hours gave a viability of 14.33 % (SE = 1.28 % of the average control value). The difference between viability with the immediately used and the stored DMEM-PAM was found to be statistically significant, with the stored liquid being less effective at reducing cell viability ($p = 0.043$).

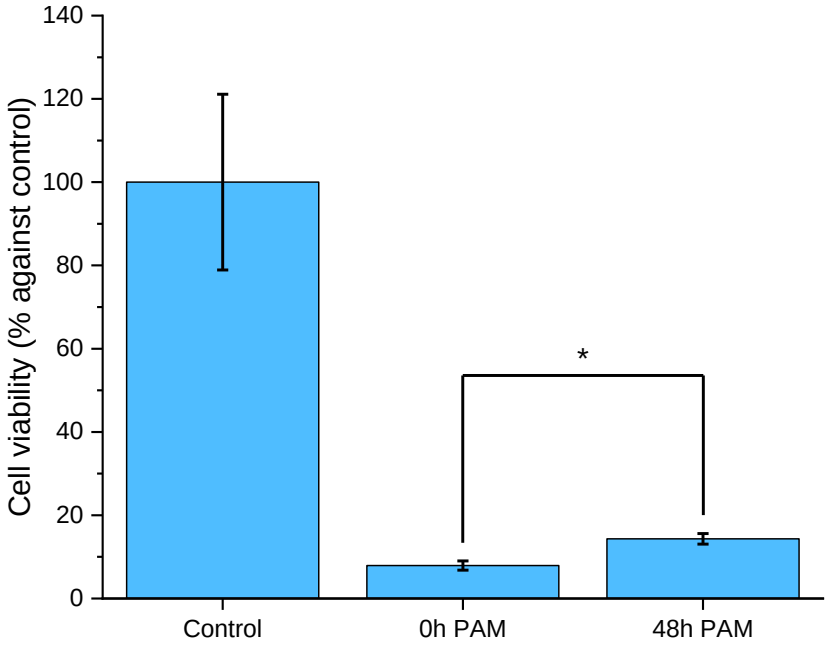

*Figure 6.6. Cell viability of 3t3 measured 24 hours following a one-hour application of DMEM-PAM, applied either immediately following its creation (0 h PAM) or after 48 hours of cold storage at 4 °C (48 h PAM). n=3, SE shown, *: $p < 0.05$, Welch with Games-Howell post-hoc test.*

A number of papers have considered the effect of delayed use of PAM on its ability to reduce viability, covering a range of storage temperatures and time periods (Table 6.3). From these, it would appear that it is more likely that a PAM maintains its potency when it is stored frozen rather than at warmer temperatures. Also, it is apparent, particularly from [223], that it

would be expected that refrigerated storage would result in reduced efficacy of PAM, but that this would not be a severe reduction, which agrees with what was observed in Figure 6.6.

Table 6.3. Key papers examining the effect of storage of PAM on its cell viability-reducing abilities.

	Author	Cell type	Storage temperature (°C)	Liquid	Storage time	Reduced PAM effect with storage?	Summary of results
1	Adachi *et al.* [223]	A569 (Human lung carcinoma) cell line	• Room temperature • 4 °C • -30 °C • -80 °C	DMEM without FBS	Up to 7 days	Yes	• Room temperature storage resulted in degradation of ability to reduce cell viability to almost no effect after 7 days. • -80 °C storage resulted in minimal degradation of PAM efficacy after 7 days. • With 4 °C and -30 °C storage, some evidence of degradation of effect present by 3 days, but not as severe as when stored at room temperature.
2	Bekeschus [122]	Primary CD4+ T helper cells	37 °C	RPMI with FBS	Up to 6 hours	Yes	Reduced efficacy with all storage times.
3	Mohades *et al.* [242]	SCaBER cell line	Room temperature	MEM (minimum essential medium)	• 15 min • 1 hour • 8 hours	Yes	Reduced efficacy with all storage times.

	Author	Cell type	Storage temperature (°C)	Liquid	Storage time	Reduced PAM effect with storage?	Summary of results
4	Nguyen *et al*. [155][81]	HeLa (Human cervix epithelioid carcinoma) cell line	-20 °C	DMEM with FBS	• 1 month • 6 months	No	Minimal reduction in efficacy.
5	Tanaka *et al* [80].	U251SP (human glioblastoma astrocytoma) cell line	Not stated, but assumed room temperature	DMEM with FBS	• 1 hour • 8 hours • 18 hours	Yes	Ability to reduce viability completely gone with 18 hours of storage.
7	Yan *et al.* [265]	MDA-MB-231 (adenocarcinoma) cell line	• 8 °C • -25 °C	PBS	3 days	No	Retained ability to reduce viability when stored at either temperature.

Due to time limitations, the H_2O_2 or NO_2^- levels in the DMEM-PAM produced by Reactor 1 were not measured following the 48-hour storage period, but evidence from the literature does support the idea that the reduction in the biological effects of PAM occur as a result of falling levels of cytotoxic ROS. Adachi *et al.* [223] found that H_2O_2 levels in PAM made from DMEM without FBS fell within 7 days from ~ 600 µM at initial creation, to ~250 µM for room temperature storage, ~400 µM for 4 °C storage, and ~250 µM for -30 °C storage. There was minimal change with -80 °C storage. This corresponds to their biological results, which showed that -80 °C storage resulted in no reduction of PAM efficacy, room temperature storage caused PAM to lose nearly all its effect, and the effects of 4°C and -30 °C storage were somewhere in between (Table 6.3, entry 1). It is not clear why the 4 °C storage was better at maintaining PAM quality than the -30 °C, as this appears counter intuitive. Another paper, that of Nguyen *et al*. [155], found that, with a similar storage temperature, -20 °C, H_2O_2 levels were maintained for 6 months. The reason for the difference between the work of Adachi *et al.* and Nguyen *et al.* is not known.

Other papers also confirmed that H_2O_2 levels reduce in stored PAM made from cell medium, although they did not link their results directly to biological effects. Yan *et al.* [265] found that H_2O_2 levels in DMEM-PAM which had been stored at 8 °C for 26 hours roughly halved, whereas storage at 22 °C resulted in a fall of around 75 %. Mohades *et al.* [177] found that H_2O_2 in MEM-based PAM stored at room temperature fell by 18 % after 1 hour, 45 % by 8 hours, and 80 % by 12 hours. Both these papers provide further evidence that the degradation of PAM over time is highly dependent upon storage temperature. It is therefore likely that the difference in effect between immediately used PAM and that used 48 hours later, seen in Figure 6.6, is due to reducing concentrations of RONS such as H_2O_2, which break down into substances which are less harmful to cells over the intervening two

days.

Although not examined on this project, there needs to be further understanding developed of the storage characteristics of PAM made from different liquid types, which will allow a better understanding of the most suitable of these for the clinical use of PAM. There has been a partial demonstration of this within the literature. Yan *et al.* [265] found that H_2O_2 levels in NTP-treated PBS remained constant at 8 °C for 7 days, contrasting with their results at the same temperature when DMEM was used and H_2O_2 levels fell. This provides an explanation for their biological results which appeared to contradict those of other researchers. They were able to link this difference between PBS and DMEM to the presence of amino acids in the DMEM, especially methionine and cysteine, neither of which would be present in PBS. Kurake *et al.* [166] stored PAM made from DMEM for 24 hours, finding that the absence of FBS allowed H_2O_2 and NO_2^- concentrations to remain stable with storage, but that this was not the case when FBS was present. Adachi *et al.* found that even slightly different formulations of medium could result in varying maintenance of H_2O_2 levels [223].

It is therefore clear that successful preservation of the chemical and biological qualities of PAM over longer treatment times is dependent upon both storage conditions and the liquid used to form the PAM, and it is likely that the maintenance of the biological effect with storage is linked to the maintenance of the chemical profile of the liquid used as the basis for the PAM. This would provide an explanation for the statistically significant, but still small, reduction in the biological efficacy of DMEM-PAM in Figure 6.6: at 4 °C it would be expected that there would be some degradation of PAM quality, probably more than if the PAM was frozen at -80 °C but less than if it was kept at room temperature, but the omission of FBS from the DMEM-PAM may have helped to maintain its initial characteristics.

6.4.5 Short exposure to DMEM-PAM

In *in vivo* and clinical settings, it may be difficult to maintain a long contact time between the biological target area and the applied PAM, and so it is important to understand the difference in the impact caused by cells in contact with PAM for short versus longer periods. The experimental work in Figure 6.7 was therefore carried out to allow comparison between the effects on cell viability (24 hours later) of a short, one-minute exposure of cells to DMEM-PAM and those of a one-hour exposure (Figure 6.1(a)) on the 3t3 cell line. Compared with control viability set to 100 % (SE = 14.87 % of control average), the samples exposed to the DMEM-PAM for one minute had an average viability of 110.27 % (SE = 16.50 % of control average) with the difference from control not being statistically significant ($p = 0.660$). This contrasts with the equivalent value with a one-hour exposure of 14.14 % (Figure 6.1(a)). Thus, it is clear that a reduction in viability is contingent upon a lengthy exposure to PAM.

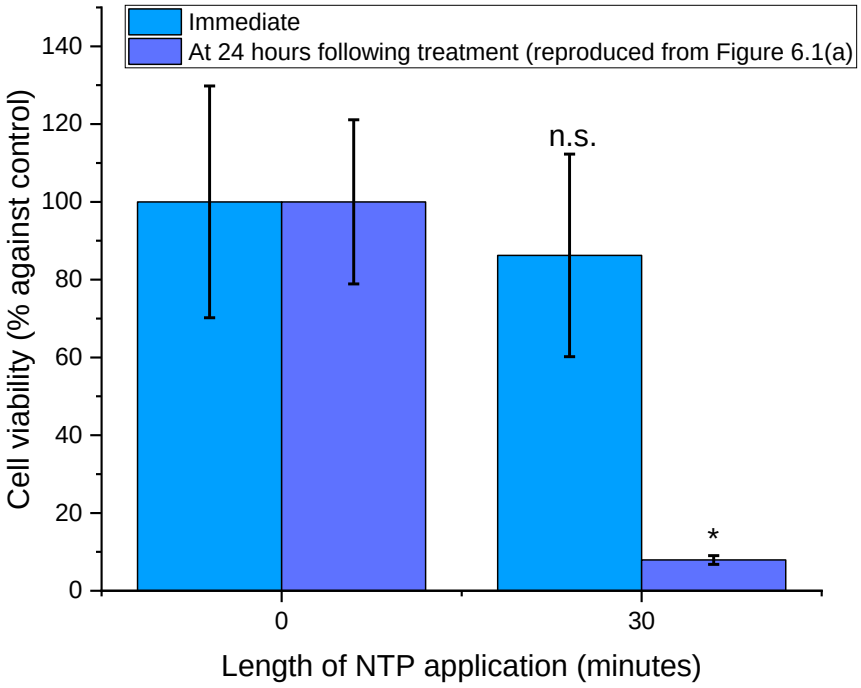

*Figure 6.7. 3t3 cell viability at 24 hours following a one-minute exposure to DMEM-PAM, shown alongside equivalent results for one hour of 3t3 exposure to DMEM-PAM, reproduced from Figure 6.1(a). For one-minute results: n=4, SE shown, n.s.= difference not statistically significant, independent t-test (2-tailed significance). For one-hour results: n=6, SE shown, *: p < 0.05, Welch test with Games-Howell post-hoc.*

Although PAM has been explored in detail by many researchers, most of this has focused on relatively long exposures of cells to PAM, with a very small number of papers having considered PAM applications to cells of under an hour. It is, however, clear from the literature, as well as from the work carried out above, that shorter contact times with PAM reduce the resultant effects on cells. Sato *et al.* [205] found that 10 minutes of exposure to PAM resulted in a viability of 88 % of the control average for the HeLa (human endocervical adenocarcinoma) cell line, measured 24 hours following the exposure, whereas leaving the

same PAM on for two hours gave a viability of 0 % of control. Similarly, Kajiyama *et al.* [266] found that, at 48 hours following initiation of PAM exposure, the average viability of K2 (human melanoma) cells against control was around 90 % for a 5-minute exposure, 80 % for a 30-minute exposure, 3 % or less for 3-hour or 48-hour exposures. Clearly, from the results presented here, short PAM exposure times have a less drastic effect on cell health than longer times. This is surprising. It would be expected that the H_2O_2, responsible for much of the effect of PAM according to the literature (4.2.1), would move extremely quickly into the cells from the PAM [265], as it passively diffuses and also travels through channels in the cell membrane (Figure 1.19). Therefore, it would be assumed that one minute of cell exposure to PAM would be sufficient for a significant amount of H_2O_2 to move into the cell. There is currently no clear explanation as to why this difference in effect occurs between PAM exposure of a few minutes and that of longer time periods, and so further research is required in this area.

This work leads to questions around the combined effect of the "strength" of PAM and the time of exposure to it:

- What is the threshold time for cell exposure to PAM which would produce a reduction in viability for the strength of DMEM-PAM used here?
- Assuming that this threshold is below one hour of cell exposure to PAM, how large is the reduction in viability in comparison to that of one hour of exposure, seen in Figure 6.1(a)? Is it the same or lower?
- Is it possible to use a strength of PAM which does in fact reduce viability after only one minute of cell exposure?
- Do these timings vary for different cell types?

- From answering these questions, and observations about how the viability level changes with different NTP treatment times of PAM (6.4.2.1), is it possible determine a formula to bring PAM strength and cell exposure time together as a combined dosage figure?

6.4.6 DPBS-PAM

In order to compare the effects on cell viability of using DPBS as the basis of PAM rather than DMEM, DPBS-PAM was immediately applied to 3t3 samples for one hour following its creation in Reactor 1, prior to viability assay 24 hours later (Figure 6.8). Compared with the control viability set as 100 % (SE = 1.89 % of control average), the treatment with DPBS-PAM gave 17.27 % of the control value (SE = 6.56 % of control average). The difference from control was statistically significant ($p < 0.001$).

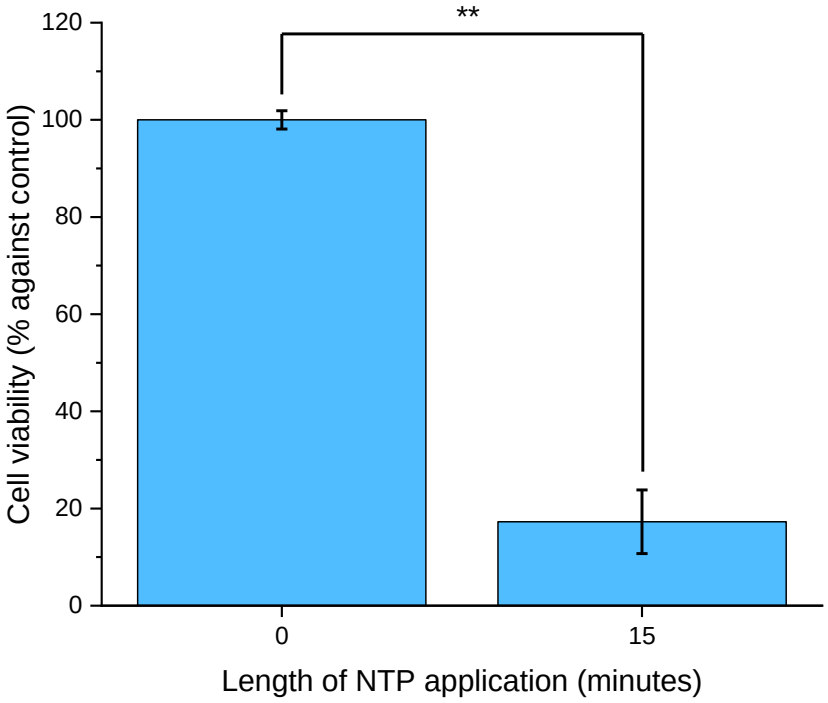

*Figure 6.8. Viability of 3t3 at 24 hours following a one-hour of exposure to DPBS-PAM, created by 15 minutes of NTP treatment. n=3, SE shown **: $p < 0.001$, independent t -test.*

Comparing this with the results of Figure 6.1(a), it can be seen that this response was nearly identical to when DMEM-PAM was used instead, and therefore the effect of the PAM does not appear to change regardless of which of these two liquids is used as its basis. This result is not surprising given the established prominence of H_2O_2 in NTP treatments, and the likelihood that most of the H_2O_2 comes from the water-based reactions in 1.2.3.5.1. Ideally, H_2O_2 and NO_2^- would also have been measured in the DPBS-PAM to confirm similar levels to those in DMEM-PAM (Figure 4.1 and Figure 4.2) but this was not possible due to time constraints. However, Yan *et al*. [265] showed that H_2O_2 levels were similar in PAM produced from DMEM versus that produced by PBS.

Despite this, there is some evidence that there are some relevant chemical differences between PAM made from cell culture medium and PAM made from PBS. Kalghatgi *et al.* [82] found that the use of PBS to create PAM did not have the effect of causing DNA damage, whereas the use of FBS-free medium did. The addition of bovine serum albumin (BSA) to the PBS resulted in PAM which caused DNA damage within the cells, and they therefore concluded DNA damage was related to amino acid peroxidation. Interestingly, they found that, unlike PAM, direct treatment with PBS did give detectable DNA damage, although the reason for this difference between the direct and indirect treatments was not discovered.

It should also be remembered that the use of DPBS and cell medium have only been considered here in terms of immediate application of PAM following its creation, and purely in terms of its biological effects. As has been discussed in 6.4.4, there is some evidence in the literature that PAM made from PBS may be more successful at maintaining its chemical profile when in prolonged storage, and this cannot be neglected when deciding on the best liquid to use as a basis for PAM. As well as this, as has been pointed out by Freund and Bekeschus [267], there are advantages to the use of liquids such as PBS and Ringer's solution, which has been used to form PAM by some researchers such as Tanaka *et al.* [268], over cell medium, as they are already clinically approved liquids with acknowledged stability. The NTP treatment of these liquids may therefore be an expanding area of research in the future as opposed to that of cell medium.

These results contrast with those for direct treatment (5.4.3), in which it appeared that using DPBS as the treatment liquid resulted in a greater viability reduction than using DMEM. The reasons for this difference in results between direct and PAM treatments are not clear, and this observation has not been noted within the literature.

6.5 Conclusions

This chapter has explored the effects of variations in PAM treatment on the viability of two cell lines, 3t3 and the differentiated form of U937. When considered at 24 hours following the removal of the PAM, cell viability was reduced in both cell lines with treatments created from NTP exposure of 5, 15 and 30 minutes, within 3t3 appearing more susceptible to PAM-induced damage than U937 at the shorter time periods. This work clearly showed that PAM created with Reactor 1 had biological effects on both cell lines, again showing the suitability of the design for plasma medicine research.

It was found that 3t3 did not show an immediate reduction in cell viability when treated with PAM created with 30 minutes of NTP exposure. This contrasted with the equivalent results for direct treatment, where an immediate reduction in viability was observed. The reasons for the difference in response between the two treatments are not clear but may be due to things such as short-lived RONS, electric fields, or concentration variances present within a directly treated well which would not be present when PAM was used instead. With differentiated U937 it was found that, unlike 3t3, there was an immediate reduction in viability following the application of PAM. Considering the 3t3 results, this was not expected as it would be assumed that a macrophage-like cell such as this would have better developed defences against RONS.

The effect on the biological efficacy of PAM following 48 hours of storage at 4 °C was considered. It was found that storage under these conditions resulted in a PAM slightly less capable of reducing cell viability than if it had been used immediately after its production. From a review of the literature, it was deemed likely that this was due to the degradation of ROS such as H_2O_2 over the storage period, and that the rate of this degradation was

possibly influenced both by the storage conditions themselves, and also by the chemical profile of the FBS-free DMEM used as the basis of the PAM.

One minute of exposure to PAM had a minimal effect on the viability of 3t3, in contrast to one hour of exposure. This finding agrees with other work within the literature, but is still somewhat surprising, given that the movement of H_2O_2 into cells should be rapid as it occurs through passive diffusion and through channels in the cell membrane. The reasons for the lack of effect with very short exposures to PAM are currently unknown.

Little difference was identified in the cell viability reduction when DPBS-PAM was used on 3t3 in comparison to that when DMEM-PAM was used. Although not measured directly, it is thought likely that this is due to the concentrations of RONS being similar in both PAMs due to the formation of these being largely the result of NTP interaction with water. However, it has been noted in the literature that there may be differences between the effects of these two types of PAM, attributed to interaction between NTP and the amino acids present in cell medium which results in DNA damage. It is also the case that the biological impact of a specific PAM is not the only thing to be taken into account when selecting a liquid as the basis for its creation, as factors such as storage characteristics and regulatory approval status may also be relevant.

Chapter 7 Diluted PAM on macrophage-like U937

7.1 Aims

The overall aim of the work presented in this chapter was to develop an understanding of how the macrophage-like form of the U937 cell line responds to Reactor 1 PAM, and how different dilutions of PAM change these responses. Specifically, the objectives of this chapter were to:

1. Develop a basic understanding of the response of the differentiated form of the U937 cell line to PAM created in Reactor 1, and contrast to the response seen in the 3t3 cell line.
2. Investigate the response of PMA-differentiated U937 to repeated applications of Reactor 1 PAM.
3. Understand whether the application of Reactor 1 PAM could modify the response of PMA-differentiated U937 in the areas of
    a. Phagocytosis
    b. Cytokine and chemokine secretion
    c. Antioxidant gene expression.

7.2 Introduction

An overview of the mammalian immune system, and the position of macrophages within it was given in 1.2.1.2. A review of the literature of NTP applied to immune cells was also given in 1.2.3.3.2, with 1.2.3.3.2.1 specifically focussed on its application to macrophages. Some background information on antioxidants was provided in 1.2.1.3.

There are several areas of work in this chapter which are novel, and have not appeared elsewhere in the literature. Investigations into the effect of NTP treatments on the phagocytic ability of macrophage-like cells has not been performed elsewhere as far as has been determined. Although the effects of NTP treatments on the secretion of chemokines and other cytokines has been examined elsewhere, this has not been carried out with either the U937 cell line, or with PAM produced in the style of NTP source used here. Further to this, the effect of different PAM strengths on this cytokine secretion does not appear to have been considered elsewhere. Although the expression of SOD1 and SOD2 in response to NTP treatments has been considered by others, this has not been with the U937 cell line, nor using an NTP source of a design such as that of Reactor 1.

7.3 Methods

7.3.1 U937 cell samples and PMA

All work within this chapter has used the U937 cell line, differentiated to a macrophage-like cell using PMA. As has been stated in 2.3.1.2, U937 is a human lymphoma-derived cell which, undifferentiated, shows monocytic characteristics [269].

For all experiments, U937 samples were set out in 96-well plate wells following the process described in 2.3.1.2. To differentiate the cells, PMA was added at a concentration of 16.2 nM, as described in 2.3.1.2.1, a choice of concentration justified by the work performed in Appendix D.

7.3.2 PAM treatment

For all experiments in this chapter, PAM-based NTP treatment was carried out rather than direct treatment. All PAM was created by exposing FBS-, antibiotic- and glutamine-free RPMI to NTP in Reactor 1 for periods of up to 30 minutes. The starting volume was always, as with previous work, 325 µL. Where the PAM was not diluted prior to use, a 40 µL volume of it was added to cell samples. Where diluted PAM was used (7.3.3), the PAM was diluted as appropriate, and then 40 µL of this diluted liquid was added to the cell samples.

Throughout this chapter, this 'RPMI-PAM' will be referred to simply as PAM, as it is the only PAM type used here.

7.3.3 PAM dilution

Much of the work presented within this chapter has used a standardised PAM created by a 15-minute NTP treatment in Reactor 1, which was then diluted. The comparison of different dilutions of PAM has received a small amount of attention in the literature, including by Nguyen *et al*. [155], Adachi *et al.* [223], Nakamura *et al.* [262] and Tokunaga *et al.* [270]. The reason for its use in the work here is that it ensures a linearity of long-lived reactive species in the PAM, thus ensuring that the change in discharge mode with Reactor 1 treatments, commented upon in 3.4.2 and 3.5, can have no effect on the comparability of the different "strengths" of treatment.

For the experiments investigating the effects of different PAM dilutions, the PAM was used at undiluted strength, and at ½-strength, ¼-strength, and 1/10-strength dilutions, as appropriate (Table 2.1). 40 µL of the final, diluted as appropriate, liquid was added per 96-well plate well of cells. The choice of dilutions was based on the introductory work within

Figure 7.1 and Figure 7.2, which provided an indication of the threshold between lethal and sub-lethal PAM. The dilutions were carried out with fresh RPMI-1640, free of FBS, antibiotics and glutamine. Based on the chemical measurements in 4.4.1, in which a value was obtained for both H_2O_2 and NO_2^- concentrations in DMEM treated for 15 minutes in Reactor 1, the estimated concentrations of H_2O_2 and NO_2^- that cells are exposed to from the diluted PAM used in this chapter can be estimated (Table 7.1).

Table 7.1. Estimated H_2O_2 and NO_2^- concentrations for different dilutions of PAM used throughout this chapter, based on measurements taken in phenol red-free DMEM treated for 15 minutes in Reactor 1 (Figure 4.1).

	H_2O_2 (mM)	**NO_2^- (mM)**
Undiluted	2.6	5.8
1/2 dilution	1.3	2.9
1/4 dilution	0.65	1.45

7.3.4 Cell viability

Viability as assessed by neutral red assay, was carried out following the techniques described at 2.3.4.

7.3.5 Latex bead addition for phagocytosis assessment

FITC-labelled 1 µm latex beads were used to assess phagocytosis. These were prepared and added to the cell samples following the process described in 2.3.8. Justification for the timings of this process is given in Appendix I.

7.3.6 ELISAs

Enzyme-linked immunosorbent assays (ELISAs) were carried out to assess levels of eight different chemokines and cytokines. This was carried out following the process described in 2.3.10.

7.3.7 RT-qPCR

RT-qPCR was carried out both as part of the work in assessing the effects of NTP treatment on phagocytic ability, and also by way of assessment of the effect on expression of genes associated with antioxidants. The sample creation and subsequent RNA isolation, cDNA creation, gene selection and RT-qPCR itself were carried out following the description in 2.3.11.2.

7.4 Results and discussion

7.4.1 Introductory experiments with differentiated U937

Prior to investigating the effects of diluted PAM, introductory viability experiments were carried out using PAM created with different lengths of NTP exposure time, and these results were compared against similar experiments carried out in the previous chapter using 3t3.

7.4.1.1 Cell viability 24 hours following PAM treatment

The viability of differentiated U937 exposed to PAM for one hour, with the PAM having been created using either 15 or 30 minutes of NTP treatment, was therefore measured at 24 hours following the removal of the PAM (Figure 7.1). Against the control samples (SE = 3.50 % of control average), the samples treated with the 15-minute PAM had a viability of

54.96 % of control (SE = 8.83 % of control average), whereas for the 30-minute PAM, the viability was 9.23 % of control (SE = 3.58 of control average). Both of these reductions against control were statistically significant ($p = 0.019$ and $p < 0.001$ respectively).

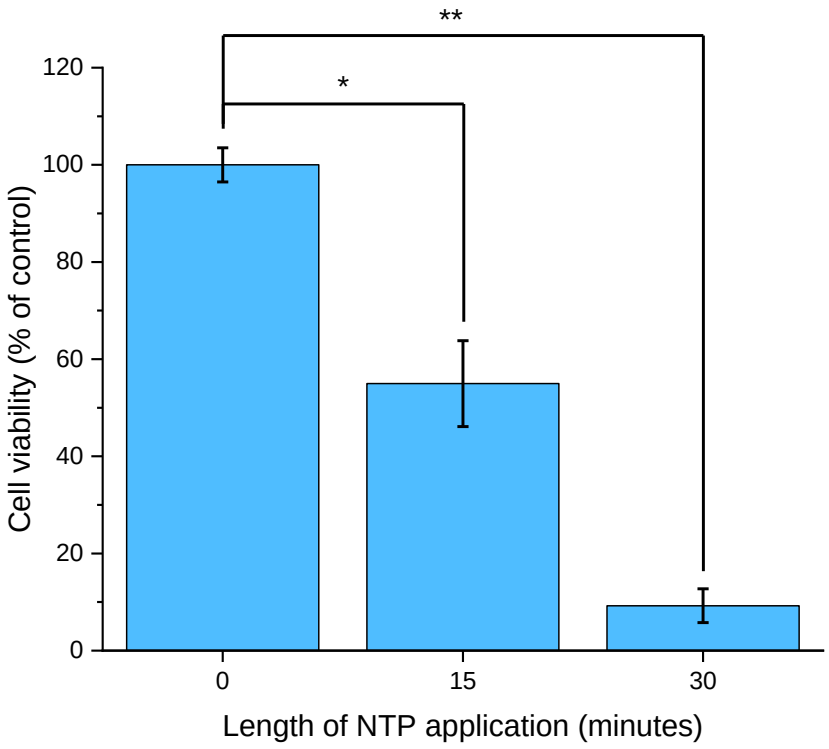

*Figure 7.1. Viability of differentiated U937 at 24 hours following one hour of exposure to PAM, created by either 15 or 30 minutes of NTP treatment. n=6, SE shown, *:p<0.05, ** p < 0.001, Welch with Games-Howell post-hoc.*

It is important to state here that this work was partially repeated as part of a later experiment within the following chapter (Figure 7.4), where, instead of giving a viability level of 54.96 % of control, one hour of exposure to PAM created from 15 minutes of NTP exposure gave a viability of 13.55 %. The reasons for the difference between the results of the two experiments are not clear.

The effects of PAM created with shorter NTP exposures was also examined, showing that it was possible to treat differentiated U937 with PAM of a strength which did not cause a reduction in viability at all (Figure 7.2). PAM created with one minute of NTP exposure resulted in a cell viability of 102 % of the control average (SE = 2.0 % of control average), while PAM created with 5 minutes of NTP exposure resulted in a viability of 106 % of control average (SE = 3.5 % of control average). Neither of these results were significantly different from control ($p = 0.987$ and $p = 0.833$ respectively). Thus, the reduction in cell viability must begin to occur with PAM created with somewhere between 5 and 15 minutes of NTP application.

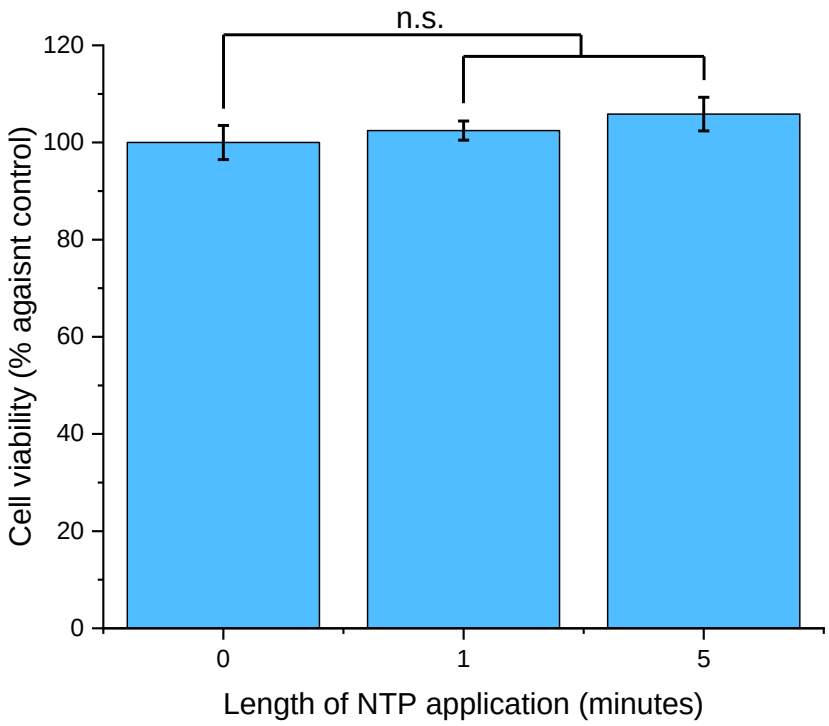

Figure 7.2. Effect of one hour of application of PAM, created with short NTP treatment times, on differentiated U937. Viability considered 24 hours following PAM exposure. n= 6, SE shown, n.s. = difference not statistically significant, Welsh with Games-Howell post-hoc.

7.4.1.2 Cell viability immediately following PAM treatment

For completeness, the viability of differentiated U937 was measured immediately following one hour of PAM exposure. Based on a control viability of 100 % (SE = 3.02 % of control average), PAM created with 15 minutes of NTP exposure gave an average viability of 14.10 % (SE = 3.57 % of control average) in differentiated U937 (Figure 7.3). This difference between the treated and control samples was statistically significant ($p < 0.001$).

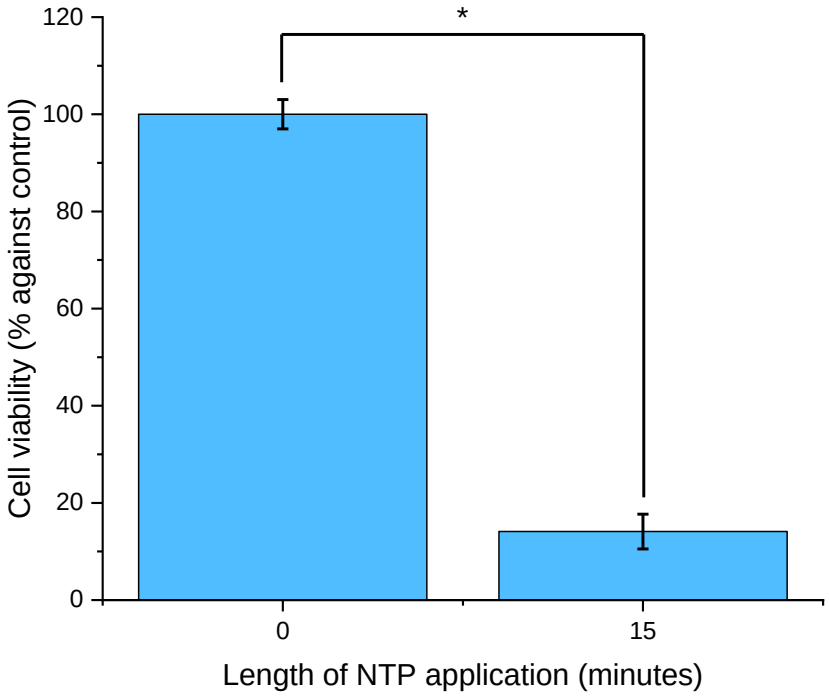

*Figure 7.3. Effect of 15-minute PAM on cell viability of differentiated U937 when exposed to the PAM for 1 hour. Viability measured immediately following PAM exposure. n=4, SE shown, *: $p < 0.001$, independent t-test.*

7.4.1.2.1 Comparison with 3t3

A comparison of the cell viability results of 24-hour post-PAM treatment for 3t3 and differentiated U937 is given below (Table 7.2). This includes the results from Figure 6.1 for

3t3 and Figure 7.1 and Figure 7.2 for U937, as well as the results from the following chapter for the latter cell line which, as discussed above, contradict those of Figure 7.1. The comparison for 15-minute PAM, although it has been included within Table 7.2, will not be commented upon further due to the contradiction in the two sets of results for U937. Examining the 30-minute and 5-minute results in Table 7.2, it is clear that at 5 minutes, 3t3 was much more vulnerable to PAM than U937. This is not unexpected. Macrophage-like cells, such as differentiated U937, produce RONS themselves as part of the inflammatory process *[271]* and they therefore have well-developed systems in place to be able to deal with high levels of these, with the nuclear factor erythroid 2-related factor 2 (nrf2) pathway considered to be the most important, alongside the forkhead box O (FOXO) pathway and others *[272][273]*. However, with the longer 30-minute treatment, the viability levels of both cell lines are almost identical, with a very small proportion of cells in the sample remaining viable. It is likely that, with such a long NTP treatment, the levels of cytotoxic substances within the liquid are now so high that even U937 can no longer cope with it, and the cells become overwhelmed.

Interestingly, when considering the immediate effect of PAM on cell viability, differentiated U937 showed a statistically significant reduction (Figure 7.3) whereas 3t3 did not (Figure 6.3). This is unexpected because, as already explained, U937 cells should be better equipped to protect themselves against high RONS levels than 3t3. The reasons for this finding are unknown, however it is acknowledged that the variances in Figure 6.3 are relatively large, and so may be obscuring an effect. Further experimentation may clarify this.

*Table 7.2. Comparison between viability of NIH 3t3 and differentiated U937, 24 hours following a one-hour application of PAM created in Reactor 1. * indicates significantly different from control.*

	Cell viability (% of control average)	
NTP exposure time (minutes)	**3t3 (Figure 6.1)**	**Differentiated U937 (Figure 7.1, Figure 7.2 Figure 7.4)**
5	43*	106
15	14*	55* or 14*
30	8*	9*

7.4.2 Cell viability effects of diluted PAM on U937

In preparation for the work performed throughout this chapter, it was important to understand the effect on the viability of differentiated U937 of the different dilutions of PAM used (Table 7.1), and therefore a viability assay was performed 24 hours following a one hour application of each of these dilutions to differentiated U937. Against a control average of 100 % (SE = 2.66 % against control average), ¼ strength PAM gave an average viability of 91.46 % (SE = 3.57 % against control average), ½ strength PAM 73.96 % (SE = 6.56 % against control average), and full-strength PAM 13.55 % (SE = 4.14 % against control average). The reductions in viability from control for both the ½-strength and full-strength PAM were statistically significant ($p = 0.003$ and $p < 0.001$ respectively), whereas the ¼-strength was not ($p = 0.742$) (Figure 7.4).

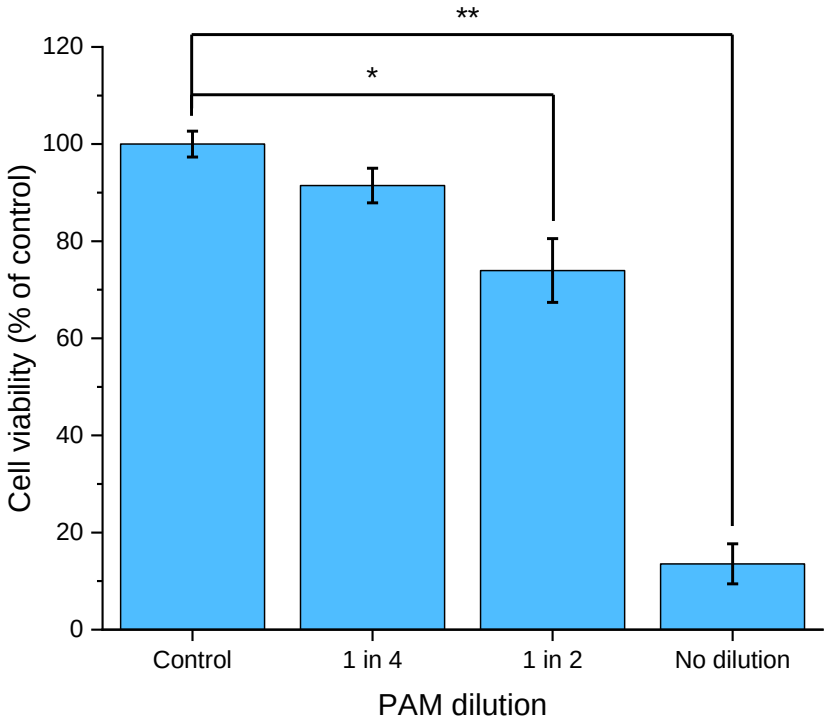

*Figure 7.4. Effect of assorted dilutions of RPMI-PAM, created with 15 minutes of NTP treatment, on cell viability of differentiated U937 when cell exposure was one hour. Viability measured 24 hours following PAM treatment. n=4, *: $p < 0.05$, **: $p < 0.001$. ANOVA with Tukey HSD post-hoc.*

7.4.3 Repeated application of diluted PAM

It has been observed in the literature that low doses of H_2O_2 can be protective against the toxicity of later-applied, higher H_2O_2 concentrations. Lee and Um [274] found that a pre-dose of 0.05 mM H_2O_2 reduced cell death in monocytic U937 when 1 mM H_2O_2 was subsequently applied. Replacing the 0.05 mM H_2O_2 with 0.25 mM was found to give an even higher level of protection. Thus, the work above was expanded to determine whether this cytoprotective effect could be obtained in differentiated U937 using the application of PAM, as it was hypothesised that, given the high concentration of H_2O_2 within PAM, it may be possible.

To decide on suitable PAM strengths for the initial and final doses for this experiment, it was decided that the first dose must be one which did not cause significant reduction in the viability of differentiated U937 on its own, whereas the second dose must be one that did cause a clear reduction when used alone. A $\frac{1}{10}$ strength PAM was therefore used for the initial dose after confirming it did not affect cell viability itself (Figure 7.5), with an undiluted PAM being used for the second dose after considering the results of Figure 7.4. From the chemical measurements performed in 4.4.1, these selections would equate to an initial exposure to PAM containing 0.26 mM H_2O_2 and a final exposure to PAM containing 2.61 mM H_2O_2. The initial PAM dose was left on the cells for 3 hours (longer than usual to try to maximise the effect), followed by one hour of exposure to the second PAM dose, with neutral red assay being performed the following day. This was compared against samples subjected to no pre-dose of PAM, and control samples which received neither dose of PAM. Viability was measured by neutral red assay the following day, with the cells having been in complete RPMI for the intervening period.

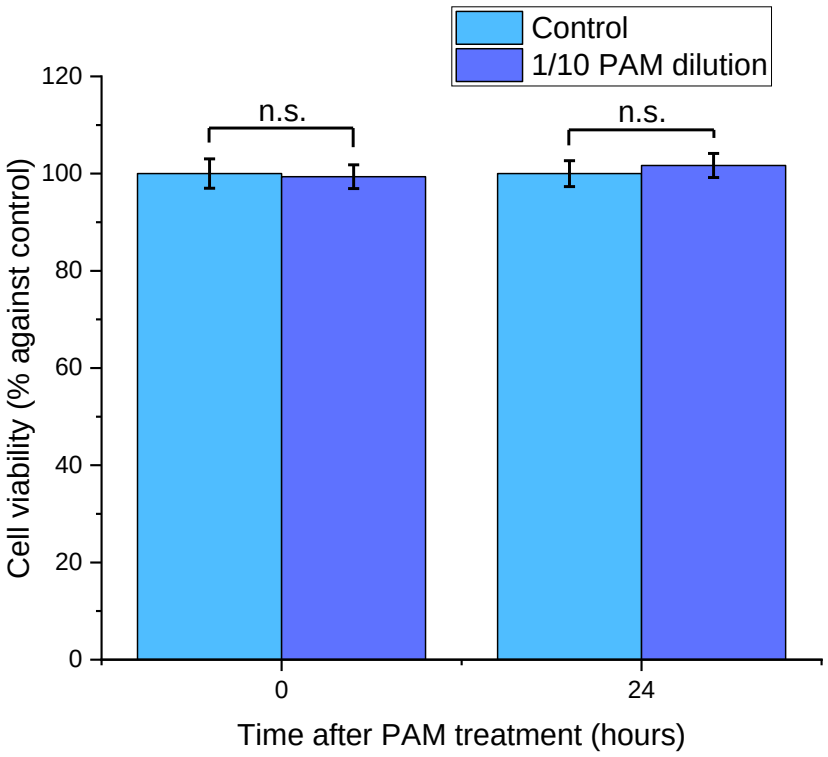

Figure 7.5. Viability of differentiated U937 at 0 and 24 hours following one hour of exposure to a 1/10 dilution of PAM created with 15 minutes of NTP treatment. n=4, SE shown n.s.: not statistically significant, independent t -test (2-tailed significance). p= 0.879 for 0 hours and p = 0.664 for 24 hours.

In comparison to the control average set as 100 % (SE = 18.1 % of control average), the treated samples had a viability average of 32.8 % (SE = 7.8 % of control value) when they did not receive a 1/10-strength initial PAM pre-dose prior to exposure to undiluted PAM and 40.8 % (SE = 9.0 % of control value) when they did (Figure 7.6). While this represented a reduction in viability in comparison to the control for both treatment groups, there was no significant difference in viability between the treated groups themselves. Thus, no cytoprotective effect was noted from exposure to low strength PAM in advance of treatment with higher strength PAM.

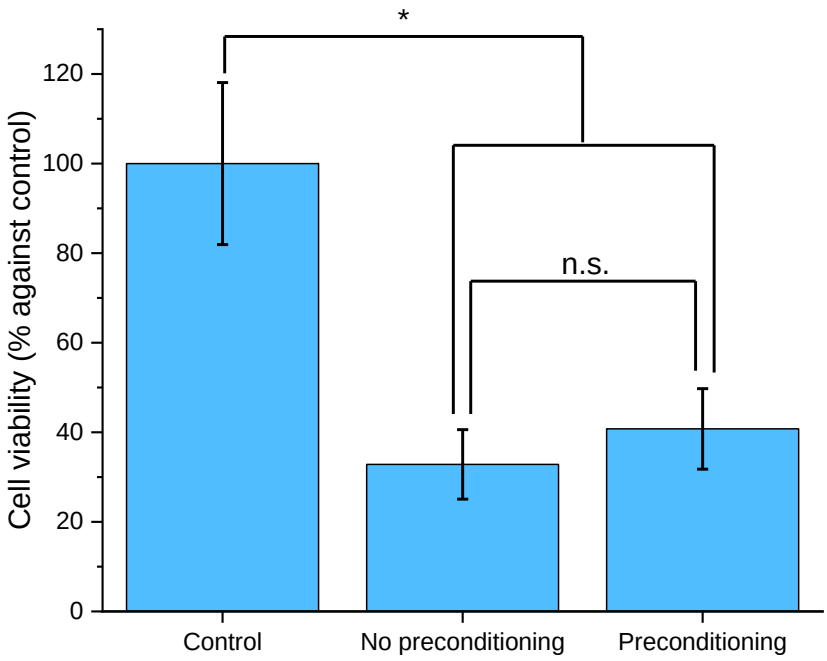

*Figure 7.6. Effect of repeated application of PAM on the viability of differentiated U937. Control is untreated FBS-free RPMI as both the first and second doses, left on the samples for three and one hours respectively. Samples without pre-dose were exposed to untreated FBS-free RPMI three hours then undiluted PAM for one hour. Samples with PAM pre-dose were exposed to ⅒-strength PAM for three hours then undiluted PAM for one hour. Viability was assessed 24 hours following the completion of these treatments. n=6, SE shown, *: $p < 0.05$, n.s.: not statistically significant, ANOVA with Tukey HSD post-hoc.*

The reasons for the absence of a protective effect from the initial dose of PAM were unclear. Lee and Um [274] found that when they used 0.25 mM H_2O_2 as the initial dose, there was an immediate enhancement of the ability of the cell to counteract increasing H_2O_2 levels, probably due to increasing levels of glutathione peroxidase, and that this enhanced ability continued long enough to be able to counteract the effects of exposure to 1 mM H_2O_2 applied 24 hours later. Given that the initial dose involved for the work in

Figure 7.5 contained around 0.26 mM H_2O_2 and was applied to the same cell line as used by Lee and Um [274], it is surprising that this effect was not observed here. Two possible explanations have been identified for this difference in response. Firstly, Lee and Um [274] used the monocytic form of U937, and thus it may be that the reaction of PMA-treated U937 to the initial dose of H_2O_2 is different to this. Secondly, it should be noted that, although the work performed here used PAM with a very similar concentration of H_2O_2 to that of the initial dose used by Lee and Um [274], the second dose had a concentration of H_2O_2 more than double what they used. It may therefore be that the ability of the cells used here to deal with toxic levels of H_2O_2 was indeed enhanced, but the concentration of H_2O_2 in the second dose was sufficiently large to overwhelm even this, and thus no protective effect was observed.

Although it did not prove possible on this project to generate this cytoprotective effect from preconditioning with PAM, other researchers have managed this with other cell lines. Horiba et *al.* [239] carried out similar work on human skin fibroblasts, suggesting that the cytoprotective effect they observed was the result of upregulation of haem oxygenase 1 (HO-1) via the involvement of the nrf2/ARE pathway (Figure 7.7), which is known to be impacted by the PI3K/Akt pathway [275]. Interestingly, Horiba *et al*. found that a preconditioning dose providing approximately 50 µM was sufficient to give this effect, a concentration which is around one fifth of that used during the work performed in Figure 7.6. It is therefore not clear why the work in Figure 7.6 did not also produce this effect, especially as it has been documented that U937 is capable of upregulating HO-1 in response to other stimuli, including PMA [276].

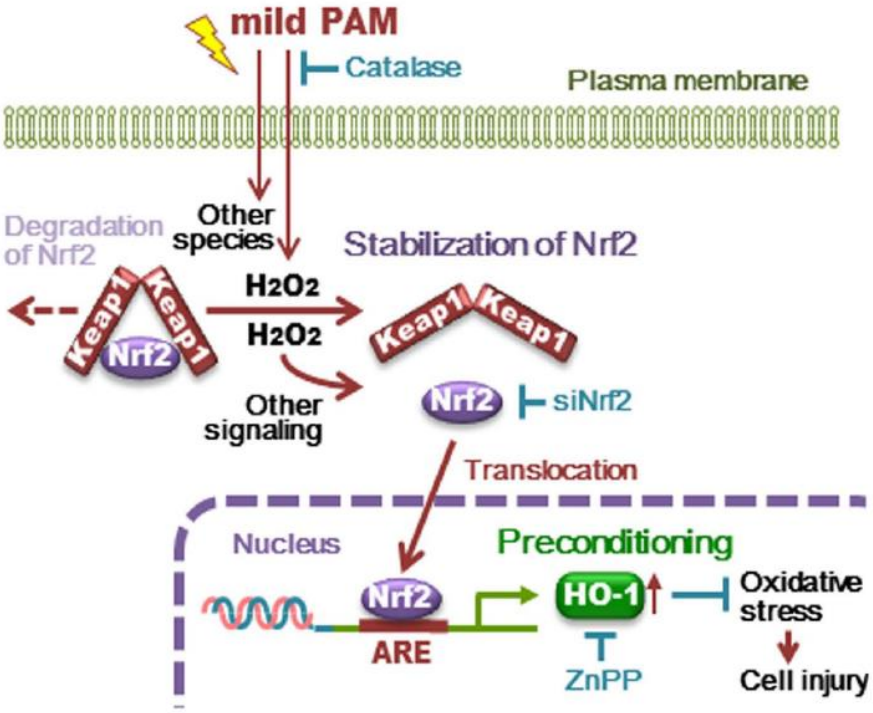

Figure 7.7. Method of action of PAM preconditioning proposed by Horiba et al. involving the nrf2/ARE pathway causing the upregulation of HO-1. Diagram taken from [239].

7.4.4 Phagocytic ability of cells treated with varying dilutions of PAM

A schematic representation of macrophages performing phagocytosis is shown in Figure 1.3 and, as explained in 1.2.1.2.1, phagocytosis by cells such as macrophages is an important part of the defences of the immune system. From Figure 7.4 it can be seen that the reduction in viability in differentiated U937 when the ¼-and ½-strength PAM treatments were applied was small (although significant for ½-strength PAM, the average reduction from control was around 26 %, with the majority of cells still remaining viable) and therefore the effect for most cells in the samples could be deemed to be non-lethal. However, it was important to understand whether these sub-lethal PAM treatments affected the ability of the cells to phagocytose, either positively or negatively.

7.4.4.1 Assessment of the effect of ¼- and ½-strength PAM on the ability of differentiated U937 to phagocytose particles

Following one hour of exposure to PAM, 1 µM FITC-labelled latex beads were added to cell samples and the cells were then subjected to light microscopy. To make the assessment of the resulting photographs more objective, cells within the photographs were individually assessed to determine the degree of phagocytosis that they had undergone. The cells were divided into 3 categories:

1) Minimal evidence of phagocytosis. This included cells in which the 2D surface had no, or a very small, area seen to be containing beads (Figure 7.8(a))
2) Moderate phagocytosis. Clear interaction of the phagocytosis of beads by the cell beyond that of minimal evidence, as described in 1) but 2D surface of the cell not wholly occupied by beads (Figure 7.8(b)).
3) High level of phagocytosis. Dark area indicative of beads covering all, or near to all, of the 2D surface of the cell (Figure 7.8(c)).

A similar method of assessing phagocytosis was used in [277]. All counts were carried out on photographs taken at random points within the well, although the edges of the well were avoided due to the accumulation of debris in this area. Three photographs from each well were used for analysis, with the counts averaged across the three.

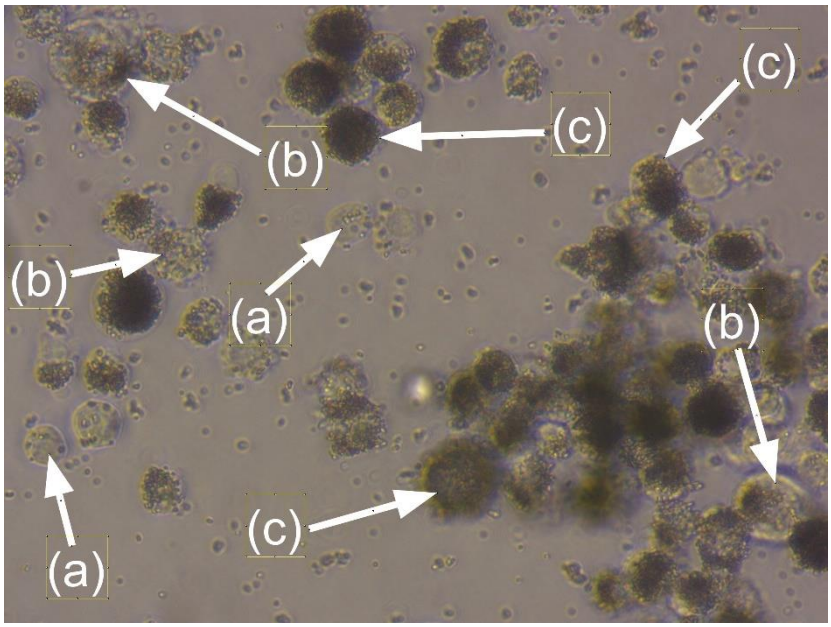

Figure 7.8. Examples of cells that would be considered to show a) minimal evidence of phagocytosis b) moderate phagocytosis and c) high level of phagocytosis.

It was clear that cells which were exposed to the ¼- and ½-strength PAM treatments maintained phagocytic ability, and that there was no reduction in competence when compared to the control cells, nor any enhancement (Figure 7.9 and Table 7.3).

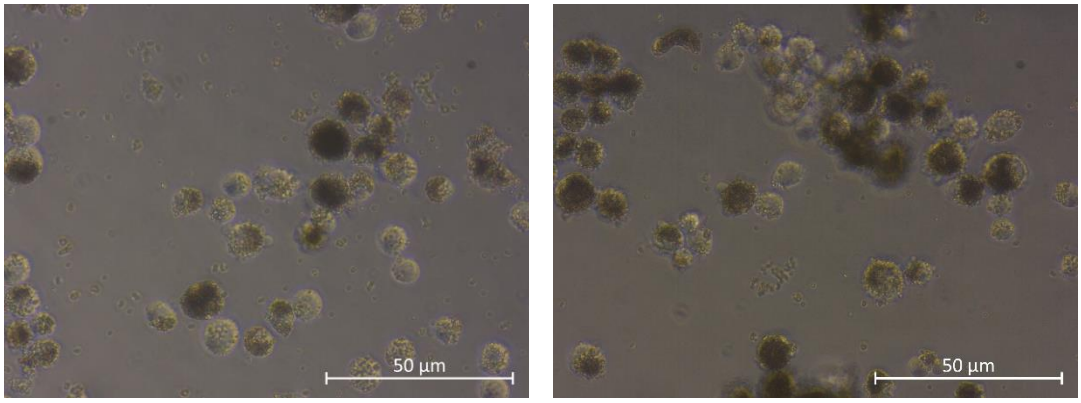

(a) (b)

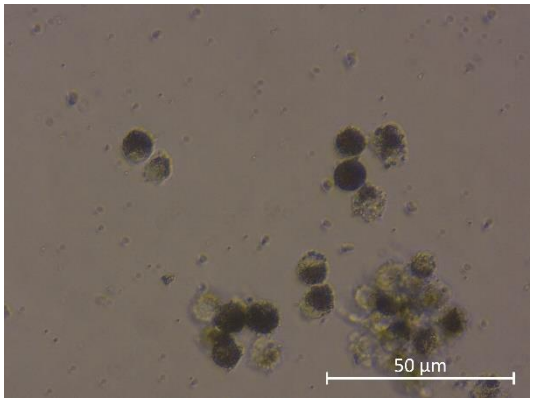

(c)

Figure 7.9. Examples of microscope photographs showing phagocytosis of 1 µM latex beads by differentiated U937 for (a) control cells which were exposed to untreated serum-free RPMI for one hour rather than PAM (b) cells treated with ¼-strength PAM and (c) cells treated with ½-strength PAM. All photographs were taken using 40x objective lens, and all are from the same biological replicate for comparability, although a further two replicates were also run.

Table 7.3. Proportion of cells showing minimal, moderate or high levels of phagocytosis for control (exposed to untreated serum-free RPMI instead of PAM) and for cells exposed to ¼-strength and ½-strength PAM. No statistically significant differences in the proportions of cells within the minimal, moderate and high categories were noted between control and treated samples. n=3, statistical significance assessed by ANOVA with Tukey HSD post-hoc.

	% of cells with each extent of phagocytosis					
	Minimal		**Moderate**		**High**	
Sample type	**Average**	**SE**	**Average**	**SE**	**Average**	**SE**
Control	18.9	4.7	38.2	3.0	43.0	1.7
¼-strength PAM	11.0 (p = 0.728)	3.6	28.8 (p = 0.564)	6.2	60.2 (p=0.510)	9.8
½-strength PAM	23.6 (p = 0.886)	10.8	23.0 (p = 0.270)	8.2	53.4 (p = 0.767)	15.0

It was thought plausible that there could be a decrease in phagocytic ability with a sub-lethal PAM treatment, with the treatment causing damage to the cell which was insufficient to result in its death but sufficient to affect its health. However, it was also thought plausible that the PAM treatment could enhance phagocytic ability, as there is evidence that H_2O_2 can enhance the ability of phagocytes. Gamaley *et al.* [278] reported an increase in phagocytic ability in murine macrophages subjected to H_2O_2 concentrations of between 0.1 and 20 µM, an effect which also corresponded to an increase in free calcium within the cytoplasm, something which has been linked to the ability of the cell to carry out non-specific, rather than receptor-mediated, phagocytosis [279]. H_2O_2-enhanced phagocytosis has also been observed in neutrophils, with Bejarano e*t al.* [280] finding that a 30-minute

exposure to 10 µM, 100 µM or 1 m of H_2O_2 all increased phagocytic efficiency in these cells, something which they also attributed to the release of stored intracellular calcium.

However, although it was thought possible that phagocytic ability may change either positively or negatively with PAM treatment, it appears to have stayed constant. No papers have been identified where the effect of NTP treatment on the phagocytic abilities of macrophages have been considered. However, the results presented here do agree with those found in the NTP treatment of neutrophils by Bekeschus [122] and Bekeschus *et al.* [124]. They concluded that the ability of neutrophils to carry out phagocytosis and kill the *Staphylococcus aureus* and *Pseudomonas aeruginosa* bacteria was not significantly changed by NTP treatment.

A note of caution should be added to the results shown in Table 7.3. The variances were found to be quite large, and of such a scale that they may be obscuring subtle changes in phagocytosis levels. The reasons for these large variances were first that grading of the cells was carried out manually and was highly subjective and secondly that the overall number of cells present within each photograph was highly variable. The best option to improve upon these results would have been to use fluorescence-activated cell sorting (FACS) which would have provided a quantitative measurement of the FITC within the cells, and thus given an indication of bead numbers. This work had been planned but it unfortunately had to be abandoned due to pandemic-related access restrictions.

On reflection, further improvements could have been made with the experiment within the experiment that was carried out. Expanding the number of biological replicates and using an even larger number of photographs per biological replicate may have helped reduce the

variances. It may also have been worth considering detaching the cells prior to photography, for example by using trypsin, and then reseeding in a new well, as this may have given a better standardisation of the cell numbers within each photograph.

7.4.4.1.1 Attempts at fluorescent imaging for phagocytic U937

Initially, it was intended that the imaging of the latex bead phagocytosis carried out in Figure 7.9 and Table 7.3 would be performed using fluorescent techniques, making use of the fact that the latex beads were labelled with FITC. PI, a nuclear stain, would be used in conjunction with this, following the method of [281]. However, a number of issues were encountered in attempting this work.

Firstly, the experiment was attempted using a confocal microscope, but it became apparent that only poor-quality images could be produced due to the fact that the imaging took place using a plastic 96-well plate, and this resulted in poor resolution as a striped interference pattern in the photographs (Figure 7.10(a)). Attempts to solve these problems were then halted by pandemic-related access restrictions meaning that it was no longer possible to access the confocal microscope. An alternative approach was then also attempted using a ZOE fluorescent cell imager. However, this was not successful at clearly distinguishing between PI and FITC staining (Figure 7.10(b)) and thus was of limited use. This line of investigation was therefore abandoned.

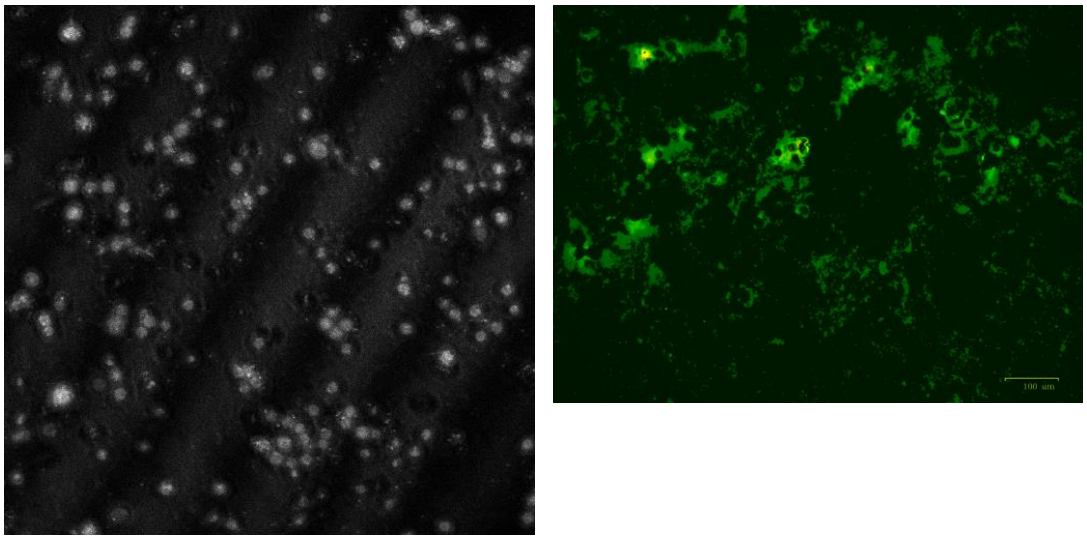

(a) (b)

Figure 7.10. Examples of imaging difficulties (a) confocal image showing poor resolution and diagonal striped interference pattern. Image presented in greyscale so interference pattern can be clearly seen (b) photograph taken using ZOE showing poor differentiation of PI and FITC.

7.4.4.2 Effect of ¼- and ½-strength PAM on phagocytic gene expression

A large number of genes have been linked to phagocytosis in U937 and the NHL-repeat-containing protein 2 (NHLRC2) gene and TM2 containing domain 1 (TM2D1) gene are two of the four genes thought to be the strongest regulators of the process [282]. The NHLRC2 protein has been implicated in other functions including regulation of apoptosis resulting from excess ROS [283], and mutations with the NHLRC2 gene have also been linked to fibrosis, neurodegeneration, and cerebral angiomatosis (FINCA) syndrome in humans [284]. TM2D1 is from a family of genes which are thought to have involvement in some neurodegenerative diseases [282] and the TM2D1 protein, also known as β-amyloid peptide binding protein, has been implicated in Alzheimer's disease, as well as to poorer outcomes in hepatocellular carcinoma [285].

The effect of NTP treatment on the expression of phagocytic genes does not appear to have been explored in the literature. Therefore, to further investigate whether it was likely that PAM was affecting phagocytic ability in differentiated U937, the impact of ¼- and ½-strength PAM treatment on the expression the NHLRC2 and TM2D1 genes was investigated using RT-qPCR and the primers and probes described in Table 7.4. It was found that there was no statistically significant change in the expression of either of these genes resulting from these PAM treatments (Table 7.5).

Table 7.4. Details of primers and probes used for phagocytic genes.

Gene name	Primer/probe	Bases	Sequence	GC Content	Tm (50mM NaCl) °C
NHLRC2, HOMO_SAPIENS (Hs.PT.58.2694219)	PrimeTime Primer 1	21	TCT TCA TTT CCA CTT CCA GCA	42.85714	54.29011
	PrimeTime Primer 2	24	AGA GGT GAC ATT TTA TGG ATA GCC	41.66667	54.5753
	PrimeTime Probe	24	/56-FAM/TGC CCA TAT /ZEN/CTG ATG AGT CCC TGC /3IABkFQ/	54.16667	60.57672
TM2D1, HOMO_SAPIENS (Hs.PT.58.2230194)	PrimeTime Primer 1	21	GCC ACT GGA ATC CTT ACA AGT	47.61905	54.86142
	PrimeTime Primer 2	23	AAT AAA TGA CGC TAC GCA AGA AC	39.13043	53.85142
	PrimeTime Probe	26	/56-FAM/TGC TGG AAA /ZEN/ACA GGA AAC ATG AGC TG/3IABkFQ/	46.15385	59.81

Table 7.5. Change in expression of genes for NHLRC2 and TM2D1 in cells treated with ¼- and ½-strength PAM. No statistically significant changes from control noted for either diluted PAM treatment. B2M used as reference gene, n=3 for both genes, ANOVA used for NHLRC2 (p = 0.998), Welch test for TM2D1 (p=0.904).

	FOLD CHANGE FROM CONTROL			
	NHLRC2		**TM2D1**	
PAM	**Average**	**SE**	**Average**	**SE**
¼-strength	1.02	0.24	1.05	0.01
½-strength	1.01	0.12	1.07	0.00

These results appear to support the conclusion from 7.4.3.1: PAM treatment with the ¼- and ½-strength PAM has no effect on phagocytic ability. However, an effect on phagocytic ability cannot be completely ruled out from the results in Table 7.5 as there are a wide range of other genes which have been associated with phagocytosis in U937 [282] and which have not been considered here, nor by other researchers with regards to their response to NTP.

7.4.5 Effect of varying dilutions of PAM on quantities of chemokines and other cytokines secreted by pro-inflammatory differentiated U937

It is known that U937 differentiated with PMA already tends to a pro-inflammatory phenotype [17][18]. The relevance of pro-inflammatory chemokines and other cytokines has been explained within 1.2.1.2.1.1, and here the effect of their secretion by PMA-differentiated U937 in response to PAM has been investigated. This was carried out by measuring the concentrations of eight of these pro-inflammatory substances in the

supernatant surrounding the cells (Figure 7.11) following the exposure to ¼-strength, ½-strength and undiluted PAM. Measuring this within the supernatant shows the pro-inflammatory changes the cells were making to their environment. The supernatant was harvested for ELISA 24 hours following the completion of the PAM treatment. The chemokines investigated were CCL2 (MCP-1), CCL5 (RANTES), CXCL8 (IL-8) and CXCL9 (MIG). The other cytokines investigated were TNF-α, IFN-γ, IL-1β and IL-6. The effects of PAM on each of these is addressed separately below.

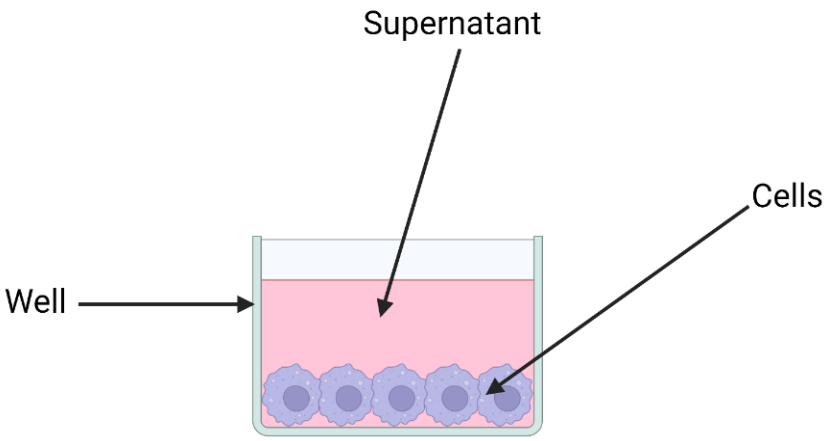

Figure 7.11. The supernatant and how it relates to cells within an in vitro sample. Created with BioRender.com [6].

7.4.5.1 CCL2

CCL2 is a chemokine which is a strong attractor of monocytes [29] as well as lymphocytes [286] and NK cells [287][3][2][1]. It is also known to enhance the expression of adhesion molecules in monocytes, thus encouraging endothelial adhesion [288]. Control samples of differentiated U937 were found to have an average supernatant concentration of 150.5 ng/ml of CCL2 (SE = 6.5 ng/ml), with ¼-strength PAM giving an average of 146.6 ng/ml (SE = 11.9 ng/ml), ½-strength PAM giving an average of 98.8 ng/ml (SE = 14.1 ng/ml), and

undiluted PAM giving an average of 8.3 ng/ml (SE 2.0 = ng/ml). The reductions for both the ½ -strength and undiluted PAM treatments were statistically significant ($p = 0.024$ and $p < 0.001$ respectively) (Figure 7.12). It can therefore be concluded that cells behaving in a manner such as that induced by ½-strength and undiluted PAM would be likely to have a reduced ability to attract monocytes, lymphocytes and NK cells, and to influence monocyte adhesion.

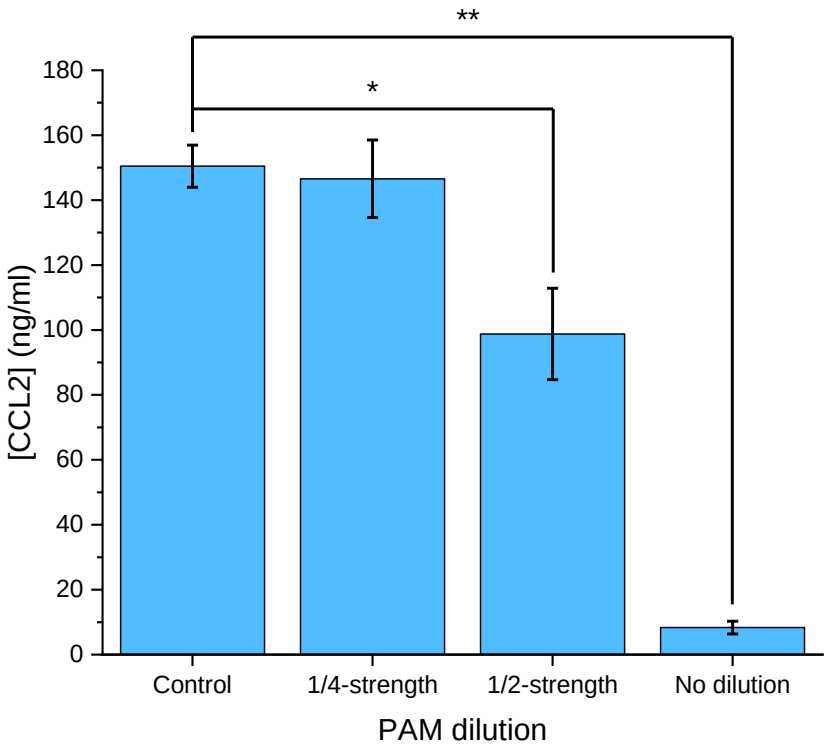

*Figure 7.12. CCL2 in supernatant measured 24 hours following 1 hour of exposure to ¼ and ½ dilution PAM, and undiluted PAM. n=3, SE shown, *: $p < 0.05$, **: $p < 0.001$, ANOVA with Tukey HSD post-hoc.*

7.4.5.2 CCL5

CCL5 is a chemokine which is known to attract lymphocytes, NK cell, basophils, eosinophils and dendritic cells, as well as interacting with macrophages and monocytes [11][289] and, like CCL2, is also known to enhance monocyte adhesion molecules [288]. Control samples

were found to contain an average CCL2 supernatant concentration of 4.8 ng/ml (SE = 0.1 pg/ml), whereas the samples subject to ¼ -strength PAM had an average of 4.3 ng/ml (SE = 0.2 ng/ml) and those subject to the ½-strength PAM had an average of 4.0 ng/ml (SE = 0.2 ng/ml). Although both of these PAM strength treatments resulted in CCL5 supernatant concentrations lower than that of the control samples, the difference was not statistically significant ($p = 0.530$ and $p = 0.167$ respectively). The samples subject to undiluted PAM, however, had a much lower level of CCL5 than control, with an average of 2.1 ng/ml (SE = 0.4 ng/ml), and this difference was statistically significant ($p < 0.001$) (Figure 7.13). This suggests that CCL5-related cell attraction in monocyte adhesion enhancement would be reduced by treatment of U937 with undiluted PAM, but perhaps not with ¼- or ½-strength PAM.

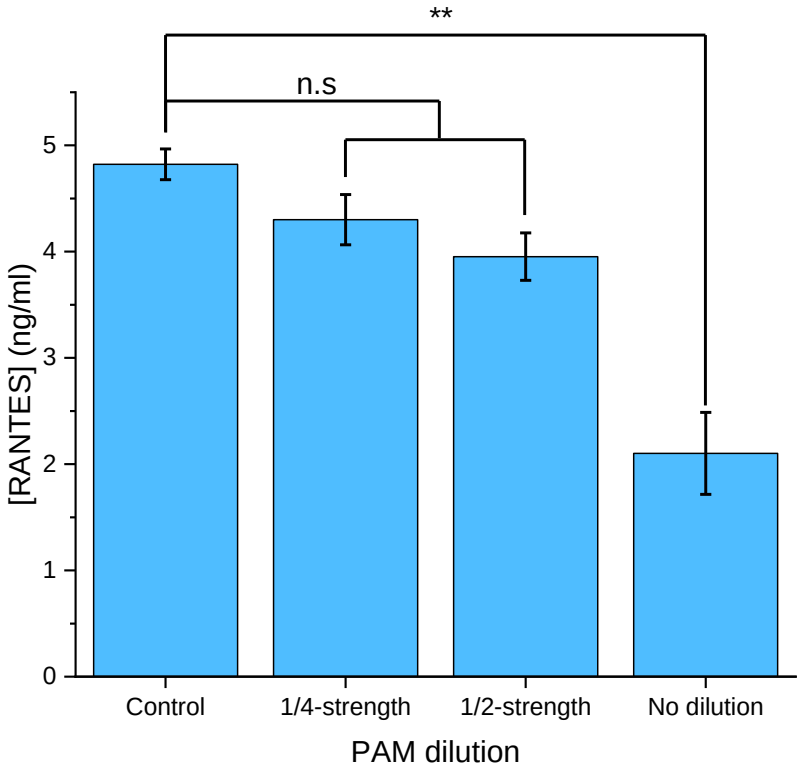

*Figure 7.13. CCL5 in supernatant measured 24 hours following 1 hour of exposure to ¼ and ½ dilution PAM, and undiluted PAM. n=6, SE shown, **: p < 0.001, n.s: not statistically significant, ANOVA with Tukey HSD post-hoc.*

7.4.5.3 CXCL8

It is known that the main function of CXCL8 is to attract and activate neutrophils, but it is known that it also acts upon basophils, CD8 cells, eosinophils endothelial cells and keratinocytes [289][11]. Against a control average concentration of 7.6 ng/ml (SE = 0.7 ng/ml) in the supernatant, treatment with ¼-dilution PAM gave an average of 19.0 ng/ml (SE = 1.2 ng/ml), ½-dilution PAM dilution gave 21.6 ng/ml (SE = 2.8 ng/ml), and undiluted PAM gave an average of 6.5 ng/ml (SE = 0.6 ng/ml). The increases in CXCL8 were statistically significant for both the ¼ and ½ dilutions ($p < 0.001$ for both), but the level

achieved with undiluted PAM was similar to that of control (Figure 7.14). This therefore suggests that treatment of U937 with lower strength PAM could enhance CXCL8-related cell attraction, with undiluted PAM it would be similar to that of control.

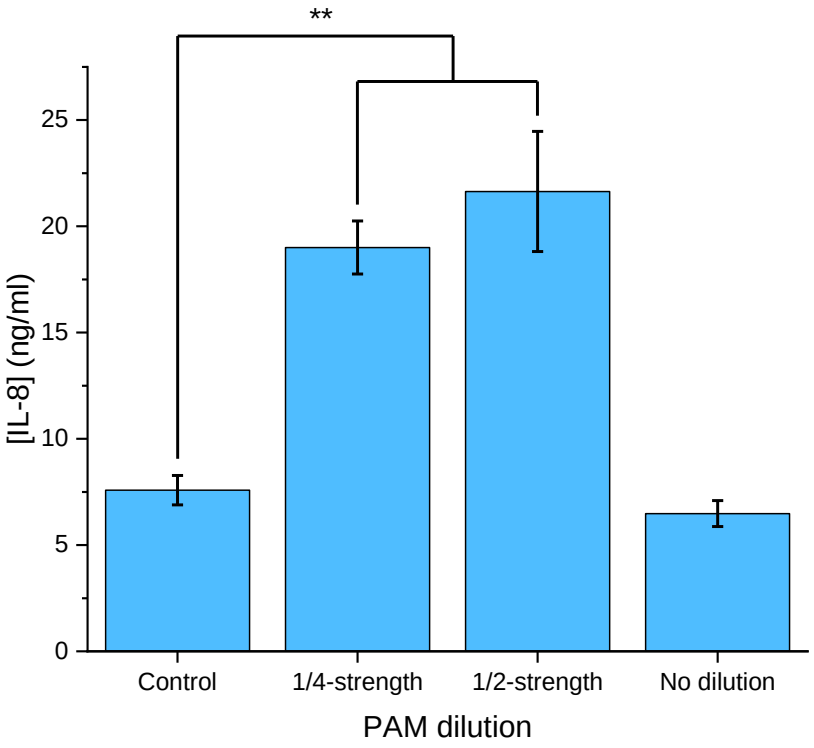

*Figure 7.14. CXCL8 in supernatant measured 24 hours following 1 hour of exposure to ¼ and ½ dilution PAM, and undiluted PAM. n=6, SE shown, **: p<0.001, ANOVA with Tukey HSD post-hoc.*

7.4.5.4 CXCL9

CXCL9 attracts T cells, and also acts against tumours and metastasis, as well as being involved in attracting inflammatory cells and those involved in tissue repair [11]. The absorbance readings for both control and PAM-treated samples for the CXCL9 ELISA were very small (Table 7.6). Therefore, it is clear that there was minimal CXCL9 present within

either the control samples of samples treated with PAM, and the PAM caused no detectable change to the levels.

Table 7.6. CXCL9 ELISA absorbance (450 nm – 570 nm) and SE for control samples and PAM treatments. The absorbance reading of a blank well was 0.450, for which the below data has been corrected.

	Average absorbance (n=3)	**SE**
Control	0.286	0.003
1 in 4 PAM	0.298	0.016
1 in 2 PAM	0.292	0.002
Undiluted PAM	0.283	0.006

7.4.5.5 TNF-α

TNF-α increases levels of corticotropic releasing hormone, causes fever, suppresses appetite, increases vasodilation and permeability of blood vessels, increases expression of cell adhesion molecules, and, alongside IL-17 acts to increase CXCL1, CXCL2 and CXCL5. As well as this it also acts on neutrophils triggering respiratory burst [11][25], and is known to polarise other macrophages to an M1 phenotype (Figure 1.4). TNF-α also has well-established roles in diseases related to inflammation such as inflammatory bowel disease and rheumatoid arthritis [11]. The average TNF-α concentration detected in the supernatant of differentiated U937 control samples was 4.23 pg/ml (SE = 0.91 pg/ml), whereas for cells treated with ¼-strength PAM the average was 31.97 pg/ml (SE = 7.31 pg/ml), with ½-strength PAM it was 71.20 pg/ml (SE = 2.95 pg/ml), and with undiluted PAM was 58.27 pg/ml (SE = 8.63 pg/ml). All three PAM treatment types resulted in statistically significant increases from the control samples ($p = 0.041$ for 1/4 -strength, $p < 0.001$ for ½

strength, $p < 0.001$ for undiluted PAM) (Figure 7.15). There was also a statistically significant increase in TNF-α between ¼-strength and ½-strength PAM ($p=0.006$). This would therefore suggest that PAM treatment is capable of enhancing the pro-inflammatory effects related to TNF-α as outlined above.

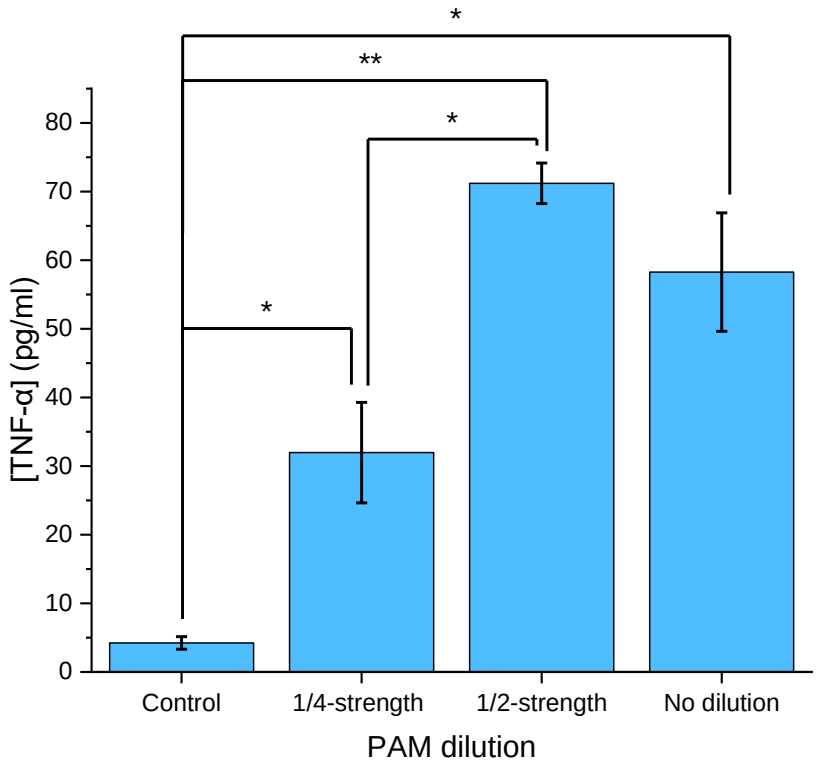

*Figure 7.15. TNF-α in supernatant measured 24 hours following 1 hour of exposure to ¼ and ½ dilution PAM, and undiluted PAM. n=3, *:p<0.05, **:p<0.001, SE shown, ANOVA with Tukey HSD post-hoc.*

7.4.5.6 IFN-γ

IFN-γ is a strong activator of macrophages [11], and it is also involved in M1 macrophage polarisation (Figure 1.4). Very low concentrations of IFN-γ were detectable in all differentiated U937 supernatant samples considered, both those of control samples and

those of samples exposed to PAM. Therefore, no PAM-related change was identified (Table 7.7).

Table 7.7. IFN-γ ELISA absorbance (450 nm – 570 nm) and SE for control samples and PAM treatments. For comparison the average blank well absorbance was 0.063, for which the values below have already been corrected.

Treatment	Average (n=3)	SE
Control	0.051	0.001
1 in 4 PAM	0.049	0.001
1 in 2 PAM	0.048	0.002
Undiluted PAM	0.048	0.003

7.4.5.7 IL-1β

Il-1β is one of the three forms of IL-1 and, along with IL-1α, is known to be pro-inflammatory. It promotes acute phase protein production in the liver and release of prostaglandins by the central nervous system, as well as encouraging IL-6 release and fever. It also encourages differentiation of T cells, attracts granulocytes and increases leukocyte and endothelial cell adhesion molecule expression, and as well as encouraging mast cells to release histamine, which increases vasodilation [11]. The average IL-1β concentrations in control sample supernatant were measured as 3.7 pg/ml (SE = 0.6 pg/ml) for control, whereas it was 14.1 pg/ml (SE = 2.0 pg/ml) for those receiving a ¼-strength PAM treatment, 12.8 pg/ml (SE = 1.1 pg/ml) for those with a ½-strength PAM treatment and 13.4 pg/ml (SE = 1.3 pg/ml) for those with an undiluted PAM treatment. All three PAM treatment types resulted in a statistically significant increase in IL-1β concentration from control ($p < 0.001$

for all) (Figure 7.16). This would therefore suggest that PAM treatment could be capable of enhancing the pro-inflammatory effects related to IFN-γ discussed above.

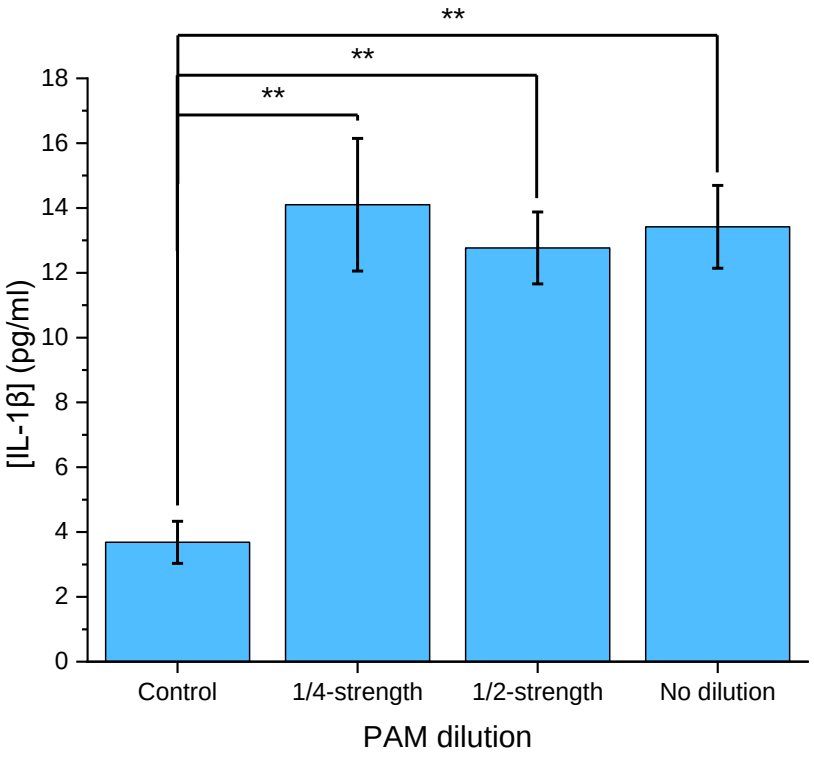

*Figure 7.16. IL-1β in supernatant measured 24 hours following 1 hour of exposure to ¼ and ½ dilution PAM, and undiluted PAM. n=6, SE shown, *: p<0.05, **: p<0.001, ANOVA with Tukey HSD post-hoc.*

7.4.5.8 IL-6

The pro-inflammatory actions of IL-6 include encouraging the in growth and differentiation of lymphocytes and reduction in their apoptosis, attraction of monocytes [25], encouragement of the production of acute phase proteins and involvement in the creation of fever [25][11]. The average supernatant concentration of IL-6 in control samples was 4.56 pg/ml (SE 2.16 pg/ml), while for the samples subject to ¼-strength PAM it was 16.11

pg/ml (SE = 2.82 pg/ml), for ½-strength PAM it was 6.99 pg/ml (SE = 0.68 pg/ml) and for undiluted PAM it was 4.28 pg/ml (SE = 0.73 pg/ml). There was a statistically significant increase from control for the ¼-strength PAM treatment (p = 0.001), but the IL-6 concentrations for both the ½-strength PAM and the undiluted PAM were lower than that of the ¼-strength PAM and did not show a statistically significant difference from control (p = 0.788 and p = 1.000 respectively) (Figure 7.17). The reduction between the IL-6 levels generated by ¼-strength PAM and the levels produced in response to ½-strength and undiluted PAM was also statistically significant (p = 0.011 and p = 0.001 respectively). Thus, ¼-strength PAM treatment of U937 may be capable of increasing the pro-inflammatory impact of IL-6, but ½-strength and undiluted PAM cannot.

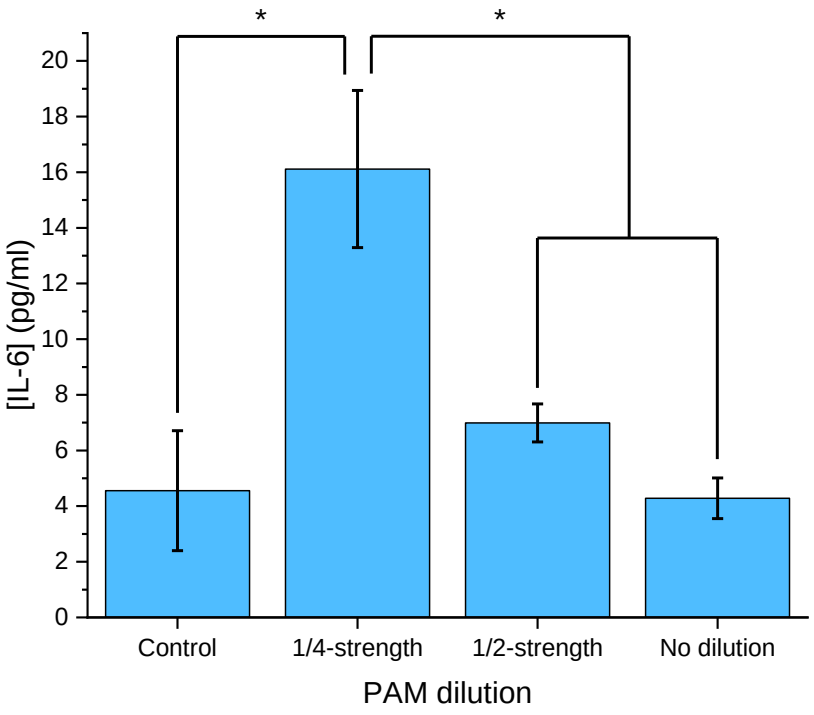

*Figure 7.17. IL-6 in supernatant measured 24 hours following 1 hour of exposure to ¼ and ½ dilution PAM, and undiluted PAM. n=6, SE shown, *: p<0.05, ANOVA with Tukey HSD post-hoc.*

7.4.5.9 Overall discussion of chemokine and cytokine results

Eight cytokines and chemokines were selected for assessment of the change in their levels around cells subject to PAM: CCL2, CCL5, CXCL8, CXCL9, TNF-α, IFN-γ, IL-1β, and IL-6. These were investigated to determine whether the pro-inflammatory activity of PMA-differentiated U937 could be enhanced by PAM treatment. It is plausible that it could give such as result given that it is known that RONS such as H_2O_2 and NO can increase the levels of some pro-inflammatory cytokines in a range of cell types [290][291][292][293][294][295].

A summary of the changes observed in the eight substances measured following PAM treatment, based on the data from 7.4.5.1 to 7.4.5.8, is given in Table 7.8. Of the eight chemokines and cytokines examined for their response to PAM treatment, six showed a change in release in response to PAM treatment, whereas two showed no change. For the six that did change, the results largely followed what would be expected after reflecting on the literature on the effects of H_2O_2 on cytokine production, given that it has been observed that high levels of H_2O_2 can result in an increase in IL-8 [291][292][293], TNF-α [295] and IL-6 [294], but not CCL5 [292]. The situation around IL-1β and H_2O_2 is unclear. For the two cytokines that did not change in response to PAM, CXCL9 and IFN-γ, there was a minimal quantity in the control samples, and this remained the same for the treated samples. It is noted that CXCL9 release is triggered by IFN-γ [294], and thus it is perhaps not surprising that they both show the same lack of effect.

Table 7.8. Summary of changes in cytokines and chemokines from control for different PAM treatments. Data taken from 7.4.4.1 to 7.4.4.8.

		% of control			
	Measurable concentrations (Y/N)	**1/4 PAM dilution**	**1/2 PAM dilution**	**Undiluted PAM**	**Commentary**
Chemokines					
CCL2	Y	$97^{n.s.}$	66*	6**	The highest value was for control sample, with the ¼-strength PAM concentrations being approximately the same as this. There was a statistically significant fall from control for the ½-strength PAM dilution, and a very large, statistically significant fall for undiluted PAM samples.
CCL5	Y	$90^{n.s.}$	$83^{n.s.}$	44**	There was a slight, statistically insignificant fall for ¼- and ½-strength PAM, and a statistically significant fall for undiluted PAM.
CXCL8	Y	250**	284**	$86^{n.s.}$	There was a significant increase in concentration with both ¼- and ½-strength PAM, but the undiluted PAM gave a concentration lower than that of the control sample (not a statistically significant difference).
CXCL9	N[1]	n/a	n/a	n/a	Due to the very low concentrations present, with the measured absorbance being around or below the blank well value for all samples, it was not possible to gain a numerical value for concentrations of

		% of control			
	Measurable concentrations (Y/N)	**1/4 PAM dilution**	**1/2 PAM dilution**	**Undiluted PAM**	**Commentary**
					CXCL9. This does, however, suggest that PAM treatment did not trigger an increase.
Other cytokines					
TNF-α	Y	756*	1683**	1378*	All PAM strengths used increased TNF-α from control. ½-strength PAM biggest increase, followed by undiluted PAM, then ¼-strength PAM. Undiluted PAM levels were nearly double the values for ¼-strength PAM.
IFN-γ	N[1]	n/a	n/a	n/a	Due to the very low concentrations present, with the measured absorbance being around or below the blank well value for all samples, it was not possible to gain a numerical value for concentrations of IFN-γ. This does, however, suggest that PAM treatment did not trigger an increase in IFN-γ.
IL-1β	Y	381**	346*	362**	All PAM increased from control by a significant amount, but notably the values for all three PAM strengths were almost identical.

		% of control			
	Measurable concentrations (Y/N)	**1/4 PAM dilution**	**1/2 PAM dilution**	**Undiluted PAM**	**Commentary**
IL-6	Y	353*	153[n.s.]	94[n.s.]	¼- and ½-strength PAM gave an increase from control, although it was much greater with the ¼-strength PAM. Undiluted PAM gave a very slight decrease from control for IL-6 which was not statistically significant.

Notes

[1] All sample types had an average absorbance of around that of the blank well.

* Statistically significant difference from control, $p < 0.05$

** Statistically significant difference from control, $p < 0.001$.

[n.s.] Difference from control not statistically significant.

It is also important to consider not only the effect PAM treatment has on the levels of individual chemokines and other cytokines, but also how the overall inflammatory profile is affected. It is clear that all three PAM strengths caused a change in the overall inflammatory profile, but that the specific way that this changed was dependent upon the strength of the PAM used (Table 7.9).

Table 7.9. Inflammatory profiles for different PAM dilutions in comparison to control. A double arrow denotes a statistically significant change, and a single arrow denotes a change which was not statistically significant.

Dilution	**CCL2**	**CCL5**	**CXCL8**	**TNF-α**	**IL-1β**	**IL-6**
1 in 4 PAM	↓	↓	↑↑	↑↑	↑↑	↑↑
1 in 2 PAM	↓↓	↓	↑↑	↑↑	↑↑	↑
Undiluted PAM	↓↓	↓↓	↓	↑↑	↑↑	↓

To summarise the functions of the individual chemokines which were found to be influenced by PAM treatment:

- CCL2 is chemoattractant for monocytes, lymphocytes and NK cells and encourages endothelial adhesion of monocytes. From Table 7.9, was reduced across all PAM strengths used, but particularly with the undiluted PAM.
- CCL5 attracts lymphocytes, NK cells, basophils, eosinophils and dendritic cells, and encourages endothelial adhesion of monocytes. The response to PAM for CCL5 followed a similar pattern to that of CCL2.
- CXCL8 attracts and activates neutrophils, as well as being chemoattractant for basophils, lymphocytes, eosinophils, endothelial cells and keratinocytes. This increased significantly for cells subjected to ¼ - and ½ - strength PAM, but there

was a small reduction, statistically insignificant reduction in concentration when undiluted PAM was used.

The functions of the non-chemokine cytokines which were found to be affected by PAM treatment can be summarised as:

- TNF-α causes vasodilation, increased permeability of blood vessels, fever, increases expression of cell adhesion molecules, and encourages neutrophils to commence respiratory burst, as well as polarising macrophages to the M1 phenotype. There was a significant increase concentrations of TNF-α in response to all three of the PAM strengths used (Table 7.9).
- IL-1β promotes the release of IL-6 and prostaglandins, and encourages vasodilation and fever, as well as the production of acute phase proteins. It is also chemoattractant for macrophages, T lymphocytes, and granulocytes and increases cell adhesion. As with TNF-α, all three PAM strengths used gave a statistically significant increase in IL-1β.
- IL-6 is a chemoattractant for monocytes and encourages growth and differentiation of lymphocytes. It also promotes the production of acute phase proteins and encourages fever. The lowest-strength PAM, ¼ -strength, resulted in a statistically significant increase in IL-6 concentration in the supernatant, whereas the two higher-strength PAMs resulted in a small decrease.

Given this information, it is possible to speculate the kind of environment the PAM-treated cells are creating around themselves, and what the effect of such an environment would be in an *in vivo* situation. With the weakest PAM used, ¼ -strength, there was a clear increase in the levels of CXCL8 from control, but there was no significant difference between control

and the treated samples for CCL2 or CCL5. It is also apparent that the supernatant produced by cells subjected to ¼-strength PAM has significant increases in TNF-α, IL-1β and IL-6. In this case of IL-6, this was the only PAM treatment which gave a significant change from control. This information would therefore suggest that there is likely enhancement of the chemoattractant nature of the environment, encouragement of the adhesion of these cells, also enhanced vasodilation and fever, and encouragement of the inflammatory properties of other cells, specifically through the activation of neutrophils and the pro-inflammatory polarisation of other macrophages. ½-strength PAM gave a significant increase in CXCL8, but a significant decrease in CCL2, with CCL5 remaining similar to control levels. TNF-α and IL-1β were significantly increased from control, with TNF-α showing a much larger increase than the level in the samples subject to ¼-strength PAM, but IL-6 did not increase as much as with the ¼-strength PAM. Therefore, the picture around chemoattraction was a mixture of enhancement and impairment, however, features such as activation and pro-inflammatory polarisation of immune cells, and vasodilation may be enhanced by the large increase in TNF-α.

With undiluted PAM, the effect on chemokine concentrations was either no change from control (CXCL8) or a significant decrease from control (CCL2, CCL5). As with the ½-strength PAM, the TNF-α and IL-1β was significantly increased from control, although in the case of TNF-α it was also significantly reduced in comparison to the ½-strength PAM. The concentration of IL-6 was similar to that of the control cells. Whilst the chemoattractant nature of the environment in comparison to control remains mixed, it appears less favourable than that of the ½-strength PAM. However, there may be enhancement beyond control of some of the other features of inflammation, such as the ability to cause

vasodilation, fever, immune cell polarisation and activation. However, this is not likely to reach the extent of that achieved by ½-strength PAM.

The impact of direct and PAM NTP treatments on cytokines and chemokines has been considered in a number of different cells types outside of the immune system, for example keratinocytes [171][296][297][298], melanoma [244][299] and stem cells [300] and some *in vivo* work has been performed on the blood levels of cytokines in mice following plasma treatment [108]. Within the immune system, the effects of NTP levels in neutrophils [124], lymphocytes [122] and monocytes [122][109][116][102] have also been considered. However, it is the work in the literature that was performed on the cytokine levels in NTP-treated macrophage-like cells which has relevance to the work performed here.

Most papers relating to the effects of PAM treatment on macrophage cytokines have, unlike the work performed here, considered a mix of pro-and anti-inflammatory substances. Kaushik *et al.* [18] found that the expression of genes for several chemokines and other cytokines increased at least two-fold when NTP-treated THP-1, differentiated by PMA, was assessed (Table 7.10). For all of the eight cytokines measured on this project, including the two in which there was no increase in concentration observed, they found that there was at least a two-fold increase in gene expression. However, the gene expression for the anti-inflammatory cytokine IL-10 was also enhanced, and therefore the extent to which the Kaushik *et al.* treatment influenced the overall pro- or anti-inflammatory nature of the macrophages is therefore unclear. This enhancement of IL-10 was also noted by Dang *et al.* [110], who found that pre-treatment of RAW264.7 murine macrophage cells with directly-applied NTP resulted in more IL-10 when cells were then stimulated with LPS, but that this was not the case with TNF-α or IL-6. Kaushik *et al.* also

examined the change in gene expression in NTP-treated macrophages when they were co-cultured with glioma cells. The results showed resulted in an increase in the expression of genes for CCL1, CCL2, CCCL4, CXCL5, CXCL8, CXCL16, IL-10, IL-1α, IL-1β, IL-6 and TNF-α. Again, this profile is mostly pro-inflammatory, but with some anti-inflammatory influence. TNF-α and IL-12 were also both measured in the macrophage and glioma co-culture supernatant, and it was found that there was significant increase in both of these with NTP-treated macrophages. In a separate work, Kaushik *et al.* [60] exposed RAW 264.7 murine macrophages to direct NTP treatment, and found that TNF-α levels in cell lysate increased, as well as genetic expression of the TNF-α gene being enhanced. They did not, however, measure any other cytokines.

Table 7.10. Genes for which expression was found to be enhanced by at least two-fold within Kaushik et al. [18].

CCL1	CCL24	CXCL12	IL-10
CCL2	CCL42	CXCL13	IL-10Ra
CCL3L3	CCR2	CXCL16	IL10-Rb
CCL4	CCR7	CXCR1	IL-12A
CCL5	CXCL2	CXCR2	IL-12B
CCL8	CXCL3	IFN-γ	IL-23D
CCL16	CXCL5	IFN-γR1	IL-R1
CCL17	CXCL8	IFN-γR2	IL-R2
CCL19	CXCL9	IL-1A	IL-Rap
CCL22	CXCL10	IL-1B	TNF
CCL23	CXCL11	IL-6	

Lacaille [112] considered PAM-induced changes of the expression of various cytokine genes in the B10R murine macrophage cell line. Of the eight chemokines and cytokines considered in 7.4.4.1 to 7.4.4.8, she considered four of them: TNF-α (1.1-fold increase), IL-6 (1.4-fold increase), CCL5 (1.5-fold decrease) and IL-1β (27.1-fold increase), however only the increase in the IL-1β expression was found to be significant. There was also, however, a significant increase in the gene expression for anti-inflammatory IL-10 (2.7-fold increase). Freud *et al.* [109] used the THP-1 monocyte cell line, differentiated using PMA to give a macrophage-like cell. Direct NTP treatment showed a significant increase in cytokines IL-1β, IL-6 and IL-8 within the supernatant, but not in IL-18, MCP-1 or the anti -inflammatory IL-10. Notably, there was also no significant increase in TNF-α, which had showed a significant increase in Figure 7.17. Bekeschus *et al*. [113], working with macrophages known to have a starting M0 phenotype, showed that PAM treatment gave little encouragement towards either a pro- or anti-inflammatory phenotype as, of cytokines considered in the supernatant (CCL2, CCL4, CXCL1, CXCL9, IL-1β, IL-2, IL-6, IL-10, IL-12, IFN-γ, TNF-α and TNF-β), only CXCL1 and CCL4 increased with PAM exposure.

The confused picture around the pro- and anti-inflammatory effects of NTP treatment is also found in the related area of the measurement of M1 and M2 polarisation markers. Kaushik *et al.* [18] found that during genetic expression of genes, both markers for M1 polarisation, such as CD86, and for M2 polarisation, such as CD163, were increased by NTP treatment and Freud *et al.* [109] found increases in some known markers of both M1 and M2 markers, but not in all of them. Crestale *et al.* [114] also noted a movement towards an anti-inflammatory phenotype from analysis of markers. Bekeschus *et al*. [113] found that there was minimal effect on the level of CD206, an M2 marker, in either M0 or M2

macrophages exposed to PAM. Lacaille [112] found M1 marker CD86 was downregulated by -2.7-fold by PAM treatment.

Therefore, some papers have shown NTP treatment to result in macrophages with a more pro-inflammatory phenotype, some anti-inflammatory, and some mixed. Some have shown significant changes in the cytokines which did not change on this project, whereas others have shown no change in cytokines that did change on this project. It is possible that some of the explanation for the difference in responses of cells to NTP treatment shown here may be due to either the different application types, direct or PAM, or the different chemical profiles produced in the treated liquids by different NTP sources. For example, Freund *et al.* [109] and Bekeschus *et al.* [113] used a kINPen as the NTP source, and thus the concentrations of both H_2O_2 and NO_2^- used for their treatments would be much lower than that those of Reactor 1 PAM (Table 4.1, Table 4.2). As well as this, treatment exposure times and measurement time points vary throughout the literature, as do measurement techniques, and it is also possible that the difference in results from different researchers also relates to the starting polarisation of the macrophage, which is usually unclear. There has also been little investigation in the literature around comparison of the effects of different "strengths" of NTP treatment on the inflammatory profile produced, such as has been performed in Table 7.9, an observation which raises the possibility of fine-tuning an immune response with NTP treatment.

7.4.5.9.1 Cytokine and chemokine secretion and viability

The work performed between 7.4.5.1 and 7.4.5.8 considers only the concentration of the cytokine in the supernatant. This measurement is important because the supernatant represents an extracellular environment, and the chemokines and cytokines are responsible

for influencing other cells in the area. However, this measurement does not consider the changes in levels of release from the individual cells within the sample. One observation which is clear for two chemokines, CCL2 and CCL5, as well as a further two cytokines, IL-1β and TNF-α, is that treatment with full-strength PAM resulted in a statistically significant increase in concentration in the supernatant, despite the fact that the viability of the cells, measured immediately following the removal of undiluted PAM, was only 14.1 % of the control value on average (Figure 7.3).

Cytokines are released from the cell by exocytosis (Figure 7.18). This is where a vesicle, in this case containing the cytokines, merges with the plasma membrane of the cell, and thus releases its contents into the extracellular environment.

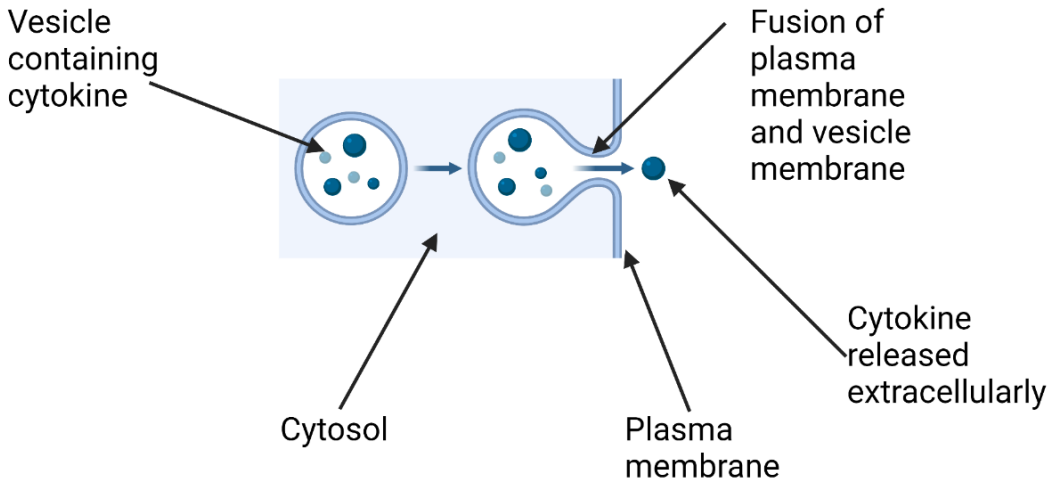

Figure 7.18. Exocytosis. Based on information within [31]. Created with BioRender.com [6].

There are two different forms of exocytosis, regulative and constitutive. The following explanation of these two terms is offered by the Encyclopaedia of Immunology:

> " Regulated exocytosis occurs on demand via secretagogues and signal transduction. Constitutive exocytosis is continuous; no secretagogue is involved, there are no storage vesicles, and the products are released apace upon synthesis." [301]

If a cytokine is one which is released by regulated exocytosis, an increased level could be a result of cell death resulting in stored substances being released in an uncontrolled manner [302]. Alternatively, if a cytokine is one which is released by constitutive exocytosis, an increase would mean that the cells which remain viable are producing unusually large amounts of the chemokine in response to the treatment. It is apparent that, due to the lack of granules in macrophages, they rely on constitutive exocytosis for the release of cytokines and chemokines [302][303][11][304]. Thus, it does appear that the undiluted PAM treatment is triggering the remaining viable cells to produce very large amounts of CCL2, CCL5, IL-1β and TNF-α, as opposed to the high concentrations of these in the supernatant being due to the high levels of cell death.

7.4.6 Effect of ¼- and ½-strength PAM on the expression of genes for the SOD1 and SOD2 antioxidant enzymes

As has been discussed in 1.2.1.3, cells have a suite of antioxidants available to them to protect against the effects of RONS. This includes the SOD family of enzymes, which dismutate the highly reactive O_2^- into the less-reactive H_2O_2.

Given that SOD has O_2^- as a substrate, and H_2O_2 as a product, and that NTP treatment seems to rely on H_2O_2 for its effects, with any O_2^- produced by the NTP being unlikely to make it directly to the cells due to its highly reactive, short-lived nature, as well as its

difficulty in crossing cell membranes [37], it may seem counterintuitive to imagine that SOD levels would increase with NTP treatment. However, it has been observed by some researchers that this is indeed the case. Having said this, it is clear that the picture remains mixed. For SOD1, one paper showed no change (Schmidt *et al.* [298]) and one showed an increase (Song *et al.* [72]), and one, that of Bekeschus *et al.* [116], showed that there was either an increase or no change depending on the cell line. This latter finding, that there is variability in the effect depending on the specific cell line, could explain the difference in results of the Schmidt *et al.* [298] and Song *et al.* [72] papers, as these used different cell lines from each other, with one using HaCaT murine keratinocyte cell line and the other the CNE-2Z human nasopharyngeal carcinoma cell line.

For SOD2, the results were even more variable across the three relevant papers identified, with a mixture of increases [116] [298], decreases [116][102], and no change [116][298] (Table 7.11). Again, this could be partially due to the fact that different cell lines were used throughout the literature, or differences in experimental techniques. It should be noted that in all three of these papers, the same plasma jet design was used as the NTP source, thus minimising the chance of the differences observed in SOD2 levels being due to differences in the NTP produced.

Table 7.11. Key papers which have considered the effect of NTP treatment on SOD1 and/or SOD2.

Author	**Cell type**	**NTP treatment**	**Gene expression or protein level measurement**	**SOD1 results**	**SOD2 results**
Bekeschus *et al.* [102]	TNP-1 monocyte	PAM, kINPen	Protein – measured in released microparticles	n/a	Decrease of SOD2 protein by 1.5-fold.
Bekeschus *et al.* [116]	THP-1, PBMC, PMN	Direct, kINPen, cells incubated in treated liquid for 4 hours prior to analysis.	Protein	THP-1: 12.33-fold increase PMBC: 2.88-fold increase PMN: change not significant	THP-1: change not significant PBMC: 2.64-fold decrease PMN: 1.79-fold increase
Schmidt *et al.* [298]	HaCaT (murine keratinocyte	PAM, kINPen	Gene expression	No change according to two gene expression measurement methods (qPCR and GeneChip)	Increased 1.65-fold according to GeneChip, but no change according to qPCR.
Song *et al.* [72]	CNE-2Z (human nasopharyngeal carcinoma)	Direct	Gene expression	CuZn-SOD/SOD1 increased	n/a

To understand how the Reactor 1 PAM affected SOD levels in differentiated U937 in comparison to these results, the change in expression of the genes for human SOD1 and SOD2 was measured following exposure to ¼- and ½ -strength PAM (Table 7.12) using RT-qPCR. The details of the primers and probes used for this work are given in Table 7.13.

Table 7.12. Change in expression of genes for SOD1 and SOD2 in cells treated with ¼- and 1/2-strength PAM. No statistically significant changes from control noted for either diluted PAM treatment. B2M used as reference gene, AVOVA for SOD1 (p = 0.943) and SOD2 (p = 0.394).

	Fold change in expression from control			
	SOD1 (n=3)		**SOD2 (n=4)**	
PAM	**Average**	**SE**	**Average**	**SE**
¼-strength	1.01	0.05	1.06	0.03
½-strength	1.04	0.06	0.93	0.07

Table 7.13. Details of primers and probes used for antioxidant genes.

Gene name	Primer/probe	Bases	Sequence	GC Content	Tm (50mM NaCl) °C
SOD1, HOMO_SAPIENS (Hs.PT.58.20593019)	PrimeTime Primer 1	20	TTA ATG CTT CCC CAC ACC TT	45	54.2950
	PrimeTime Primer 2	17	CCT CGG AAC CAG GAC CT	64.7059	56.4985
	PrimeTime Probe	22	/56-FAM/TCG CCA TAA /ZEN/CTC GCT AGG CCA C/3IABkFQ/	59.0909	61.3448
SOD2, HOMO_SAPIENS (Hs.PT.58.2512947)	PrimeTime Primer 1	19	TGC TCC CAC ACA TCA ATC C	52.6316	55.0703
	PrimeTime Primer 2	22	GGT TGG CTT GGT TTC AAT AAG G	45.4546	54.5522
	PrimeTime Probe	26	/56-FAM/TGC TTG TCC /ZEN/AAA TCA GGA TCC ACT GC/3IABkFQ/	50	61.2547

The results for SOD2 throughout the literature (Table 7.11), and the results presented here (Table 7.12), range across increases, decreases and no effect, and it is not clear why this is so variable. One possible explanation for situations in the literature in which there was an increase in SOD2 could relate to an increase TNF-α by NTP treatment, as it is known that TNF-α and IL-1β can induce both O_2^- production in some cells, as well as that of SOD2 in some cell types [305]. It has been confirmed both in this project, and by other researchers, that both of these substances can be increased by NTP treatment (7.4.5.5, 7.4.5.7 and 7.4.5.9), and therefore it can be seen that there could be a link between an increase in SOD2 and the effects of NTP treatment on cytokine levels. It is notable about the research into the interaction of TNF-α increases and SOD2 increases that it has revealed that it does not apply equally to all cell types [306]. It appears that it does not apply to U937, at least not in its monocytic form [306], which could explain why no increase in SOD2 was observed here, whereas it was observed in other work using other cell types. The mechanism by which some of the research in Table 7.11 resulted in a decrease in SOD2 is not clear, but again the explanation may be due to the quirks of specific cell types, particularly as, in one of the papers where a decrease was noted on one cell type, other cell types showed an increase or no change in SOD2 in response to the exactly the same NTP treatment [116].

Although this is a possible explanation for the variable effects on SOD2 levels seen with NTP treatment, the same cannot be said of SOD1. It appears that TNF-α does not have the same effect on SOD1 levels as it can do on SOD2 [307][308]. This is an area that would require further investigation.

7.5 Conclusions

A number of different measurements were taken during the work in this chapter to understand the effect of Reactor 1 PAM treatment of various strengths on key attributes of macrophages, with a particular focus on phagocytosis and the cytokine environment that they create around them. It was found that, at sublethal levels of PAM, phagocytosis did not seem to be inhibited, something that was verified both by counting beads and also by examining two genes that are related in phagocytosis, specifically NHLRC2 and TM2D1. Work in the area of phagocytosis was hampered significantly by pandemic-related access restrictions as this meant that both FACS and advanced imaging techniques could not be pursued as had originally been planned and ideally these would therefore be performed in the future to get a more accurate set of results than it was possible to achieve here. As well as this, there are a large number of genes associated with phagocytosis beyond the two that have been considered here, and a broader assessment of these genes could be enlightening.

It was clear that Reactor 1 PAM treatment could enhance the pro-inflammatory nature of the environment around differentiated U937. Four chemokines and four further cytokines were assessed in the cell supernatant following application of PAM of various dilutions. The results varied depending on the specific protein being measured: some went up, some went down, and some did not change. This was also dependent upon the particular PAM dilution used, and it was clear that the different PAM dilutions gave different inflammatory profiles. However, with the work performed it is not clear whether the amounts of anti-inflammatory cytokines are also enhanced and, as has been shown in the literature, the balance between the pro- and anti-inflammatory attributes of NTP-treated macrophages can be quite nuanced. Therefore, it would be useful to consider a much wider range of

cytokines, both pro- and anti-inflammatory, as well as M1 and M2 markers, to better understand the response of macrophages to Reactor 1 PAM.

There was little change in the expression of SOD1 and SOD2 following PAM treatment of differentiated U937. Reflecting on the literature, this may not be unexpected due to the varying responses of cells to NTP treatment which have been observed, as well as what is known about the characteristics of U937 specifically. Further investigation into the effects of PAM on a wider range of antioxidant genes would be useful.

Attempts were also made to see if using a weak pre-dose of PAM could protect against a later strong dose, a hypothesis based on work in the literature which showed that such as effect could occur with H_2O_2. It was, however, not possible to achieve this affect with the PAM. It may be that this effect is possible with these cells, as it seems likely given that PAM contains H_2O_2, but the strengths of PAM used were perhaps not the right ones to use.

Overall, there were several novel findings in the work performed in this chapter which add to the understanding of the effects of PAM application to macrophage-like cells. In particular, it was shown that sublethal PAM treatment had no effect on phagocytic ability in such cells, nor on the expression of two specific phagocytosis-related genes, NHLRC2 and TM2D1. It was also found that, as well as the PAM treatment causing the cells to become more strongly pro-inflammatory in terms of cytokine secretion, the exact inflammatory profile could be varied by differing PAM dilutions, allowing deliberate tuning.

Chapter 8 Conclusion

8.1 Progress against stated aims

The aims of the project, as stated in section 1.3 were:

1. To develop a simple DBD-type NTP source suitable for application to *in vitro* cell samples, and carry out appropriate electrical, chemical, and biological testing to develop an understanding of its operation and confirm its suitability for use in plasma medicine research.
2. To investigate the effect NTP treatment generated by this reactor on the U937 monocyte cell line, differentiated to a macrophage-like cell with PMA, through the use of different dilutions of PAM. The effects considered as part of this would be viability, phagocytic ability, antioxidant gene expression, and levels of certain pro-inflammatory chemokines and other cytokines.

Both of these aims have been met over the course of the project, as detailed below.

8.1.1 Aim 1

Reactor 1, of a pin-plate DBD device style, was designed for use in the bulk of the work on this project, and electrical, chemical and biological testing considered overall confirmed that it was suitable for use within plasma medicine research.

8.1.1.1 Electrical characteristics of Reactor 1

The initial discharge power of Reactor 1 was found to be an average of 439 mW, and this remained stable up to the maximum treatment time used in this project, 30 minutes. It was also found that the character of the discharge changed across this time, thought to be

a consequence of the reducing liquid level in the well due to evaporation being caused by the treatment. However, as confirmed in the chemical and biological testing detailed below, this change in discharge mode appeared to have minimal effect on the efficacy of the reactor in terms of its practical use in plasma medicine research.

Although a basic assessment of the electrical characteristics of Reactor 1 has been carried out, further work is required to have a full understanding. Ideally, intensified charge-coupled device (ICCD) imaging to view the discharge would be employed, as well as examination of the optical emission spectra of the NTP. Further refinement of the reactor with the aim of designing out the transition in discharge mode would also be worthwhile, as well as modification of the design for *in vivo* use. Clearly, the use of either a 96-well plate or Petri dish is not possible would not be possible if direct treatment were to be applied, and therefore a possible design would be to instead place the subject upon a dielectric plate.

8.1.1.2 Chemical effects on NTP-treated liquid

Two of the most important substances in plasma medicine are H_2O_2 and NO_2^-, and Reactor 1 was found to be capable of producing both of these substances in liquids in concentrations that were broadly in line with those seen within the plasma medicine literature, suggesting that the Reactor 1 design was indeed suitable for use in this context (Chapter 4). The change in concentration of both substances was approximately linear with treatment times of up to 30 minutes, despite the apparent change of discharge mode observed mentioned in 8.1.1.1, with concentrations reaching 5.2 mM of H_2O_2 and 13.0 mM of NO_2^-. Temperature and pH change in treated liquid were found to be minimal.

Work with a modified version of Reactor 1 (Reactor 2) demonstrated the highly targeted nature of an NTP treatment of liquid created using a pin-plate style device, showing the potential of this design in a medical setting. However, this work also showed that precision of treatment area is lost with longer treatment times, and as well as highlighting the post-treatment diffusion of the RONS, something which does not seem to have been widely considered in the plasma medicine literature.

Ideally, future work could be carried out to develop a more complete understanding of the chemical profile of the NTP-treated liquid produced by Reactor 1, beyond simply H_2O_2 and NO_2^-. This could be achieved using techniques such as nuclear magnetic resonance (NMR) spectroscopy. Experimentation using gases other than atmospheric air to form the NTP of Reactor 1 could also be interesting.

8.1.1.3 Basic biological testing

From the work performed on the NIH 3t3 cell line in Chapters 5 and 6, the suitability of Reactor 1 for *in vitro* work was confirmed, as it showed that both the direct and PAM treatments produced were capable of achieving repeatable, measurable biological effects.

Direct and PAM treatment experiments on the NIH 3t3 cell line, and PAM treatments of differentiated U937 produced an at-times confusing picture around the effects of Reactor 1 treatment on viability. With 3t3, although direct NTP treatments produced significant reductions in cell viability, and appeared apoptotic, when considered 24 hours later, there was a larger reduction when the cells were considered immediately after treatment instead. It is thought that this observation could be due to the cells which are not killed outright by the treatment going on to divide in the following 24 hours. Interestingly, when

treated with PAM rather than direct treatment, this immediate response was absent in 3t3, but it was present in U937. The reasons behind these differences are not clear.

The 3t3 cell line was also used in investigations into effects of PAM storage conditions, with it being found that there was a reduction in its ability to affect cell viability if it was stored, refrigerated, for 48 hours, as opposed to being applied to cells immediately following its creation, with the viability of the cells treated with the stored PAM being approximately double that of those treated with the immediately-used PAM. An understanding of optimal storage conditions is important if PAM is ever to progress to clinical use, as in such a setting it is unlikely to be produced immediately prior to application to a patient. The effects of differing cell exposure times to PAM were also investigated, with it being found that PAM had no effect on viability if only applied to cells for very short periods, perhaps surprising given the known rapid movement of H_2O_2 through the cell membrane. Again, this has important implications for any clinical use, as the optimum time of exposure, and indeed how that exposure could be practically controlled, needs to be determined. Unexpectedly, it was also found that in direct treatment, using DBPS as the treatment liquid was more effective at reducing viability than DMEM, something that was not the case when these liquids were instead used as the basis for PAM. The reason for this difference between the two treatment methods is not clear, but it highlights the need for a thorough understanding of how different liquids react to NTP exposure, and which are the most suitable for medical applications.

8.1.2 Aim 2

Chapter 7 considered whether PAM treatment could influence the immune activities of differentiated U937, a macrophage-like cell. The effects on phagocytic ability were investigated, from which it was found that sublethal levels of PAM did not inhibit the ability of the cells to phagocytose particles, nor did it significantly influence the expression of two genes associated with phagocytosis, NHLRC2 and TM2D1. The change in expression of two genes relating to the production of superoxide, SOD1 and SOD2, was also considered, and again little difference was found from the control samples.

It was clear, however, that PAM treatment could modify the immune properties of U937 in other ways, with the assessment of the cell supernatant showing changes in the levels of several pro-inflammatory chemokines and other cytokines present following PAM treatment. The extent and direction of these changes was dependent upon the protein being considered, and also the specific PAM dilution used. This raises the possibility of using PAM to delicately tune an inflammatory environment.

The work performed to assess phagocytosis of latex beads was hampered significantly by pandemic-related access restrictions and, therefore, this would ideally be improved upon. Specifically, this could involve the use of FACS and advanced imaging techniques. It would also be interesting to investigate the effects of PAM on the expression of the many other genes relating to phagocytosis, beyond NHLRC2 and TM2D1, as well as looking into the into the effects of PAM exposure on cytokines beyond those examined, including anti-inflammatory cytokines.

8.2 Overall conclusions

A novel source, named Reactor 1, suitable for the production of NTP from atmospheric pressure air, and the application of that NTP to in vitro cell samples was successfully designed and characterised. It was proven that reactors which used a pin electrode are capable of applying NTP to a highly targeted area. It was also determined that there can be post-treatment diffusion of the reactive species produced by NTP treatment, something that does not appear to have been considered elsewhere within the plasma medicine literature.

Reactor 1 was found to be able to reduce cell viability via both direct and PAM NTP treatments, something that would be expected from a source suitable for plasma medicine research, given the similar effects found in the literature.

Novel work was performed in the application of PAM to macrophage-like cells. The work performed within this project was the first to show that sublethal PAM treatments do not affect phagocytic ability in such cells. It was also shown, as far as has been determined for the first time, that use of different strengths of PAM result in different inflammatory profiles, raising the possibility of the use of PAM to finely tune macrophage actions, something which could be useful in clinical settings.

References

[1] E. Martin and R. Hine, *A Dictionary of Biology*, 7th ed. Oxford: OUP Oxford, 2015.

[2] B. Alberts, A. Johnson, J. Lewis, D. Morgan, M. Raff, K. Roberts, and P. Walter, "Molecular Biology of the Cell ," 6th ed., New York: Garland Science, 2015, pp. 1–42.

[3] "Biorender Templates." [Online]. Available: https://app.biorender.com/biorender-templates

[4] K. Murphy and C. Weaver, "Janeway's Immunobiology," 9th ed., New York: Garland Science, 2016, pp. 1–36.

[5] P. K. Mahalingaiah, T. Palenski, and T. R. Van Vleet, "An *in vitro* model of hematotoxicity: differentiation of bone marrow-derived stem/progenitor cells into hematopoietic lineages and evaluation of lineage-specific hematotoxicity," *Current Protocols in Toxicology*, vol. 76, no. 1, p. e45, 2018.

[6] "BioRender." [Online]. Available: biorender.com

[7] J. Punt, S. Stranford, P. Jones, and J. Owen, "Kuby Immunology," 8th ed., New York: Macmillan Learning, 2018, pp. 47–115.

[8] J. K. Actor, "Introductory Immunology: Basic Concepts for Interdisciplinary Applications," 2nd ed., Cham: Academic Press, 2019, pp. 17–30.

[9] A. Viola, F. Munari, R. Sánchez-Rodriguez, T. Scolaro, and A. Castegna, "The metabolic signature of macrophage responses," *Frontiers in Immunology*, vol. 10, p. 1462, 2019.

[10] J. Punt, S. Stranford, P. Jones, and J. Owen, "Kuby Immunology," 8th ed., New York: Macmillan Learning, 2018, pp. 116–198.

[11] G. Arango Duque and A. Descoteaux, "Macrophage cytokines: involvement in immunity and infectious diseases," *Frontiers in Immunology*, vol. 5, p. 491, 2014.

[12] A. L. Coelho, C. M. Hogaboam, and S. L. Kunkel, "Chemokines provide the sustained inflammatory bridge between innate and acquired immunity," *Cytokine & Growth Factor Reviews*, vol. 16, no. 6, pp. 553–560, 2005.

[13] M. A. Sugimoto, L. P. Sousa, V. Pinho, M. Perretti, and M. M. Teixeira, "Resolution of inflammation: what controls its onset?," *Frontiers in Immunology*, vol. 7, p. 160, 2016.

[14] J. R. de Sousa, P. F. Da Costa Vasconcelos, and J. A. S. Quaresma, "Functional aspects, phenotypic heterogeneity, and tissue immune response of macrophages in infectious diseases," *Infection and Drug Resistance*, pp. 2589–2611, 2019.

[15] A. Shapouri-Moghaddam, S. Mohammadian, H. Vazini, M. Taghadosi, S.-A. Esmaeili, F. Mardani, B. Seifi, A. Mohammadi, J. T. Afshari, and A. Sahebkar, "Macrophage plasticity, polarization, and function in health and disease," *Journal of Cellular Physiology*, vol. 233, no. 9, pp. 6425–6440, 2018.

[16] A. N. Orekhov, V. A. Orekhova, N. G. Nikiforov, V. A. Myasoedova, A. V. Grechko, E. B. Romanenko, D. Zhang, and D. A. Chistiakov, "Monocyte differentiation and macrophage polarization," *Vessel Plus*, vol. 3, no. 10, pp. 2574–1209, 2019.

[17] M. Song, I. Ryoo, H. Choi, B. Choi, S.-T. Kim, T.-H. Heo, J. Y. Lee, P.-H. Park, and M.-K. Kwak, "NRF2 signaling negatively regulates phorbol-12-myristate-13-acetate (PMA)-induced differentiation of human monocytic U937 cells into pro-inflammatory macrophages," *PLoS One*, vol. 10, no. 7, p. e0134235, 2015.

[18] N. K. Kaushik, N. Kaushik, M. Adhikari, B. Ghimire, N. N. Linh, Y. K. Mishra, S.-J. Lee, and E. H. Choi, "Preventing the solid cancer progression via release of anticancer-cytokines in co-culture with cold plasma-stimulated macrophages," *Cancers*, vol. 11, no. 6, p. 842, 2019.

[19] P. R. Taylor, L. Martinez-Pomares, M. Stacey, H.-H. Lin, G. D. Brown, and S. Gordon, "Macrophage receptors and immune recognition," *Annual Review of Immunology*, vol. 23, no. 1, pp. 901–944, 2005.

[20] T. Ito, "PAMPs and DAMPs as triggers for DIC," *Journal of Intensive Care*, vol. 2, no. 1, pp. 1–9, 2014.

[21] K. Murphy and C. Weaver, "Janeway's Immunobiology," 9th ed., New York: Garland Science, 2016, pp. 37–76.

[22] T. H. Mogensen, "Pathogen recognition and inflammatory signaling in innate immune defenses," *Clinical Microbiology Reviews*, vol. 22, no. 2, pp. 240–273, 2009.

[23] M. van Lookeren Campagne, C. Wiesmann, and E. J. Brown, "Macrophage complement receptors and pathogen clearance," *Cellular Microbiology*, vol. 9, no. 9, pp. 2095–2102, 2007.

[24] H. Lee, M. B. Fessler, P. Qu, J. Heymann, and J. B. Kopp, "Macrophage polarization in innate immune responses contributing to pathogenesis of

chronic kidney disease," *BMC Nephrology*, vol. 21, no. 1, pp. 1–13, 2020.

[25] K. Murphy and C. Weaver, "Janeway's Immunobiology," 9th ed., New York: Garland Science, 2016, pp. 811–813.

[26] H. Mühl and J. Pfeilschifter, "Anti-inflammatory properties of pro-inflammatory interferon-γ," *International Immunopharmacology*, vol. 3, no. 9, pp. 1247–1255, 2003.

[27] C. P. Verschoor, A. Puchta, and D. M. Bowdish, "The macrophage," in *Leucocytes: Methods and Protocols*, Ashman, Robert B, Ed. Totowa, NJ: Humana Press, 2012, pp. 139–156.

[28] J. L. Owen and M. Mohamadzadeh, "Macrophages and chemokines as mediators of angiogenesis," *Frontiers in Physiology*, vol. 4, p. 159, 2013.

[29] M. Brault and R. A. Kurt, "Impact of tumor-derived CCL2 on macrophage effector function," *Journal of Biomedicine and Biotechnology*, vol. 2005, no. 1, pp. 37–43, 2005.

[30] K. Murphy and C. Weaver, "Janeway's Immunobiology," 9th ed., New York: Garland Science, 2016, pp. 77–137.

[31] B. Alberts, A. Johnson, J. Lewis, D. Morgan, M. Raff, K. Roberts, and P. Walter, *Molecular Biology of the Cell*. New York: Garland Science, 2015.

[32] B. Halliwell and J. M. Gutteridge, "Free Radicals in Biology and Medicine," 5th ed., Oxford: Oxford University Press, 2015, pp. 411–462.

[33] J. Punt, S. Stranford, P. Jones, and J. Owen, "Kuby Immunology," 8th ed., New York: Macmillan Learning, 2018, pp. 306–425.

[34] D. B. Graves, "The emerging role of reactive oxygen and nitrogen species in redox biology and some implications for plasma applications to medicine and biology," *Journal of Physics D: Applied Physics*, vol. 45, no. 26, p. 263001, 2012.

[35] B. Halliwell and J. M. Gutteridge, "Free Radicals in Biology and Medicine," 5th ed., Oxford: Oxford University Press, 2015, pp. 199–283.

[36] H. Sies, "Oxidative eustress and oxidative distress: introductory remarks," in *Oxidative Stress*, Sies, Helmut, Ed. San Diego: Elsevier, 2020, pp. 3–12.

[37] B. Halliwell and J. M. Gutteridge, "Free Radicals in Biology and Medicine," 5th ed., Oxford: Oxford University Press, 2015, pp. 30–76.

[38] T. Iannitti and B. Palmieri, "Antioxidant therapy effectiveness: an up to date," *European Review for Medical and Phamacological Sciences*, vol. 13, no. 4,

pp. 245–278, 2009.

[39] B. Halliwell and J. M. Gutteridge, “Free Radicals in Biology and Medicine,” 5th ed., Oxford: Oxford University Press, 2015, pp. 77–152.

[40] F. Johnson and C. Giulivi, “Superoxide dismutases and their impact upon human health,” *Molecular Aspects of Medicine*, vol. 26, no. 4–5, pp. 340–352, 2005.

[41] Y. Wang, R. Branicky, A. Noë, and S. Hekimi, “Superoxide dismutases: dual roles in controlling ROS damage and regulating ROS signaling,” *Journal of Cell Biology*, vol. 217, no. 6, pp. 1915–1928, 2018.

[42] K. H. Becker, U. Kogelschatz, K. Schoenbach, and R. Barker, *Non-equilibrium Air Plasmas at Atmospheric Pressure*. CRC press, 2004.

[43] A. Fridman, “Introduction to theoretical and applied plasma chemistry: plasma as the fourth state of matter,” in *Plasma Chemistry*, Cambridge: Cambridge University Press, 2008, pp. 1–11.

[44] N. Bibinov, P. Rajasekaran, P. M. D. Wandke, W. Viöl, and P. Awakowicz, “Basics and biomedical applications of dielectric barrier discharge (DBD),” in *Biomedical Engineering, Trends in Materials Science*, InTech, 2011.

[45] P. Lu, P. Cullen, and K. Ostrikov, “Atmospheric pressure nonthermal plasma sources,” in *Cold Plasma in Food and Agriculture*, Elsevier, 2016, pp. 83–116.

[46] A. Fridman, “Electric discharges in plasma chemistry,” in *Plasma Chemistry*, Cambridge: Cambridge University Press, 2008, pp. 157–258.

[47] M. Kushner and M. Kong, “Fundamentals of non-equilibrium plasmas,” in *Plasma Medicine: Applications of Low-Temperature Gas Plasmas in Medicine and Biology*, M. Laroussi, M and Kong, MG and Morfill, G and Stolz, W, Ed. Cambridge: Cambridge University Press, 2012, pp. 2–27.

[48] A. Fridman, *Plasma Chemistry*. Cambridge: Cambridge University Press, 2008.

[49] N. Misra, O. Schlüter, and P. J. Cullen, “Plasma in food and agriculture,” in *Cold Plasma in Food and Agriculture: Fundamentals and Applications*, Misra, NN and Schlüter, Oliver and Cullen, Patrick J, Ed. San Diego: Academic Press, 2016, pp. 10–17.

[50] T. Von Woedtke, S. Reuter, K. Masur, and K.-D. Weltmann, “Plasmas for medicine,” *Physics Reports*, vol. 530, no. 4, pp. 291–320, 2013.

[51] E. Stoffels, I. Kieft, and R. Sladek, “Superficial treatment of mammalian cells using plasma needle,” *Journal of Physics D: Applied Physics*, vol. 36, no. 23, p. 2908, 2003.

[52] E. Stoffels, R. Sladek, and I. Kieft, “Gas plasma effects on living cells,” *Physica Scripta*, vol. 2004, no. T107, p. 79, 2004.

[53] I. Kieft, J. Broers, V. Caubet-Hilloutou, D. Slaaf, F. Ramaekers, and E. Stoffels, “Electric discharge plasmas influence attachment of cultured CHO K1 cells,” *Bioelectromagnetics: Journal of the Bioelectromagnetics Society, The Society for Physical Regulation in Biology and Medicine, The European Bioelectromagnetics Association*, vol. 25, no. 5, pp. 362–368, 2004.

[54] E. Stoffels, Y. Sakiyama, and D. B. Graves, “Cold atmospheric plasma: charged species and their interactions with cells and tissues,” *IEEE Transactions on Plasma Science*, vol. 36, no. 4, pp. 1441–1457, 2008.

[55] E. Stoffels, A. Flikweert, W. Stoffels, and G. Kroesen, “Plasma needle: a non-destructive atmospheric plasma source for fine surface treatment of (bio) materials,” *Plasma Sources Science and Technology*, vol. 11, no. 4, p. 383, 2002.

[56] M. Laroussi, “Plasma medicine: a brief introduction,” *Plasma*, vol. 1, no. 1, p. 5, 2018.

[57] D. Yan, J. H. Sherman, and M. Keidar, “Cold atmospheric plasma, a novel promising anti-cancer treatment modality,” *Oncotarget*, vol. 8, no. 9, p. 15977, 2017.

[58] A. Lin, N. Chernets, J. Han, Y. Alicea, D. Dobrynin, G. Fridman, T. A. Freeman, A. Fridman, and V. Miller, “Non-equilibrium dielectric barrier discharge treatment of mesenchymal stem cells: charges and reactive oxygen species play the major role in cell death,” *Plasma Processes and Polymers*, vol. 12, no. 10, pp. 1117–1127, 2015.

[59] N. Kaushik, P. Attri, N. Kaushik, and E. Choi, “A preliminary study of the effect of DBD plasma and osmolytes on T98G brain cancer and HEK non-malignant cells,” *Molecules*, vol. 18, no. 5, pp. 4917–4928, 2013.

[60] N. K. Kaushik, N. Kaushik, B. Min, K. H. Choi, Y. J. Hong, V. Miller, A. Fridman, and E. H. Choi, “Cytotoxic macrophage-released tumour necrosis factor-alpha (TNF-α) as a killing mechanism for cancer cell death after cold plasma activation,” *Journal of Physics D: Applied Physics*, vol. 49, no. 8, p. 084001, 2016.

[61] M. Laroussi, X. Lu, and M. Keidar, “Perspective: The physics, diagnostics, and applications of atmospheric pressure low temperature plasma sources used in plasma medicine,” *Journal of Applied Physics*, vol. 122, no. 2, p. 020901,

2017.

[62] J. Balzer, K. Heuer, E. Demir, M. A. Hoffmanns, S. Baldus, P. C. Fuchs, P. Awakowicz, C. V. Suschek, and C. Opländer, "Non-thermal dielectric barrier discharge (DBD) effects on proliferation and differentiation of human fibroblasts are primary mediated by hydrogen peroxide," *PLoS One*, vol. 10, no. 12, p. e0144968, 2015.

[63] G. Fridman, M. Peddinghaus, M. Balasubramanian, H. Ayan, A. Fridman, A. Gutsol, and A. Brooks, "Blood coagulation and living tissue sterilization by floating-electrode dielectric barrier discharge in air," *Plasma Chemistry and Plasma Processing*, vol. 26, no. 4, pp. 425–442, 2006.

[64] K. D. Weltmann, E. Kindel, R. Brandenburg, C. Meyer, R. Bussiahn, C. Wilke, and T. Von Woedtke, "Atmospheric pressure plasma jet for medical therapy: plasma parameters and risk estimation," *Contributions to Plasma Physics*, vol. 49, 2009.

[65] N. Kaushik, S. J. Lee, T. G. Choi, K. Y. Baik, H. S. Uhm, C. H. Kim, N. K. Kaushik, and E. H. Choi, "Non-thermal plasma with 2-deoxy-D-glucose synergistically induces cell death by targeting glycolysis in blood cancer cells," *Scientific Reports*, vol. 5, 2015.

[66] G. E. Conway, A. Casey, V. Milosavljevic, Y. Liu, O. Howe, P. J. Cullen, and J. F. Curtin, "Non-thermal atmospheric plasma induces ROS-independent cell death in U373MG glioma cells and augments the cytotoxicity of temozolomide," *British Journal of Cancer*, vol. 114, no. 4, p. 435, 2016.

[67] I. C. Gerber, C. T. Mihai, L. Gorgan, M. Ciorpac, A. Nita, V. Pohoata, I. Mihaila, and I. Topala, "Air dielectric barrier discharge plasma source for *in vitro* cancer studies," *Clinical Plasma Medicine*, vol. 9, p. 4, 2018.

[68] S. Kalghatgi, C. Kelly, E. Cerchar, and J. Azizkhan-Clifford, "Selectivity of non-thermal atmospheric-pressure microsecond-pulsed dielectric barrier discharge plasma induced apoptosis in tumor cells over healthy cells," *Plasma Medicine*, vol. 1, no. 3–4, 2011.

[69] S. B. Karki, E. Yildirim-Ayan, K. M. Eisenmann, and H. Ayan, "Miniature dielectric barrier discharge nonthermal plasma induces apoptosis in lung cancer cells and inhibits cell migration," *BioMed Research International*, vol. 2017, 2017.

[70] G. Kim, S. Park, G. Kim, and J. K. J. Lee, "Targeted cancer treatment using anti-EGFR and-TFR antibody-conjugated gold nanoparticles stimulated by nonthermal air plasma," *Plasma Medicine*, vol. 1, no. 1, 2011.

[71] K. Panngom, K. Y. Baik, Y. H. Ryu, H. S. Uhm, and E. H. Choi, "Differential responses of cancer cell lines to non-thermal plasma from dielectric barrier

discharge," *Current Applied Physics*, vol. 13, pp. S6–S11, 2013.

[72] W. Song, E. Wang, Y. Gao, Q. Wu, S. Rao, H. Wang, and L. Bao, "Low temperature plasma induced apoptosis in CNE-2Z cells through endoplasmic reticulum stress and mitochondrial dysfunction pathways," *Plasma Processes and Polymers*, vol. 15, no. 3, p. 1600249, 2018.

[73] M. Vandamme, E. Robert, S. Lerondel, V. Sarron, D. Ries, S. Dozias, J. Sobilo, D. Gosset, C. Kieda, B. Legrain, and others, "ROS implication in a new antitumor strategy based on non-thermal plasma," *International Journal of Cancer*, vol. 130, no. 9, pp. 2185–2194, 2012.

[74] U. Kogelschatz, B. Eliasson, and W. Egli, "Dielectric-barrier discharges. Principle and applications," *Le Journal de Physique IV*, vol. 7, no. C4, pp. C4–47, 1997.

[75] G. Isbary, T. Shimizu, Y.-F. Li, W. Stolz, H. M. Thomas, G. E. Morfill, and J. L. Zimmermann, "Cold atmospheric plasma devices for medical issues," *Expert Review of Medical Devices*, vol. 10, no. 3, pp. 367–377, 2013.

[76] U. Kogelschatz, "Dielectric-barrier discharges: their history, discharge physics, and industrial applications," *Plasma Chemistry and Plasma Processing*, vol. 23, no. 1, pp. 1–46, 2003.

[77] R. Brandenburg, "Dielectric barrier discharges: progress on plasma sources and on the understanding of regimes and single filaments," *Plasma Sources Science and Technology*, vol. 26, no. 5, p. 053001, 2017.

[78] L. Bundscherer, K. Wende, K. Ottmüller, A. Barton, A. Schmidt, S. Bekeschus, S. Hasse, K.-D. Weltmann, K. Masur, and U. Lindequist, "Impact of non-thermal plasma treatment on MAPK signaling pathways of human immune cell lines," *Immunobiology*, vol. 218, no. 10, pp. 1248–1255, 2013.

[79] M. Ishaq, S. Kumar, H. Varinli, Z. J. Han, A. E. Rider, M. D. Evans, A. B. Murphy, and K. Ostrikov, "Atmospheric gas plasma-induced ROS production activates TNF-ASK1 pathway for the induction of melanoma cancer cell apoptosis," *Molecular Biology of the Cell*, vol. 25, no. 9, pp. 1523–1531, 2014.

[80] H. Tanaka, M. Mizuno, K. Ishikawa, K. Nakamura, H. Kajiyama, H. Kano, F. Kikkawa, and M. Hori, "Plasma-activated medium selectively kills glioblastoma brain tumor cells by down-regulating a survival signaling molecule, AKT kinase," *Plasma Medicine*, vol. 1, no. 3–4, 2011.

[81] N. H. Nguyen, H. J. Park, S. S. Yang, K. S. Choi, and J.-S. Lee, "Anti-cancer efficacy of nonthermal plasma dissolved in a liquid, liquid plasma in heterogeneous cancer cells," *Scientific Reports*, vol. 6, p. 29020, 2016.

[82] S. Kalghatgi, C. M. Kelly, E. Cerchar, B. Torabi, O. Alekseev, A. Fridman, G. Friedman, and J. Azizkhan-Clifford, “Effects of non-thermal plasma on mammalian cells,” *PloS One*, vol. 6, no. 1, p. e16270, 2011.

[83] H. J. Ahn, K. I. Kim, G. Kim, E. Moon, S. S. Yang, and J.-S. Lee, “Atmospheric-pressure plasma jet induces apoptosis involving mitochondria via generation of free radicals,” *PloS One*, vol. 6, no. 11, p. e28154, 2011.

[84] H. J. Ahn, K. I. Kim, N. N. Hoan, C. H. Kim, E. Moon, K. S. Choi, S. S. Yang, and J.-S. Lee, “Targeting cancer cells with reactive oxygen and nitrogen species generated by atmospheric-pressure air plasma.,” *PLoS One*, vol. 9, no. 1, p. e86173, 2014.

[85] R. Furuta, N. Kurake, K. Ishikawa, K. Takeda, H. Hashizume, H. Tanaka, H. Kondo, M. Sekine, and M. Hori, “Intracellular responses to reactive oxygen and nitrogen species, and lipid peroxidation in apoptotic cells cultivated in plasma-activated medium,” *Plasma Processes and Polymers*, vol. 14, no. 11, p. 1700123, 2017.

[86] E. Stoffels, I. Kieft, R. Sladek, L. Van den Bedem, E. Van der Laan, and M. Steinbuch, “Plasma needle for in vivo medical treatment: recent developments and perspectives,” *Plasma Sources Science and Technology*, vol. 15, no. 4, p. S169, 2006.

[87] B. Alberts, A. Johnson, J. Lewis, D. Morgan, M. Raff, K. Roberts, and P. Walter, “Molecular Biology of the Cell,” New York: Garland Science, 2015, pp. 1021–1034.

[88] M. S. D’arcy, “Cell death: a review of the major forms of apoptosis, necrosis and autophagy,” *Cell Biology International*, vol. 43, no. 6, pp. 582–592, 2019.

[89] O. Volotskova, T. S. Hawley, M. A. Stepp, and M. Keidar, “Targeting the cancer cell cycle by cold atmospheric plasma,” *Scientific Reports*, vol. 2, p. 636, 2012.

[90] N. Georgescu and A. R. Lupu, “Tumoral and normal cells treatment with high-voltage pulsed cold atmospheric plasma jets,” *IEEE Transactions on Plasma Science*, vol. 38, no. 8, pp. 1949–1955, 2010.

[91] J. Köritzer, V. Boxhammer, A. Schäfer, T. Shimizu, T. G. Klämpfl, Y.-F. Li, C. Welz, S. Schwenk-Zieger, G. E. Morfill, J. L. Zimmermann, and others, “Restoration of sensitivity in chemo—resistant glioma cells by cold atmospheric plasma,” *PloS One*, vol. 8, no. 5, p. e64498, 2013.

[92] G. Kim, W. Kim, K. Kim, and J. Lee, “DNA damage and mitochondria dysfunction in cell apoptosis induced by nonthermal air plasma,” *Applied Physics Letters*, vol. 96, no. 2, p. 021502, 2010.

[93] B. Alberts, A. Johnson, J. Lewis, D. Morgan, M. Raff, K. Roberts, and P. Walter, “Molecular Biology of the Cell ,” 6th ed., New York: Garland Science, 2015, pp. 173–236.

[94] B. Alberts, A. Johnson, J. Lewis, D. Morgan, M. Raff, K. Roberts, and P. Walter, “Molecular Biology of the Cell ,” 6th ed., New York: Garland Science, 2015, pp. 299–368.

[95] W. J. Cannan and D. S. Pederson, “Mechanisms and consequences of double-strand DNA break formation in chromatin,” *Journal of Cellular Physiology*, vol. 231, no. 1, pp. 3–14, 2016.

[96] R. B. Mikkelsen and P. Wardman, “Biological chemistry of reactive oxygen and nitrogen and radiation-induced signal transduction mechanisms,” *Oncogene*, vol. 22, no. 37, pp. 5734–5754, 2003.

[97] H. L. Borges, R. Linden, and J. Y. Wang, “DNA damage-induced cell death: lessons from the central nervous system,” *Cell Research*, vol. 18, no. 1, pp. 17–26, 2008.

[98] X. Yan, F. Zou, S. Zhao, X. Lu, G. He, Z. Xiong, Q. Xiong, Q. Zhao, P. Deng, J. Huang, and others, “On the mechanism of plasma inducing cell apoptosis,” *IEEE Transactions on Plasma Science*, vol. 38, no. 9, pp. 2451–2457, 2010.

[99] A. McLennan, A. Bates, P. Turner, and M. White, *BIOS Instant Notes in Molecular Biology*, 4th ed. Garland Science, 2013.

[100] I. E. Kieft, M. Kurdi, and E. Stoffels, “Reattachment and apoptosis after plasma-needle treatment of cultured cells,” *IEEE Transactions on Plasma Science*, vol. 34, no. 4, pp. 1331–1336, 2006.

[101] V. Miller, A. Lin, G. Fridman, D. Dobrynin, and A. Fridman, “Plasma stimulation of migration of macrophages,” *Plasma Processes and Polymers*, vol. 11, no. 12, pp. 1193–1197, 2014.

[102] S. Bekeschus, A. Schmidt, L. Bethge, K. Masur, T. von Woedtke, S. Hasse, and K. Wende, “Redox stimulation of human THP-1 monocytes in response to cold physical plasma,” *Oxidative Medicine and Cellular Longevity*, vol. 2016, 2016.

[103] X.-M. Shi, G.-J. Zhang, Y.-K. Yuan, Y. Ma, G.-M. Xu, and Y. Yang, “Effects of low-temperature atmospheric air plasmas on the activity and function of human lymphocytes,” *Plasma Processes and Polymers*, vol. 5, no. 5, pp. 482–488, 2008.

[104] S. Bekeschus, K. Masur, J. Kolata, K. Wende, A. Schmidt, L. Bundscherer, A. Barton, A. Kramer, B. Bröker, and K.-D. Weltmann, “Human mononuclear cell survival and proliferation is modulated by cold atmospheric plasma jet,”

Plasma Processes and Polymers, vol. 10, no. 8, pp. 706–713, 2013.

[105] A. Lin, B. Truong, A. Pappas, L. Kirifides, A. Oubarri, S. Chen, S. Lin, D. Dobrynin, G. Fridman, A. Fridman, and others, "Uniform nanosecond pulsed dielectric barrier discharge plasma enhances anti-tumor effects by induction of immunogenic cell death in tumors and stimulation of macrophages," *Plasma Processes and Polymers*, vol. 12, no. 12, pp. 1392–1399, 2015.

[106] A. Lin, B. Truong, S. Patel, N. Kaushik, E. H. Choi, G. Fridman, A. Fridman, and V. Miller, "Nanosecond-pulsed DBD plasma-generated reactive oxygen species trigger immunogenic cell death in A549 lung carcinoma cells through intracellular oxidative stress," *International Journal of Molecular Sciences*, vol. 18, no. 5, p. 966, 2017.

[107] A. G. Lin, B. Xiang, D. J. Merlino, T. R. Baybutt, J. Sahu, A. Fridman, A. E. Snook, and V. Miller, "Non-thermal plasma induces immunogenic cell death in vivo in murine CT26 colorectal tumors," *Oncoimmunology*, vol. 7, no. 9, p. e1484978, 2018.

[108] A. Schmidt, T. V. Woedtke, J. Stenzel, T. Lindner, S. Polei, B. Vollmar, and S. Bekeschus, "One year follow-up risk assessment in SKH-1 mice and wounds treated with an argon plasma jet," *International Journal of Molecular Sciences*, vol. 18, no. 4, p. 868, 2017.

[109] E. Freund, J. Moritz, M. Stope, C. Seebauer, A. Schmidt, and S. Bekeschus, "Plasma-derived reactive species shape a differentiation profile in human monocytes," *Applied Sciences*, vol. 9, no. 12, p. 2530, 2019.

[110] C. P. Dang, S. Weawseetong, A. Charoensappakit, K. Sae-Khow, D. Thong-Aram, and A. Leelahavanichkul, "Non-thermal atmospheric pressure argon-sourced plasma flux promotes wound healing of burn wounds and burn wounds with infection in mice through the anti-inflammatory macrophages," *Applied Sciences*, vol. 11, no. 12, p. 5343, 2021.

[111] A. Lin, B. Truong, G. Fridman, A. A. Fridman, and V. Miller, "Immune cells enhance selectivity of nanosecond-pulsed DBD plasma against tumor cells," *Plasma Medicine*, vol. 7, no. 1, 2017.

[112] I. Lacaille, "Design of an Atmospheric Pressure Non-thermal Miniature Plasma Jet and Exploration of Its Potential as a Treatment for Cutaneous Leishmaniasis," 2014.

[113] S. Bekeschus, L. Scherwietes, E. Freund, K. R. Liedtke, C. Hackbarth, T. von Woedtke, and L.-I. Partecke, "Plasma-treated medium tunes the inflammatory profile in murine bone marrow-derived macrophages," *Clinical Plasma Medicine*, vol. 11, pp. 1–9, 2018.

[114] L. Crestale, R. Laurita, A. Liguori, A. Stancampiano, M. Talmon, A. Bisag, M. Gherardi, A. Amoruso, V. Colombo, and L. G. Fresu, “Cold atmospheric pressure plasma treatment modulates human monocytes/macrophages responsiveness,” *Plasma*, vol. 1, no. 2, pp. 261–276, 2018.

[115] N. Kaushik, N. Kumar, C. H. Kim, N. K. Kaushik, and E. H. Choi, “Dielectric barrier discharge plasma efficiently delivers an apoptotic response in human monocytic lymphoma,” *Plasma Processes and Polymers*, vol. 11, no. 12, pp. 1175–1187, 2014.

[116] S. Bekeschus, J. Moritz, A. Schmidt, and K. Wende, “Redox regulation of leukocyte-derived microparticle release and protein content in response to cold physical plasma-derived oxidants,” *Clinical Plasma Medicine*, vol. 7, pp. 24–35, 2017.

[117] Y. Tabuchi, H. Uchiyama, Q.-L. Zhao, T. Yunoki, G. Andocs, N. Nojima, K. Takeda, K. Ishikawa, M. Hori, and T. Kondo, “Effects of nitrogen on the apoptosis of and changes in gene expression in human lymphoma U937 cells exposed to argon-based cold atmospheric pressure plasma,” *International Journal of Molecular Medicine*, vol. 37, no. 6, pp. 1706–1714, 2016.

[118] S. Bekeschus, J. Kolata, A. Muller, A. Kramer, K.-D. Weltmann, B. Broker, and K. Masur, “Differential viability of eight human blood mononuclear cell subpopulations after plasma treatment,” *Plasma Medicine*, vol. 3, no. 1–2, 2013.

[119] L. Bundscherer, S. Nagel, S. Hasse, H. Tresp, K. Wende, R. Walther, S. Reuter, K.-D. Weltmann, K. Masur, and U. Lindequist, “Non-thermal plasma treatment induces MAPK signaling in human monocytes,” *Open Chemistry*, vol. 13, no. 1, pp. 606–13, 2015.

[120] H. Mohamed, E. Gebski, R. Reyes, S. Beane, B. Wigdahl, F. C. Krebs, K. Stapelmann, and V. Miller, “Differential effect of non-thermal plasma RONS on two human leukemic cell populations,” *Cancers*, vol. 13, no. 10, p. 2437, 2021.

[121] S. Bekeschus, R. Clemen, L. Haralambiev, F. Niessner, P. Grabarczyk, K.-D. Weltmann, J. Menz, M. Stope, T. von Woedtke, R. Gandhirajan, and others, “The plasma-induced leukemia cell death is dictated by the ROS chemistry and the HO-1/CXCL8 axis,” *IEEE Transactions on Radiation and Plasma Medical Sciences*, vol. 5, no. 3, pp. 398–411, 2020.

[122] S. Bekeschus, “Effects of Cold Physical Plasma on Human Leukocytes,” 2015.

[123] S. Bekeschus, T. von Woedtke, A. Kramer, K.-D. Weltmann, and K. Masur, “Cold physical plasma treatment alters redox balance in human immune

cells," *Plasma Medicine*, vol. 3, no. 4, 2013.

[124] S. Bekeschus, C. C. Winterbourn, J. Kolata, K. Masur, S. Hasse, B. M. Bröker, and H. A. Parker, "Neutrophil extracellular trap formation is elicited in response to cold physical plasma," *Journal of Leukocyte Biology*, vol. 100, no. 4, pp. 791–799, 2016.

[125] B. Haertel, F. Volkmann, T. von Woedtke, and U. Lindequist, "Differential sensitivity of lymphocyte subpopulations to non-thermal atmospheric-pressure plasma," *Immunobiology*, vol. 217, no. 6, pp. 628–633, 2012.

[126] D. Dobrynin, G. Fridman, G. Friedman, and A. Fridman, "Physical and biological mechanisms of direct plasma interaction with living tissue," *New Journal of Physics*, vol. 11, no. 11, p. 115020, 2009.

[127] S. Bekeschus, K. Rödder, A. Schmidt, M. B. Stope, T. von Woedtke, V. Miller, A. Fridman, K.-D. Weltmann, K. Masur, H.-R. Metelmann, and others, "Cold physical plasma selects for specific T helper cell subsets with distinct cells surface markers in a caspase-dependent and NF-κB-independent manner," *Plasma Processes and Polymers*, vol. 13, no. 12, pp. 1144–1150, 2016.

[128] S. Bekeschus, S. Iséni, S. Reuter, K. Masur, and K.-D. Weltmann, "Nitrogen shielding of an argon plasma jet and its effects on human immune cells," *IEEE Transactions on Plasma Science*, vol. 43, no. 3, pp. 776–781, 2015.

[129] S. Bekeschus, J. Kolata, C. Winterbourn, A. Kramer, R. Turner, K. Weltmann, B. Bröker, and K. Masur, "Hydrogen peroxide: A central player in physical plasma-induced oxidative stress in human blood cells," *Free Radical Research*, vol. 48, no. 5, pp. 542–549, 2014.

[130] S. Bekeschus, S. Iséni, P. Luettjohann, and K.-D. Weltmann, "Tailored power of an RF plasma jet with admixture of nitrogen or oxygen and its effects on human immune cells," *IEEE Transactions on Plasma Science*, vol. 49, no. 11, pp. 3336–3343, 2021.

[131] S. Bekeschus, D. Meyer, K. Arlt, T. von Woedtke, L. Miebach, E. Freund, and R. Clemen, "Argon plasma exposure augments costimulatory ligands and cytokine release in human monocyte-derived dendritic cells," *International Journal of Molecular Sciences*, vol. 22, no. 7, p. 3790, 2021.

[132] L. Bundscherer, S. Bekeschus, H. Tresp, S. Hasse, S. Reuter, K.-D. Weltmann, U. Lindequist, and K. Masur, "Viability of human blood leukocytes compared with their respective cell lines after plasma treatment," *Plasma Medicine*, vol. 3, no. 1–2, 2013.

[133] Y. Ma, C. S. Ha, S. W. Hwang, H. J. Lee, G. C. Kim, K.-W. Lee, and K. Song, "Non-thermal atmospheric pressure plasma preferentially induces

apoptosis in p53-mutated cancer cells by activating ROS stress-response pathways," *PloS One*, vol. 9, no. 4, p. e91947, 2014.

[134] H. Pelicano, D. Carney, and P. Huang, "ROS stress in cancer cells and therapeutic implications," *Drug Resistance Updates*, vol. 7, no. 2, pp. 97–110, 2004.

[135] C.-H. Kim, S. Kwon, J. H. Bahn, K. Lee, S. I. Jun, P. D. Rack, and S. J. Baek, "Effects of atmospheric nonthermal plasma on invasion of colorectal cancer cells," *Applied Physics Letters*, vol. 96, no. 24, p. 243701, 2010.

[136] F. Utsumi, H. Kajiyama, K. Nakamura, H. Tanaka, M. Mizuno, K. Ishikawa, H. Kondo, H. Kano, M. Hori, and F. Kikkawa, "Effect of indirect nonequilibrium atmospheric pressure plasma on anti-proliferative activity against chronic chemo-resistant ovarian cancer cells *in vitro* and *in vivo*," *PloS One*, vol. 8, no. 12, p. e81576, 2013.

[137] K. R. Liedtke, E. Freund, C. Hackbarth, C.-D. Heidecke, L.-I. Partecke, and S. Bekeschus, "A myeloid and lymphoid infiltrate in murine pancreatic tumors exposed to plasma-treated medium," *Clinical Plasma Medicine*, vol. 11, pp. 10–17, 2018.

[138] M. Keidar, R. Walk, A. Shashurin, P. Srinivasan, A. Sandler, S. Dasgupta, R. Ravi, R. Guerrero-Preston, and B. Trink, "Cold plasma selectivity and the possibility of a paradigm shift in cancer therapy," *British Journal of Cancer*, vol. 105, no. 9, p. 1295, 2011.

[139] H.-R. Metelmann, C. Seebauer, V. Miller, A. Fridman, G. Bauer, D. B. Graves, J.-M. Pouvesle, R. Rutkowski, M. Schuster, S. Bekeschus, and others, "Clinical experience with cold plasma in the treatment of locally advanced head and neck cancer," *Clinical Plasma Medicine*, vol. 9, pp. 6–13, 2018.

[140] A. Sakudo, Y. Yagyu, and T. Onodera, "Disinfection and sterilization using plasma technology: Fundamentals and future perspectives for biological applications," *International Journal of Molecular Sciences*, vol. 20, no. 20, p. 5216, 2019.

[141] S.-J. Sung, J.-B. Huh, M.-J. Yun, B. M. W. Chang, C.-M. Jeong, and Y.-C. Jeon, "Sterilization effect of atmospheric pressure non-thermal air plasma on dental instruments," *The Journal of Advanced Prosthodontics*, vol. 5, no. 1, pp. 2–8, 2013.

[142] Y. Tian, P. Sun, H. Wu, N. Bai, R. Wang, W. Zhu, J. Zhang, and F. Liu, "Inactivation of Staphylococcus aureus and Enterococcus faecalis by a direct-current, cold atmospheric-pressure air plasma microjet," *Journal of Biomedical Research*, vol. 24, no. 4, pp. 264–269, 2010.

[143] L. Guo, R. Xu, Y. Zhao, D. Liu, Z. Liu, X. Wang, H. Chen, and M. G. Kong, “Gas plasma pre-treatment increases antibiotic sensitivity and persister eradication in methicillin-resistant Staphylococcus aureus,” *Frontiers in Microbiology*, vol. 9, p. 537, 2018.

[144] S. Arndt, A. Schmidt, S. Karrer, and T. von Woedtke, “Comparing two different plasma devices kINPen and Adtec SteriPlas regarding their molecular and cellular effects on wound healing,” *Clinical Plasma Medicine*, 2018.

[145] “PlasmaDerm.” [Online]. Available: https://plasmaderm.de/?lang=en. [Accessed: 28–11-2022]

[146] “The kINPenVet.” [Online]. Available: https://neoplas.eu/. [Accessed: 28–11-2022]

[147] “Technology of PlasmaDerm.” [Online]. Available: https://plasmaderm.de/technology-of-plasmaderm/?lang=en

[148] B. Alberts, A. Johnson, J. Lewis, D. Morgan, M. Raff, K. Roberts, and P. Walter, “Molecular Biology of the Cell ,” 6th ed., New York: Garland Science, 2015, pp. 1217–1262.

[149] T. Dittmar and K. S. Zanker, “Introduction,” in *Stem Cell Biology in Health and Disease*, Dittmar, Thomas and Zanker, Kurt S, Ed. Dordrecht: Springer, 2009, pp. 1–7.

[150] J. W. Choi, S. U. Kang, Y. E. Kim, J. K. Park, S. S. Yang, Y. S. Kim, Y. S. Lee, Y. Lee, and C.-H. Kim, “Novel therapeutic effects of non-thermal atmospheric pressure plasma for muscle megeneration and differentiation,” *Scientific Reports*, vol. 6, 2016.

[151] M. J. Steinbeck, N. Chernets, J. Zhang, D. S. Kurpad, G. Fridman, A. Fridman, and T. A. Freeman, “Skeletal cell differentiation is enhanced by atmospheric dielectric barrier discharge plasma treatment,” *PloS One*, vol. 8, no. 12, p. e82143, 2013.

[152] F. Utsumi, H. Kajiyama, K. Nakamura, H. Tanaka, M. Hori, and F. Kikkawa, “Selective cytotoxicity of indirect nonequilibrium atmospheric pressure plasma against ovarian clear-cell carcinoma,” *SpringerPlus*, vol. 3, no. 1, p. 398, 2014.

[153] M. Hoentsch, T. von Woedtke, K.-D. Weltmann, and J. B. Nebe, “Time-dependent effects of low-temperature atmospheric-pressure argon plasma on epithelial cell attachment, viability and tight junction formation *in vitro*,” *Journal of Physics D: Applied Physics*, vol. 45, no. 2, p. 025206, 2011.

[154] X. Yan, Z. Xiong, F. Zou, S. Zhao, X. Lu, G. Yang, G. He, and K. K. Ostrikov, “Plasma-induced death of HepG2 cancer cells: intracellular effects of reactive species,” *Plasma Processes and Polymers*, vol. 9, no. 1, pp. 59–66, 2012.

[155] N. H. Nguyen, H. J. Park, S. Y. Hwang, J.-S. Lee, and S. S. Yang, “Anticancer Efficacy of Long-Term Stored Plasma-Activated Medium,” *Applied Sciences*, vol. 9, no. 4, p. 801, 2019.

[156] K. Wende, P. Williams, J. Dalluge, W. Van Gaens, H. Aboubakr, J. Bischof, T. Von Woedtke, S. M. Goyal, K.-D. Weltmann, A. Bogaerts, and others, “Identification of the biologically active liquid chemistry induced by a nonthermal atmospheric pressure plasma jet,” *Biointerphases*, vol. 10, no. 2, p. 029518, 2015.

[157] D. Yan, H. Xiao, W. Zhu, N. Nourmohammadi, L. G. Zhang, K. Bian, and M. Keidar, “The role of aquaporins in the anti-glioblastoma capacity of the cold plasma-stimulated medium,” *Journal of Physics D: Applied Physics*, vol. 50, no. 5, p. 055401, 2017.

[158] F. Saadati, H. Mahdikia, H.-A. Abbaszadeh, M.-A. Abdollahifar, M. S. Khoramgah, and B. Shokri, “Comparison of direct and indirect cold atmospheric-pressure plasma methods in the B 16 F 10 melanoma cancer cells treatment,” *Scientific Reports*, vol. 8, no. 1, pp. 1–15, 2018.

[159] S. Kalghatgi, A. Fridman, J. Azizkhan-Clifford, and G. Friedman, “DNA damage in mammalian mells by non-thermal atmospheric pressure microsecond pulsed dielectric barrier discharge plasma is not mediated by ozone,” *Plasma Processes and Polymers*, vol. 9, no. 7, pp. 726–732, 2012.

[160] I. Trizio, E. Sardella, V. Rizzi, G. Dilecce, P. Cosma, M. Schmidt, T. von Woedtke, R. Gristina, and P. Favia, “Characterization of reactive oxygen/nitrogen species produced in PBS and DMEM by air DBD plasma treatments,” *Plasma Medicine*, vol. 6, no. 1, 2016.

[161] P.-M. Girard, A. Arbabian, M. Fleury, G. Bauville, V. Puech, M. Dutreix, and J. S. Sousa, “Synergistic effect of H_2O_2 and NO_2 in cell death induced by cold atmospheric He plasma,” *Scientific Reports*, vol. 6, p. 29098, 2016.

[162] F. Girard, V. Badets, S. Blanc, K. Gazeli, L. Marlin, L. Authier, P. Svarnas, N. Sojic, F. Clément, and S. Arbault, “Formation of reactive nitrogen species including peroxynitrite in physiological buffer exposed to cold atmospheric plasma,” *RSC Advances*, vol. 6, no. 82, pp. 78457–78467, 2016.

[163] J. Chauvin, F. Judée, M. Yousfi, P. Vicendo, and N. Merbahi, “Analysis of reactive oxygen and nitrogen species generated in three liquid media by low temperature helium plasma jet,” *Scientific Reports*, vol. 7, no. 1, p. 4562,

2017.

[164] H. Mokhtari, L. Farahmand, K. Yaserian, N. Jalili, and K. Majidzadeh-A, "The antiproliferative effects of cold atmospheric plasma-activated media on different cancer cell lines, the implication of ozone as a possible underlying mechanism," *Journal of Cellular Physiology*, vol. 234, no. 5, pp. 6778–6782, 2019.

[165] H. Jablonowski, J. S. Sousa, K.-D. Weltmann, K. Wende, and S. Reuter, "Quantification of the ozone and singlet delta oxygen produced in gas and liquid phases by a non-thermal atmospheric plasma with relevance for medical treatment," *Scientific Reports*, vol. 8, no. 1, p. 12195, 2018.

[166] N. Kurake, H. Tanaka, K. Ishikawa, T. Kondo, M. Sekine, K. Nakamura, H. Kajiyama, F. Kikkawa, M. Mizuno, and M. Hori, "Cell survival of glioblastoma grown in medium containing hydrogen peroxide and/or nitrite, or in plasma-activated medium," *Archives of Biochemistry and Biophysics*, vol. 605, pp. 102–108, 2016.

[167] J. Winter, H. Tresp, M. Hammer, S. Iseni, S. Kupsch, A. Schmidt-Bleker, K. Wende, M. Dünnbier, K. Masur, K. Weltmann, and others, "Tracking plasma generated H_2O_2 from gas into liquid phase and revealing its dominant impact on human skin cells," *Journal of Physics D: Applied Physics*, vol. 47, no. 28, p. 285401, 2014.

[168] C.-H. Lin, S.-Y. Lee, and Y.-M. Lin, "Plasma treatment in conjunction with EGM-2 medium increases endothelial and osteogenic marker expressions of bone marrow mesenchymal stem cells," *Journal of Materials Science*, vol. 51, no. 19, pp. 9145–9154, 2016.

[169] R. S. Tipa and G. M. Kroesen, "Plasma-stimulated wound healing," *IEEE Transactions on Plasma Science*, vol. 39, no. 11, pp. 2978–2979, 2011.

[170] S. Arndt, P. Unger, E. Wacker, T. Shimizu, J. Heinlin, Y.-F. Li, H. M. Thomas, G. E. Morfill, J. L. Zimmermann, A.-K. Bosserhoff, and others, "Cold atmospheric plasma (CAP) changes gene expression of key molecules of the wound healing machinery and improves wound healing in vitro and in vivo," *PloS One*, vol. 8, no. 11, 2013.

[171] A. Barton, K. Wende, L. Bundscherer, S. Hasse, A. Schmidt, S. Bekeschus, K.-D. Weltmann, U. Lindequist, and K. Masur, "Nonthermal plasma increases expression of wound healing related genes in a keratinocyte cell line," *Plasma Medicine*, vol. 3, no. 1–2, 2013.

[172] J. Park, H. Lee, H. J. Lee, G. C. Kim, D. Y. Kim, S. Han, and K. Song, "Non-thermal atmospheric pressure plasma efficiently promotes the proliferation of adipose tissue-derived stem cells by activating NO-response pathways,"

Scientific Reports, vol. 6, no. D122, 2016.

[173] M. N. Möller, E. Cuevasanta, F. Orrico, A. C. Lopez, L. Thomson, and A. Denicola, "Diffusion and transport of reactive species across cell membranes," in *Bioactive Lipids in Health and Disease, Advances in Experimental Biology and Medicine 1127*, Trostchansky, A and Rubbo, H, Ed. Cham: Springer, 2019, pp. 3–19.

[174] S. G. Rhee, "H_2O_2, a necessary evil for cell signaling," *Science*, vol. 312, no. 5782, pp. 1882–1883, 2006.

[175] M. Sundaresan, Z.-X. Yu, V. J. Ferrans, K. Irani, and T. Finkel, "Requirement for generation of H_2O_2 for platelet-derived growth factor signal transduction," *Science*, vol. 270, no. 5234, pp. 296–299, 1995.

[176] H. Sies, "Hydrogen peroxide as a central redox signaling molecule in physiological oxidative stress: oxidative eustress," *Redox Biology*, vol. 11, pp. 613–619, 2017.

[177] S. Mohades, N. Barekzi, H. Razavi, V. Maruthamuthu, and M. Laroussi, "Temporal evaluation of the anti-tumor efficiency of plasma-activated media," *Plasma Processes and Polymers*, vol. 13, no. 12, pp. 1206–1211, 2016.

[178] S. Roy, S. Khanna, K. Nallu, T. K. Hunt, and C. K. Sen, "Dermal wound healing is subject to redox control," *Molecular Therapy*, vol. 13, no. 1, pp. 211–220, 2006.

[179] A. E. K. Loo, Y. T. Wong, R. Ho, M. Wasser, T. Du, W. T. Ng, and B. Halliwell, "Effects of hydrogen peroxide on wound healing in mice in relation to oxidative damage," *PloS One*, vol. 7, no. 11, 2012.

[180] B. Halliwell and J. M. C. Gutteridge, *Free Radicals in Biology and Medicine*, 3rd ed. New York: Oxford University Press, 1999, pp. 36–104.

[181] A. M. Gardner, F. Xu, C. Fady, F. J. Jacoby, D. C. Duffey, Y. Tu, and A. Lichtenstein, "Apoptotic vs. nonapoptotic cytotoxicity induced by hydrogen peroxide," *Free Radical Biology and Medicine*, vol. 22, no. 1–2, pp. 73–83, 1997.

[182] O. Lyublinskaya and F. Antunes, "Measuring intracellular concentration of hydrogen peroxide with the use of genetically encoded H_2O_2 biosensor HyPer," *Redox Biology*, vol. 24, p. 101200, 2019.

[183] N. S. Bryan, B. O. Fernandez, S. M. Bauer, M. F. Garcia-Saura, A. B. Milsom, T. Rassaf, R. E. Maloney, A. Bharti, J. Rodriguez, and M. Feelisch, "Nitrite is a signaling molecule and regulator of gene expression in mammalian tissues," *Nature Chemical Biology*, vol. 1, no. 5, pp. 290–297,

2005.

[184] D. A. Guimaraes, C. Reyes, and S. Shiva, “The mitochondrion: a physiological target of nitrite,” in *Nitrite and Nitrate in Human Health and Disease*, 2nd ed., Bryan, Nathan S and Loscalzo, Joseph, Ed. Cham: Springer, 2011.

[185] N. Bryan and J. Loscalzo, “Introduction,” in *Nitrite and Nitrate in Human Health and Disease*, 2nd ed., Bryan, NS and Loscalzo J, Ed. Cham: Springer, 2011, pp. 3–10.

[186] J. M. Berg, J. L. Tymoczko, G. J. Gatto Jr., and L. Stryer, “Biochemistry,” 9th ed., New York: Macmillan Learning, 2019, pp. 1276–1366.

[187] E. E. Van Faassen, S. Bahrami, M. Feelisch, N. Hogg, M. Kelm, D. B. Kim-Shapiro, A. V. Kozlov, H. Li, J. O. Lundberg, R. Mason, and others, “Nitrite as regulator of hypoxic signaling in mammalian physiology,” *Medicinal Research Reviews*, vol. 29, no. 5, pp. 683–741, 2009.

[188] J. O. Lundberg, E. Weitzberg, and M. T. Gladwin, “The nitrate-nitrite-nitric oxide pathway in physiology and therapeutics,” *Nature Reviews Drug Discovery*, vol. 7, no. 2, pp. 156–167, 2008.

[189] W. Bechtel and G. Bauer, “Catalase protects tumor cells from apoptosis induction by intercellular ROS signaling,” *Anticancer Research*, vol. 29, no. 11, pp. 4541–4557, 2009.

[190] B. Böhm, S. Heinzelmann, M. Motz, and G. Bauer, “Extracellular localization of catalase is associated with the transformed state of malignant cells,” *Biological Chemistry*, vol. 396, no. 12, pp. 1339–1356, 2015.

[191] G. Bauer, “The synergistic effect between hydrogen peroxide and nitrite, two long-lived molecular species from cold atmospheric plasma, triggers tumor cells to induce their own cell death,” *Redox Biology*, vol. 26, p. 101291, 2019.

[192] G. Bauer and D. B. Graves, “Mechanisms of selective antitumor action of cold atmosphericplasma-derived reactive oxygen and mitrogen species,” *Plasma Processes and Polymers*, vol. 13, no. 12, pp. 1157–1178, 2016.

[193] O. Augusto, M. G. Bonini, A. M. Amanso, E. Linares, C. C. Santos, and S. L. De Menezes, “Nitrogen dioxide and carbonate radical anion: two emerging radicals in biology,” *Free Radical Biology and Medicine*, vol. 32, no. 9, pp. 841–859, 2002.

[194] P. Bruggeman and C. Leys, “Non-thermal plasmas in and in contact with liquids,” *Journal of Physics D: Applied Physics*, vol. 42, no. 5, p. 053001, 2009.

[195] A. Phaniendra, D. B. Jestadi, and L. Periyasamy, “Free radicals: properties, sources, targets, and their implication in various diseases,” *Indian Journal of Clinical Biochemistry*, vol. 30, pp. 11–26, 2015.

[196] M. Kelm, “Nitric oxide metabolism and breakdown,” *Biochimica et Biophysica Acta (BBA)-Bioenergetics*, vol. 1411, no. 2–3, pp. 273–289, 1999.

[197] Q. Cai, W. Zhang, and Z. Yang, “Stability of nitrite in wastewater and its determination by ion chromatography,” *Analytical Sciences/Supplements*, vol. 17, no. 0, pp. i917–i920, 2002.

[198] G. R. Stratton, C. L. Bellona, F. Dai, T. M. Holsen, and S. M. Thagard, “Plasma-based water treatment: conception and application of a new general principle for reactor design,” *Chemical Engineering Journal*, vol. 273, pp. 543–550, 2015.

[199] Y. Y. Zhao, T. Wang, M. P. Wilson, S. J. MacGregor, I. V. Timoshkin, and Q. C. Ren, “Hydroxyl radicals and hydrogen peroxide formation at nonthermal plasma-water interface,” *IEEE Transactions on Plasma Science*, vol. 44, no. 10, pp. 2084–2091, 2016.

[200] P. Jamróz, K. Greda, P. Pohl, and W. Zyrnicki, “Atmospheric pressure glow discharges generated in contact with flowing liquid cathode: production of active species and application in wastewater purification processes,” *Plasma Chemistry and Plasma Processing*, vol. 34, no. 1, pp. 25–37, 2014.

[201] B. R. Locke and K.-Y. Shih, “Review of the methods to form hydrogen peroxide in electrical discharge plasma with liquid water,” *Plasma Sources Science and Technology*, vol. 20, no. 3, p. 034006, 2011.

[202] P. Lukes, E. Dolezalova, I. Sisrova, and M. Clupek, “Aqueous-phase chemistry and bactericidal effects from an air discharge plasma in contact with water: evidence for the formation of peroxynitrite through a pseudo-second-order post-discharge reaction of H_2O_2 and HNO_2,” *Plasma Sources Science and Technology*, vol. 23, no. 1, p. 015019, 2014.

[203] M. N. Möller, Q. Li, J. R. Lancaster Jr, and A. Denicola, “Acceleration of nitric oxide autoxidation and nitrosation by membranes,” *IUBMB Life*, vol. 59, no. 4–5, pp. 243–248, 2007.

[204] T. Tian, H. Rabat, M. Magureanu, O. Aubry, and D. Hong, “Electrical investigation of a pin-to-plane dielectric barrier discharge in contact with water,” *Journal of Applied Physics*, vol. 130, no. 11, p. 113301, 2021.

[205] T. Sato, M. Yokoyama, and K. Johkura, “A key inactivation factor of HeLa cell viability by a plasma flow,” *Journal of Physics D: Applied Physics*, vol. 44, no. 37, p. 372001, 2011.

[206] T. Manley, “The electric characteristics of the ozonator discharge,” *Transactions of the Electrochemical Society*, vol. 84, no. 1, pp. 83–96, 1943.

[207] H.-E. Wagner, R. Brandenburg, K. Kozlov, A. Sonnenfeld, P. Michel, and J. Behnke, “The barrier discharge: basic properties and applications to surface treatment,” *Vacuum*, vol. 71, no. 3, pp. 417–436, 2003.

[208] L. C. Green, D. A. Wagner, J. Glogowski, P. L. Skipper, J. S. Wishnok, and S. R. Tannenbaum, “Analysis of nitrate, nitrite, and [15N] nitrate in biological fluids,” *Analytical biochemistry*, vol. 126, no. 1, pp. 131–138, 1982.

[209] “ECACC General Cell Collection: NIH 3T3.” [Online]. Available: https://www.phe-culturecollections.org.uk/products/celllines/generalcell/detail.jsp?refId=93061524&collection=ecacc_gc. [Accessed: 04-Feb-2022]

[210] “ECACC General Cell Collection: U937.” [Online]. Available: https://www.phe-culturecollections.org.uk/products/celllines/generalcell/detail.jsp?refId=85011440&collection=ecacc_gc. [Accessed: 04-Feb-2022]

[211] W. Kues, M. Anger, J. Carnwath, D. Paul, J. Motlik, and H. Niemann, “Cell cycle synchronization of porcine fetal fibroblasts: effects of serum deprivation and reversible cell cycle inhibitors,” *Biology of Reproduction*, vol. 62, no. 2, pp. 412–419, 2000.

[212] M. Hewison, A. Brennan, R. Singh-Ranger, J. Walters, D. Katz, and J. O’Riordan, “The comparative role of 1, 25-dihydroxycholecalciferol and phorbol esters in the differentiation of the U937 cell line,” *Immunology*, vol. 77, no. 2, p. 304, 1992.

[213] J. W. Larrick, D. Fischer, S. Anderson, and H. Koren, “Characterization of a human macrophage-like cell line stimulated in vitro: a model of macrophage functions.,” *The Journal of Immunology*, vol. 125, no. 1, pp. 6–12, 1980.

[214] G. Repetto, A. Del Peso, and J. L. Zurita, “Neutral red uptake assay for the estimation of cell viability/cytotoxicity,” *Nature Protocols*, vol. 3, no. 7, p. 1125, 2008.

[215] E. Borenfreund and J. A. Puerner, “A simple quantitative procedure using monolayer cultures for cytotoxicity assays (HTD/NR-90),” *Journal of Tissue Culture Methods*, vol. 9, no. 1, pp. 7–9, 1985.

[216] B. Halliwell and J. M. Gutteridge, “Free Radicals in Biology and Medicine,” 5th ed., Oxford: Oxford University Press, 2015, pp. 1–29.

[217] S. Kamiloglu, G. Sari, T. Ozdal, and E. Capanoglu, “Guidelines for cell viability assays,” *Food Frontiers*, vol. 1, no. 3, pp. 332–349, 2020.

[218] C. Horlock, “Enzyme-linked immunosorbent assay (ELISA).” [Online]. Available: https://www.immunology.org/public-information/bitesized-immunology/experimental-techniques/enzyme-linked-immunosorbent-assay. [Accessed: 07–02-2023]

[219] L. Brody, “Gene Expression.” [Online]. Available: https://www.genome.gov/genetics-glossary/Gene-Expression. [Accessed: 09–02-2023]

[220] B. Alberts, A. Johnson, J. Lewis, D. Morgan, M. Raff, K. Roberts, and P. Walter, “Molecular Biology of the Cell,” New York: Garland Science, 2015, pp. 439–528.

[221] L. Shi, L. Yu, F. Zou, H. Hu, K. Liu, and Z. Lin, “Gene expression profiling and functional analysis reveals that p53 pathway-related gene expression is highly activated in cancer cells treated by cold atmospheric plasma-activated medium,” *PeerJ*, vol. 5, p. e3751, 2017.

[222] T. Adachi, S. Nonomura, M. Horiba, T. Hirayama, T. Kamiya, H. Nagasawa, and H. Hara, “Iron stimulates plasma-activated medium-induced A549 cell injury,” *Scientific Reports*, vol. 6, no. 1, p. 20928, 2016.

[223] T. Adachi, H. Tanaka, S. Nonomura, H. Hara, S. Kondo, and M. Hori, “Plasma-activated medium induces A549 cell injury via a spiral apoptotic cascade involving the mitochondrial-nuclear network,” *Free Radical Biology and Medicine*, vol. 79, pp. 28–44, 2015.

[224] T. Adachi, A. Kano, S. Nonomura, T. Kamiya, and H. Hara, “Histone deacetylase inhibitors stimulate the susceptibility of A549 cells to a plasma-activated medium treatment,” *Archives of Biochemistry and Biophysics*, vol. 606, pp. 120–127, 2016.

[225] T. K. Archer, H.-L. Lee, M. G. Cordingley, J. S. Mymryk, G. Fragoso, D. S. Berard, and G. L. Hager, “Differential steroid hormone induction of transcription from the mouse mammary tumor virus promoter.,” *Molecular Endocrinology*, vol. 8, no. 5, pp. 568–576, 1994.

[226] “QuantStudio™ 5 Real-Time PCR System for Human Identification, 96-well, 0.2 mL, desktop.” [Online]. Available: QuantStudio 5 Real-Time PCR System . [Accessed: 07–02-2023]

[227] “PCR Primer Design Tips.” [Online]. Available: https://www.thermofisher.com/blog/behindthebench/pcr-primer-design-tips/ . [Accessed: 25–07-2023]

[228] "How to Simplify PCR Optimization Steps for Primer Annealing." [Online]. Available: https://www.thermofisher.com/uk/en/home/brands/thermo-scientific/molecular-biology/molecular-biology-learning-center/molecular-biology-resource-library/spotlight-articles/pcr-annealing-optimization-universal-annealing.html#:~:text=The%20recommended%20melting%20temperature%20of,ms)%20between%20the%20two. [Accessed: 25–07-2023]

[229] F. Xie, P. Xiao, D. Chen, L. Xu, and B. Zhang, "miRDeepFinder: a miRNA analysis tool for deep sequencing of plant small RNAs," *Plant Molecular Biology*, vol. 80, no. 1, pp. 75–84, 2012.

[230] "RefFinder." [Online]. Available: https://www.heartcure.com.au/reffinder/. [Accessed: 01-Feb-2022]

[231] "National Center for Biotechnology Information." [Online]. Available: https://www.ncbi.nlm.nih.gov/. [Accessed: 20–09-2022]

[232] K. J. Livak and T. D. Schmittgen, "Analysis of relative gene expression data using real-time quantitative PCR and the $2^{-\Delta\Delta CT}$ method," *Methods*, vol. 25, no. 4, pp. 402–408, 2001.

[233] E. Kuffel, W. Zaengl, and J. Kuffel, "High Voltage Engineering Fundamentals," 2nd ed., Oxford: Elsevier, 2000, pp. 281–366.

[234] A. Küchler, "Electric strength," in *High Voltage Engineering: Fundamentals-Technology-Applications*, Berlin, Heidelberg: Springer, 2017, pp. 141–268.

[235] Y. Zhou, T. Wang, S. MacGregor, I. Timoshkin, M. Wilson, and M. Given, "Pulsed filament current characteristics in dielectric barrier discharge," in *2015 IEEE Pulsed Power Conference (PPC)*, 2015, pp. 1–4.

[236] E. Van Veldhuizen and W. Rutgers, "Corona discharges: fundamentals and diagnostics," *Invited paper, Proc. Frontiers in Low Temp. Plasma Diagn. IV, Rolduc, Netherlands*, pp. 40–49, 2001.

[237] Y. S. Akishev, A. Dem'yanov, V. Karal'nik, A. Monich, and N. Trushkin, "Comparison of the AC barrier corona with DC positive and negative coronas and barrier discharge," *Plasma Physics Reports*, vol. 29, no. 1, pp. 82–91, 2003.

[238] S. Bekeschus, A. Schmidt, H. Jablonowski, L. Bethge, S. Hasse, K. Wende, K. Masur, T. von Woedtke, and K.-D. Weltmann, "Environmental control of an argon plasma effluent and its role in THP-1 monocyte function," *IEEE Transactions on Plasma Science*, vol. 45, no. 12, pp. 3336–3341, 2017.

[239] M. Horiba, T. Kamiya, H. Hara, and T. Adachi, "Cytoprotective effects of mild plasma-activated medium against oxidative stress in human skin

fibroblasts," *Scientific Reports*, vol. 7, p. 42208, 2017.

[240] J.-R. Liu, L.-G. Gao, Y.-M. Wu, G.-M. Xu, Y. Ma, Y. Hao, X.-M. Shi, and G.-J. Zhang, "Low-temperature plasma-activated medium inhibited invasion and metastasis of melanoma cells via suppressing the Wnt/β-catenin pathway," *Plasma Processes and Polymers*, vol. 17, no. 1, p. 1900060, 2020.

[241] J.-R. Liu, Y.-M. Wu, G.-M. Xu, L.-G. Gao, Y. Ma, X.-M. Shi, and G.-J. Zhang, "Low temperature plasma induced melanoma apoptosis by triggering P53/PIGs/caspase-dependent pathway in vivo and in vitro," *Journal of Physics D: Applied Physics*, 2019.

[242] S. Mohades, M. Laroussi, J. Sears, N. Barekzi, and H. Razavi, "Evaluation of the effects of a plasma activated medium on cancer cells," *Physics of Plasmas*, vol. 22, no. 12, p. 122001, 2015.

[243] K. Wende, S. Bekeschus, A. Schmidt, L. Jatsch, S. Hasse, K. Weltmann, K. Masur, and T. von Woedtke, "Risk assessment of a cold argon plasma jet in respect to its mutagenicity," *Mutation Research/Genetic Toxicology and Environmental Mutagenesis*, vol. 798, pp. 48–54, 2016.

[244] K. Rödder, J. Moritz, V. Miller, K.-D. Weltmann, H.-R. Metelmann, R. Gandhirajan, and S. Bekeschus, "Activation of murine immune cells upon co-culture with plasma-treated B16F10 melanoma cells," *Applied Sciences*, vol. 9, no. 4, p. 660, 2019.

[245] Y. Zhao, "Non-Thermal Plasma for Water Treatment," 2017.

[246] N. Takamura, D. Wang, T. Satoh, T. Namihira, H. Saitoh, and H. Akiyama, "Effect of atmospheric-pressure helium plasma jet on cell culture medium," *Electronics and Communications in Japan*, vol. 97, no. 11, pp. 65–73, 2014.

[247] H. Tresp, M. U. Hammer, K.-D. Weltmann, and S. Reuter, "Effects of atmosphere composition and liquid type on plasma-generated reactive species in biologically relevant solutions," *Plasma Medicine*, vol. 3, no. 1–2, 2013.

[248] S. Maheux, D. Duday, T. Belmonte, C. Penny, H.-M. Cauchie, F. Clément, and P. Choquet, "Formation of ammonium in saline solution treated by nanosecond pulsed cold atmospheric microplasma: a route to fast inactivation of E. coli bacteria," *RSC Advances*, vol. 5, no. 52, pp. 42135–42140, 2015.

[249] R. M. Walk, J. A. Snyder, P. Srinivasan, J. Kirsch, S. O. Diaz, F. C. Blanco, A. Shashurin, M. Keidar, and A. D. Sandler, "Cold atmospheric plasma for the ablative treatment of neuroblastoma," *Journal of Pediatric Surgery*, vol. 48, no. 1, pp. 67–73, 2013.

[250] K. C. Kim, M. J. Piao, M. Hewage, S. R. Kumara, X. Han, K. A. Kang, J. O. Jo, Y. S. Mok, J. H. Shin, Y. Park, and others, "Non-thermal dielectric-barrier

discharge plasma damages human keratinocytes by inducing oxidative stress," *International Journal of Molecular Medicine*, vol. 37, no. 1, pp. 29–38, 2016.

[251] S. Iseki, K. Nakamura, M. Hayashi, H. Tanaka, H. Kondo, H. Kajiyama, H. Kano, F. Kikkawa, and M. Hori, "Selective killing of ovarian cancer cells through induction of apoptosis by nonequilibrium atmospheric pressure plasma," *Applied Physics Letters*, vol. 100, no. 11, p. 113702, 2012.

[252] R. Tiede, J. Hirschberg, W. Viöl, and S. Emmert, "A µs-pulsed dielectric barrier discharge source: physical characterization and biological effects on human skin fibroblasts," *Plasma Processes and Polymers*, vol. 13, no. 8, pp. 775–787, 2016.

[253] B. Alberts, A. Johnson, J. Lewis, D. Morgan, M. Raff, K. Roberts, and P. Walter, "Molecular Biology of the Cell ," 6th ed., New York: Garland Science, 2015, pp. 963–1020.

[254] H. Akcakaya, F. Dal, S. Tok, S.-A. Cinar, and R. Nurten, "K562 cells display different vulnerability to H_2O_2 induced oxidative stress in differing cell cycle phases," *Cell Biology International*, vol. 39, no. 2, pp. 201–209, 2015.

[255] R. G. Syljuåsen, "Cell cycle effects in radation oncology," in *Radiation Oncology*, Wenz, Frederik, Ed. Cham: Springer, 2019, pp. 1–8.

[256] B. Alberts, A. Johnson, J. Lewis, D. Morgan, M. Raff, K. Roberts, and P. Walter, "Molecular Biology of the Cell ," 6th ed., New York: Garland Science, 2015, pp. 1021–1034.

[257] G. Fridman, A. Shereshevsky, M. M. Jost, A. D. Brooks, A. Fridman, A. Gutsol, V. Vasilets, and G. Friedman, "Floating electrode dielectric barrier discharge plasma in air promoting apoptotic behavior in melanoma skin cancer cell lines," *Plasma Chemistry and Plasma Processing*, vol. 27, no. 2, pp. 163–176, 2007.

[258] S. Kang, J. Cho, J. Chang, Y. Shin, K. Kim, J. Park, S. Yang, J. Lee, E. Moon, K. Lee, and others, "Nonthermal plasma induces head and neck cancer cell death: the potential involvement of mitogen-activated protein kinase-dependent mitochondrial reactive oxygen species," *Cell death and disease*, vol. 5, no. 2, p. e1056, 2014.

[259] K. Torii, S. Yamada, K. Nakamura, H. Tanaka, H. Kajiyama, K. Tanahashi, N. Iwata, M. Kanda, D. Kobayashi, C. Tanaka, and others, "Effectiveness of plasma treatment on gastric cancer cells," *Gastric Cancer*, vol. 18, no. 3, pp. 635–643, 2015.

[260] H. Hara, S. Sueyoshi, M. Taniguchi, T. Kamiya, and T. Adachi, "Differences in intracellular mobile zinc levels affect susceptibility to plasma-activated medium-induced cytotoxicity," *Free Radical Research*, vol. 51, no. 3, pp.

306–315, 2017.

[261] A. Laurent, C. Nicco, C. Chéreau, C. Goulvestre, J. Alexandre, A. Alves, E. Lévy, F. Goldwasser, Y. Panis, O. Soubrane, and others, “Controlling tumor growth by modulating endogenous production of reactive oxygen species,” *Cancer Research*, vol. 65, no. 3, pp. 948–956, 2005.

[262] K. Nakamura, Y. Peng, F. Utsumi, H. Tanaka, M. Mizuno, S. Toyokuni, M. Hori, F. Kikkawa, and H. Kajiyama, “Novel intraperitoneal treatment with non-thermal plasma-activated medium inhibits metastatic potential of ovarian cancer cells,” *Scientific Reports*, vol. 7, no. 1, p. 6085, 2017.

[263] B. B. Lopes, M. B. de P. L. Kraft, J. Rehder, F. R. X. Batista, and M. B. Puzzi, “The interactions between non-thermal atmospheric pressure plasma and ex-vivo dermal fibroblasts,” *Procedia Engineering*, vol. 59, pp. 92–100, 2013.

[264] Y. F. Yue, S. Mohades, M. Laroussi, and X. Lu, “Measurements of plasma-generated hydroxyl and hydrogen peroxide concentrations for plasma medicine applications,” *IEEE Transactions on Plasma Science*, vol. 44, no. 11, pp. 2754–2758, 2016.

[265] D. Yan, N. Nourmohammadi, K. Bian, F. Murad, J. H. Sherman, and M. Keidar, “Stabilizing the cold plasma-stimulated medium by regulating medium’s composition,” *Scientific Reports*, vol. 6, no. 1, pp. 1–11, 2016.

[266] H. Kajiyama, F. Utsumi, K. Nakamura, H. Tanaka, M. Mizuno, S. Toyokuni, M. Hori, and F. Kikkawa, “Possible therapeutic option of aqueous plasma for refractory ovarian cancer,” *Clinical Plasma Medicine*, vol. 4, no. 1, pp. 14–18, 2016.

[267] E. Freund and S. Bekeschus, “Gas plasma-oxidized liquids for cancer treatment: Pre-clinical relevance, immuno-oncology, and clinical obstacles,” *IEEE Transactions on Radiation and Plasma Medical Sciences*, 2020.

[268] H. Tanaka, K. Nakamura, M. Mizuno, K. Ishikawa, K. Takeda, H. Kajiyama, F. Utsumi, F. Kikkawa, and M. Hori, “Non-thermal atmospheric pressure plasma activates lactate in Ringer’s solution for anti-tumor effects,” *Scientific Reports*, vol. 6, p. 36282, 2016.

[269] H. S. Koren, S. J. Anderson, and J. W. Larrick, “In vitro activation of a human macrophage-like cell line,” *Nature*, vol. 279, no. 5711, p. 328, 1979.

[270] T. Tokunaga, T. Ando, M. Suzuki-Karasaki, T. Ito, A. Onoe-Takahashi, T. Ochiai, M. Soma, and Y. Suzuki-Karasaki, “Plasma-stimulated medium kills TRAIL-resistant human malignant cells by promoting caspase-independent cell death via membrane potential and calcium dynamics modulation,” *International Journal of Oncology*, vol. 52, no. 3, pp. 697–708, 2018.

[271] D. L. Laskin, V. R. Sunil, C. R. Gardner, and J. D. Laskin, “Macrophages and tissue injury: agents of defense or destruction?,” *Annual Review of Pharmacology and Toxicology*, vol. 51, p. 267, 2011.

[272] P. Wang, J. Geng, J. Gao, H. Zhao, J. Li, Y. Shi, B. Yang, C. Xiao, Y. Linghu, X. Sun, and others, “Macrophage achieves self-protection against oxidative stress-induced ageing through the Mst-Nrf2 axis,” *Nature Communications*, vol. 10, no. 1, pp. 1–16, 2019.

[273] L. Virág, R. I. Jaén, Z. Regdon, L. Boscá, and P. Prieto, “Self-defense of macrophages against oxidative injury: Fighting for their own survival,” *Redox Biology*, p. 101261, 2019.

[274] B. R. Lee and H.-D. Um, “Hydrogen peroxide suppresses U937 cell death by two different mechanisms depending on its concentration,” *Experimental Cell Research*, vol. 248, no. 2, pp. 430–438, 1999.

[275] D. Martin, A. I. Rojo, M. Salinas, R. Diaz, G. Gallardo, J. Alam, C. M. R. De Galarreta, and A. Cuadrado, “Regulation of heme oxygenase-1 expression through the phosphatidylinositol 3-kinase/Akt pathway and the Nrf2 transcription factor in response to the antioxidant phytochemical carnosol,” *Journal of Biological Chemistry*, vol. 279, no. 10, pp. 8919–8929, 2004.

[276] T. Miyazaki, Y. Kirino, M. Takeno, S. Samukawa, M. Hama, M. Tanaka, S. Yamaji, A. Ueda, N. Tomita, H. Fujita, and others, “Expression of heme oxygenase-1 in human leukemic cells and its regulation by transcriptional repressor Bach1,” *Cancer Science*, vol. 101, no. 6, pp. 1409–1416, 2010.

[277] P. Pagliara, R. Lanubile, M. Dwikat, L. Abbro, and L. Dini, “Differentiation of monocytic U937 cells under static magnetic field exposure,” *European Journal of Histochemistry*, pp. 75–86, 2005.

[278] I. A. Gamaley, I. V. Klyubin, and others, “Activation of murine macrophages by hydrogen peroxide,” *Cellular Signalling*, vol. 6, no. 8, pp. 949–957, 1994.

[279] T. Hishikawa, J. Y. Cheung, R. V. Yelamarty, and D. W. Knutson, “Calcium transients during Fc receptor-mediated and nonspecific phagocytosis by murine peritoneal macrophages.,” *The Journal of Cell Biology*, vol. 115, no. 1, pp. 59–66, 1991.

[280] I. Bejarano, M. Terrón, S. Paredes, C. Barriga, A. Rodriguez, and J. Pariente, “Hydrogen peroxide increases the phagocytic function of human neutrophils by calcium mobilisation,” *Molecular and Cellular Biochemistry*, vol. 296, no. 1, pp. 77–84, 2007.

[281] O. M. Posada Estefan, “Study of the Toxicity, Immunological and Gene Expression Effects of Cobalt Ions and Wear Debris Derived from Metal-On-

Metal Hip Implants," 2013.

[282] M. S. Haney, C. J. Bohlen, D. W. Morgens, J. A. Ousey, A. A. Barkal, C. K. Tsui, B. K. Ego, R. Levin, R. A. Kamber, H. Collins, and others, "Identification of phagocytosis regulators using magnetic genome-wide CRISPR screens," *Nature Genetics*, vol. 50, no. 12, pp. 1716–1727, 2018.

[283] K. Nishi, Y. Iwaihara, T. Tsunoda, T. Sakata, S. Shirasawa, S. Ishikura, and others, "ROS-induced cleavage of NHLRC2 by caspase-8 leads to apoptotic cell death in the HCT116 human colon cancer cell line," *Cell Death and Disease*, vol. 8, no. 12, pp. 1–13, 2017.

[284] M. Badura-Stronka, R. Śmigiel, K. Rutkowska, K. Szymańska, A. S. Hirschfeld, M. Monkiewicz, J. Kosińska, E. Wolańska, M. Rydzanicz, A. Latos-Bieleńska, and others, "FINCA syndrome—Defining neurobehavioral phenotype in survivors into late childhood," *Molecular Genetics and Genomic Medicine*, vol. 10, no. 4, p. e1899, 2022.

[285] J.-W. Hu, Y. Yin, Y. Gao, Y.-Y. Nie, P.-Y. Fu, J.-B. Cai, K. Zhu, C. Huang, X.-W. Huang, X.-R. Yang, and others, "TM2D1 contributes the epithelial-mesenchymal transition of hepatocellular carcinoma via modulating AKT/β-catenin axis," *American Journal of Cancer Research*, vol. 11, no. 4, p. 1557, 2021.

[286] M. W. Carr, S. J. Roth, E. Luther, S. S. Rose, and T. A. Springer, "Monocyte chemoattractant protein 1 acts as a T-lymphocyte chemoattractant.," *Proceedings of the National Academy of Sciences*, vol. 91, no. 9, pp. 3652–3656, 1994.

[287] P. Allavena, G. Bianchi, D. Zhou, J. Van Damme, P. Jilek, S. Sozzani, and A. Mantovani, "Induction of natural killer cell migration by monocyte chemotactic protein- 1,- 2 and- 3," *European Journal of Immunology*, vol. 24, no. 12, pp. 3233–3236, 1994.

[288] K. Vaddi and R. C. Newton, "Regulation of monocyte integrin expression by beta-family chemokines.," *The Journal of Immunology*, vol. 153, no. 10, pp. 4721–4732, 1994.

[289] K. Murphy and C. Weaver, "Janeway's Immunobiology," 9th ed., New York: Garland Science, 2016, pp. 814–815.

[290] M. Jaramillo and M. Olivier, "Hydrogen peroxide induces murine macrophage chemokine gene transcription via extracellular signal-regulated kinase-and cyclic adenosine 5′-monophosphate (cAMP)-dependent pathways: involvement of NF-κB, activator protein 1, and cAMP response element binding protein," *The Journal of Immunology*, vol. 169, no. 12, pp. 7026–7038, 2002.

[291] L. E. DeForge, A. M. Preston, E. Takeuchi, J. Kenney, L. A. Boxer, and D. Remick, “Regulation of interleukin 8 gene expression by oxidant stress.,” *Journal of Biological Chemistry*, vol. 268, no. 34, pp. 25568–25576, 1993.

[292] V. Lakshminarayanan, D. W. Beno, R. H. Costa, and K. A. Roebuck, “Differential regulation of interleukin-8 and intercellular adhesion molecule-1 by H_2O_2 and tumor necrosis factor-α in endothelial and epithelial cells,” *Journal of Biological Chemistry*, vol. 272, no. 52, pp. 32910–32918, 1997.

[293] P. Andrew, H. Harant, and I. Lindley, “Nitric oxide regulates IL-8 expression in melanoma cells at the transcriptional level,” *Biochemical and Biophysical Research Communications*, vol. 214, no. 3, pp. 949–956, 1995.

[294] C. Sgadari, J. M. Farber, A. L. Angiolillo, F. Liao, J. Teruya-Feldstein, P. R. Burd, L. Yao, G. Gupta, C. Kanegane, and G. Tosato, “Mig, the monokine induced by interferon-γ, promotes tumor necrosis in vivo,” *Blood, The Journal of the American Society of Hematology*, vol. 89, no. 8, pp. 2635–2643, 1997.

[295] G. Valen, W. Erl, P. Eriksson, D. Wuttge, G. Paulsson, and G. K. Hansson, “Hydrogen peroxide induces mRNA for tumour necrosis factor α in human endothelial cells,” *Free Radical Research*, vol. 31, no. 6, pp. 503–512, 1999.

[296] S. Arndt, M. Landthaler, J. L. Zimmermann, P. Unger, E. Wacker, T. Shimizu, Y.-F. Li, G. E. Morfill, A.-K. Bosserhoff, and S. Karrer, “Effects of cold atmospheric plasma (CAP) on ß-defensins, inflammatory cytokines, and apoptosis-related molecules in keratinocytes in vitro and in vivo,” *PLoS One*, vol. 10, no. 3, 2015.

[297] A. Schmidt, S. Bekeschus, H. Jablonowski, A. Barton, K.-D. Weltmann, and K. Wende, “Role of ambient gas composition on cold physical plasma-elicited cell signaling in keratinocytes,” *Biophysical Journal*, vol. 112, no. 11, pp. 2397–2407, 2017.

[298] A. Schmidt, K. Wende, S. Bekeschus, L. Bundscherer, A. Barton, K. Ottmüller, K.-D. Weltmann, and K. Masur, “Non-thermal plasma treatment is associated with changes in transcriptome of human epithelial skin cells,” *Free Radical Research*, vol. 47, no. 8, pp. 577–592, 2013.

[299] G. Pasqual-Melo, S. K. Sagwal, E. Freund, R. K. Gandhirajan, B. Frey, T. von Woedtke, U. Gaipl, and S. Bekeschus, “Combination of gas plasma and radiotherapy has immunostimulatory potential and additive toxicity in murine melanoma cells in vitro,” *International Journal of Molecular Sciences*, vol. 21, no. 4, p. 1379, 2020.

[300] J. Park, D. Suh, T. Tang, H. J. Lee, J.-S. Roe, G. C. Kim, S. Han, and K. Song, “Non-thermal atmospheric pressure plasma induces epigenetic modifications that activate the expression of various cytokines and growth factors in human mesoderm-derived stem cells,” *Free Radical Biology and Medicine*, vol. 148,

pp. 108–122, 2020.

[301] J. Padawer, “Exocytosis,” in *Encyclopedia of Immunology* , 2nd ed., Delves, Peter J and Roitt, Ivan M, Ed. San Diego: Academic Press, 1998, pp. 849–856.

[302] P. Lacy and J. L. Stow, “Cytokine release from innate immune cells: association with diverse membrane trafficking pathways,” *Blood, The Journal of the American Society of Hematology*, vol. 118, no. 1, pp. 9–18, 2011.

[303] R. Z. Murray and J. L. Stow, “Cytokine secretion in macrophages: SNAREs, Rabs, and membrane trafficking,” *Frontiers in Immunology*, vol. 5, p. 538, 2014.

[304] J. L. Stow, P. C. Low, C. Offenhäuser, and D. Sangermani, “Cytokine secretion in macrophages and other cells: pathways and mediators,” *Immunobiology*, vol. 214, no. 7, pp. 601–612, 2009.

[305] P. L. Jones, D. Ping, and J. M. Boss, “Tumor necrosis factor alpha and interleukin-1β regulate the murine manganese superoxide dismutase gene through a complex intronic enhancer involving C/EBP-β and NF-κB,” *Molecular and Cellular Biology*, vol. 17, no. 12, pp. 6970–6981, 1997.

[306] G. H. Wong, “Protective roles of cytokines against radiation: induction of mitochondrial MnSOD,” *Biochimica et Biophysica Acta (BBA)-Molecular Basis of Disease*, vol. 1271, no. 1, pp. 205–209, 1995.

[307] G. H. Wong and D. V. Goeddel, “Induction of manganous superoxide dismutase by tumor necrosis factor: possible protective mechanism,” *Science*, vol. 242, no. 4880, pp. 941–944, 1988.

[308] Y. Lewis-Molock, K. Suzuki, N. Taniguchi, Dee-dee H Nguyen, and others, “Lung manganese superoxide dismutase increases during cytokine-mediated protection against pulmonary oxygen toxicity in rats,” *American Journal of Respiratory Cell and Molecular Biology*, vol. 10, no. 2, p. 133, 1994.

[309] “DMEM 4.5 g/L glucose w/L-Gln w/ sodium pyruvate.” [Online]. Available: https://bioscience.lonza.com/lonza_bs/CH/en/Culture-Media-and-Reagents/p/000000000000183918/DMEM-4-5-g-L-glucose-w-L-Gln-w-sodium-pyruvate. [Accessed: 05-May-2022]

[310] “RPMI 1640 medium without L-glutamine.” [Online]. Available: https://bioscience.lonza.com/lonza_bs/GB/en/Culture-Media-and-Reagents/p/000000000000183913/RPMI-1640-Medium-without-L-Glutamine. [Accessed: 26-May-2022]

[311] D. Fischer, M. Pike, H. Koren, and R. Snyderman, “Chemotactically responsive and nonresposive forms of a continuous human monocyte cell

line," *The Journal of Immunology*, vol. 125, no. 1, pp. 463–465, 1980.

[312] Y.-S. Baek, S. Haas, H. Hackstein, G. Bein, M. Hernandez-Santana, H. Lehrach, S. Sauer, and H. Seitz, "Identification of novel transcriptional regulators involved in macrophage differentiation and activation in U937 cells," *BMC Immunology*, vol. 10, no. 1, p. 18, 2009.

[313] G. Carruba, P. D'Agostino, M. Miele, M. Calabrò, C. Barbera, G. D. Bella, S. Milano, V. Ferlazzo, R. Caruso, M. L. Rosa, L. Cocciadiferro, I. Campisi, L. Castagnetta, and E. Cillari, "Estrogen regulates cytokine production and apoptosis in PMA-differentiated, macrophage-like U937 cells.," *Journal of Cellular Biochemistry*, vol. 90, no. 1, pp. 187–96, 2003.

[314] A. Garcia, A. Serrano, E. Abril, P. Jimenez, L. M. Real, J. Canton, F. Garrido, and F. Ruiz-Cabello, "Differential effect on U937 cell differentiation by targeting transcriptional factors implicated in tissue-or stage-specific induced integrin expression," *Experimental Hematology*, vol. 27, no. 2, pp. 353–364, 1999.

[315] M. Hewison, A. Brennan, R. Singh-Ranger, J. C. Walters, D. R. Katz, and J. L. O'Riordan, "The comparative role of 1,25-dihydroxycholecalciferol and phorbol esters in the differentiation of the U937 cell line," *Immunology*, vol. 77, no. 2, pp. 304–11, 1992.

[316] J. Leβig, B. Neu, H.-J. Glander, J. Arnhold, and U. Reibetanz, "Phagocytotic competence of differentiated U937 cells for colloidal drug delivery systems in immune cells," *Inflammation*, vol. 34, no. 2, pp. 99–110, 2011.

[317] T. Matsusaki, K. Kawanabe, K. Ise, T. Nakayama, J. Toguchida, and T. Nakamura, "Gene expression profile of macrophage-like U937 cells in response to polyethylene particles: a novel cell-particle culture system," *The Journal of Arthroplasty*, vol. 22, no. 7, pp. 960–965, 2007.

[318] S. Teimourian and N. Masoudzadeh, "CARD15 gene overexpression reduces effect of etanercept, infliximab, and adalimumab on cytokine secretion from PMA activated U937 cells," *European Journal of Pharmacology*, vol. 762, pp. 394–401, 2015.

[319] M. Vongsakul, J. Kasisith, P. Noisumdaeng, and P. Puthavathana, "The difference in IL-1β], MIP-1α, IL-8 and IL-18 production between the infection of PMA activated U937 cells with recombinant vaccinia viruses inserted 2004 H5N1 influenza HA genes and NS genes," *Asian Pacific Journal of Allergy and Immunology*, vol. 29, no. 4, p. 349, 2011.

[320] H. Yue, N. Leng, Z. Wu, H. Li, X. Li, and P. Zhu, "Expression of CD147 on phorbol-12-myris-tate-13-acetate (PMA)-treated U937 cells differentiating into foam cells," *Archives of Biochemistry and Biophysics*, vol. 485, no. 1, pp.

30–34, 2009.

[321] E. Bastonini, L. Verdone, S. Morrone, A. Santoni, G. Settimo, G. Marsili, M. La Fortezza, E. Di Mauro, and M. Caserta, “Transcriptional modulation of a human monocytic cell line exposed to PM10 from an urban area,” *Environmental Research*, vol. 111, no. 6, pp. 765–774, 2011.

[322] M. Bernhard and K. Ulrich, “Rt-PCR study of purinergic P2 receptors in hematopoietic cell lines,” *Biochemistry (Moscow)*, vol. 71, no. 6, pp. 607–611, 2006.

[323] W. Chai, J. Zhang, Y. Duan, D. Pan, W. Liu, Y. Li, X. Yan, and B. Chen, “Pseudomonas pyocyanin stimulates IL-8 expression through MAPK and NF-κB pathways in differentiated U937 cells,” *BMC Microbiology*, vol. 14, no. 1, pp. 1–12, 2014.

[324] A. Kadl, J. Huber, F. Gruber, V. N. Bochkov, B. R. Binder, and N. Leitinger, “Analysis of inflammatory gene induction by oxidized phospholipids in vivo by quantitative real-time RT-PCR in comparison with effects of LPS,” *Vascular Pharmacology*, vol. 38, no. 4, pp. 219–227, 2002.

[325] Y. Y. Liew, E. Docter, D. Ray, I. Hutchinson, and I. Brogan, “Effect of rapamycin and prednisolone in differentiated THP-1 and U937 cells,” in *Transplantation Proceedings*, 2002, vol. 34, no. 7, pp. 2872–2873.

[326] W. C. Lim and V. T. Chow, “Gene expression profiles of U937 human macrophages exposed to Chlamydophila pneumoniae and/or low density lipoprotein in five study models using differential display and real-time RT-PCR,” *Biochimie*, vol. 88, no. 3–4, pp. 367–377, 2006.

[327] Y. Lin, G. Zhang, Z. Leng, Z. Lu, L. Bu, G. Shen, and S. Yang, “Study on the bone marrow mesenchymal stem cells induced drug resistance in the U937 cells and its mechanism,” *Chinese Medical Journal*, vol. 119, no. 11, pp. 905–910, 2006.

[328] Z. Molaeipour, K. Shamsasanjan, A. A. Movassaghpour, P. Akbarzadehlaleh, F. Sabaghi, and M. Saleh, “The effect of bone marrow mesenchymal stem cells on vitamin D3 induced monocytic differentiation of U937 cells,” *Advanced Pharmaceutical Bulletin*, vol. 6, no. 1, p. 23, 2016.

[329] W. Wen, S. Chen, Y. Cao, Y. Zhu, and Y. Yamamoto, “HIV-1 infection initiates changes in the expression of a wide array of genes in U937 promonocytes and HUT78 T cells,” *Virus Research*, vol. 113, no. 1, pp. 26–35, 2005.

[330] Z. Xiaoxia, N. Weihua, Z. Qingyong, W. Fengli, L. Yingying, S. Xiaxia, L. Zhonghui, and T. Guixiang, “Maltose-binding protein isolated from Escherichia coli induces Toll-like receptor 2-mediated viability in U937

cells," *Clinical and Translational Oncology*, vol. 13, no. 7, pp. 509–518, 2011.

[331] L. Zang, H. He, Q. Xu, Y. Yu, N. Zheng, W. Liu, T. Hayashi, S. Tashiro, S. Onodera, and T. Ikejima, "Reactive oxygen species H_2O_2 and OH, but not O2- promote oridonin-induced phagocytosis of apoptotic cells by human histocytic lymphoma U937 cells," *International Immunopharmacology*, vol. 15, no. 2, pp. 414–423, 2013.

[332] W. Zhu, L. Huang, X. Xu, H. Qian, and W. Xu, "Anti-proliferation effect of BMI-1 in U937 cells with siRNA," *International Journal of Molecular Medicine*, vol. 25, no. 6, pp. 889–895, 2010.

[333] S. Bekeschus, A. Lin, A. Fridman, K. Wende, K.-D. Weltmann, and V. Miller, "A Comparison of Floating-Electrode DBD and kINPen Jet: Plasma Parameters to Achieve Similar Growth Reduction in Colon Cancer Cells Under Standardized Conditions," *Plasma Chemistry and Plasma Processing*, vol. 38, no. 1, pp. 1–12, 2018.

[334] S. Bekeschus, R. Clemen, F. Nießner, S. K. Sagwal, E. Freund, and A. Schmidt, "Medical gas plasma jet technology targets murine melanoma in an immunogenic fashion," *Advanced Science*, vol. 7, no. 10, p. 1903438, 2020.

[335] C.-Y. Chen, Y.-C. Cheng, and Y.-J. Cheng, "Synergistic effects of plasma-activated medium and chemotherapeutic drugs in cancer treatment," *Journal of Physics D: Applied Physics*, vol. 51, no. 13, p. 13LT01, 2018.

[336] N. K. Kaushik, N. Kaushik, D. Park, and E. H. Choi, "Altered antioxidant system stimulates dielectric barrier discharge plasma-induced cell death for solid tumor cell treatment," *PloS One*, vol. 9, no. 7, p. e103349, 2014.

[337] A. Siu, O. Volotskova, X. Cheng, S. S. Khalsa, K. Bian, F. Murad, M. Keidar, and J. H. Sherman, "Differential effects of cold atmospheric plasma in the treatment of malignant glioma," *PloS One*, vol. 10, no. 6, p. e0126313, 2015.

[338] K. Wende, S. Straßenburg, B. Haertel, M. Harms, S. Holtz, A. Barton, K. Masur, T. von Woedtke, and U. Lindequist, "Atmospheric pressure plasma jet treatment evokes transient oxidative stress in HaCaT keratinocytes and influences cell physiology," *Cell Biology International*, vol. 38, no. 4, pp. 412–425, 2014.

[339] J. Ikeda, H. Tanaka, K. Ishikawa, H. Sakakita, Y. Ikehara, and M. Hori, "Plasma-activated medium (PAM) kills human cancer-initiating cells," *Pathology International*, vol. 68, no. 1, pp. 23–30, 2018.

[340] H. Tanaka, M. Mizuno, K. Ishikawa, K. Takeda, H. Hashizume, K. Nakamura, F. Utsumi, H. Kajiyama, Y. Okazaki, S. Toyokuni, and others, "Glioblastoma cell lines display different sensitivities to plasma-activated medium," *IEEE*

Transactions on Radiation and Plasma Medical Sciences, vol. 2, no. 2, pp. 99–102, 2017.

[341] K. Wende, S. Reuter, T. von Woedtke, K.-D. Weltmann, and K. Masur, "Redox-based assay for assessment of biological impact of plasma treatment," *Plasma Processes and Polymers*, vol. 11, no. 7, pp. 655–663, 2014.

[342] D. Yan, A. Talbot, N. Nourmohammadi, X. Cheng, J. Canady, J. Sherman, and M. Keidar, "Principles of using cold atmospheric plasma stimulated media for cancer treatment," *Scientific Reports*, vol. 5, p. 18339, 2015.

Appendix A Formulations of cell media

Table A.1. Formulation of Lonza DMEM high glucose with L-glutamine (BE12-604F).

Information taken from manufacturer website at [309].

Description	CAS #	Chemical formula	Concentration (mg/L)	Concentration (µM)
Calcium Chloride Anhydrous	10043-52-4	$CaCl_2$	200	1.80E+03
Dextrose	50-99-7	$C_6H_{12}O_6$	4.50E+03	2.50E+04
Ferric Nitrate Nonahydrate	7782-61-8	$Fe(NO_3)_3{\cdot}9H_2O$	0.1	0.248
Magnesium Sulfate Anhydrous	7487-88-9	$MgSO_4$	97.67	811.415
Potassium Chloride	7447-40-7	KCl	400	5.37E+03
Sodium Bicarbonate	144-55-8	$NaHCO_3$	3.70E+03	4.40E+04
Sodium Chloride	7647-14-5	NaCl	6.40E+03	1.10E+05
L-Arginine Monohydrochloride	1119-34-2	$C_6H_{14}N_4O_2{\cdot}HCl$	84	398.747
L-Glutamine	56-85-9	$C_5H_{10}N_2O_3$	584	4.00E+03
Glycine	56-40-6	$HO_2CCH_2NH_2$	30	399.627
L-Histidine Monohydrochloride Monohydrate	5934-29-2	$C_6H_9N_3O_2{\cdot}HCl{\cdot}H_2O$	42	200.382
L-Isoleucine	73-32-5	$HO_2CCH(NH_2)CH(CH_3)CH_2CH_3$	104.8	798.963
L-Leucine	61-90-5	$HO_2CCH(NH_2)CH_2CH(CH_3)_2$	104.8	798.963
L-Lysine Monohydrochloride	657-27-2	$C_6H_{14}N_2O_2{\cdot}HCl$	146.2	800.438
L-Methionine	63-68-3	$HO_2CCH(NH_2)CH_2CH_2SCH_3$	30	201.072
L-Phenylalanine	63-91-2	$HO_2CCH(NH_2)CH_2C_6H_5$	66	399.54

Description	CAS #	Chemical formula	Concentration (mg/L)	Concentration (µM)
L-Serine	56-45-1	$HO_2CCH(NH_2)CH_2OH$	42	399.657
L-Threonine	72-19-5	$HO_2CCH(NH_2)CH(OH)CH_3$	95.2	799.194
L-Tryptophan	73-22-3	$C_{11}H_{12}N2O_2$	16	78.343
L-Valine	72-18-4	$HO_2CCH(NH_2)CH(CH_3)_2$	93.6	799.317
D-Calcium Pantothenate (Vitamin B5)	137-08-6	$C_{18}H_{32}CaN_2O_{10}$	4	8.394
Choline Chloride	67-48-1	$HOCH_2CH_2N(CH_3)_3Cl$	4	28.647
Folic Acid	59-30-3	$C_{19}H_{19}N_7O_6$	4	9.062
I-Inositol	87-89-8	$C_6H_{12}O_6$	7	38.846
Niacinamide (Nicotinamide)	98-92-0	$C_6H_6N_2O$	4	32.757
Pyridoxine Monohydrochloride	58-56-0	$C_8H_{11}NO_3$	4	19.455
Riboflavin (Vitamin B2)	83-88-5	$C_{17}H_{20}N_4O_6$	0.4	1.063
Thiamine Monohydrochloride (Vitamin B1)	67-03-8	$C_{12}H_{18}N_4OSCl_2$	4	11.859
Phenol Red	34487-61-1	$C_{19}H_{14}O_5S$	15	39.851
Pyruvic Acid Sodium Salt	113-24-6	CH_3COCO_2Na	110	999.636
L-Tyrosine Disodium Salt, Dihydrate	122666-78-9	$C_9H_9NO_3Na_2{\cdot}2H_2O$	103.79	397.374
L-Cystine Dihydrochloride	30925-07-6	$C_6H_{12}N_2O_4S_2{\cdot}2HCl$	62.58	199.808
Sodium Phosphate Monobasic, Anhydrous	7558-80-7	NaH_2PO_4	108.69	905.75

Table A.2. Formulation of RPMI 1640 without L-glutamine (BE12-167F). Information taken from manufacturer website at [310].

Description	CAS #	Chemical formula	Concentration (mg/L)	Concentration (μM)
Sodium Bicarbonate	144-55-8	$NaHCO_3$	2.00E+03	2.38E+04
Sodium Chloride	7647-14-5	NaCl	6.00E+03	1.03E+05
Ca(NO3)2.4H2O	13477-34-4	$Ca(NO_3)_2$, $4H_2O$	100	423.46
Choline Chloride	67-48-1	$HOCH_2CH_2N(CH_3)_3Cl$	3	21.485
D-Biotin (Vitamin H) (00129)	58-85-5	$C_{10}H_{16}N_2O_3S$	0.2	0.819
D-Calcium Pantothenate (Vitamin B5)	137-08-6	$C_{18}H_{32}CaN_2O_{10}$	0.25	0.525
D-Glucose anhydrous	50-99-7	$C_6H_{12}O_6$	2.00E+03	1.11E+04
Folic Acid	59-30-3	$C_{19}H_{19}N_7O_6$	1	2.266
Glutathione Reduced	70-18-8	$C_{10}H_{17}N_3O_6S$	1	3.254
Glycine	56-40-6	$HO_2CCH_2NH_2$	10	133.209
Potassium Chloride	7447-40-7	KCl	400	5.37E+03
L-Arginine Hydrochloride (00095)	1119-34-2	$C_6H_{14}N_4O_2{\cdot}HCl$	241.86	1.15E+03
L-Asparagine Monohydrate	5794-13-8	$NH_2COCH_2CH(NH_2)COOH{\cdot}H_2O$	56.81	378.405
L-Aspartic Acid	56-84-8	$HO_2CCH(NH_2)CH_2CO_2H$	20	150.263
L-Cystine Dihyrohydrochloride	30925-07-6	$C_6H_{12}N_2O_4S_2{\cdot}2HCl$	65.19	208.13
L-Glutamic Acid	56-86-0	$C_5H_9NO_4$	20	135.962

Description	CAS #	Chemical formula	Concentration (mg/L)	Concentration (µM)
L-Histidine Monohydrochloride Monohydrate	5934-29-2	$C_6H_9N_3O_2 \cdot HCl \cdot H_2O$	20.27	96.708
L-Hydroxyproline	51-35-4	$C_5H_9NO_3$	20	152.52
L-Isoleucine	73-32-5	$HO_2CCH(NH_2)CH(CH_3)CH_2CH_3$	50	381.185
L-Leucine	61-90-5	$HO_2CCH(NH_2)CH_2CH(CH_3)_2$	50	381.185
L-Lysine Monohydrochloride	657-27-2	$C_6H_{14}N_2O_2 \cdot HCl$	40	218.998
L-Methionine	63-68-3	$HO_2CCH(NH_2)CH_2CH_2SCH_3$	15	100.536
L-Phenylalanine	63-91-2	$HO_2CCH(NH_2)CH_2C_6H_5$	15	90.805
L-Proline	147-85-3	$C_5H_9NO_2$	20	173.717
L-Serine	56-45-1	$HO_2CCH(NH_2)CH_2OH$	30	285.442
L-Threonine	72-19-5	$HO_2CCH(NH_2)CH(OH)CH_3$	20	167.898
L-Tryptophane	73-22-3	$C_{11}H_{12}N_2O_2$	5	24.482
L-Tyrosine Disodium Salt, Dihydrate	122666-87-9	$C_9H_9NO_3Na_2 \cdot 2H_2O$	28.83	110.379
L-Valine	72-18-4	$HO_2CCH(NH_2)CH(CH_3)_2$	20	170.794
Magnesium Sulfate Anhydrous	7487-88-9	$MgSO_4$	48.83	405.666
Myo-Inositol	87-89-8	$C_6H_{12}O_6$	35	194.272
Sodium Phosphate Dibasic, Anhydrous	7558-79-4	Na_2HP0_4	800.49	5.64E+03
Niacinamide (Nicotinamide)	98-92-0	$C_6H_6N_2O$	1	8.189
P-Aminobenzoic Acid	150-13-0	$C_7H_7NO_2$	1	7.292

Description	CAS #	Chemical formula	Concentration (mg/L)	Concentration (µM)
Phenol Red Sodium Salt	34487-61-1	$C_{19}H_{13}O_5SNa$	5.1	13.549
Pyridoxine Monohydrochloride	58-56-0	$C_8H_{11}NO_3$	1	4.864
Riboflavin (Vitamin B2)	83-88-5	$C_{17}H_20N_4O_6$	0.2	0.531
Thiamine Monohydrochloride (Vitamin B1)	67-03-8	$C_{12}H_{18}N_4OSCl_2$	1	2.965
Cyanocobalamin (Vitamin B12)	68-19-9	$C_{63}H_{88}CoN_{14}O_{14}P$	5.00E-03	3.69E-03

Appendix B Abandoned reactor designs

Four DBD-style NTP source designs were prototyped and tested over the course of the project, but were then found to be unsuitable for further use (Table B.1).

Table B.1. Abandoned prototype reactors

.

Reactor no.	Diagram	Reason for abandonment
3	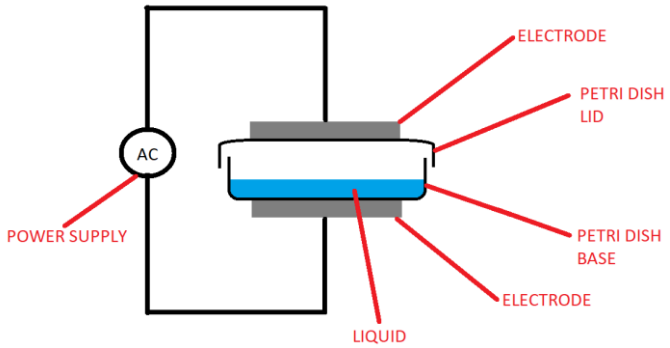	Treatment liquid tended to rise up and stick to lid, therefore removing the air gap and causing discharge to fail.
4	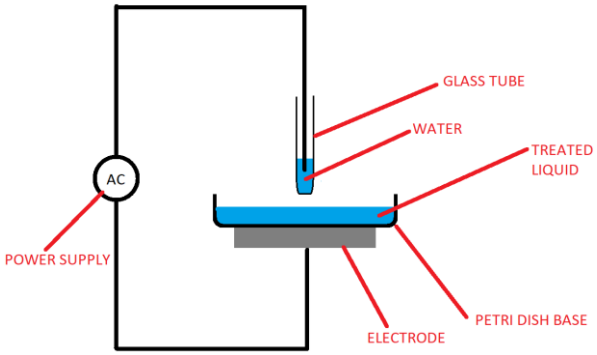	No detectable H_2O_2 formed in treated liquid.

Reactor no.	Diagram	Reason for abandonment
5	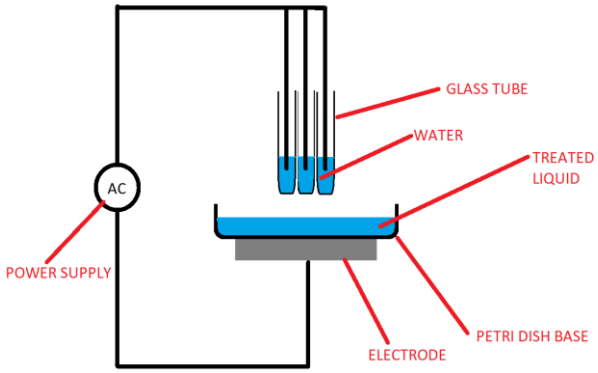	No detectable H_2O_2 formed in treated liquid.
6	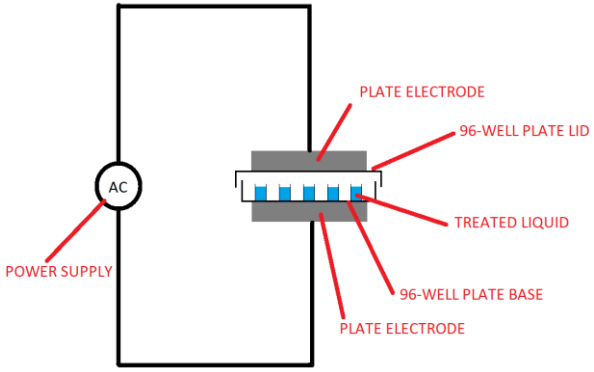	Failed to produce reliable reduction in cell viability with 3t3.

Appendix C MATLAB code for power calculation using Lissajous method

```
C3charge=Ampl1*10*10^(-9) %conversion of voltage across 10 nF measurement (Ampl1) capacitor to charge.

A=polyarea(Ampl,C3charge) %calculation of area contained within Lissajous diagram of voltage across reactor (Ampl) and C3charge, calculated above.  This gives the energy per cycle.

PowerW=A*4000 %Conversion of energy per cycle to power, given 4 kHz being used.

PowermW=PowerW*1000 %conversion to mW from W.

AmplkV=Ampl/1000 %conversion to kV for graph

C3chargeuC = C3charge*1000000 %conversion to uC for graph

plot(AmplkV,C3chargeuC) %Plot of Lissajous diagram.
grid
```

Appendix D Determination of process for differentiation of the U937 cell line into a macrophage-like phenotype

D.1 Introduction

The focus of the latter part of this project was to investigate the effects of plasma on macrophage-like cells, and therefore the U937 used would need to be differentiated into this cell type prior to use. It has long been known that U937 can be induced to behave as a macrophage [311], and that it is therefore capable of acting like a macrophage model in *in vitro* experimentation. A well-established way of doing so is by use of PMA.

To determine an appropriate concentration of PMA to achieve the desired effects, and the accompanying application process, a literature review was carried out for papers which used PMA on U937 to achieve differentiation to a macrophage phenotype. From this, it was noted that a wide range of different protocols were used, with variations in both the concentration of PMA used and the time of application to the cells (Table D.1).

*Table D.1. Concentrations of PMA in a selection of papers in which this substance has been used to differentiate U937. *For these papers, the concentrations were expressed in ng/L, and therefore this has been converted to nM using the molar mass of PMA of 616.83 g/mol.*

Author	**[PMA] (nM)**	**Exposure time (hours)**
Baek *et al.* [312]	10.0	48
Carruba *et al.* [313]	16.2*	48
Garcia *et al.* [314]	32.4*	120
Hewison *et al.* [315]	Up to 8.0	48
Leβig *et al.* [316]	16.2*	24
Matsusaki *et al.* [317]	100.0	72
Teimourian *et al.* [318]	81.1*	24
Vonsakul *et al.* [319]	10.0	24
Yue *et al.* [320]	200.0	168

D.2 Assessment of PMA concentration effects

When monocytes differentiate into macrophages, there are several key changes that occur. These include an increase in size, improved phagocytic ability [11], the development of pseudopodia, and the development of adherent abilities [316][277]. Therefore, in order to determine the most suitable concentration of PMA to use to obtain a macrophage-like phenotype in U937, the following three attributes were assessed in U937 treated with a range of PMA concentrations:

1. Phagocytic ability
2. Morphological characteristics
3. Adherent ability.

As well as this, neutral red and MTT viability assays were also carried out for each PMA concentration. These assays could be described as giving a combined measurement of two different changes that may be expected in differentiated U937. For both assay types, the number of adherent cells present is a factor in the quantity of dye present at the point of assay. However, as well as this, increased activity of lysosomes is known to occur in the differentiation of monocytes to macrophages [316] and this would be likely to increase uptake of neutral red, while metabolism is also likely to be altered, affecting uptake of MTT.

PMA concentrations of 1, 10, 16.2, 32.4, 81 and 100 nM were investigated, covering the range of most of the papers listed in Table D.1. All cell samples were created following the procedures described in 2.3.1.2. PMA-exposed cells were only considered after 48 hours following the addition of PMA, as preliminary experiments showed that shorter (24-hour) exposures did not result in the attributes seen with 48-hours, whereas longer (72-hour) exposures did not result in these attributes being any more prominent than at 48 hours. Therefore, 24- and 72-hour exposures were not investigated in detail, and only results for 48 hours are given here.

D.2.1 Assessment of phagocytic ability

It would be expected that macrophage-like U937 would have significant phagocytic ability [277]. The effect of exposure to differing concentrations of PMA was assessed using FITC-labelled 1 µm latex beads, prepared and used as described in 2.3.8. These were added to samples 24 hours following addition of PMA, with the cells and beads remaining in the PMA for a further 24 hours. Following this time period, the medium was removed and wells were washed twice with DPBS to remove any remaining free beads.

From the microscope photographs taken of these samples (Figure D.1) it is apparent that, for the small number of control cells (not exposed to PMA) that remained in the sample following the double wash, their phagocytic ability was minimal. This was also the case for 1 nM PMA, suggesting that this concentration may be too low for U937 to differentiate sufficiently. All the concentrations above this which were used, from 10 nM to 100 nM showed a significant amount of phagocytic ability in the cell population and no concentration appeared to produce a better effect than any other.

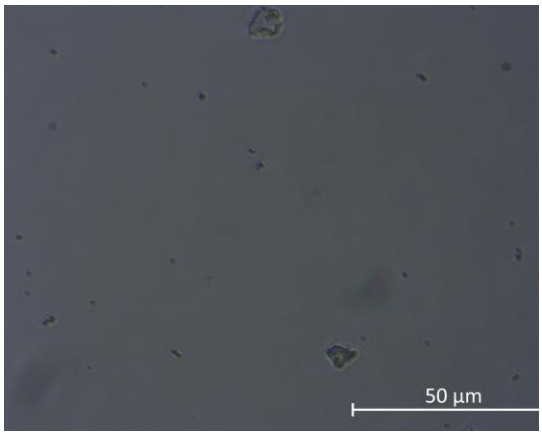

(a)

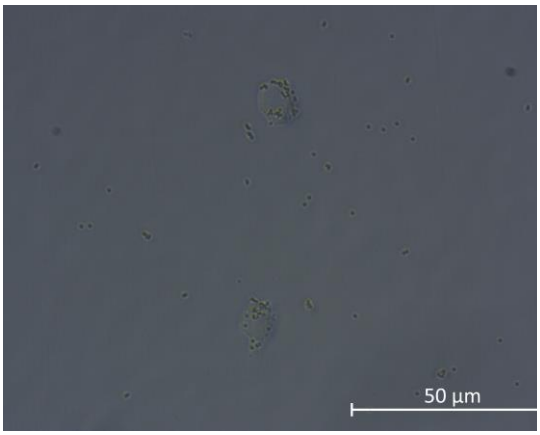

(b)

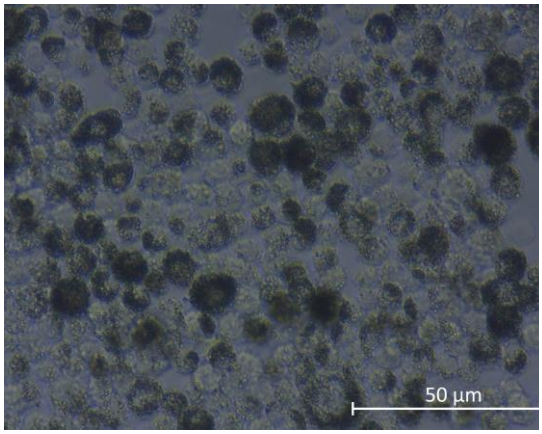

(c)

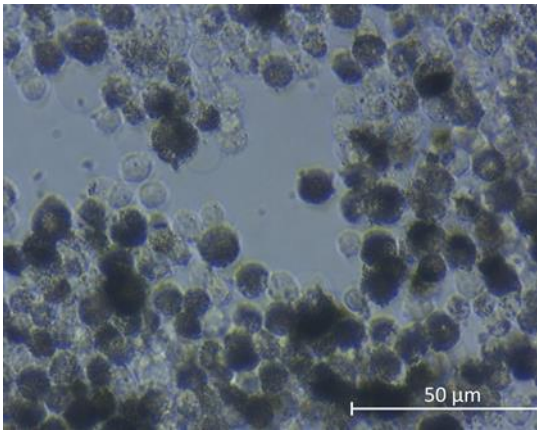

(d)

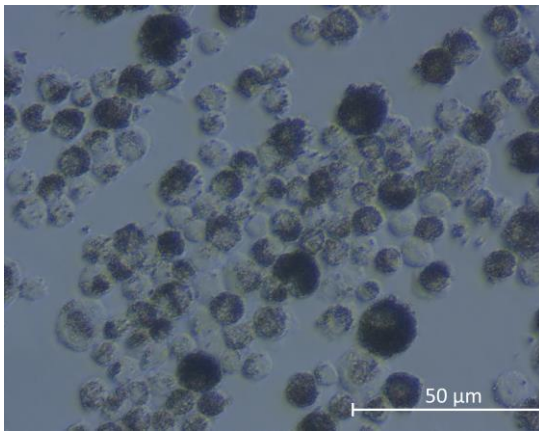

(e)

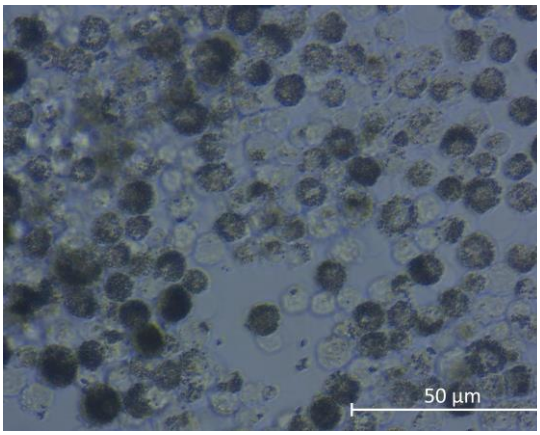

(f)

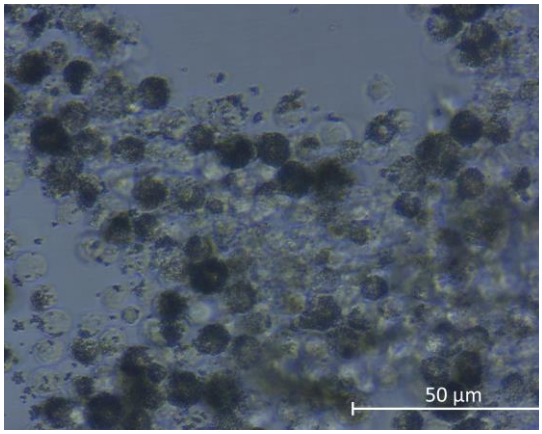

(g)

Figure D.1. Phagocytosis of 1 µM latex beads by U937 following 48-hour exposure to PMA concentrations of (a) 0 nM (b) 1 nM (c) 10 nM (d) 16.2 nM (e) 32.4 nM (f) 81 nM (g) 100 nM. The latex beads appear as dark areas within the cells where they have been phagocytosed. 40x magnification used.

Ideally, FACS would have been used to quantify beads present. However, as with the similar work performed in 7.4.4.1, this did not prove possible due to access restrictions within the University due to the COVID-19 pandemic.

D.2.2 Assessment of morphological characteristics

Photographs taken also showed evidence of pseudopodia with at least some of the cells at for all PMA concentrations used (Figure D.2). This is seen by the bumpy texture of the cell surface, and in some instances, long projections emanating from the cell.

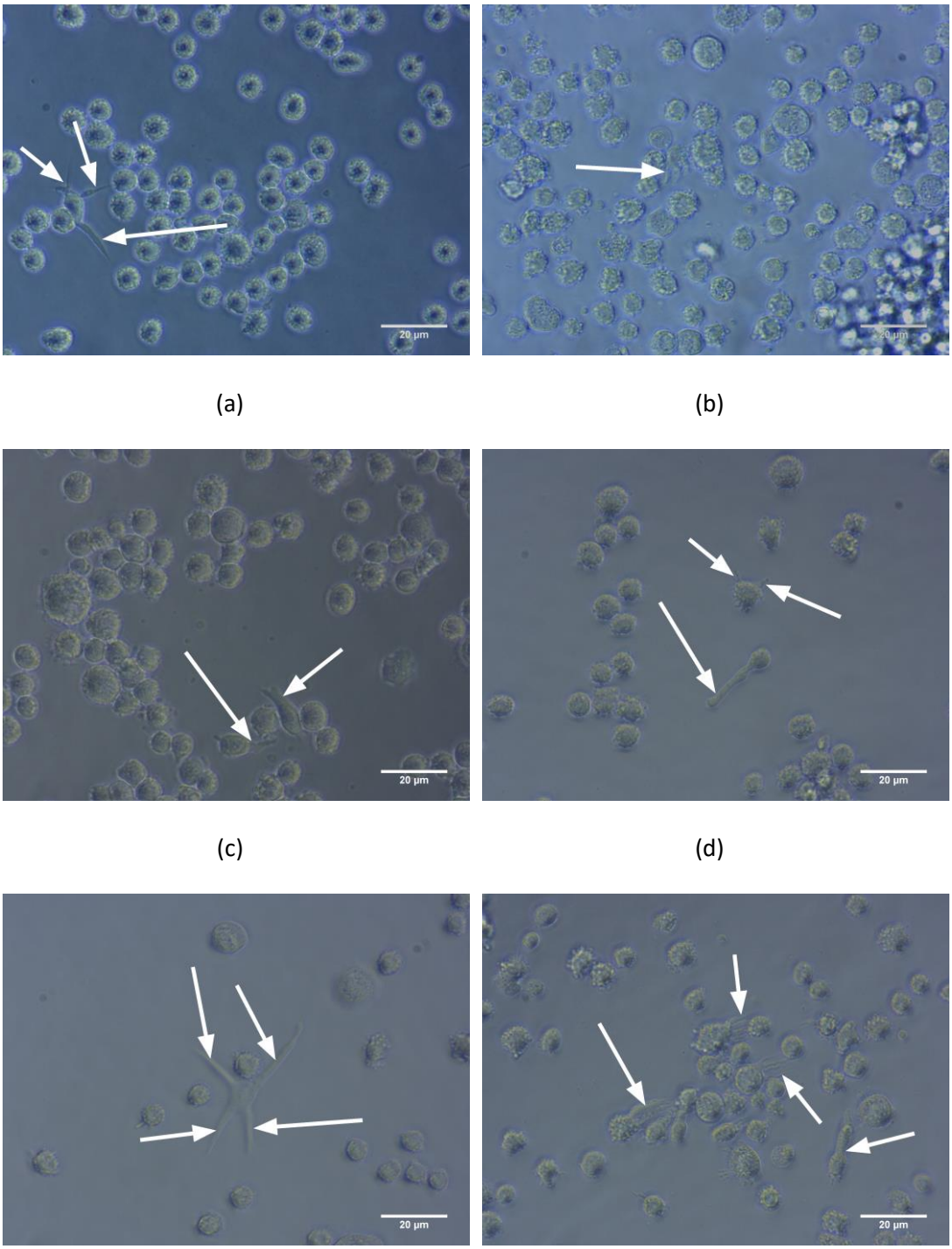

(a) (b)

(c) (d)

Figure D.2. Pseudopodia present in U937 following 48 hours of exposure to PMA of concentrations of (a) 1 nM (b) 10 nM (c) 16.2 nM (d) 32.4 nM (e) 81 nM and f) 100 nM. White arrows show prominent pseudopodia. 40x magnification used.

Some evidence of cell enlargement was also clearly seen in all PMA concentrations (Figure D.3).

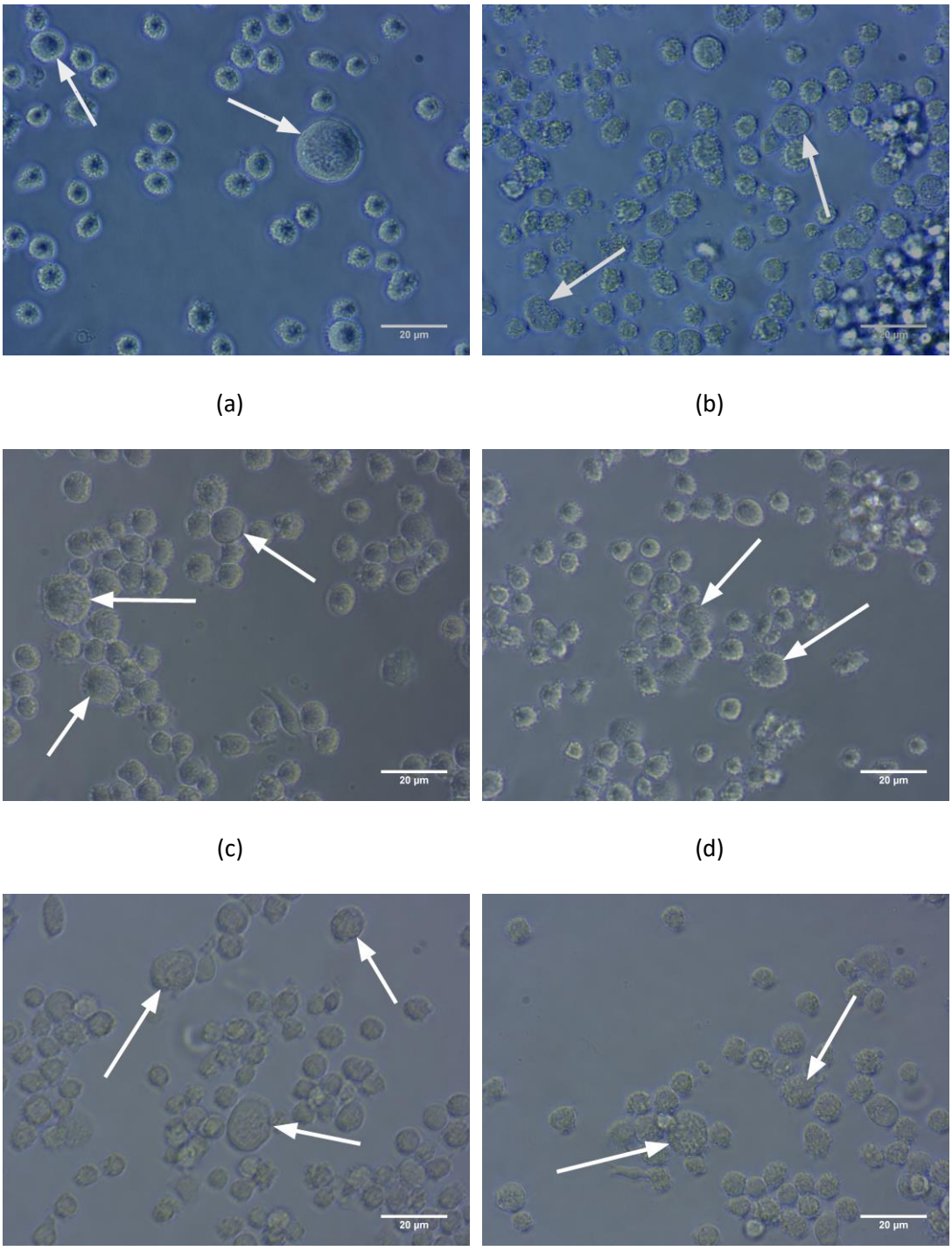

(a) (b)

(c) (d)

(e) (f)

Figure D.3. Size comparisons at 48 hours after exposure to PMA of concentrations (a) 1 nM (b) 10 nM (c) 16.2 nM (d) 32.4 nM (e) 81 nM and (f) 100 nM. White arrows show particularly prominent enlarged cells. 40x magnification used.

D.2.3 Assessment of adherent ability

To assess adherent ability, samples of PMA-treated cells were first photographed at 48 hours following the PMA addition, without the cells being disturbed (Figure D.4(i)). Following this, the sample was washed twice with DPBS to remove unadhered cells, and it was then rephotographed (Figure D.4(ii)). From this, it could be seen that all the PMA concentrations used enhanced cell adhesion well beyond that of the control samples, and thus all could be deemed to be enhancing adherent ability in U937.

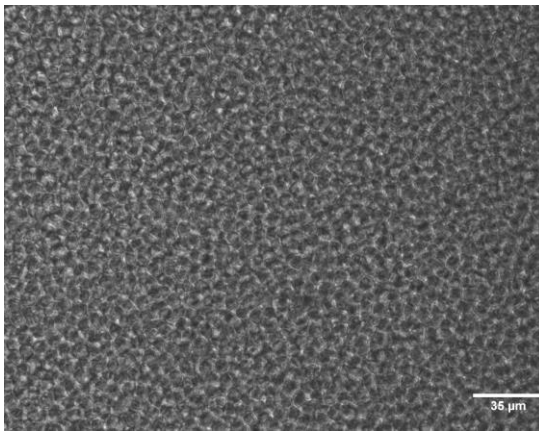

(a)*(i)*

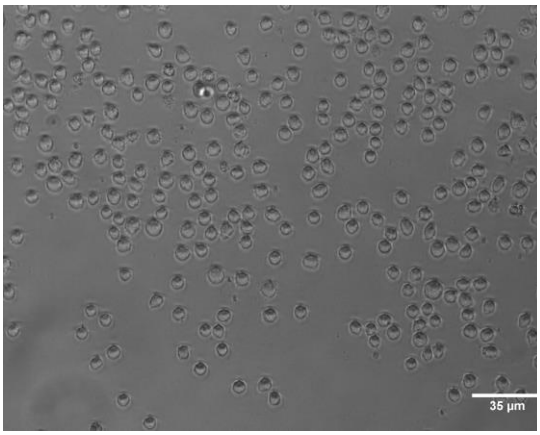

(a)*(ii)*

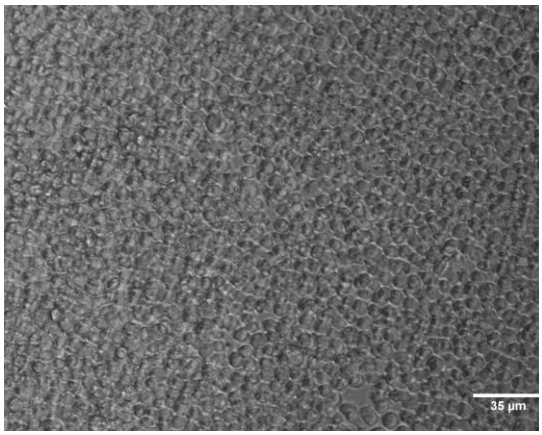

(b)*(i)*

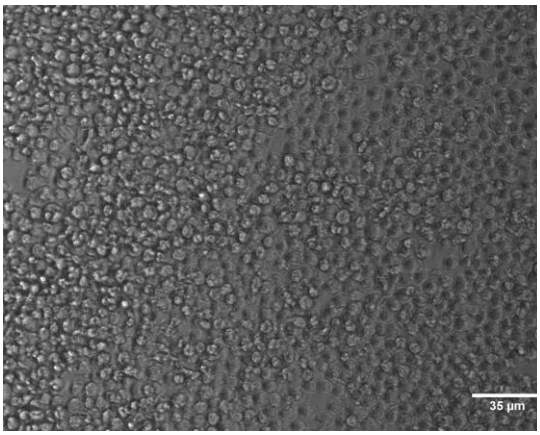

(b)*(ii)*

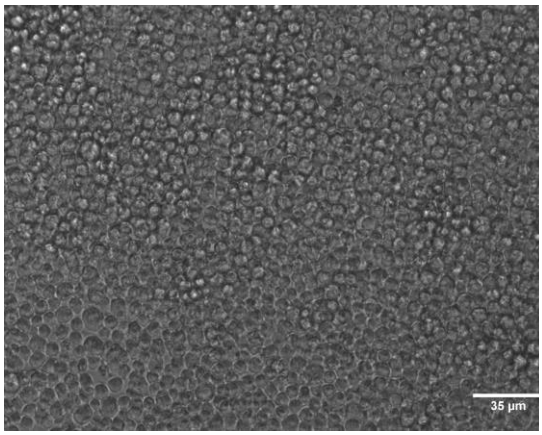

(c)*(i)*

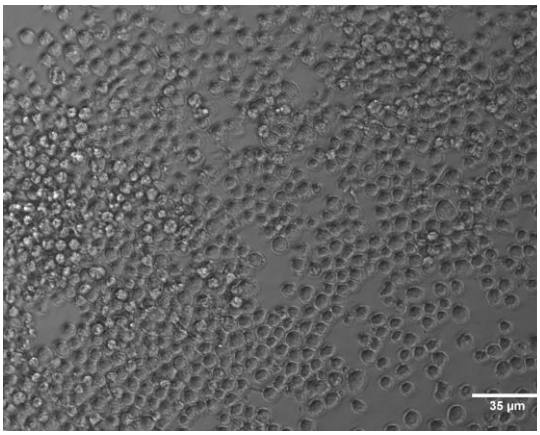

(c)*(ii)*

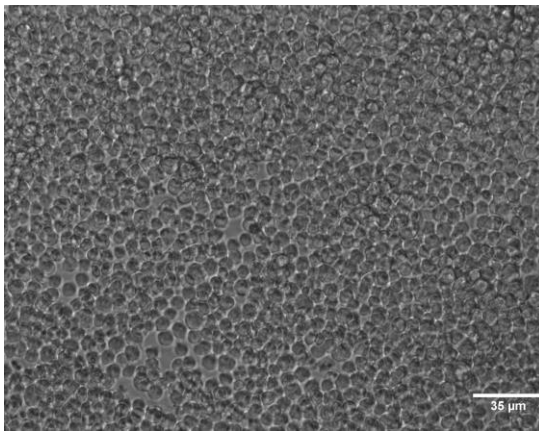

(d)*(i)*

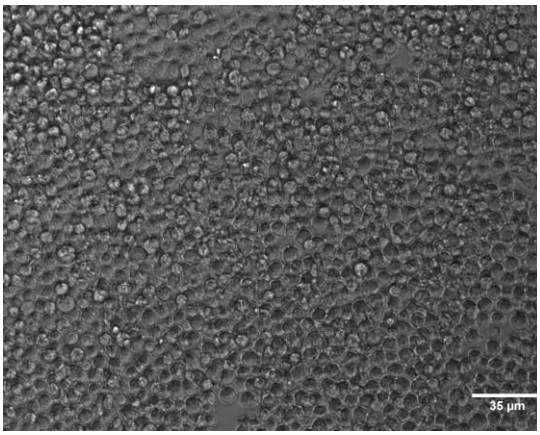

(d)(ii)

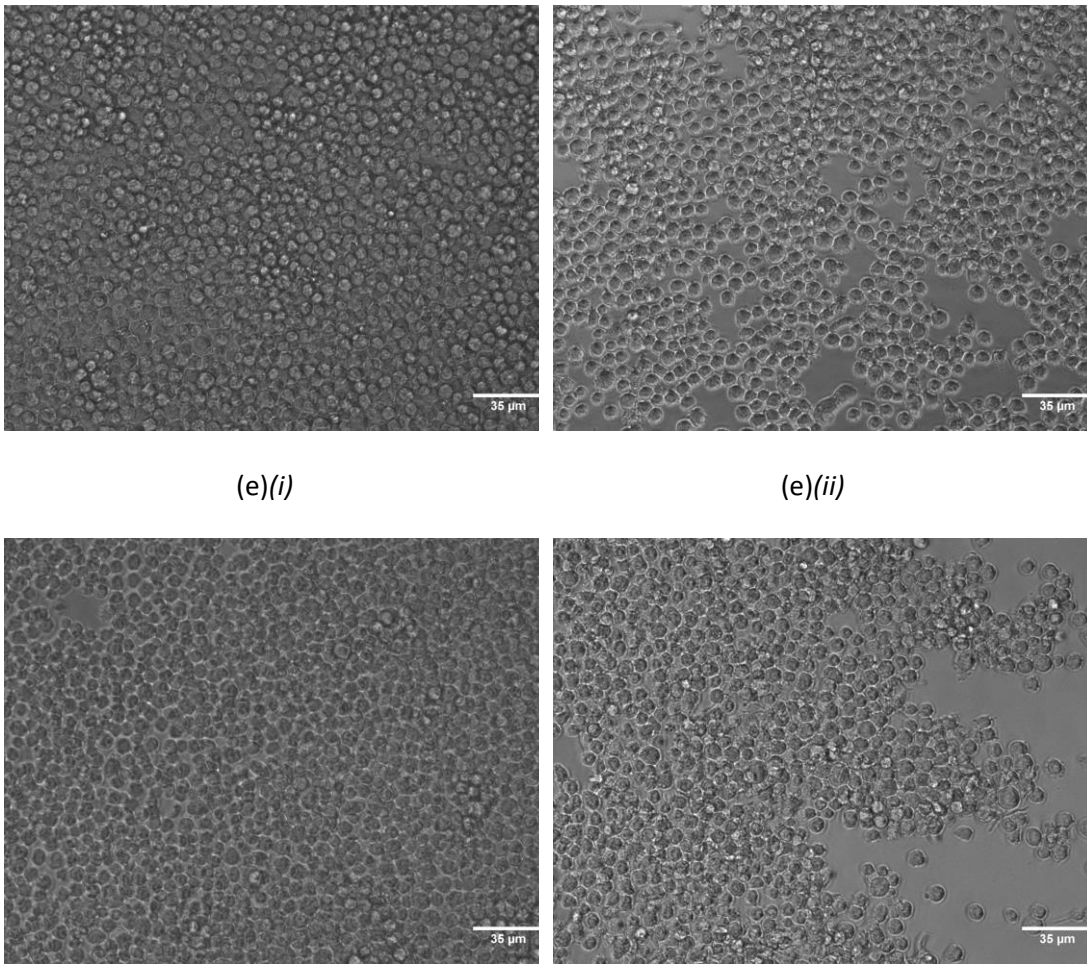

(e)*(i)* (e)*(ii)*

(f)*(i)* (f)*(ii)*

Figure D.4. Differentiated U937 (i) before and (ii) after DPBS wash following 48 hours of exposure to PMA concentrations of (a) 0 nM (b) 10 nM PMA (c) 16.2 nM (d) 32.4 nM (e) 81 nM (f) 100 nM. All photographs taken with 20x objective lens. Note that 1 nM concentration was omitted from the experiment in error. However, given this concentration had already been shown to be unsuitable from the work presented in Figure D.1, this is not a significant issue.

D.2.4 Viability assays

Neutral red and MTT assays were carried out on U947 samples exposed to different concentrations of PMA for 48 hours (Figure D.5 and Figure D.6). Prior to assay, the cells

were washed twice with DPBS to remove non-adherent cells, and thus only adherent cells, which were assumed therefore to be differentiated, were included in the assay. With MTT, it was found that all samples apart from those which used 1 nM PMA gave a statistically significant increase in absorbance value, with 16.2 nM, 32.4 nM, 81 nM, and 100 nM having the highest confidence. However, in the neutral red experiment, the higher PMA concentrations (81 nM and 100 nM) were not found to have a statistically significant difference from the control samples.

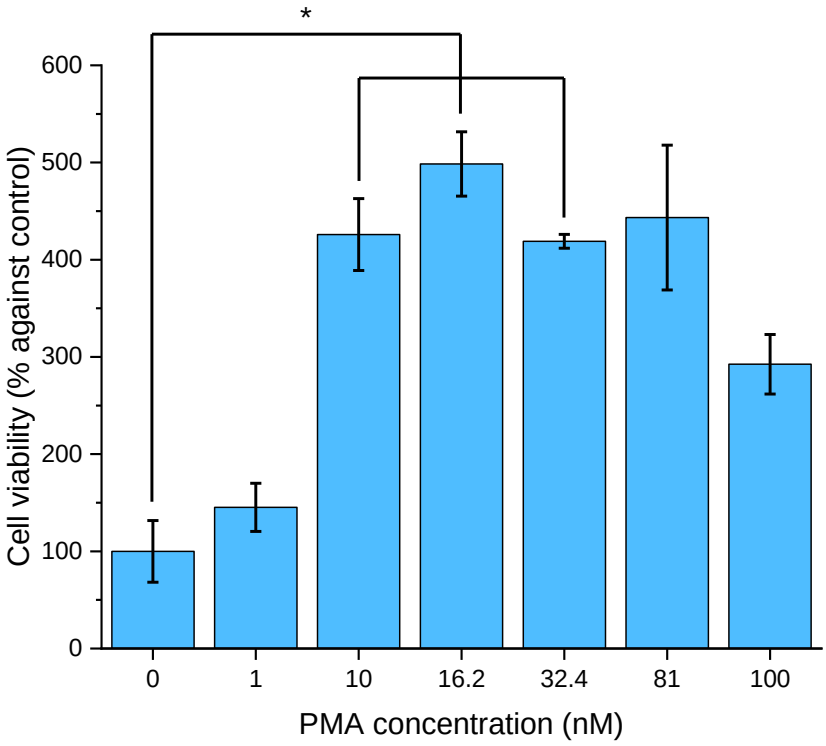

*Figure D.5. Neutral red assay on U937 following 48 hours of exposure to a range of concentrations of PMA. n=3, SE shown, *: p<0.05, Welch with Games-Howell post-hoc.*

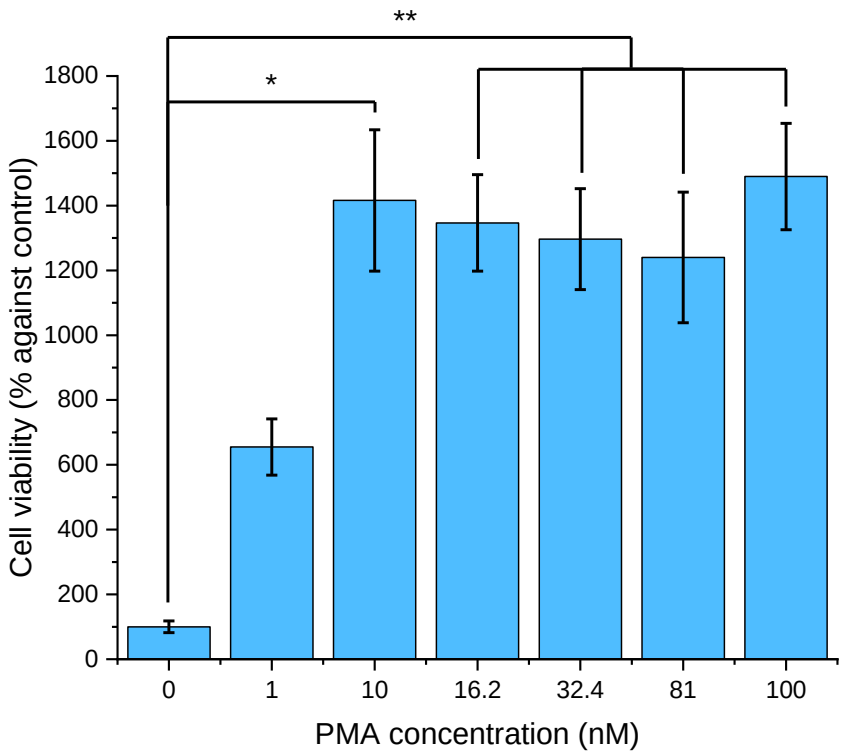

*Figure D.6. MTT assay on U937 following 48 hours of exposure to a range of concentrations of PMA. n=6, SE shown, *: p<0.05, **p<0.001, ANOVA with Tukey HSD post-hoc.*

D.3 Conclusion

There was little difference in most measurements between 10 nM, 16.2 nM, 32.4 nM, 81 nM and 100 nM PMA concentrations. However, the MTT and neutral red assays did raise the possibility of 10 nM, 81 nM and 100 nM being less effective at inducing differentiation than 16.2 nM and 32.4 nM. Between 16.2 nM and 32.4 nM, there was little identifiable difference in their effects from any of the work performed. The decision was therefore made to use 16.2 nM for all experiments from this point forward, as this was commonly used in the literature.

Appendix E Selection of reference genes used for RT-qPCR

RT-qPCR was performed in Chapter 7 to investigate the effects of PAM on the expression of certain genes associated with phagocytosis (7.4.4.2), and others associated with some antioxidants (7.4.6) within differentiated U937. The selection of four possible reference genes (GAPDH, HRPT1, B2M and ACTB) was made by considering papers which had used PCR within both the plasma medicine literature and those outside of this which had used U937 (Table E.1).

Table E.1. Papers and theses considered when selecting reference genes for NTP-treated U937.

Author	**U937?**	**NTP treated?**	**Reference gene(s)**
Adachi *et al*.[223]	No	Yes	β-actin
Adachi *et al*.[222]	No	Yes	β-actin
Arndt *et al.* [296]	No	Yes	β-actin
Bastonini *et al.* [321]	Yes	No	β-actin GAPDH HRPT1
Bernhard and Ulrich [322]	Yes	No	GAPDH
Chai *et al.* [323]	Yes	No	β-actin
Kadl *et al.* [324]	Yes	No	B2M
Liew *et al.* [325]	Yes	No	HRPT1 β-actin
Lim and Chow [326]	Yes	No	GAPDH
Lin *et al.* [168]	No	Yes	GAPDH
Lin *et al.* [327]	Yes	No	β-actin
Molaeipour *et al.* [328]	Yes	No	GAPDH
Posada Estefan [281]	Yes	No	HRPT1
Song *et al.* [17]	Yes	No	GAPDH
Song *et al.* [72]	No	Yes	β-actin
Tabuchi *et al.* [117]	Yes	Yes	GAPDH
Teimourian and Masoudzadeh [318]	Yes	No	β-actin

Author	U937?	NTP treated?	Reference gene(s)
Wen *et al.* [329]	Yes	No	β-actin
Xiaoxia *et al.* [330]	Yes	No	β-actin
Zang *et al.* [331]	Yes	No	β-actin
Zhu *et al.* [332]	Yes	No	GAPDH

Appendix F Lissajous diagrams over first 5 minutes of Reactor 1 treatment

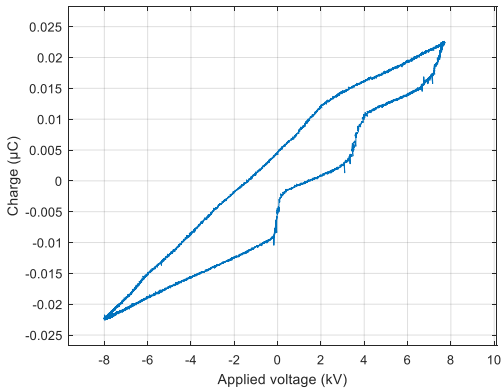

(a)

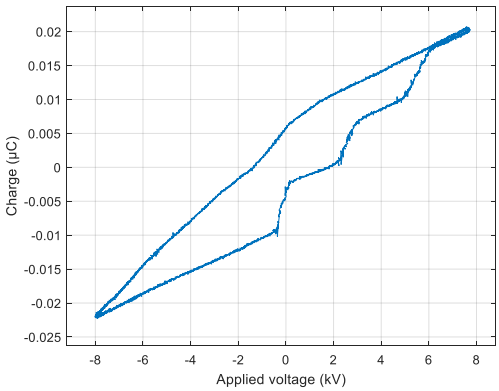

(b)

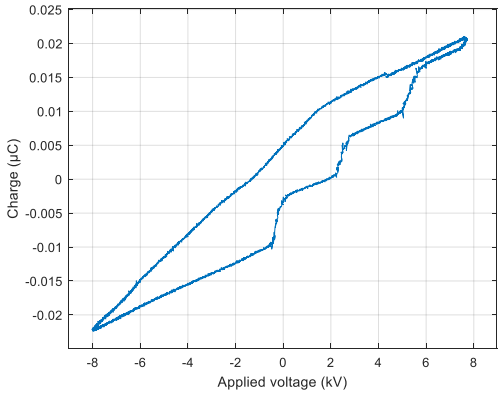

(c)

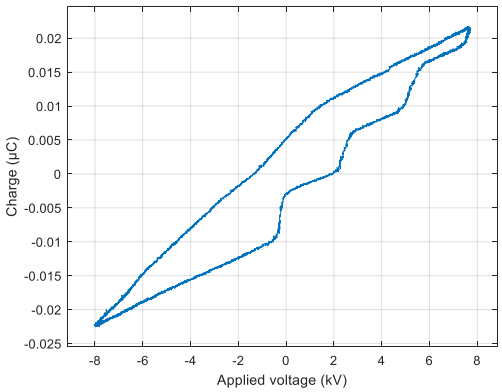

(d)

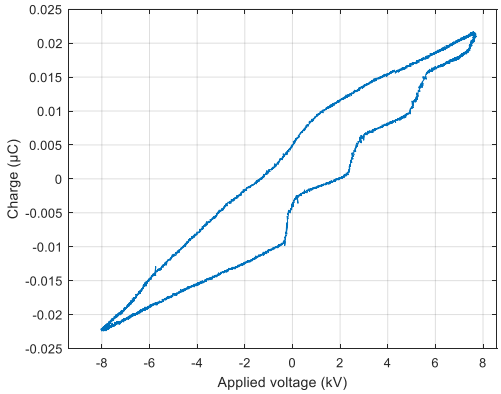
Charge (μC)
Applied voltage (kV)

(e)

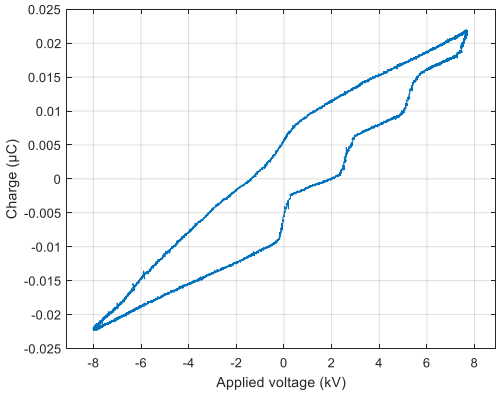
Charge (μC)
Applied voltage (kV)

(f)

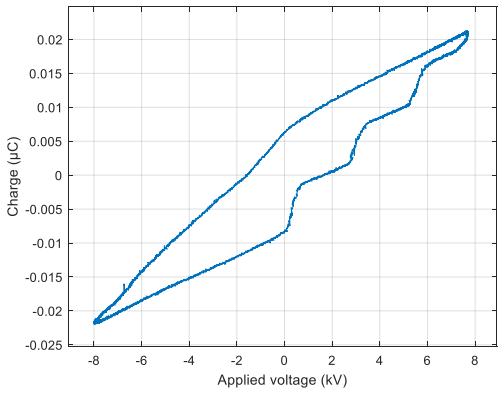
Charge (μC)
Applied voltage (kV)

(g)

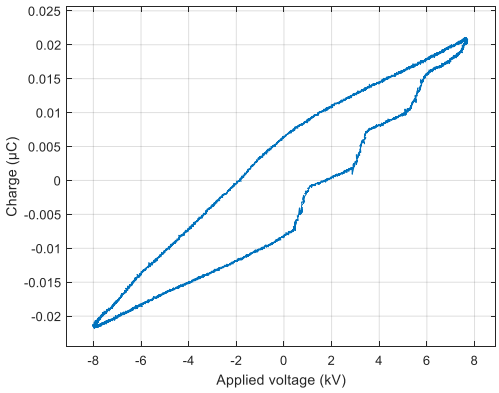
Charge (μC)
Applied voltage (kV)

(h)

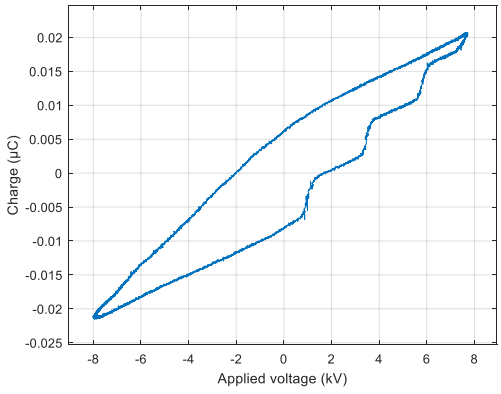
Charge (μC)
Applied voltage (kV)

(i)

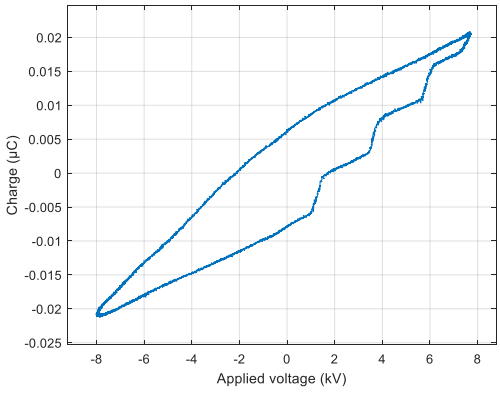
Charge (μC)
Applied voltage (kV)

(j)

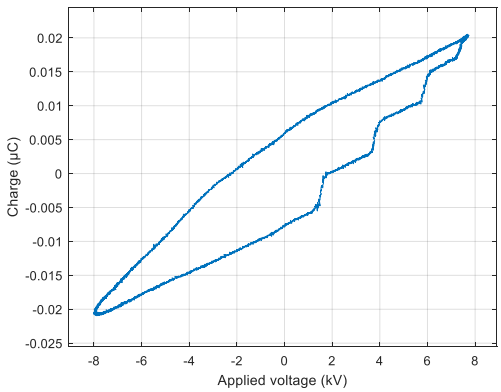
Charge (μC)
0.02
0.015
0.01
0.005
0
-0.005
-0.01
-0.015
-0.02
-0.025
-8
-6
-4
-2
0
2
4
6
8
Applied voltage (kV)

(k)

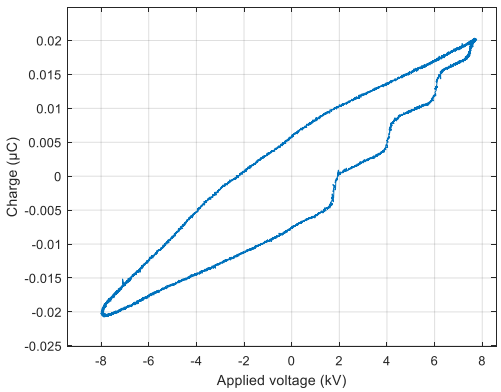
Charge (μC)
0.02
0.015
0.01
0.005
0
-0.005
-0.01
-0.015
-0.02
-0.025
-8
-6
-4
-2
0
2
4
6
8
Applied voltage (kV)

(l)

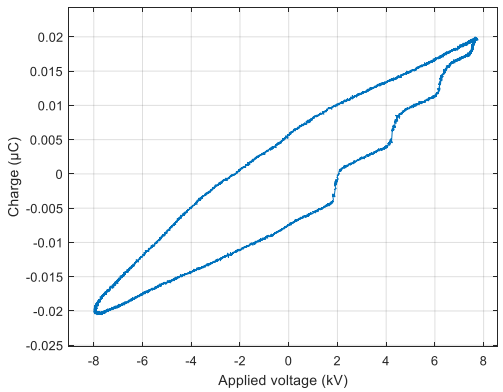
Charge (μC)
Applied voltage (kV)

(m)

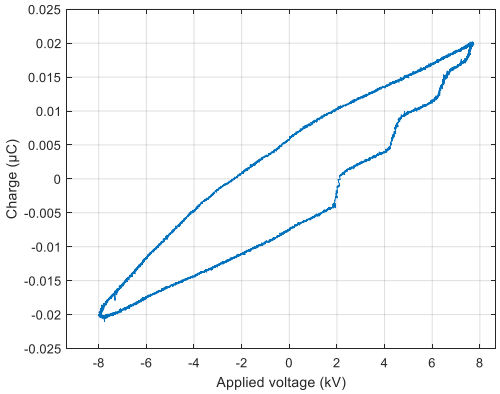
Charge (μC)
Applied voltage (kV)

(n)

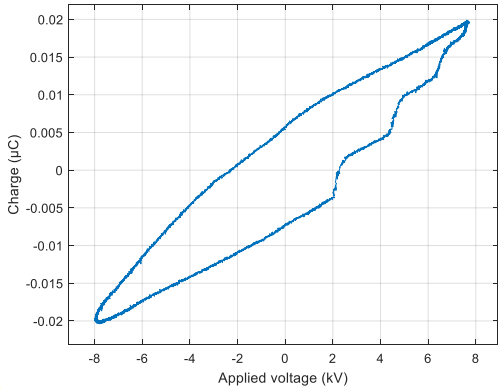
Charge (μC)
Applied voltage (kV)

(o)

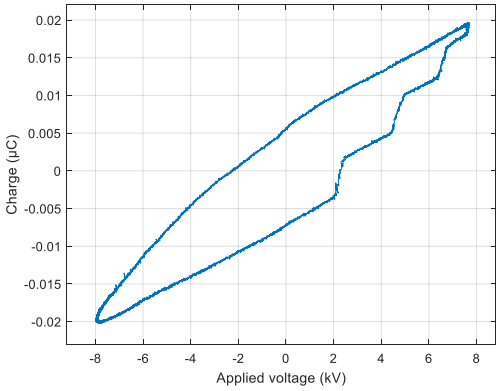
Charge (μC)
Applied voltage (kV)

(p)

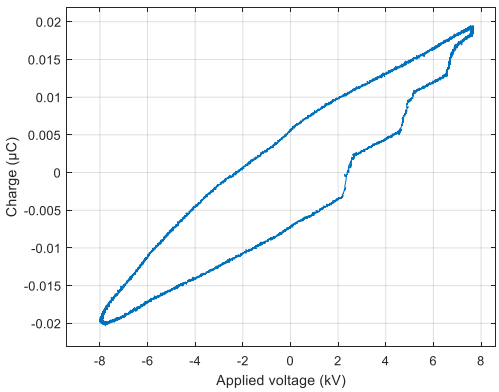
Charge (μC)
Applied voltage (kV)

(q)

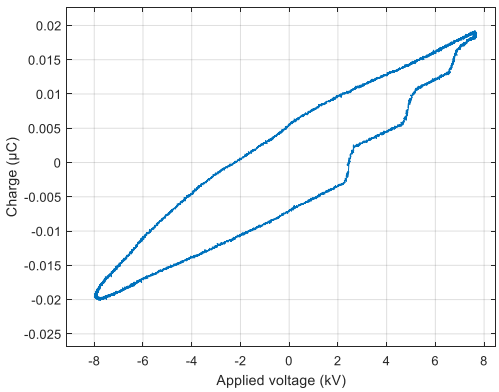
Charge (μC)
Applied voltage (kV)

(r)

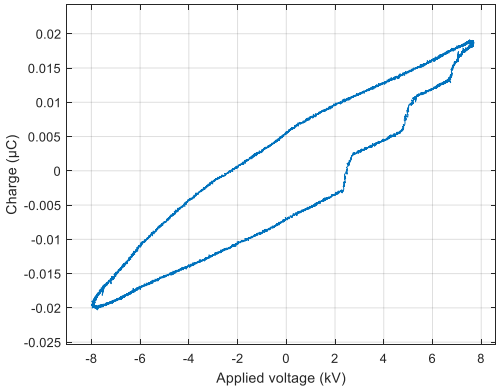
Charge (μC)
Applied voltage (kV)

(s)

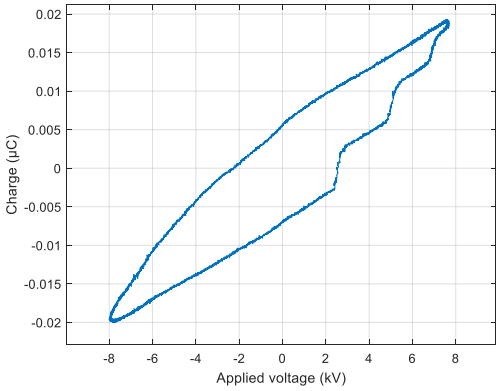
Charge (μC)
Applied voltage (kV)

(t)

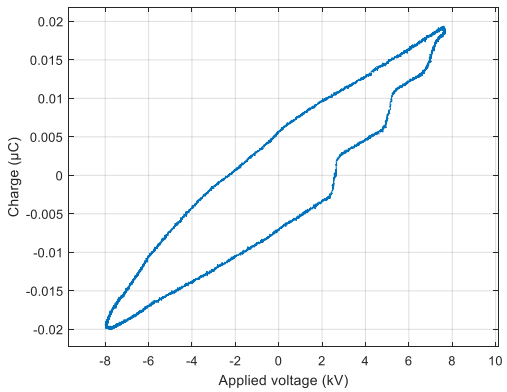

(u)

Figure F.1. Time series of Lissajous diagrams of Reactor 1 for taken at 15-second intervals during the first 5 minutes of treatment (a) 0 minutes 0seconds (b) 0 minutes 15 seconds (c) 0 minutes 30 seconds (d) 0 minutes 45 seconds (e) 1 minute 0 seconds (f) 1 minute 15 seconds (g) 1 minute 30 seconds (h) 1 minute 45 seconds (i) 2 minutes 0 seconds (j) 2 minutes 15 seconds (k) 2 minutes 30 seconds (l) 2 minutes 45 seconds (m) 3 minutes 0 seconds (n) 3 minutes 15 seconds (o) 3 minutes 30 seconds (p) 3 minutes 45 seconds (q) 4 minutes 0 seconds (r) 4 minutes 15 seconds (s) 4 minutes 30 seconds (t) 4 minutes 45 seconds (u) 5 minutes 0 seconds.

Appendix G Discharge power of Reactor 2

G.1 Introduction

Reactor 2 was created to be a similar design to Reactor 1, but capable of treating cells within a 9.6 cm^2 Petri dish rather than a 96-well plate. Reactor 2 was used only for the work performed in 4.4.5. The reason for this was that the area of the cell layer affected by NTP treatment with Reactor 2 was a very small percentage of the surface area of the dish, and thus the effects of the treatment would be easily obscured in biological assays, given the large number of unaffected cells present.

G.2 Design of Reactor 2

The design of Reactor 2 is detailed in 2.1.1.2.

G.3 Power matching and electrical characteristics

To determine an appropriate applied voltage for the work of 4.4.5, a range of different voltages were tried to find one which gave a discharge power close to that of Reactor 1, which was in the region of 0.5 W. This was achieved with Reactor 2 with a power supply output voltage of 100 V_m via a 220:10000 transformer, resulting in the voltage applied to the reactor being around of 4.5 kV_m. The discharge power with this voltage was found to remain largely consistent across a 30-minute treatment, although it did rise slightly from an average of 0.53 W (SE = 0.03 W) at the beginning to 0.63 W (SE = 0.04 W) at the end. The discharge power of Reactor 2 was measured using the Lissajous method, as described in 2.1.3.4, and the circuit diagram for this work is given in Figure G.1.

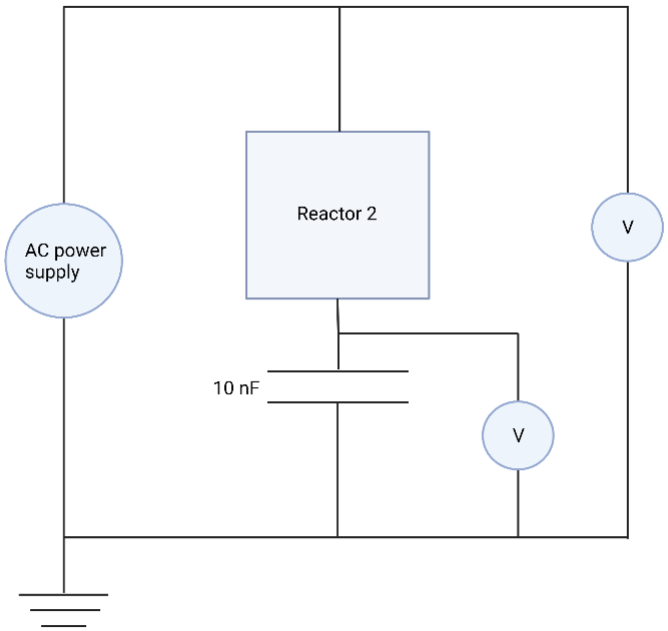

Figure G.1. Circuit diagram for Reactor 2 discharge power. Created with Biorender.com [6].

G.4 Comparisons to Reactor 1

The set of experiments carried out with Reactor 2 are illustrative only, to demonstrate the level of precision of moderate treatments with a DBD reactor design with needle electrode and to show the importance of diffusion effects in NTP treatments, and the treatment provided by Reactor 2 cannot be said to be identical to that of Reactor 1. That the treatment is not the same can be confirmed by examination of the Lissajous figures for both Reactor 1 (Figure 3.5) and Reactor 2 (Figure G.2). As has been discussed at length in 3.4.2 and 3.5, the character of the discharge of Reactor 1 clearly changes over the course of a 30-minute treatment, whereas for Reactor 2, it remains consistent throughout. This is not surprising as, unlike Reactor 1, where the change in discharge character appears linked

to the rapidly reducing liquid level in the 96-well plate well (surface area 0.32 cm^2), the liquid level in Reactor 2 barely falls due to its large surface area (9.6 cm^2).

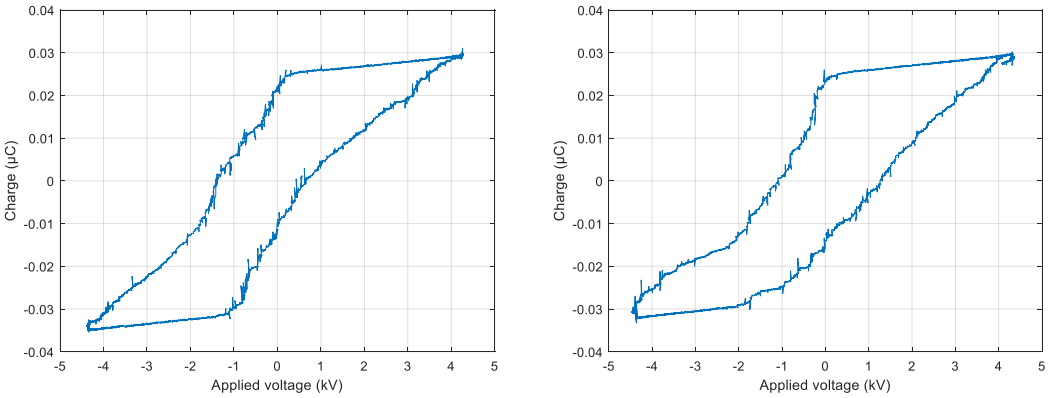

(a) (b)

Figure G.2. Example Lissajous figures for Reactor 2 taken (a) at beginning of 30-minute treatment time and (b) at end of 30-minute treatment time.

Appendix H Key papers in direct and PAM treatments

Table H.1. Key papers considering cell viability at 24 hours or longer following direct NTP treatment.

Author	**NTP source**	**Year of publication**	**Cell type**
Ahn et al. [84]	Air plasma jet	2014	HeLa, A549
Bekeschus *et al.* [129]	kINPen Ar plasma jet	2014	Primary T helper cells
Bekeschus [122]	kINPen Ar plasma jet	2015	Primary monocytes, B cells, natural killer cells, T helper cells, Cytotoxic T cells, γδ T cells.
Bekeschus *et al.* [238]	kINPen Ar plasma jet	2017	THP-1

Author	NTP source	Year of publication	Cell type
Bekeschus *et al*. [333]	kINPen Ar plasma jet	2018	CT26
Bekeschus *et al.* [334]	kINPen Ar plasma jet	2020	B16F10
Chen et al. [335]	He plasma jet	2018	HepG2, A549
Conway *et al.* [66]	DBD with sample held between two layers of dielectric.	2016	HeLa, U373MG
Fridman *et al.* [257]	Floating electrode (FE) DBD	2007	ATCC A2058
Girard *et al.* [161]	He plasma jet	2016	HCT116, LUI205

Author	NTP source	Year of publication	Cell type
Hoentsch *et al.* [153]	Ar plasma jet	2012	mHepR1
Kalghatgi *et al.* [68]	DBD with quartz covered powered electrode and grounded dish.	2011	MCF10A
Kaushik *et al.* [336]	DBD with mesh ground electrode allowing diffusion down to sample dish	2014	T98G, SNU80, KB,HEK
Kim *et al.* [70]	DBD operated in air, without sample being part of circuit (diffusion down to sample dish)	2011	G361
Ma *et al.* [133]	He plasma jet	2014	Many, including HeLa, adipose-derived stem cells, G361, YD-9 HCT116, HT29
Nguyen *et al.* [81]	Air plasma jet	2016	HeLa

Author	NTP source	Year of publication	Cell type
Nguyen *et al*. [155]	Air plasma jet	2019	HeLa
Panngom *et al.* [71]	DBD with mesh ground electrode, allowing diffusion of RONS to sample.	2013	KB, MCF-7, HeLa, H460, SNU-80, T98G
Sato *et al.* [205]	DBD with needle electrode, and culture tube embedded in grounded metal holder.	2011	HeLa
Siu *et al*. [337]	He plasma jet	2015	A172, U373, U87, NHA, HUVEC
Song *et al.* [72]	DBD in flowing He atmosphere	2018	CNE-2Z
Vandamme *et al.* [73]	FE-DBD	2012	U87MF, HCT116

Author	NTP source	Year of publication	Cell type
Volotskova *et al.* [89]	He plasma jet	2012	WTK, 308, PAM 212
Wende *et al.* [338]	kINPen	2013	HaCaT
Wende *et al.* [156]	RF Ar jet, kINPen	2015	HaCaT, CRFK
Yan *et al.* [154]	He-O2 plasma jet	2012	HepG2

Table H.2. Key papers showing cell viability effects of PAM application, considered at 24 hours or more following the application.

	Author	**NTP source**	**Year of publication**	**Cell type**
1	Chen *et al.* [335]	He plasma jet	2018	HepG2, A549
2	Hoentsch *et al.* [153]	Ar plasma jet	2012	mHepR1
3	Ikeda *et al.* [339]	Ar plasma jet (flat head)	2018	HEC-1, GCIY
4	Kajiyama *et al.* [266]	Ar plasma jet (flat head)	2016	K2
5	Liu *et al.* [240]	He plasma jet	2020	B16
6	Mohades *et al*.[242]	He plasma jet	2015	SCaBER

	Author	NTP source	Year of publication	Cell type
7	Mohades *et al.* [177]	He plasma jet	2016	SCaBER, MDCK
8	Nguyen *et al.* [81]	Air plasma jet	2016	HeLa
9	Nguyen *et al.* [155]	Air plasma jet	2019	HeLa
10	Panngom *et al.* [71]	DBD with mesh ground electrode, allowing diffusion of RONS to sample.	2013	KB, MCF-7, HeLa, H460, SNU-80, T98G
11	Tanaka *et al.* [340]	Ar plasma jet	2018	U251SP, LN-229, T98G
12	Tanaka *et al.* [80]	Ar plasma jet	2011	U251SP

	Author	NTP source	Year of publication	Cell type
13	Tokunaga *et al.* [270]	He plasma jet	2018	A375, A2058, SAOS, NB-1, SK-N-SH, LM8, K7M3, MC3t3-E1 17, 143B, nFOB.
14	Utsumi *et al.*[152]	Ar plasma jet	2014	TOV21G
15	Utsumi *et al.* [136]	Ar plasma jet	2013	NOS2, NOS3
16	Wende *et al.* [341]	kINPen	2014	HaCaT
17	Wende *et al.* [156]	RF Ar jet, kINPen	2015	HaCaT, CRFK
18	Yan *et al.* [342]	He plasma jet	2015	U87, MDA-MB-231, MCF-7

	Author	NTP source	Year of publication	Cell type
19	Yue *et al.* [264]	He plasma jet	2016	SCaBER

Appendix I Determination of process for use of FITC-labelled 1 µM latex beads to assess phagocytosis

To determine the length of time required for cells to phagocytose a sufficient number of latex beads to be noticeable under a microscope, an experiment was carried out to compare two different lengths of exposure: 2 hours and 24 hours. It was found that 2 hours was an insufficient exposure time for significant phagocytosis to have occurred (Figure I.1(a)) and it was apparent that 24 hours (Figure I.1(b)) would be more suitable. Therefore, for the phagocytosis experiments within this project, latex beads were applied for to cells for 24 hours prior to analysis.

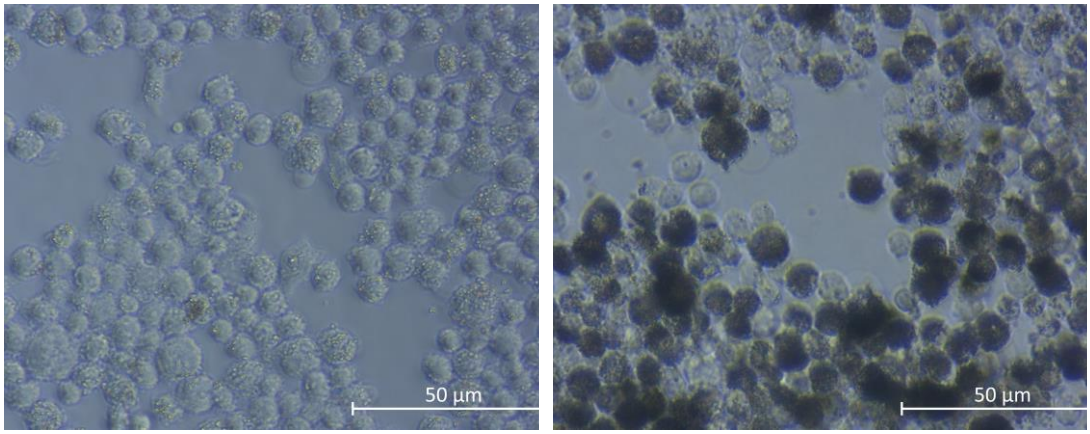

(a) *(b)*

Figure I.1. Differentiated U937 (differentiated by exposure to 16.2 nM PMA for 48 hours) incubated with latex beads for (a) 2 hours and (b) 24 hours. Both samples were washed twice with DPBS to remove as many non-phagocytosed beads as possible prior to photography.

Appendix J Poster presented at International School on Low Temperature Plasma Physics, 5th to 12th October 2019, Bad Honnef, Germany

Cell viability reduction in the 3t3 murine fibroblast cell line treated with dielectric barrier discharge in a pin-plate reactor

R. B. Pirie[1], M. H. Grant[2], T. Wang[1]

1. Department of Electronic and Electrical Engineering, University of Strathclyde, Royal College Building, 204 George Street, Glasgow G1 1XW, UK
2. Department of Biomedical Engineering, University of Strathclyde, Graham Hills Building, 50 George Street, Glasgow G1 1QE, UK
Contact: rachael.pirie@strath.ac.uk

University of Strathclyde Engineering

INTRODUCTION

The purpose of this work was to develop a simple system capable of applying plasma to the liquid cell medium used for *in vitro* cell samples, and to begin basic exploration of its effects on cells. An atmospheric-pressure air dielectric barrier discharge (DBD) design was selected as the basis for the system, as this allowed for simple construction and also operated in the ambient environment, without the need for a gas supply. Unlike many other DBD systems developed for biomedical application, in which flat plates are used as electrodes, the use of a needle electrode in this design creates a narrow filament of discharge, allowing precise application. Following the initial development of the reactor design, the nitrite (NO_2^-), and hydrogen peroxide (H_2O_2) levels produced in cell medium during treatment were measured. These two long-lived substances are thought to be largely responsible for the fatal effects seen when a liquid pre-treated with plasma is later added to cells [4]. Temperature and pH of the treated liquid were also measured, as extremes of these also have biological effects.

Cell viability experiments were then carried out with plasma treatment applied to the 3t3 (murine fibroblast) cell line. Initially, this section of work focused on what is often called a "direct" plasma treatment, where the cells sit within liquid medium as it is receiving the treatment. A comparison was then made with the effects on the cells of a plasma treated medium (PAM) method, sometimes known as "indirect" treatment, where the liquid was treated in the reactor without the cells being present, before then being added to the cells. The neutral red assay method was used to measure the cell viability.

SYSTEM DESIGN

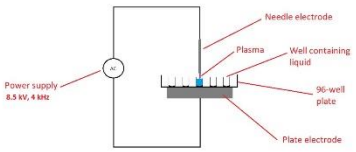

Figure 1. Schematic diagram of designed plasma reactor showing application to single treatment well in 96-well plate

- Dielectric barrier discharge (DBD) operating in ambient air
- Applied voltage 8.5 kV A.C at 4 kHz
- Well undergoing treatment contains 325 µL of serum-free Dulbecco's Modified Eagle Medium (DMEM)
- When cells are used within the reactor in a "direct" treatment, they form a layer on the bottom of the well
- Discharge power measured as 0.5 W by Lissajous method
- Individual current pulses approximately 4 ns at up to 1 A

NO_2^- MEASUREMENT

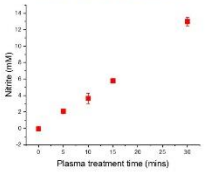

Figure 2. Nitrite concentration, measured by Griess method, in treated serum-free DMEM, against plasma treatment time.

- Relationship between NO_2^- concentration and plasma treatment time of liquid is linear (R^2=0.9971)
- Rate of increase of nitrite concentration is around 0.4 mM/minute. Although this is in line with some similar biomedical plasma devices, it is at the higher end of the range

H_2O_2 MEASUREMENT

H_2O_2 testing, using Amplex Red, is not presently fully complete, but concentration is around 2.0 – 2.5 mM after 30 minutes of treatment of serum-free DMEM. This rate of H_2O_2 production is in line with other biomedical plasma devices.

TEMPERATURE AND pH EFFECTS

Temperature change in the liquid with 30 minutes of plasma treatment is an average of 1.2 °C. pH change was found to be negligible.

BIOLOGICAL MEASUREMENTS

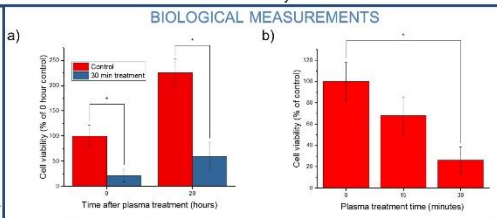

Figure 3. a) Cell viability of 3t3 shown 0 hours after a 30 minute "direct" plasma treatment of cells held in serum-free DMEM, and also at 20 hours. Immediately after plasma treatment, the medium was removed and replaced with fresh medium, which the cells were held in until the cell viability assay was carried out. Both the immediate and 20 hour samples showed a similar proportional decrease from control (79 % for the immediate samples, and 74 % for the 20 hour samples) b) Cell viability at 20 hours following "direct" plasma treatment of 3t3 for either 15 or 30 minutes. Statistically significant reduction noted for 30 minute treatment but not for 15 minute treatment (p<0.05).*

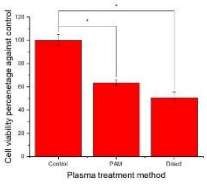

*Figure 4. Comparison of 3t3 cell viability after PAM treatment versus that after "direct" treatment. PAM-treated samples were held within immediately pre-treated serum-free DMEM for 1 hour prior to its replacement with fresh complete DMEM. "Direct" treatment was applied to serum-free DMEM containing the cells for 10 minutes, prior to the cells being held within this liquid for a further 50 minutes post-treatment, before this was then replaced with fresh complete DMEM. In both cases, cell viability was considered 20 hours after treatment. Results show statistically significant difference from control for both PAM and "direct" treatment (36 % reduction on average for PAM treatment and 49 % average reduction for "direct" treatment) but no statistically significant difference between the two treatment types . This is in line with other work seen in the literature, such as at [5] (*p≤0.001).*

CONCLUSIONS

- Two key chemicals, NO_2^- and H_2O_2, were measured in treated cell medium. Levels of both were found to be comparable with other devices used for similar purposes, although the NO_2^- was at the higher end of this range
- Temperature and pH change in treated liquid was minimal
- Viability of 3t3 cells was significantly reduced by a 30 minute "direct" plasma treatment, but not by a 15 minute treatment
- There was no significant difference in the viability reduction given by "direct" and "indirect" treatment.
- Future work will involve the investigation of the effects of plasma treatment on a second cell line, U937 (human monocyte)

DIFFICULTIES DURING PROJECT

- A number of different reactor designs were rejected due to either movement of liquid during treatment, or due to failure to produce a detectable chemical modification to the treatment liquid
- There were difficulties in getting repeatable results with the biological experiments, and it was problematic to determine whether this was due to variances in the plasma application or variances in the cell samples
- There is a significant breadth of knowledge required for the project

REFERENCES

[1] I. E. Kieft, M. Kurdi, and E. Stoffels, "Reattachment and apoptosis after plasma-needle treatment of cultured cells," IEEE transactions on Plasma Science, vol. 34, no. 4, pp. 1331–1336, 2006.
[2] V. Miller, A. Lin, G. Fridman, D. Dobrynin, and A. Fridman, "Plasma stimulation of migration of macrophages," Plasma Processes and Polymers, vol. 11, no. 12, pp. 1193–1197, 2014.
[3] J. W. Choi, S. U. Kang, Y. E. Kim, J. K. Park, S. S. Yang, Y. S. Kim, Y. S. Lee, Y. Lee, and C.-H. Kim, "Novel Therapeutic Effects of Non-thermal atmospheric pressure plasma for Muscle Regeneration and Differentiation," Scientific reports, vol. 6, 2016.
[4] N. Kurake, H. Tanaka, K. Ishikawa, T. Kondo, M. Sekine, K. Nakamura, H. Kajiyama, F. Kikkawa, M. Mizuno, and M. Hori, "Cell survival of glioblastoma grown in medium containing hydrogen peroxide and/or nitrite, or in plasma-activated medium," Archives of biochemistry and biophysics, vol. 605, pp. 102–108, 2016.
[5] S. Bekeschus, K. Masur, J. Kolata, K. Wende, A. Schmidt, L. Bundscherer, A. Barton, A. Kramer, B. Bröker, and K.-D. Weltmann, "Human mononuclear cell survival and proliferation is modulated by cold atmospheric plasma jet," *Plasma Processes and Polymers*, vol. 10, no. 8, pp. 706–713, 2013.